

**Development of a Hybrid and Open Architecture  
Controlled Laser Workstation**

by

**Hasan Sinan Bank**

**A Thesis Submitted to the  
Graduate School of Engineering  
in Partial Fulfillment of the Requirements for  
the Degree of**

**Master of Science  
in  
Mechanical Engineering**

**Koç University**

**August 2011**

**Koç University  
Graduate School of Sciences and Engineering**

This is to certify that I have examined this copy of a master's thesis by

Hasan Sinan Bank

and have found that it is complete and satisfactory in all respects,  
and that any and all revisions required by the final  
examining committee have been made.

Committee Members:

---

Assoc. Prof. Dr. Ismail Lazoglu (Advisor)

---

Prof. Dr. İskender Yılgör

---

Assoc. Prof. Dr. Murat Sözer

---

Prof. Dr. Erhan Budak

---

Prof. Dr. Alphan Sennaroğlu

Date:

---

## **ABSTRACT**

Development of a machine in order to impose a manufacturing technology is crucial improvement for mankind. Generally there is parallelism between the scientific evolution and current available key manufacturing technology. Development of laser technology has affected our lives significantly. The methods such as laser marking, laser cutting, laser machining and laser sintering are some of the key usage of this technology as a tool. In addition to that the progresses, the digital technology yields to control this tool in a precise manner. Virtual artifacts that are generated by computer aided design (CAD) programs might be carried out in wide range areas from macro to micro applications.

This dissertation describes the development of a versatile laser workstation which is capable of using subtractive-additive manufacturing (SAM) methods such as laser cutting, laser machining, laser marking and direct selective laser sintering (SLS). The design and manufacturing of the mechanical components; the selection and programming firmware of programmable electronics and the computer software are developed in this manner. In the aim of this thesis, virtual 3D CAD geometries (in stereo lithography (STL) or G-Code format) are planned to manufacture by developed workstation. Therefore, an in-house built 3D scanner is also implemented to the system and the scanned point clouds would also be converted in STL file by using some commercial software packages. In addition to that, there isn't any geometrical constraint in the developed software which confirms the possibility of calculation of toolpath for any application such as custom biomedical implants, MEMS (Micro Electro Mechanical Systems) devices or even a jet turbine's complex impeller blade.

The current software and hardware technology are used to solve some of engineering problems in laser based manufacturing. The proposed general solutions in the engineering problems (i.e. three-dimensional freeform geometry slicing and toolpath generation, servo system (position/ velocity) control, multitasking equipment control by simultaneous signal

generation (via Field Programmable Gate Arrays (FPGA) and microcontrollers), reverse engineering of freeform surfaces etc.) are available to use in different machines and methods (i.e. laser marking, laser machining and SLS).

In the light of forgoing points, the production of permanent high resolution images on most of the engineering materials (i.e. polymers or metals) is possible in a fast, non-contact manner via laser machining. The most popular used laser's wavelengths are 10640 nm and 1064 nm. The developed toolpath (rastering or continuous scanning) are control points for the FPGA controlled mirrors oscillating along orthogonal axes in this study. The minimum resolution is depends on the optics on the galvanometric scanner which is capable of using in mentioned laser wavelengths ( $CO_2$  10640 nm, Ytterbium Fiber Laser 1064nm) due to the specific coating that the mirror has.

Another application of this workstation is direct SLS, which is a laser based rapid manufacturing technology that enables production of functional, metal or polymeric components via the direct, layerwise consolidation of constituent powders. Specifically, this dissertation focuses on a different laser wavelength usage to consolidate different type of materials due to material dependent absorption without changing any structural components. Moreover, the fundamental machine technology development was established with processing science to enable aforementioned additive manufacturing technology composed of polymers (e.g. Polyamide). This process is intended as a significantly faster, low cost, versatile, highly automated and hopefully replaceable with the laser workstations which are recently used in the industry.

All of the mentioned processes based on a physical facts behind it. Therefore, a study of some of the important laser material processing mathematical models is completed and an analytical one is built. This model was undertaken especially for laser material interactions to obtain a fundamental understanding of the underlying process physics. In addition to that, this model helps in developing selection schemes (i.e. starting parameters) for the

materials that are most amenable to the process. This physical understanding is the paramount importance in the development of machine and process control technology.

The development of machine, processing and control technologies during this research effort enabled successful production of a number of different geometries by two-dimensional (2D) and three-dimensional (3D) manner. In order to show this, sub-scaled demonstration components in different materials processed by laser workstation are given.

The overall goal of this research was to develop a laser workstation which is capable of laser machining (laser drilling, laser cutting and laser marking) and direct (SLS) armed with a fundamental understanding of the underlying physics behind it. The knowledge gained from experimental (with technological demonstration) and analytical work is essential for machine design, process development and control.

## ÖZET

Herhangi bir üretim teknolojisi geliřtirmek ve bunu makinalařtırmak insanlık için büyük önem arz etmektedir. Bunun sebebi bilimsel ilerleme ile ilerlemeyi saęlayan anahtar üretim teknolojisi üzerinde paralellik olmasıdır. Örnek olarak Galile'nin teleskobu (1609 yılında yeni geliřtirilen camdan lens üretme teknolojisi) veya James Gregory ve Isaac Newton'un yansıtmalı teleskobu (1660 yılında metal aynaların tařlama ve parlatma teknolojileri), o yıllarda varolan üretim teknolojileri sayesinde bilimsel ilerlemede kullandıkları araçları geliřtirmişlerdir. Bu verilen örneklerin ötesinde 20. yüzyılın en büyük icatlarından bir tanesi lazerdir. İlk kullanılan lazerden günümüze lazer teknolojisi hayatımız üzerinde büyük etkiye sahiptir. Bu teknoloji kullanılarak lazer markalama, lazer kesme, lazer işleme ve lazer sinterleme gibi üretim metodlarında lazer teknolojisi araç olarak kullanılmaktadır. Buna ek olarak geliřen dijital teknoloji sayesinde bu araç hassas bir şekilde kontrol edilebilmektedir. Bilgisayar destekli yazılım (BDT) programları kullanılarak yaratılan sanal nesnelere mikrodan makro uygulamaya kadar büyük bir yelpazede üretilebilmektedirler.

Bu tezde çok amaçlı bir lazer işstasyonunun geliřtirilmesini kapsamaktadır. Kullanılan üretim metodları lazer markalama, lazer kesme, lazer işleme ve direkt lazer sinterleme olarak sayılabilir. Mekanik komponentlerin tasarımı ve üretimi; programlanabilir elektronik malzemelerin seçimi ve programlanması; bilgisayar yazılımının geliřtirilmesi bu amaçla yapılan işlerin konu başlıklarıdır. Bu tezde amaçlanan, planlanan BDT geometrilerinin üç boyutlu tarayıcı, stereolitografi (STL) veya G-Code (G programlama dili, Massachusetts Institute of Technology) gibi geometri bilgilerini kullanarak üretilmesidir. Bundan dolayı, üç-boyutlu tarayıcı geliřtirilmiştir ve sisteme dahil edilmiştir. Buradan elde edilen nokta bulutları daha sonra ticari yazılımlar kullanılarak STL dosya formatına dönüřtürülebilmektedir. Buna ek olarak, geliřtirilen bilgisayar programında herhangi bir geometrik kısıt bulunmamaktadır. MEMS cihazları, biyomedikal implantlar veya kompleks

geometriye sahip jet türbinlerini üretmek için gerekli matematiksel hesaplamalar yapılabilmektedir.

Bütün yapılan çalışmalarda günümüz teknolojisini üretimde ortaya çıkan sorunları çözebilmek için birleştirmek amaçlanmaktadır. Üç boyutlu serbest yüzey geometrilerinin dilimlenmesi ve lazer yollarının çıkarılması; servo sistem pozisyon ve hız kontrolü; aynı anda çoklu işlem yapabilecek sinyal sistemlerinin geliştirilmesi ; serbest yüzey geometrilerinin tersine mühendislikte kullanımı ile ilgili önerilen çözümler farklı makinalarda farklı uygulamalar için kullanılabilir.

Yukarıda anlatılanların ışığında, yüksek çözünürlüklü imgelerin mühendislik malzemelerinde kalıcı, hızlı ve temas etmeden üretilmesi lazer markalama olarak tanımlanabilir. En çok kullanılan lazer dalga boyları 10640 nm ve 1064 nmdir. Geliştirilen takım yolları (duraksayarak veya sürekli tarama) FPGA aygıtı için komut zincirlerini oluşturur. Böylece tarama işlemini gerçekleştiren aynalar ortogonal eksenlerde hareket etmektedirler. En küçük elde edilen hassasiyet kullanılan merceğe bağlıdır ve bu sebepten seçilen galvo  $CO_2$  (10640 nm) ve Ytterbium (1064 nm) için kullanılabilir.

Geliştirilen sistemle uygulanabilecek bir başka uygulama da direkt lazer sinterlemedir. Metalik veya polimerik toz malzemenin katmanları olarak birleştirilmesi ile tasarlanan geometri üretilmeye çalışılır. Özellikle bu tezde yapısal herhangi bir değişikliğe gitmeden çoklu dalga boyunda çalışan bir sistem yapılması planlanmaktadır. Temel makina tasarımı ilkeleri yanında polimerik malzeme (poliamid) üzerinde proses çalışmaları yapılmıştır. Bu süreç önemli ölçüde hızlı, düşük maliyetli, farklı kullanım alanlarına sahip, otomatik ve endüstriyel uygulamadaki muadillerinin yerine geçebilir şekilde tasarlanmıştır.

Yukarıda bahsedilen üretim metotları içerisinde fiziksel gerçekleri barındırır. Bundan dolayı bazı önemli lazer malzeme işlem süreci matematik modelleri literatürden incelenmiş ve analitik bir tanesi oluşturulmuştur. Bu model özellikle lazer malzeme etkileşimlerinin temellerini anlamak ve altında yatan süreç fiziğini kavramak için kullanılmıştır. Buna ek

olarak, bu model bu işlemde kullanıma en uygun malzemeler için başlangıç parametrelerinin belirlenmesinde yardımcı olmaktadır. Bu tezde, üzerinde çalışılan sürecin kontrolü ve bu süreci gerçekleştiren makina teknolojisinin yaratılmasında arkasında yatan fiziksel nedenleri anlamak en önemli kısmı olarak düşünülebilir.

Tez sırasında bir makinanın tasarımı, makinanın çalıştırılması ve kontrol teknolojileri sayesinde farklı iki-boyutlu ve üç-boyutlu geometriler üzerinde çalışılmıştır. Bu çalışmalarını göstermek için farklı ölçeklerde ve farklı malzemeler kullanan parça örnekleri verilmiştir.

Tezde nihai olarak yapılmak istenen daha önceden de belirtildiği gibi lazer kesme, lazer markalama, lazer işleme ve direkt lazer sinterleme işlemlerini yapabilen bir lazer iş istasyonunun yazılımı ve bütün donanımıyla geliştirilmesi; bunun yanında, bu işlemlerin arkasındaki fiziksel nedenleri de ele alarak temeldeki amaç olan makina tasarımı, süreç gelişimi ve kontrolünü tamamlamaktır.



## **ACKNOWLEDGEMENTS**

It is my duty first and foremost to acknowledge the role of my advisor Dr. Ismail Lazođlu in my professional development by giving me the chance to be part of his team and the infrastructures that he provides during this research. I am also grateful for his faith and patient.

I would like to thank the committee members of my thesis defense, Dr. Erhan Budak, Dr. İskender Yılgör, Dr. Alphan Sennarođlu and Dr. Murat Sözer for reading this thesis and offering constructive criticism.

I would like to extend my appreciation to Dr. Zeki Bayraktarođlu and Dr. Cevza Candan for their guidance, inspiration and help during my undergraduate study.

I am thankful to Laser Research Group members Dr. Huseyin Çankaya and Natali Çizmeciyen for their technical support.

I specially thank to Adnan Kurt for providing valuable advice and technical guidance throughout this thesis.

Several colleagues and associates deserve special thanks. I thank my friends and MARC members Daulet Izbassarov, Coskun Islam, Enis Akgün, Canberk Manav for sharing their knowledge with me. I am grateful to the summer researcher Aniqa Arif and Mariam Khalid. They are very productive and supportive during their existence in MARC.

I extremely appreciate the valuable technical help of Selim Ölçer, Muzaffer Bütün, Emre Ayarođlu and the outstanding assistance given by Can Franko and Mehmet Aydın Baytas. Without their help, this thesis would not be completed.

A substantial portion of the work described in this dissertation was done under the sponsorship of Science Technology and Industrial Administration of Turkish Republic and Laser Micron Company with project number 00470.STZ.2009-2. Therefore, I wish to thank Birhan U. Güzel, who made this funding possible.

Special thanks go to my family, because it would not be possible without their undying support during my educational life.

Finally, thanks to my greatest chance in my life, Pırl Ertem, for sharing my happiest moments in Koç University and motivating me continuously during this study.

## Table of Contents

|  |      |
|--|------|
| LIST OF TABLES .....   | xiv  |
| LIST OF FIGURES .....  | xv   |
| NOMENCLATURE .....   | xvii |
| 1. Introduction.....   | 18   |
| 1.1 Motivation of this study.....  | 18   |
| 1.2 Dissertation Outline .....   | 18   |
| 2. General Review of Laser Materials Processing.....                               | 20   |
| 2.1 Introduction.....  | 20   |
| 2.2 An Overview for Laser Material Processing Methods .....                        | 22   |
| 2.3 Analytical Thermal Modeling of Laser Material Processing.....                  | 27   |
| 2.4 The Temperature Distribution.....  | 33   |
| 2.4 Material Characterizations for Laser Material Processing.....                  | 35   |
| 2.4.1 Absorption Coefficient.....  | 36   |
| 2.4.2. Specific Heat Capacity.....   | 38   |
| 2.4.3. Thermal Conductivity .....  | 39   |
| 2.4.4. Density .....   | 40   |
| 2.4.5 Thermal Diffusivity .....  | 40   |
| 2.4.5. Coefficient of Thermal Expansion.....                                       | 40   |
| 2.4.6. Transformation Temperatures.....  | 41   |
| 3. Laser Workstation Design.....   | 43   |
| 3.1 Introduction.....  | 43   |
| 3.2 Design Procedure of Subtractive-Additive Manufacturing (SAM) Workstation ..... | 43   |
| 3.3 Developing Methodology of Machine Specifications .....                         | 45   |
| 3.3.1 The First Generation Additive Manufacturing (AM) Machine .....               | 46   |
| 3.3.2 The Second Generation Additive Manufacturing (AM) Machine.....               | 50   |
| 3.3.3 Laser Material Processing [LMP].....   | 51   |
| 3.4 Design Strategies .....  | 54   |
| 3.4.1 Accuracy .....   | 54   |

|  |     |
|--|-----|
| 3.4.2 Stiffness and Damping Outlook for Designed Workstation .....                           | 58  |
| 3.4.3 Structural Stability .....   | 61  |
| 3.4.5 Productivity and Manufacturability .....   | 63  |
| 3.5 Design Layouts .....   | 66  |
| 3.7 Recommendations for Design of Laser Workstation.....                                     | 78  |
| 4. Development of Optic-Electronic Hardware and Computer Software for Laser Workstation..... | 80  |
| 4.1 Introduction.....  | 80  |
| 4.2 Laser Beam Delivery .....  | 83  |
| 4.3 Hardware Interfaces .....  | 88  |
| 4.3.1 Scan Control for Flying Optics (Module I) and Galvoscaner (Module II).....             | 91  |
| 4.3.2 Laser Power Control .....  | 95  |
| 4.3.3 Optical Feedback System.....   | 102 |
| 4.4 Developed Laser Processing Software.....   | 110 |
| 4.4.1 Importing Geometry by Reverse Engineering .....  | 111 |
| 4.4.2 Geometry Importing and Processing .....  | 120 |
| 4.4.3 Software Process Parameters .....  | 132 |
| 5. Conclusion: Technological Demonstration.....  | 137 |
| 5.1 Introduction.....  | 137 |
| 5.2 General solution from the plan into the motion G-code Approach .....                     | 137 |
| 5.2.1 Scaffold production.....   | 137 |
| 5.2.2 Laser cutting operation .....  | 139 |
| 5.3 Three-dimensional (3D) Applications of Developed Laser Workstation.....                  | 141 |
| 5.3.1 Powder Sintering Applications .....  | 142 |
| Appendix 2.1 – Mathematical Derivation of Analytical Model .....                             | 147 |
| A.2.1.1 The Point Source Solution .....  | 147 |
| A.2.1.2 Applications of the point source solution .....                                      | 152 |
| A.2.1.3 Line Source Solution.....  | 155 |
| Appendix 2.2 Thermal Model Codes.....  | 164 |

|  |     |
|--|-----|
| A3.1.1 Chassis Assembly .....  | 166 |
| A3.1.2 Fly-optics X-axis.....  | 167 |
| A3.1.3 Laser Feedback Assembly .....                                 | 168 |
| A3.1.4 Work Table (Module I) Assembly .....                          | 169 |
| A3.1.5 Y Axis (Module I) Assembly.....                               | 170 |
| A3.1.6 Part Drawings.....  | 171 |
| Appendix 3.2 - Optic Component List.....                             | 188 |
| Appendix 5.1 - Technological Demonstration Material Properties ..... | 190 |
| References.....  | 191 |
| Chapter 2 References .....   | 191 |
| Chapter 3 References .....   | 194 |
| Chapter 4 References .....   | 196 |

## LIST OF TABLES

|  |     |
|--|-----|
| Table 2-1 Sources of data for metals, ceramics, glasses, polymers and composites .....                               | 28  |
| Table 2-2 Sources of data for metals, ceramics, glasses, polymers and composites .....                               | 29  |
| Table 2-3 Analytical equations for the temperature fields around a surface energy source                             | 30  |
| Table 2-4 Absorbance of powders, Ytterbium ( $\lambda=1.06 \mu\text{m}$ ) and $CO_2(\lambda=10.6 \mu\text{m})$ ..... | 32  |
| Table 2-5 Absorbance of powders, Ytterbium ( $\lambda=1.06 \mu\text{m}$ ) and $CO_2(\lambda=10.6 \mu\text{m})$ ..... | 33  |
| Table 2-6 Material Characterization Techniques.....  | 36  |
| Table 3-1 Laser Processing Parameters from the Literature Survey .....   | 52  |
| Table 3-2 Specifications of commercial laser workstations[28].....   | 53  |
| Table 3-3 Design Iterations of the developed laser workstation.....  | 70  |
| Table 3-4 Design Iterations of the developed laser workstation.....  | 71  |
| Table 3-5 The masses of the given assemblies .....   | 72  |
| Table 3-6 Measurement results of the points in Fig. 3.12 .....   | 75  |
| Table 4-1 Commercial 3D Scanners .....   | 116 |
| Table 4-2 List of important laser material processing parameters.....  | 133 |
| Table 4-3 List of important laser material processing parameters.....  | 134 |
| Table 5-1 The given G-code, in order to produce the scaffolds in Fig. 5.1 .....                                      | 139 |
| Table 5-2 G-Code Command for the given test pattern of front part .....  | 141 |

## LIST OF FIGURES

|   |    |
|---|----|
| Figure 2.1 Schematic of Selective Laser Sintering Process.....  | 25 |
| Figure 2.2 Laser Beam Machining Schematics, a) Laser Cutting b) Laser Drilling .....  | 26 |
| Figure 2.3 Integrated Sphere Reflectometer – experimental setup [69] .....  | 36 |
| Figure 2.4 Wavelength – Absorptivity relation for metals, alloys and organic materials ...  | 38 |
| Figure 3.1 The first developed additive manufacturing machine .....   | 46 |
| Figure 3.2 (I,II,III) The former designed four different type of extrusion head .....   | 47 |
| Figure 3.3 The produced part from the first generation of AM machine .....  | 48 |
| Figure 3.4 Developed MATLAB software output in first generation of AM machine .....   | 49 |
| Figure 3.5 The second generation of AM machine.....   | 50 |
| Figure 3.6 S shaped belt tensioner .....  | 56 |
| Figure 3.7 Industrial CMM Y(a)– Z (counter-balaced)(b) axes belt drive systems .....  | 56 |
| Figure 3.8 Lumped system model of belt-drive model.....   | 57 |
| Figure 3.9 Bottom part of the chassis without vibration dampers .....   | 63 |
| Figure 3.10 (a) Cleaned surfaces of bought aluminum components (b) Pre-assembled parts<br>after machining according to technical drawings ..... | 64 |
| Figure 3.11 Final schematic of the designed laser workstation .....   | 66 |
| Figure 3.12 Modal analysis results of the final version of the machine .....  | 67 |
| Figure 3.13 X axis sub-assembly modal analysis result .....   | 73 |
| Figure 3.14 Implementation of sensor for measuring paralelity, offset calculation (top) and<br>axes detection (bottom).....                     | 74 |
| Figure 3.15 Measurement points of the machine.....  | 74 |
| Figure 3.16 Top chassis modal analysis without bottom chassis.....  | 77 |
| Figure 3.17 Total chassis modal analysis .....  | 77 |
| Figure 3.18 Modal analysis of recommended chasis design.....  | 79 |
| Figure 4.1 Knife edge test setup for <i>CO2</i> laser .....   | 85 |
| Figure 4.2 (a) Knife-edge test result, (b) Hyperbolic profile of <i>CO2</i> laser beam propagation<br>.....                                     | 86 |
| Figure 4.3 Modules of the designed laser workstation .....  | 89 |
| Figure 4.4 The wiring of the developed electronic interface (a) Arduino Board (b)<br>Electrical Panel .....                                     | 90 |
| Figure 4.5 Pololu A4983 Step Motor Driver Wiring Schematic .....  | 91 |
| Figure 4.6 Scanning system field size and bit number relation .....   | 92 |
| Figure 4.7 A Schematic of the Scan Field .....  | 93 |
| Figure 4.8 Micro-vector Operation.....  | 93 |
| Figure 4.9 The wiring schematic of Arduino.....   | 95 |
| Figure 4.10 Actel FPGA Based Raylase IPG Interface Board .....  | 96 |
| Figure 4.11 Interface Pin and Module Relations of IPG YLP-1-120-50-50-HC Ytterbium<br>Fiber Laser .....   | 98 |

|   |     |
|---|-----|
| Figure 4.12 Laser Power Control Signals (a) Mode 0 – (CO <sub>2</sub> ), (b) Mode 1- (Ytterbium)  | 101 |
| Figure 4.13 Audible sound, acoustic emission, infrared and ultraviolet sensing feedback system .....  | 103 |
| Figure 4.14 Blackbody energy distribution (a) log scale (b) linear scale [23] .....   | 105 |
| Figure 4.15 A graybody and non-graybody energy distribution [23].....   | 106 |
| Figure 4.16 Developed Laser Feedback System Schematic (a) Final optical system (b) Designed Optical System.....   | 108 |
| Figure 4.17 Optic Triangulation Schematic.....  | 114 |
| Figure 4.18 System Design Overview v.2.0 .....  | 117 |
| Figure 4.19 Scanned free-form geometries of (a) cow sculpture and (b) air-wick.....   | 120 |
| Figure 4.20 ASCII STL geometry file.....  | 122 |
| Figure 4.21 The flowchart for plane triangle intersection algorithm.....  | 123 |
| Figure 4.22 Sliced geometry examples, Slice Thickness 3mm a) Hip Implant b) Tiger Figure c) Ataturk Mask (Multi contour example) d) Impeller (Flat start point example) [The Ataturk mask and impeller blade is created by HSB©2011]..... | 124 |
| Figure 4.23 Developed Laser Workstation Software GUI (a) 3D Geometry Panel (b) G-Code Panel .....   | 125 |
| Figure 4.24 The flowchart for ordering the line intersections into complete outlines.....   | 127 |
| Figure 4.25 The flowchart of raster-scanning to generate G-code for Module I or Module II .....   | 128 |
| Figure 4.26 The output of the selected algorithms for laser material processing .....   | 128 |
| Figure 4.27 The galvoscaner outputs without grid compensation (a) Pincushion Distortion (b) Pillow Distortion .....   | 130 |
| Figure 4.28 G-code file for the developed system.....   | 131 |
| Figure 5.1 G programming output of Open-Architecture Rapid Prototyping Machine V.1 (a) CIMCO Software Simulation (b) Manufactured scaffold example .....  | 138 |
| Figure 5.2 Test pattern for the Module I of the developed laser workstation.....  | 140 |
| Figure 5.3 Single track testing wells for depth 0.4 [mm] and 0.6 [mm].....  | 142 |
| Figure 5.4 Single scan track results with microscopic pictures 0.4 [mm] and 0.6 [mm] ..   | 143 |
| Figure 5.5 Example geometries, toolpath and manufactured parts.....   | 144 |
| Figure 5.6 Example geometries, toolpath and manufactured parts.....   | 145 |
| Figure 5.7 Vernier caliper measurements of the manufactured two-dimensional and three-dimensional parts .....   | 146 |



## **NOMENCLATURE**

|        |   |
|--------|---|
| STL:   | Stereolithography                                       |
| LASER: | Light Amplification of Stimulated Emission of Radiation |
| RP:    | Rapid Prototyping                                       |
| LL:    | Laser Lithography                                       |
| LOM:   | Laminated Object Manufacturing                          |
| SLS:   | Selective Laser Sintering                               |
| SAM:   | Subtractive-Additive Manufacturing                      |
| FDM:   | Fused Deposition Manufacturing                          |
| CAM:   | Computer Aided Manufacturing                            |
| CLSF:  | Cutter Location Source File                             |
| FEA:   | Finite Element Analysis                                 |
| LBM:   | Laser Beam Machining                                    |
| AC:    | Alternative Current                                     |
| FPGA:  | Field Programmable Gate Array                           |
| SFF:   | Solid Free-form fabrication                             |
| CNC:   | Computer Numeric Control                                |
| CW:    | Continuous Wave   |
| TEM:   | Transverse Electromagnetic Mode                         |
| MO:    | Master Oscillator                                       |
| PRR:   | Pulsed Repetition Rate                                  |
| BS:    | Booster   |

## 1. Introduction

### 1.1 Motivation of this study

Manufacturing brings key thoughts and ideas into being. In this project, one of the most complex manufacturing tools, laser light, is used to cut, machine or combine materials to any desired two-dimensional or three-dimensional shape. This technology could be considered for use in cost efficient, fast and local in manufacturing of medical devices such as heart pump impellers; complex shaped hip implants for patients or in manufacturing of micro devices such as MEMS based biosensors, light scanners for advanced technology developments.

Due to the physical characteristic of the mentioned manufacturing technologies, functional products can be manufactured without any post-processing methods. Unfortunately, there is no laser workstation developed and manufactured in Turkey which has such developed software (capable of processing all types of STL geometries without defects) or versatile construction. Therefore, the intention with such and following efforts is to create a know-how and capacity for our industry.

### 1.2 Dissertation Outline

*Chapter 2* digs into the physics of the target manufacturing technologies. Thereafter, an analytical model is written in MATLAB with the details of intended goals, objectives and potential pay-offs.

*Chapter 3* details the design of the subtractive-additive manufacturing (SAM) laser workstation built for polymer sintering and engineering materials cutting, marking, and machining. In addition to the former studies at the Koç University Manufacturing and Automation Research Center, the current contributions and different design studies are given with one detailed analysis result.

*Chapter 4* focuses on the optical, electronic and software parts which comprise the workstation. In order to develop the open-architecture scheme, the current device properties, which are used in processing, are identified from the datasheets and applied tests. Elaborate hardware explanations are given in order to ease future progress in the study. Every controllable parameter and how to control them are explained. In addition, geometrical aspects, which includes importing (by 3D scan or STL, slicing, toolpath generation etc.) of the software is added for understanding of reader.

*Chapter 5* concentrates on the technological demonstration of the developed software and hardware. Through the developed G-code parsing algorithm scaffold meshed structures are built. For laser cutting, some two-dimensional geometry is cut and the kinematic errors are understood by examining these test geometries. Single line track sintering tests are completed in order to understand the warping, sintering with different laser powers or scan speeds for different polymeric materials. Finally a few primitive and complex shaped geometries are tried to manufacture and their errors are discussed.

The references are given at the end of each chapter, after the recommendations related to the presented chapter. Hopefully, these endeavors are for something which will be developed further for future of our industry.

## 2. General Review of Laser Materials Processing

### 2.1 Introduction

In 1900, quanta theory was named by Planck and in 1920, it was admitted distinctly from the wavelike characteristics of light it also shows particle nature while interacting with matter and exchanges energy in the form of photons[1]. The theory of stimulated emission was laid by Einstein in 1917[2], and this theory was put into application 50 years later in 1957 by Townes and Schawlow with a ruby laser at Bell Labs. [3] At the end of 1950's, a graduate student of Columbia University, Gordon Gould, was also looking into the conditions required for stimulated emission at visible wavelengths and patented his applications [4].

LASER is an acronym which stands for "light amplification of stimulated emission of radiation," denoting a coherent and amplified beam of electro-magnetic radiation. The key element in making a practical laser is the light amplification achieved by stimulated emission due to the incident photons of high energy. Three principal components are required: the lasing medium, means for exciting the lasing medium into its amplified state (lasing energy source), and an optical delivery/feedback system. Additional provisions could be added into the system such as beam guidance, cooling systems and the target manipulation etc. The laser medium may be solid, liquid or gas. Laser light differs from ordinary light because it has all of its photons have the same frequency, wavelength and phase. In addition, unlike ordinary light; laser beams are highly directional, have high power density, and have better focusing characteristics. These unique characteristics of laser beams are useful in the processing of materials. Among different type of lasers, *Ytterbium fiber* and  $CO_2$  [Carbondioxide] are the ones most widely used for laser beam machining applications and therefore, these are selected for the our machine design.  $CO_2$  lasers have wavelength of  $10 \mu m$  in the far infrared region. It has high average beam power, good efficiency and beam quality. It is suitable for fine cutting of sheet metal at high speeds. *Ytterbium fiber* lasers have low average beam power; but when operating in

pulsed mode, high peak power enables them to machine even thicker materials. In our design, the selected laser's pulse mode is Q-Switched between 20-200 kHz [5]. The machining of thinner materials would be possible with shorter pulse duration. This shorter wavelength of the *Ytterbium fiber laser*, 1064 nm, allows the processing of reflective materials which are difficult to machine by  $CO_2$  lasers. On the other hand, it is also limited in comparison to other shorter wavelengths than *Ytterbium fiber*.

The processing mechanism of material removal in LBM comprises melting, vaporization, and degradation (chemical bonds are broken and the material is degraded). As stated before, when the laser beam is focused on the workpiece, thermal energy is absorbed by the workpiece, which changes its state into molten and vaporized so that the material can be removed by flow of pressurized air. Thermal machining is affected by following material properties: Favorable materials for laser processing have common properties such as low thermal diffusivity and conductivity, and high degree of brittleness or hardness (i.e. Ti6Al4V, Inconel etc.). The advantages of laser machining with respect to conventional machining are the lack of tool wear, machine vibration (w/ galvoscaner) and material damage. In addition to that, there is no maximum tool force, build up edge formation or tool chatter. The major laser machining configurations in this thesis covers drilling (1D), cutting (2D) and machining (3D). The processes are given in following sections. In this section, the process details by means of analytical models are given in order to understand the workstation system clearly.

In this work, first, a short literature study is given in order to understand the processes by using mathematical models. The mathematical model gives the temperature distribution, roughly predicted by an analytical solution strategy, on the workpiece during laser material interactions. The mentioned processes are given according to the capabilities of the Laser Workstation. The modeling efforts provide qualitative insight to the process of interest and give quantitative system-specific information. While numerical heat transfer solutions are often tedious to develop and computationally intensive, there isn't any general solution which can be easily employed by other researchers. However, development of an analytical

solution or application of an existing analytical solution for predicting the temperature distribution in the workpiece would provide a good starting point for parameter estimation for laser material processing applications. For example, Rosenthal [5] provides a mathematical solution to a point-like moving heat source, which is used to give information regarding to the temperature distribution for the heat affected zone during a welding operation; the model is frequently used for benchmarking with new thermal models of the welding process. Rosenthal's model is specifically used for welding since the mathematical equations of this physical scenario are well represented especially for this process.

In the following paragraphs, analytical heat transfer solutions which have applicability to laser material processing will be reviewed. These models are generally analytic instead of being finite element, difference volume or boundary problems. Therefore, in the literature review part of the modeling effort, other approaches than finite element solutions are employed. In the former research and during this thesis, several simplifications and assumptions are made about the material properties and geometry of the system.

At the first look, the challenge of modeling is unsurpassable. In addition, some phenomena, such as free surface deformation, are shrouded under plasma during the process and are difficult to measure for model validation. Therefore, some researchers approach this modeling effort saying "why bother;" while others say "why not" and plunge in with curiosity regardless of direction. On the other hand, an intelligent application of boundary conditions can make the mathematical challenge more amenable, and the availability of fast computer power has made modeling of many complicated processes possible in recent times. There are even software packages, such as ANSYS, SIMPLE, ABAQUS, FLUENT, SOLA, FIDAP etc., which simplify the coding and modeling of the processes, so that even the uninitiated can have a go.

## **2.2 An Overview for Laser Material Processing Methods**

The reasons for investigating the laser material processing by using mathematical models are simple. First of all, the heat and the fluid flow that occur during laser processing

influence the microstructures (through grain structure and phases that are formed), residual stresses (through the thermal stresses that result from differential strains), and distortions that evolve during the process. Secondly, these in turn affect the mechanical properties of the final product and thus the quality of the process. In addition to these, due to the following general reasons such as a semi-quantitative understanding of the process mechanisms for the design of experiments and displaying results (dimensional analysis, order of magnitude); and parametric understanding for control purposes (empirical and statistical processing diagrams), a system model is needed for laser material interactions. However, because of the versatility of the developed laser workstation, the literature survey is covered for the processes such as Laser-induced Rapid Prototyping, Laser Machining [LM], Laser Marking [LM], Laser Cutting [LC].

Among the common and mature RP processes, those based on the use of a laser for materials processing are the Stereolithography (SL) process, the Laminated Object Manufacturing (LOM), the Selective Laser Sintering (SLS) and SLS-like processes. The basic building-block mechanisms of the SL and SLS processes, which are the most important laser-induced RP processes, are presented in literature widely [6, 7].

The Laser Lithography process creates three-dimensional parts by selectively solidifying polymeric materials layer-by-layer upon exposure to UV radiation or laser beams. It is still the most accurate RP process in terms of dimensional accuracy and capability in creating small, fine features [8] in industrial level. On the other hand, the selective laser sintering (SLS) process was developed at the University of Austin by Beaman and Deckard. In the SLS process, a layer of powder is deposited on a support and leveled by the combination of cylinders and sweep mechanism as shown in Fig. 2.1. Similar, to LL process, a laser beam scans a two-dimensional pattern on the deposited powder to sinter a powder layer. After sintering of a layer, a new layer of powder is deposited in the same manner. This is one type of consolidation mechanism for powder fusion mechanism, along with selective laser melting (SLM) and selective laser cladding (SLC). As the word implies this powder fusion mechanism occurs when the powder materials are fused in their solid state at elevated

temperatures. The advantage of SLS is that it requires only a low power laser. In addition to that, there is a possibility to get more accurate than LL based system by using Selective Micro Sintering [9] at the research level (used currently in the industry with low production rates). However, since the powder is not totally melted during laser scanning, the SLS-processed parts are not fully dense and hence, have relatively low strength compared to SLM and SLC manufactured parts. In order to overcome these disadvantages of traditional SLS, SLM and SLC processes have been developed that enable full melting of powder or post processing (i.e. Hot Isostatic Pressing etc.) is added into the SLS manufacturing process. Fundamentally, the SLM process is the same as SLS except for the much higher laser energy density used. There are many ways in which liquid phase sintering (LPS) can be utilized as a fusion mechanism in additive manufacturing processes. For purposes of clarity, the classification proposed by Kruth et al. has formed the basis for the distinctions discussed in [10]. The powder bed is fully or partially melted directly to form metallic bonding [11]. This might occur also for polymers between one half of the absolute melting temperature and the melting temperature [12, 13]; for other materials, for instance, metals, there are other practical useful approaches the reader may see [14]. After patenting the system [15] in 1988 and building the conceptual structure, Sun et al. present a one dimensional model of the LS process which considers the sintering of a single layer in 1990 [16]. The beam energy is modeled as a moving square flux, convective heat loss at the powder surface is not considered and temperature independent material properties are assumed in the solution of this heat transfer problem. Nelson et al. 1993 [17], Childs et al. 1994 [18], Weissman and Hsu 1991 [19], Williams and Deckard 1998 [20], Cervera and Lombera 1999 [21], Tontowi and Childs 2001[22] are other important LS models in the literature.



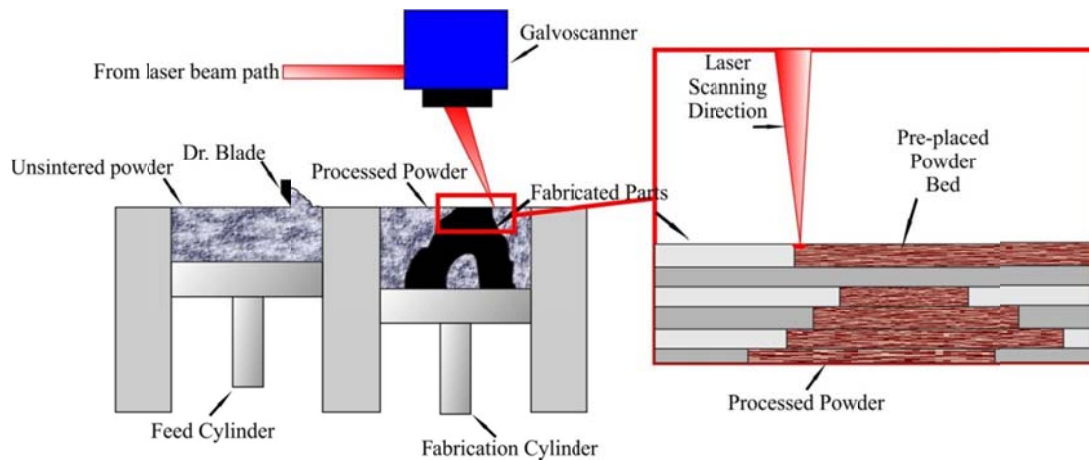


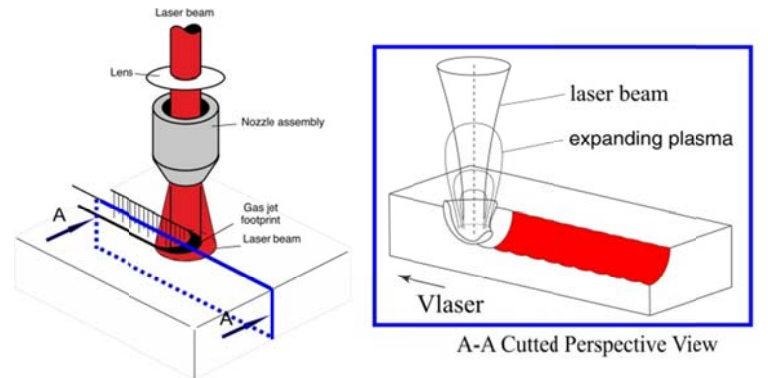
Figure 2.1 Schematic of Selective Laser Sintering Process

Thermal laser machining is referred in this thesis as laser machining for convenience. Marking and drilling techniques are included in laser machining, based on both thermal and athermal modes of processing. Athermal mechanisms, which are out of the topic of this thesis, involve breaking chemical bonds using ultraviolet or short pulsed laser beams, and were described in [23]. Laser machining given in Fig. 2.2., where the objective is to remove material as quickly as possible, within specified dimensional tolerances and with minimal negative effect on parent material; is based on conventional mechanisms of laser beam heating, including melting and vaporization.

The process competes with conventional methods of mechanical and thermal machining, capable of operating with tolerances on the order of micrometers. Procedures and performance data, provided for a range of engineering materials, are given in Table 2.1. For example, the first industrial application of thermal laser drilling (and of laser material processing) involved punching holes in a diamond for wire-drawing dies.

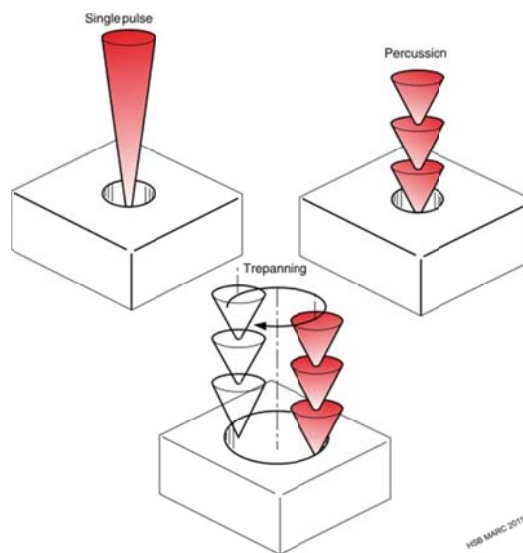
Laser machining processes dominate when the interaction time of the laser beam with the material is on the order of microseconds, and the power density is sufficient to initiate melting or vaporization. The melt fusion mechanism is similar to that used in cutting, in which material is expelled by the kinetic energy of a process gas, which may be inert or

active, delivered coaxially or at an angle to the beam. A relatively rough surface is produced with material removal rates on the order of a few cubic millimeters per minute.



HSB MARC 2011 (c)

(a)



HSB MARC 2011(d)

(b)

Figure 2.2 Laser Beam Machining Schematics, a) Laser Cutting b) Laser Drilling

With the controlled oxidation mechanism, material is melted and reacts with oxygen to form a brittle oxide, which breaks away. Material removal rates up to  $100 \text{ m}^3/\text{min}$  are then possible [24]. Engraving can be performed by increasing the power density to about  $10^6 \text{ W}/\text{mm}^2$ , causing material to be removed principally by vaporization (i.e. ablation).

The other laser machining application is drilling, which is a continuation of scribing and the beam is normally stationary with respect to the workpiece. The aim is to produce a cavity with a very high aspect ratio. The beam heats the material to the vaporization temperature, after which it penetrates to form a cavity, in a similar manner to keyhole welding. The pressure induced by vaporized material, together with any assist gas, forces molten material at the cavity wall to its outer rim where it is expelled. Radiation becomes trapped in the keyhole, inducing plasma formation. A portion of the energy may then be absorbed by the plasma and reradiated to the cavity wall, increasing the process efficiency; however, plasma formation has to be limited through careful control of an assist gas. Holes can be formed by three practical techniques: direct drilling (roughest), multi-pulse percussion drilling (for tighter tolerances) and trepanning (for larger holes).

The aforementioned process methods mainly depend on the material to be worked up and laser wavelength to be used. Generally speaking, there is a close relation between the selected laser beam wavelength and material to be processed. The laser beam wavelength is chosen to match the absorptive characteristics of the material, i.e. short wavelength light is used to machine metals, alloys and some ceramics, whereas organic materials absorb relatively long wavelength far infrared light sufficiently for efficient machining. Materials with high values of specific heat capacity require larger amounts of energy to raise their temperature to that required for melting. Similarly, materials with high latent heats of melting and vaporization require more energy for the changes in state relevant to the processing mechanism. The material-laser wavelength correlation is given in Table 2.4-2.5.[25].

### **2.3 Analytical Thermal Modeling of Laser Material Processing**

Analytical process modeling is applied to illustrate the effects of changes in processing variables on performance, and to enable practical processing parameters to be selected as mentioned before. All the processes have used some parts of analytical model solutions from the literature in the beginning part of the research and these models could be used like

Table 2-1 Sources of data for metals, ceramics, glasses, polymers and composites

| <b>Material</b>    | <b>Laser</b>                                | <b>Reference</b>                 |
|--------------------|---|----------------------------------|
| Fe, Ti             | Cu-vapor                                    | (Lash et al, 1993, [26])         |
| C-Mn Steel         | $CO_2$                                      | (O'Neill et al. 1995, [27])      |
| C-Mn Steel         | Cu vapor                                    | (Chang, et al., 1996, [28])      |
| Co-based Hayes 188 | Cu vapor                                    | (Knowles et al., 1995, [29])     |
| Cu                 | Nd:YAG ( $\lambda/2, \lambda/3$ Q-switched) | (Tunna et al., 2001, [30])       |
| Ni on ceramic      | Cu vapor                                    | (Knowles, 2000, [31])            |
| Nimonic            | Nd:YAG                                      | (Kamalu et al. 2002, [32])       |
| Various            | Cu vapor                                    | (Chang, et al. 1998, [33, 34])   |
| Alumina            | $CO_2$                                      | (Olson, et al. 1992, [35])       |
| Ceramics           | Nd:YAG                                      | (Pffeferkorn et al., 2003, [36]) |
| Cordierite         | Nd:YAG                                      | (Kirby et al., 1998, [37])       |
| Diamond            | Cu vapor                                    | (Barnes, 2001, [38])             |
|                    | Nd:YAG                                      | (Miyazawa et al., 1994, [39])    |
|                    | Ruby  | (Anon., 1966, [40])              |
| Diamond(CVD)       | Nd:YLF                                      | (Shaeffer, 1995, [41])           |
| Eng. Ceramics      | Nd:YAG                                      | (Harryson, et al., 1987, [42])   |
| Glass              | Nd:YAG ( $\lambda/4$ ), $CO_2$ (Q-switched) | (Schaeffer et al., 2002, [43])   |
|                    | Various                                     | (Atanasov, et al., 1987, [44])   |

Table 2-2 Sources of data for metals, ceramics, glasses, polymers and composites

| Material       | Laser                                      | Reference                      |
|----------------|--|--------------------------------|
| Rocks          | COIL                                       | (Hallada, et al., 2000, [45])  |
| Sandstone      | HF   | (Graves, et al., 1998, [46])   |
| $Si_3N_4$      | $CO_2$                                     | (Bang et al., 1993, [47])      |
| $Si_3N_4$      | Nd:YAG                                     | (Rozzi et al., 2000, [48])     |
| $Si_3N_4, SiC$ | $CO_2$                                     | (Kitagawa, et al, 1990, [49])  |
| Paint          | $CO_2(TEA)$                                | (Cottam et al., 1998, [50])    |
| PMMA           | $CO_2$                                     | (Berrie, et. al, 1980,[51])    |
| Polymers       | $CO_2$ (Q-switched), Nd:YAG<br>$\lambda/3$ | (Schaeffer, et al, 2002, [52]) |

modules if needed. Some of the important models are listed in Table 2.2 without giving their equations.

However, before using one of these, understanding the correct assumptions are critical such as the homogeneity and isotropicity of the materials, conduction dominated heat flow, energy-free the material transformation, thermally independent material properties etc.

Before starting into more details, one important mathematical aspect should be considered: the dimensional analysis of heat flow or any other physical problem implies a total knowledge of all the variables involved, but no knowledge of how they are related. For any equation describing a physical relationship, we know that the units must balance and that therefore there is a restriction on the number of ways the variables can be related. The way to take advantage of this is to arrange for the variables to be grouped as dimensionless groups, in which case the units will automatically balance and we are left with a reduced number of variables – the groups. Once that has been done, then some experiments must be performed to show how the groups are related. For instance, the Buckingham  $\Pi$  Theorem tells us how many groups to expect: the number of independent groups,  $n = i - r$ , where  $i$  is the number of variables, and  $r$  is the greatest number of these

which will not form a dimensionless group (usually the same as the number of basic dimensions, except where there is an unusual symmetry). The usual dimensionless groups involved in heat transfer problems are: Fourier Number [Form of dimensionless time]; Andrew Number [A measure of the energy deposited per unit area over the surface of material by moving energy source][61]; Péclet Number [Form of dimensionless velocity (ratio of convection to conduction)]; Reynolds Number [Another form of dimensionless velocity (ratio of viscous to inertial forces)]; Weber Number [Ratio of internal forces to surface tension forces]; Dimensionless Temperature; Dimensionless Power, Dimensionless Distance etc. Some other parameters are given in the nomenclature of this thesis. In the following equations, these variables are used as they are needed.

Table 2-3 Analytical equations for the temperature fields around a surface energy source

| Type        | Shape       | Energy Distribution | Source  |
|-------------|-------------|---------------------|---|
| Stationary  | Area $A_B$  | Uniform             | Carslaw et al., 1959 [53]   |
| Stationary  | Square      | Uniform             | Carslaw et al., 1959 [53]   |
| Stationary  | Circular    | Uniform             | Bass, 1983[54]  |
| Stationary  | Rectangular | Uniform             | Bass, 1983[54]  |
| Stationary  | Circular    | Gaussian            | Ready, 1971, [55]   |
| Moving      | Point       | -                   | Ready, 1971[55];<br>Rosenthal 1941&1946<br>[56, 57]; Ashby &<br>Easterling, 1982 [58] |
| Fast moving | Circular    | Gaussian            | Rykalin et al., 1978[59]  |
| Moving      | Circular    | Gaussian            | Ashby & Easterling,<br>1984[60]   |

To find the appropriate power rating to use in the analytical model; there exists a well-known relationship among laser peak power, average laser power, repetition rate, and pulse width, which can be expressed as follows in case of a pulsed laser usage [62]:

$$\text{Peak Power [kW]} = \frac{\text{Average power [W]} \times 1000}{\text{Repetition Rate [kHz]} \times \text{Pulse Width [ns]}} \quad [2.1]$$

$$\text{Energy per Pulse [mJ]} = \frac{\text{Average Power [W]}}{\text{Repetition Rate [kHz]}} \quad [2.2]$$

The pulse width, the laser peak power and energy per pulse are used in these equations. An increment on these parameters is caused by an increment in the average laser power and/or a decrement on the repetition rate. After laser irradiating, the absorbed laser energy heats up a volume of the target material, which is transformed into liquid and/or vapor phase, and then this material removed [63].

The following table gives the measured absorbance using *Ytterbium fiber* and *CO<sub>2</sub>* lasers for different materials. Thus, in the analytical model the following list might be used in order to do a rough estimation of the initial process condition [25].

As a rule of thumb, the reflectivity of a material is the most dependent on its electrical conductivity. A metal with high electrical conductivity has the highest reflectivity; for example, copper. Hence a high energy density is required to process a material like copper. A material with high thermal diffusivity will normally allow a greater depth of processing penetration with no thermal shock or cracking. In addition to that, materials in powder form exhibit higher absorbance than their bulk form [64].

Table 2-4 Absorbance of elemental and compound powders, Ytterbium ( $\lambda=1.06 \mu\text{m}$ ) and  $\text{CO}_2(\lambda=10.6 \mu\text{m})$

| Material                           | Absorbance                 |                            |
|------------------------------------|----------------------------|----------------------------|
|                                    | $\lambda=1.06 \mu\text{m}$ | $\lambda=10.6 \mu\text{m}$ |
| Cu                                 | 0.59                       | 0.26                       |
| Fe                                 | 0.64                       | 0.45                       |
| Sn                                 | 0.66                       | 0.23                       |
| Ti                                 | 0.77                       | 0.59                       |
| Pb                                 | 0.79                       |                            |
| Co-Alloy (1%C; 28% Cr; 4%)         | 0.58                       | 0.25                       |
| Cu-Alloy (10% Al)                  | 0.63                       | 0.32                       |
| Ni-Alloy I (13%Cr; 3%B;4%Si;0.6%C) | 0.64                       | 0.42                       |
| Ni-Alloy II(15%Cr; 3.1%Si; 0.8%C)  | 0.72                       | 0.51                       |
|                                    |                            |                            |
| ZnO                                | 0.02                       | 0.94                       |
| $\text{Al}_2\text{O}_3$            | 0.03                       | 0.96                       |
| $\text{SiO}_2$                     | 0.04                       | 0.96                       |
| BaO                                | 0.04                       | 0.92                       |
| SnO                                | 0.05                       | 0.95                       |
| CuO                                | 0.11                       | 0.76                       |
| SiC                                | 0.78                       | 0.66                       |
| $\text{Cr}_3\text{C}_2$            | 0.81                       | 0.7                        |



Table 2-5 Absorbance of elemental and compound powders, Ytterbium ( $\lambda=1.06 \mu\text{m}$ ) and  $\text{CO}_2$  ( $\lambda=10.6 \mu\text{m}$ )

| Material                     |                            |                            |
|------------------------------|----------------------------|----------------------------|
|                              | $\lambda=1.06 \mu\text{m}$ | $\lambda=10.6 \mu\text{m}$ |
| TiC                          | 0.82                       | 0.46                       |
| WC                           | 0.82                       | 0.48                       |
| $\text{NaNO}_3$              | 0.16                       | 0.8                        |
| NaCl                         | 0.17                       | 0.6                        |
| Polytetrafluoroethylene      | 0.05                       | 0.73                       |
| Polymethylacrylate           | 0.06                       | 0.75                       |
| Epoxypolyether-based polymer | 0.09                       | 0.94                       |

#### 2.4 The Temperature Distribution

In many forms of laser technology, the coherent light from the laser forms a spot that can be a concentrated source of heat or, in laser surface treatment, for example, a rather more diffused region of heating. Some of techniques used in the simpler mathematical models that first found use in welding problems in fact prove to be of considerable value in more general context. In particular, the point and line source solutions associated in the context of welding with Rosenthal as stated before [56, 57], but also very well described from a rather different point of view by Carslaw and Jaeger [53], have proved to be extremely useful. They will be derived first, before considering specific applications, after which they will be used to obtain simple descriptions of the temperature in a workpiece. Since then Carslaw and Jaeger's study has taken more than 18351 citations in the literature until June 2011 which also proves its reliability by over 300 citations per year.

From these elementary solutions, it is possible to build up more complex solutions to describe different incident intensity distributions at the surface of the workpiece. They can be extended to cover time-dependent situations. The line solution can be applied to a plate of finite thickness as well as an infinite or semi-infinite workpiece. The point solution in its

basic form only applies to an infinite or semi-infinite workpiece, but it can be extended very simply to cover other cases, such as a plate of finite thickness, for example.

In various ways it is therefore possible to solve more complicated problems in terms of these simple analytical solutions, an approach that can lead to better understanding before resorting to more complicated computational methods.

Whatever approach is used to calculate the power of the incident radiation and the energy transfer mechanism, the result is a prediction for the temperature distribution in the workpiece. This result can then be used as the basis for further calculation to obtain such quantities as

- the thermal history of individual points in the workpiece;
- metallurgical properties deduced from the thermal histories;
- more accurate solutions for the temperature distribution, using the scheme, which might be analytical or, more usually numerical;
- the consequences of varying the absorption models in order to test their validity and reliability;
- the distribution of thermal stress on the workpiece;
- the deformation of the workpiece resulting from thermal stress

The developed MATLAB model discussed in this thesis calculates the temperature profile (temp structure) in a semi-infinite solid, induced by a moving heat source-i.e. induced by absorbed laser energy. That is, the temperature rise is calculated in a homogenous solid (so no melting, nor vaporization) of infinite thickness, with constant material properties. Solution of classical heat conduction problems were presented by Carslaw and Jaeger as mentioned before [53], but the implementation of most functions of the proposed MATLAB code were based on the solutions derived in a more recent book on thermal modeling of laser material processing by Dowden [65], including point heat source and line heat source solutions. The derivations are given in the - Appendix 2.1 Derivation of the Analytical Model-. For more complex analytical model, the MATLAB Laser Toolbox would be useful [66]. The developed MATLAB code is given in Appendix 2.2.

As a rule of thumb, the following approaches might be useful in their application to the following models. As if the application is a thick plate with a moving heat source, this might be the case, for example, in conduction mode welding. If the workpiece is considered to be a thin plate and the line heat source penetrates through the thickness and involves 2D heat flow, this would be example for keyhole welding or laser cutting. The concepts of these analytical solutions might be used in these manners.

#### **2.4 Material Characterizations for Laser Material Processing**

The principal mechanical and thermal properties of engineering materials are described below. Material Properties play a dominant role in determining the interaction between the laser beam and engineering materials, dictating the processing mechanisms. Many material properties change with temperature; although this would at first sight appear to present problems in modeling, it is an interesting phenomenon that could be exploited in novel laser treatments. These values are also valuable in order to simulate the system properly by using the committed analytical model.

These parameters are determined experimentally material by material. Following analysis are generally used for that purpose. Unfortunately, in this thesis, none of them are used but in future these are highly recommended. These experiments cover, relevant material properties for polymers, metals and ceramics are able to be determined using the characterization techniques listed in Table 2.6. In case of SLS, the particle size distributions of the as-received powders will be used directly after getting diameter distribution of powders.

Table 2-6 Material Characterization Techniques

| Characterization technique for materials   | Properties determined   |
|--|---|
| Differential Scanning Calorimetry(DSC)     | Glass transition temperature, melting temperature, enthalpy of melting, recrystallization temperature |
| Thermogravimetric Analysis(TGA)            | Degradation temperature   |
| Scanning Electron Microscopy               | Qualitative characterization of powder size and shape   |
| Small amplitude oscillatory shear rheology | Storage and loss moduli as a function of frequency and temperature                                    |
| Powder packing analysis                    | Tap density, pour density   |
| Powder Reflection Measurement              | Estimation Reflection/ Absorption coef.,  |

### 2.4.1 Absorption Coefficient

The attenuation of an incident beam width depth in a material is a property named absorption coefficient. If the transmittance of the substances is neglected, this would be experimentally determined by using an experimental setup as demonstrated in Fig. 2.3. [69].

For the materials which has opaque characteristics ( $a = 1 - R$ ) is valid [70].

Theoretically, for a beam of incident energy  $E_0$ , the transmitted energy,  $E$ , at a depth  $z$ , is given by Beer-Lambert law  $E = E_0 e^{-az}$ .

$a$  is the absorption coefficient (i.e. for metals the absorption coefficient is around  $5 \times 10^5 \text{ cm}^{-1}$  for metals in the visible spectrum). Incident radiation takes place in a very shallow region with a fraction of the wavelength. Absorption is also the first direct effective material property which can be seen in the given analytical model.

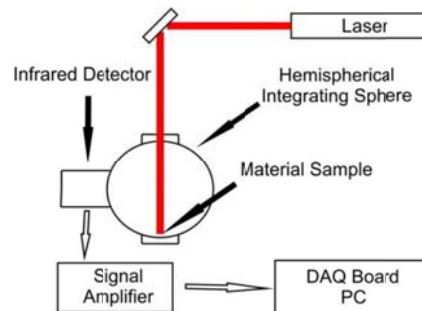


Figure 2.3 Integrated Sphere Reflectometer – experimental setup [69]

Laser light impinging on the surface of a material may be absorbed, reflected, transmitted or re-radiated. On the macroscopic scale, absorptivity is a measure of the fraction of incident radiation absorbed. As the absorption coefficient indicates, radiation is absorbed by electrons in the upper  $10^{-6}$  to  $10^{-5}$  cm of the surface the electromagnetic skin depth. The absorption mechanism is known as the inverse Bremsstrahlung (braking radiation) effect, which means energy is subsequently transferred into the material by a mechanism that depends on the energy of the photons of that material. The classical thermal conduction through collision with lattice defects and other electrons is the dominant heat transfer mechanism because the photon energy of material processing lasers that emit with a wavelength that lies above ultra violet region of the electromagnetic spectrum, in the literature these and other properties are included [71-75]. As the interaction time approaches that of the mean free time of electrons ( $10^{-13}$  s in a conductor), classical thermal conduction laws are no longer valid and athermal processing mechanisms, associated with rapid picosecond ( $10^{-12}$  s) and femtosecond ( $10^{-15}$  s) pulses apply. The absorptivity versus wavelength for Ag and Fe is shown schematically in Fig. 2.4. The angle of incident is also important factor for absorption of laser light. For vertical condition ( $\theta = 0$ ), the beam oriented parallel to the incidence, the absorption of  $R_p$  increases and  $R_s$  decreases. In Brewster angle, the absorption of  $R_p$  reaches a maximum value and  $R_s$  drops to zero (Brewster effect).

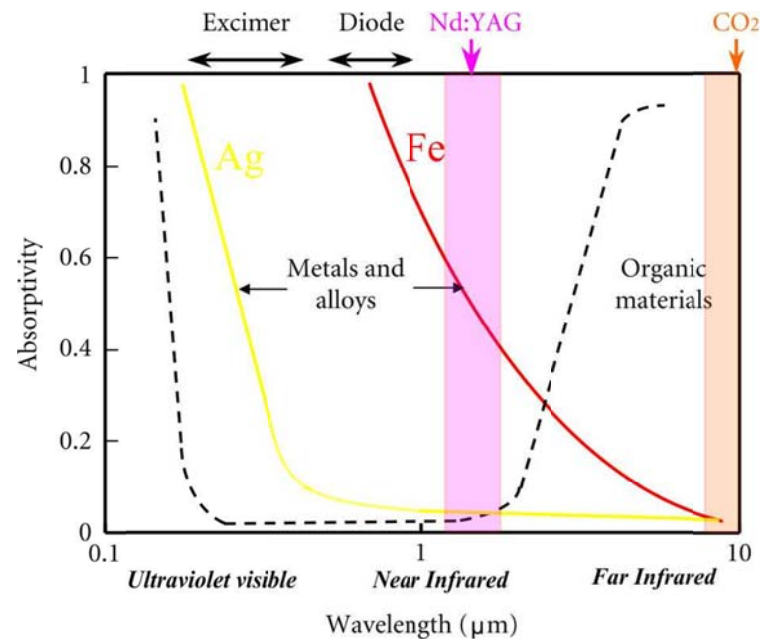


Figure 2.4 Wavelength – Absorptivity relation for metals, alloys and organic materials

Depending on its optical properties and modifications to the surface, as the temperature of a material changes, the absorptivity can increase or decrease (e.g. due to oxidation reactions or phase transformations). Absorptivity also varies with surface roughness. Therefore, a rough surface presents a greater surface area to the laser beam, and causes light to be reflected several times, thereby increasing the total absorptivity. In the process development part of this study, the surface roughness is also taken into account before experimenting. In addition to that, as formerly state, in the analytical model these variations are neglected.

#### 2.4.2. Specific Heat Capacity

The energy required to raise its temperature by one Celsius degree at constant pressure is named the specific heat of a material. The units of specific heat capacity is [ $Jkg^{-1}K^{-1}$ ] or as a volumetric quantity as [ $Jm^{-3}K^{-1}$ ]. The volumetric specific heat capacity for homogenous materials at room temperature is about  $3 \times 10^{-6} Jm^{-3}K^{-1}$ . The heat capacity of metals and alloys increases with temperature until it reaches a limiting value

around  $25 \text{ Jmol}^{-1}\text{K}^{-1}$ . The heat capacity increases with temperature to about  $1000 \text{ }^\circ\text{C}$  for ceramics and glasses, above this temperature remains approximately constant. On the other hand, in polymers the heat capacity increases steadily up to the glass transition temperature.

### 2.4.3. Thermal Conductivity

Thermal conductivity is the parameter which heat flows through material and it is crucial esp. in steady state thermal processes. It is proportional to the amount of energy present (the volumetric heat capacity), the number and velocity of energy carriers (electrons and phonons) and the amount of energy dissipation the amount of scattering of the attenuation distance of lattice waves, i.e., the mean free path. When the temperature rises, the amount of energy dissipated increases by collisions, and naturally the thermal conductivity decreases. Oppositely, the carriers in ceramics and glasses are phonons, which can be thought as lattice vibrations that occur on discrete energy levels or quanta. Electrons are restrained in ionic and covalent bonds, and so cannot participate in thermal conduction at low temperatures. Thermal conductivity is highest in materials that have an orderly structure comprising single element or elements of similar atomic weight because the strong periodic bonds transfer lattice waves efficiently. Structurally two dimensional layered materials have high the thermal conductivity in the direction of bonding; however in the perpendicular direction the van der Waals forces attenuate vibrations, which decrease conductivity. As mentioned before, in ceramics the thermal conductivity is decreases as temperature increases due to the inverse proportion of the mean free path with temperature. The amorph-structure of the glasses has a relatively short mean free path which does not change significantly with temperature. However, the thermal conductivity is also increase with the temperature because of its increment in the heat capacity. The thermal conductivity of the polymers is low with compare to the other materials. The reason behind it is generally the electrons are bounded covalently, molecular sizes are large and the crystallinity is low.

#### 2.4.4. Density

Density is commonly known material property shows the mass quantity in a unit volume. Therefore close packing of atoms results in high density and a high melting temperature. This is generally true for accounts for high values in metals and alloys, and low values in polymers.

#### 2.4.5 Thermal Diffusivity

Thermal diffusivity  $\kappa$  [ $m^2/s$ ] is the ratio of the energy transmitted by conduction to the energy stored in unit volume material. Thermal diffusivity is also referred as the diffusion coefficient of heat and determines how rapidly material will accept and conduct thermal energy. It is very important for characterization of transient thermal processing.

$$\kappa = \frac{\lambda}{\rho c_p} \quad [2.3]$$

Especially in pulsed laser treatment or moving heat source analysis this parameter is crucial. It determines the penetration depth of the material. It is also important for laser heating processes. As a rule of thumb the relation between penetration depth, heating time and thermal diffusivity Eq. 2.25 is valid.

$$z = \sqrt{4\kappa t} \quad [2.4]$$

The diffusivity of alloys is generally lower than of the pure metal in the alloy; stainless steel is particularly low in comparison with plain carbon steels.

#### 2.4.5. Coefficient of Thermal Expansion

The ratio of The change in length,  $\Delta l$ , and in temperature,  $\Delta T$ , with respect to length (at known temperature) is clarified as the coefficient of thermal expansion,  $\alpha$ , and given as,

$$\alpha = \Delta l / l_0 \Delta T.$$

The thermal expansion coefficient is mainly controlled by atomic and molecular vibration; as the temperature increases, the amplitude of vibration increases.

In metals and alloys, which have close-packed structures, the increment in atomic vibrations is accumulated in neighboring atoms, producing relatively high expansion in the lattice.



The predominantly ionic bonded ceramics has also high values of thermal expansion due to this close-packed structure. The structures which contain spaces such as in covalently bonded ones the thermal expansions are reducing because of the absorption of vibrations.

The thermal history, structure and composition are the most important control parameters for thermal expansion of glasses. However, thermal shock, which generally occurs in glasses, can be notified by proper heat treatment of the glasses. Isotropy and anisotropy is another important characteristic of materials while investigating the thermal expansion. Anisotropic materials have different expansivity along different axes.

The heating may stretch (depends on their types) extensively polymers and elastomers before failing.

#### **2.4.6. Transformation Temperatures**

Heating, melting and vaporization are three important dependences of laser material processing principles. These transformations state the phases such as solid, liquid and vapor. In literature, for the most important phase transformations, some empirical formulae are derived. Sodium potassium like alkali metals are bonded with low energy electrons, which result in weak bonding. Therefore have low strength and melting temperatures. Chromium, tungsten and iron like transition metals are bonded by inner electron, and exhibit high strength and melting temperature. The covalent bonding type in glasses (esp. silica) gives them high strength, stability and softening temperature. A softening or melting temperature,  $T_m$ , would be identified in polymers that contain a high degree of crystallinity. This is becomes with an increase in energy named as latent heat of melting. As the temperature is raised there is a continuous increment in the heat capacity for amorphous polymers, until the glass transition temperature,  $T_g$ , in which the rate of energy absorption increases without any discontinuity[76]. The amorphous polymers have not any latent heat of melting and the melting temperature is approximately  $1.5 \times T_g$ . For metals and alloys the vaporization temperature is about the twice of the melting temperature. [77]

The required energy change from free vibrated solid state to a free rotated liquid state is stated as the latent heat of melting without a change in temperature. The  $L_m/T_m$  is approximately constant with a similar value as gas constant ( $8.314 \text{ Jmol}^{-1}\text{K}^{-1}$ ) for most of the metals (Richards Rule, [78]).

If the materials hold the relationship due to such as Van der Waals bonding this rule is not valid. Richard's Rule is good with high bond strength which has high values for latent of fusion and melting temperature.

On the other hand, the latent heat of vaporization presents the energy required to convert from liquid state to gas at the vaporization temperature. The ratio of  $L_v/T_v$  is appx. constant and about  $83.14 \text{ Jmol}^{-1}\text{K}^{-1}$  for most metals with some assumptions (Trouton's Rule, [79]). Similar to Richard's rule, in Trouton's rule the materials with high bond strengths have high values for latent heat of vaporization and vaporization temperature. This rule is invalid for small and light molecules such as  $H_2$  or He and for materials which have strong hydrogen bonding such as  $H_2O$ .

These aforementioned thermal properties could be found in literature easily. Ashby describes means of charting and relating the basic mechanical and thermal properties of engineering materials by using Material Property Charts[80]. These charts give also valuable information for materials which are processed with laser or being processed with laser instead of using analytical model.

### **3. Laser Workstation Design**

#### **3.1 Introduction**

The machine design stage is the main and the most important part of machine tool research projects. Without a good mechanical design, the rest of the machine will be ineffective, even if the most advanced and expensive controllers or electronics are implemented. In this part of thesis, from the design and analysis of machine structure to fine details of the designed sub-components of SAM workstation will be explained. Fundamentally, some topics should be included such as stiffness requirements, damping requirements, structural configurations for machine and other structural system configurations for a machine conceptual design approach.

In precision machine design strategy; accuracy, kinematic design, system elasticity, passive or active temperature control, structural configurations and damping are the main concerns. In the following paragraphs, most of the design fundamentals are considered with this respect. However, there are some limitations and tradeoffs due to lack of time and funding.

Beyond the design strategy and approach, the purpose of this study is to demonstrate the use of methods and strategies for designing high accuracy workstation for industry and research. The challenge is to achieve the productivity and the precision that needs for a price that the project is able to handle. While many of the decisions made will be unique to this example, the process and logic behind the decisions should be quite simple and applicable to other types and sizes of future machine design studies in Manufacturing and Automation Research Center (MARC), Koç University.

#### **3.2 Design Procedure of Subtractive-Additive Manufacturing (SAM) Workstation**

In order to follow the design procedure the first step will be the definition of the problem. In SAM workstation design procedure, the main aim is to produce the designed

geometry as accurate as possible by optimum conditions. Thereby, this dimensional accuracy need depends on production method that the SAM workstation is using at that moment. For instance, if the machine is set to work in FDM mode (if possible), the resolution of the manufacturing will be theoretically in between 100-500  $\mu\text{m}$  at each slice and in dimension (height-, width-, lengthwise) due to mechanical constraints. Moreover, the machine designer must be conscious of the purpose which is satisfying the needs and a well-defined set of design goals should represent the best vision of the end product or demonstrate the know-how of how to get there.

The highest level of guidance must be provided by the functional requirements and these requirements must properly represent the industrial and research necessities. Some of them may be listed as follows

- The workstation must capable of removing metal and polymeric based or sintering powder based material by using  $CO_2$ ( $\lambda$ :10640 nm) and Ytterbium Fiber ( $\lambda$ : 1064nm) lasers.
- The most general configuration requires the three-degree-of-freedom relationship between laser optics due to the physics of the desired manufacturing methodologies. The workstation is going to work mainly  $2^{1/2}$  axes kinematic movement while in processing.
- The horizontal axes which are capable of reaching to all exposed sides of the workspace as provided. In all cases this relationship must be sufficiently accurate and rigid to meet the requirements.
- The work table must be perfectly horizontal to facilitate the manufacturing methodology.
- The working range of the machine must be roughly equal in three spatial directions X, Y and Z.

- The atmospheric environment should be arranged in order to constitute proper process condition and to avoid suffocation of operator during operation due to hazardous gases. Therefore, the work volume must be enclosed and proper air circulation must be provided within the machine.
- The selected subcomponents and design should be compatible to automation. This means that after succeeding the process control, the main process is going to be automated by all manner such as atmosphere, temperature etc.
- The system must be readily transportable to the locations where it is going to operate on standard utilities.

### **3.3 Developing Methodology of Machine Specifications**

After completing detailed literature survey, the specification of the developed machine versus the forgoing machines could be compared. Therefore, the developed ideas in this recent machine might fill the missing points on the literature. For example, in the literature, there isn't any machine which is capable of working such a versatile manner by usage of different wavelengths and different manufacturing methodologies. In addition, there isn't any machine which has 3D scanner on it. These specifications should also require iterations to be better since the decision depends on the design solutions that evolve over the course of the project. This is why the specifications are considered design goals at this stage.

The completed studies in University of Michigan, Ann Arbor (Center for Laser-Aided Intelligent Manufacturing)[1-6]; University of Texas, Austin (Laboratory for Freeform Fabrication)[7-10]; Katholieke Universiteit Leuven (Division of Production Engineering, Machine design and Automation [Division of PMA] ) [11-13]; University of Applied Science Mittweida (Lasereinstitute der HochschuleMittweida)[14] show great efforts in literature since the invention of first laser based workstation.

On the other hand, at Manufacturing and Automation Research Center (MARC), the development of an additive manufacturing machine design has been a long sought goal of

researchers. In pursuit of this goal, substantial efforts have been undertaken in the design and fabrication of SAM workstation by reconsidering the former studies. During machine design, emphasis was placed on reconfigurable, highly adaptable machines intended to perform a variety of laser based or FDM based research. The eventual goal however, is to transition mature technology embodiments from that research into the industry.

This section presents the chronological development of a workstation design which mainly used FDM based structure in MARC. In the following paragraphs a short explanation of former thesis will be given shortly. Thereby, the comparison with the current design may be seen easier with this respect.

### **3.3.1 The First Generation Additive Manufacturing (AM) Machine**

The first machine was developed in between 2005 - 2008 with a TUBITAK research project, the sole purpose was building polymer based parts by using four different designed polymer extrusion heads. The first developed mechanical structure is a simple open loop G type structure which would be found by means of terminology in [15]. The structure has 2 axes moving work table in X-Y and one axis working in Z direction as in Fig.3.1.

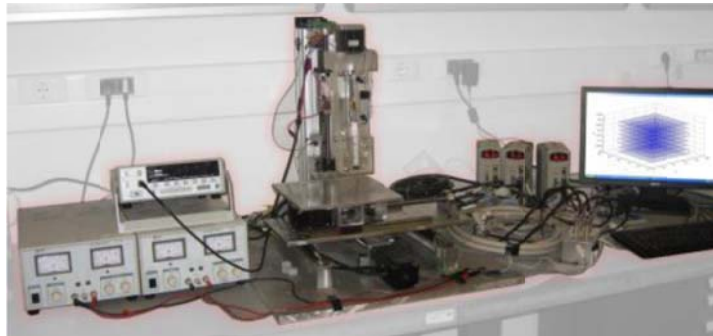


Figure 3.1 The first developed additive manufacturing machine

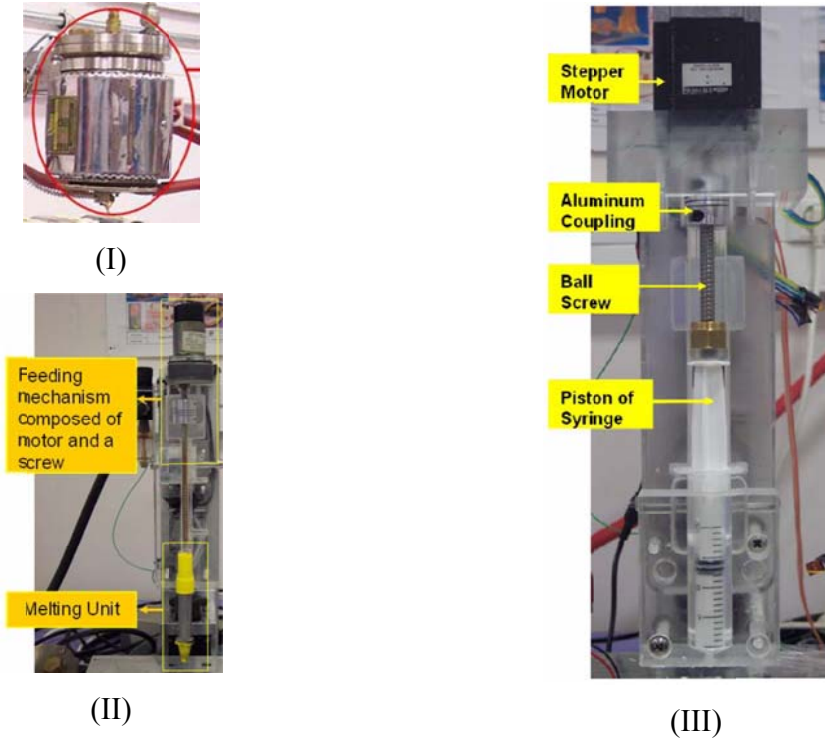


Figure 3.2 (I,II,III) The former designed four different type of extrusion head

The AM machine assures the kinematic entailment for  $2\frac{1}{2}$  axes manufacturing due to the nature of that method. In addition, the dynamic response of the system and stiffness values seems fine in order to manufacture the designed parts in sub-millimeter level tolerances. Even there isn't any stiffness calculation or dynamical analysis to show the positional accuracy of the design in the former thesis, some trial-error based experimental results are shown because of dedicated work of former students[16]. Their results of their dedicated efforts might be seen as in Fig.3.3.

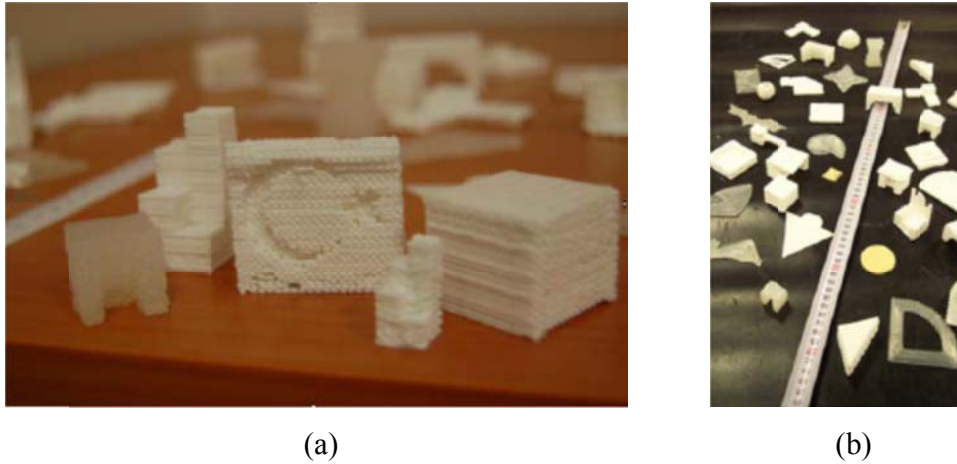


Figure 3.3 The produced part from the first generation of AM machine

In the software part of the first AM machine, MATLAB based software programmed which is cleaning Cutter Location Source File (CLSF). CLSF is the output of the Computer Aided Manufacturing (CAM) programs such as Unigraphics NX6. The MATLAB software send signals to servo drivers through microcontroller circuit via serial communication (RS-232) [17]. In this work, there isn't any STL slicer algorithm to generate any toolpath. If the operator doesn't have any CAM background, the desired geometries wouldn't be a complex geometry. The CAM program output and the developed software are shown in Fig 3.3. In addition to that, the given method requires working in the same MATLAB version which is 7.1. If the edition is changed the same algorithm would not work properly.



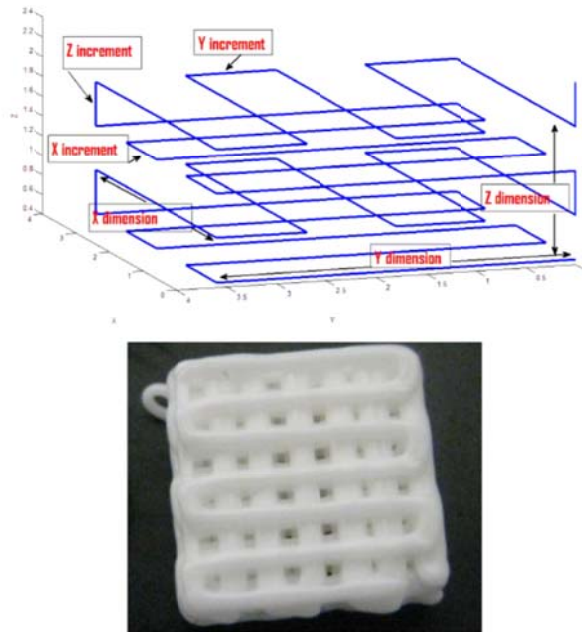


Figure 3.4 Developed MATLAB software output in first generation of AM machine

Some of the drawbacks in the designed machine are,

- In extrusion head design I (Fig. 3.2 I), the temperature gradient is too hard to control in type I extrusion head due to improper selection of thermal pool.
- In extrusion head design II (Fig. 3.2 II), the glue is low viscosity to build 3D artifacts.
- In extrusion head design III (Fig. 3.2 III), the material continuously flows out due to the back suction deficiency.
- The generated software is mainly used CAM package and needs CAM program background.
- The deposited polymeric material, which solved in solvent and filled in a syringe, has limited area of usage.
- The base structure is heavy and prone to the error in Z axis.

Even the first generation machine has lots of disadvantages in engineering perspective, this study is sufficient in order to understand the process parameters and their effects to robocasting.

### 3.3.2 The Second Generation Additive Manufacturing (AM) Machine

The thesis work of Izbassarov[18] resulted in second generation AM machine making overall huge advances over first generation of AM machine, especially in terms of construction, component standardization, mobilization, electronics and software. Therefore, the system mainly designed on RepRap, Fab@Home and first generation AM machine [19, 20].

The second generation of AM machine is demonstrated in Fig. 3.4. As seen from this figure the complete structure changed into Plexiglas (acrylic) chassis in order to increase the mobility of the machine by decreasing the mass. However, the material properties of Plexiglas and the laser cutting manufacturing method results in inaccuracies in that system. Similar to the former study, there weren't completed any basic calculation of machine design.

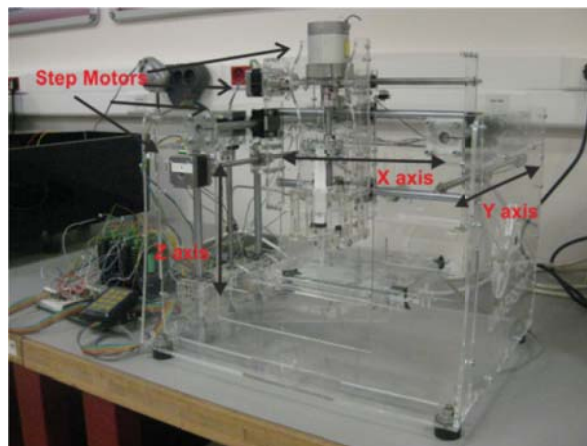


Figure 3.5 The second generation of AM machine

Oppositely, developed syringe injection head, which is compatible with multiple type of syringe such as 5mL, 10 mL and 20 mL has promising results by means of design. With this head the injector may be pushed or pulled, in order to provide continuity and stop of the polymeric solvent. The former experience on polymeric solutions leads this thesis focusing more on bio application side of the additive manufacturing. Thereby, several solvent and materials is tried for producing scaffolds and there are several successful trials completed by using different cell types.

In the developed control system, the former 100 MHz 8050 based Cyrix microcontroller is redundant for this project, so a 20 MHz 16F877PIC microcontroller is used. In addition, the micro stepping behavior of POLOLU step motor driver and the 2.5 mm pitch sized ball screws enhanced theoretical resolution of the system. On the other hand, the newly developed firmware is still need for CAM program in order to produce desired geometries with a G-code parsing algorithm.

These efforts affect great the current state of the specifications and followed procedure in this thesis. The specifications presented in the following sections are developed rather for a potential application field.

### **3.3.3 Laser Material Processing [LMP]**

The laser material processing model (Chapter 2), relates different laser material interaction conditions to the corresponding requirements for the workstation. These necessities are given shortly in 3.2 Design Procedure section. In addition, a short literature survey would be indicated for conceptual design and represented the boundary parameters for designed workstation. These parameters are not as highest possible parameters in the literature but these will give some rough ideas on that topic. In the literature survey, several fundamental parameters of LMP and FDM are focused such as SS: Scanning Speed, HD: Hatch Distance, LP: Laser Power, EHF: Extrusion Head Feedrate, PF: Piston Feedrate, T: Temperature, OL: Oxygen Level, PTC: Preheat Temperature Condition as indicated in

Table 3.1. The selected components of the proposed design should provide these parameters. Further reading is suggested to the reader in order to inspect not mentioned properties such as material, optical systems etc. from the given references of this chapter.

Table 3-1 Laser Processing Parameters from the Literature Survey

| Parameters \ Literature         | $SS^1$  | $HD^2$ | $LP^3$ | $EHF^4$                  | $PF^5$ | $BD^6$ | $GL^7$                | $PTC^8$            | $LW^9$ | -   |  |
|---------------------------------|---------|--------|--------|--------------------------|--------|--------|-----------------------|--------------------|--------|-----|--|
| <i>Martin</i> <sup>1991</sup>   | 0.104   | -      | 18     | -                        | -      | 254    | -                     | -                  | 10640  | SLS |  |
| <i>Das</i> <sup>1998</sup>      | 0.71    | 127    | 130    | -                        | -      | 500    | 10 <sup>-6</sup> Torr | -                  | 1064   | SLS |  |
| <i>Chen</i> [21]                | 1.27e-2 | -      | 2      | -                        | -      | 38     | 30 [psi]              | -                  | 1064   | LM  |  |
| <i>Kruth</i> [22]               | 0.1-0.6 | 200    | 300    | -                        | -      | 600    | Ni                    | -                  | 1064   | SLM |  |
| <i>Kuar</i> [23]                |         |        |        |                          |        |        |                       |                    |        | LMD |  |
| <i>Lamikiz</i> [24]             | 0.033   | -      | 900    | -                        | -      | 930    | -                     | -                  | 1064   | LMP |  |
| <i>Fischer</i> [25]             | 2       | 75     | 23     | -                        | -      | 30     | -                     | -                  | 355    | LM  |  |
| <i>Li</i> [26]                  | 0.12    | -      | 475    | -                        | -      | 14     | Ar, 25 [L/min]        | -                  | 1075   | LW  |  |
| 1- Scanning Speed [m/s]         |         |        |        | 2- Hatch Distance [um]   |        |        |                       | 3- Laser Power [W] |        |     |  |
| 4- Extrusion Head Feedrate[m/s] |         |        |        | 5- Piston Feedrate [m/s] |        |        |                       | 6- Beam Dia.[um]   |        |     |  |
| 7- Gas Level [-]                |         |        |        | 8- Preheat Temp. [K]     |        |        |                       | 9- Las. Wave.[nm]  |        |     |  |

There are 5 different laser material processing operations on Table 3.1, which are LM: Laser Machining; SLS: Selective Laser Sintering; SLM: Selective Laser Melting; LMD: Laser Micro Drilling; LMP: Laser Marking/Polishing; LW: Laser Welding.

In the first step of the designing stage, the thermal calculations and models should be concluded, because the proposed SAM method in this thesis is a thermal based laser processing method. The effective parameters on thermal model is mainly the laser scanning speed, laser power, spot diameter and hatch distance, which constitute the energy density or Andrew Number. In order to understand this in details, a model is also given in Chapter 2 to adjust the parameters according to processed material in a scientific outlook, instead of estimation by infinite trials. However, the limit conditions are still needed for conceptual design of the SAM workstation. Therefore, for different laser processing methods and their

conditions are given in Table 3.1. For example, the fastest condition of laser scanning speed from the table might seem as 2m/s for laser machining operation of composite materials[25] and the slowest operating condition with 0.033 m/s was in[24].

In second stage, due to this thermal effect, other concerns in the conceptual design should be included such as selection of the structural material of the SAM workstation, insulation of the workstation construction and design-evaluate atmospheric conditions. The small changes on the temperature may cause some undesired conditions in the processed material (i.e. insufficient interlayer bonding, undesired porous micro/macrostructure, agglomeration of the material etc.). These micro/macro structural concerns may be avoided by preheating and adjusting the atmospheric conditions of processing chamber. In addition to that, the limit values regarding to preheating and atmospheric gas/pressure are mainly depends on the material that is processed. Das is used rough vacuum conditions (30 mTorr) and high vacuum conditions  $3 \times 10^{-5} Torr$  in his experiments on Inconel 625 and Ti6Al4V [27]. Moreover, the preheating temperatures that he is dealing with is in between 300-600 °C.

Table 3.1 demonstrates some of the pure scientific push on a developed manufacturing technology in between 1990-2011. Moreover, the industry pulls this research area and design laser stations in order to use this technology. In table 3.2 some of the examples from industrial systems are given.

Table 3-2 Specifications of commercial laser workstations[28]

|                               | <b>EOSINT M 250</b>           | <b>DTM Sinterstation 2000</b> |
|-------------------------------|-------------------------------|-------------------------------|
| <b>Work Volume</b>            | 250x250x150 [ $mm^3$ ]        | 304.81[ $\phi$ ]x381 [L] [mm] |
| <b>Laser Type/ Power</b>      | $CO_2$ / 200 W                | $CO_2$ / 50 W                 |
| <b>Laser Scan Speed</b>       | Up to 3 m/s                   | Up to 5 m/s                   |
| <b>Layer Thickness</b>        | 0.05 – 0.1 [mm]               | 0.0752-0.508 [mm]             |
| <b>Interface CAD Standard</b> | STL, CLI, VDA-FS, IGES, CATIA | STL                           |

Working with the tables as in 3.1 and 3.2, that is, by entering parameters and reviewing the calculated values from literature and industry, is a judgment process based on anticipated machine capabilities and the expected operation conditions. The variety of operations represented in the Table 3.1-3.2 tax the workstation in different ways. The specifications developed using this approach should result in a machine that is versatile and well balanced.

### **3.4 Design Strategies**

The strategies for satisfying the design goals should clearly guide the designer to the basic technologies to use and how to approach the fundamental problems. This section is important to this study because many of ideas may not appeared or be obvious in the conceptual design drawings.

#### **3.4.1 Accuracy**

Friction, backlash and temperature change are the sources of unrepeatability and instability. The accuracy of the workstation, whether software corrected or mechanically compensated, is fundamentally limited by the repeatability of the axes and the stability of the metrology loop. In order to support repeatability and robustness to flying optic or FDM head movement, the axis should have widely spaced bearings for greater moment stiffness and a minimum lever arm between the moving stage and the feedback device of the moving component. In addition to that, greater dynamic stiffness and reduced dynamic moments would be provided by acting actuators through center of mass.

In this concept design, the compensation are not fully effective on errors, it might be easily corrected by mechanical alignments by axis correction. Axis correctness significantly reduces sine errors that result from errors acting through Abbé offsets. X-Y-Z alignment reduces to a minimum those errors associated with volumetric property of designed machine.

In general aspect, the design of accurate machine tools includes preloaded rolling-elements such as thrust bearings, ball screws and linear guides. These components have almost zero backlash, low frictional hysteresis and relatively low heat generation. In addition to that, increased contact surfaces results in high capacity, stiffness and smooth repeatable motion. On the other hand, the designed workstation has to have some limits such as velocity boundaries, as stated before, in all axes which require faster transmission system response (e.g. 0 - 10 m/s) than ball screw without any additional inertial effect. The additional mass and inertia of the ball screw transmission is decreased the system response even increased the robustness of the system.

Belt drives consist of flexible elements running on either pulley. A belt drive transmits power between shafts by using a belt to connect pulleys on the shafts by means of frictional contact or mechanical interference. In this current design, the constant speed ratio or synchronization of angular position of the driving and driven shaft is critical to operation due to the need for controlling position and velocity. This requirement can be achieved by means of special toothed belts, called synchronous or timing belt. Belt drives have numerous advantages over other power transmission systems such as easy transmission, low maintenance (no lubrication need), high reliability, adaptability to non-parallel drives and -most important for our case is- high transmission speed with lowest inertia. The principle disadvantages of synchronous belt drives are their limited power transmission capacity, susceptibility to environmental conditions (e.g. chemicals, vibration shock), generated noise by compression of air between teeth especially at high speeds and limited speed ratio capability. In this study the selected synchronous belts are steel wired inside, which decrease the elasticity and increase the positional accuracy. Moreover, in order to increase the tension on the belt, S shaped parts are manufactured on ThingoMatic and plugged through the belt as shown in Fig. 3.6.

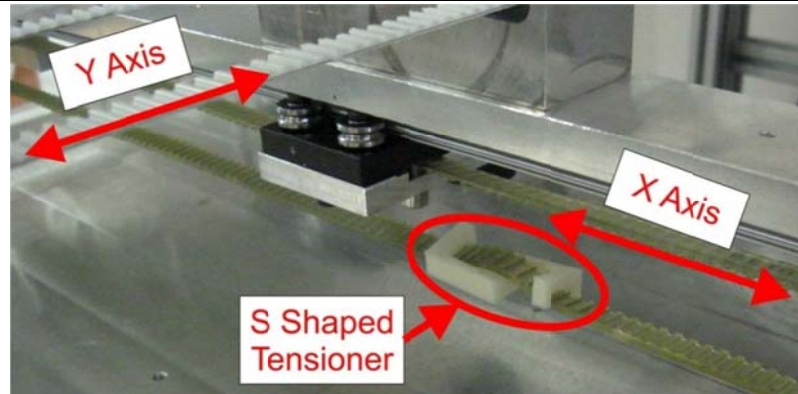


Figure 3.6 S shaped belt tensioner

In control engineering perspective the positional accuracy of belt driven system is lower than the ball screw based systems. However, these systems are generally used even in metrology industry with suitable rotary or linear encoders such as in CMM machines at Manufacturing and Automation Research Center in Fig. 3.7.



(a)



(b)

Figure 3.7 Industrial CMM Y(a)– Z (counter-balanced)(b) axes belt drive systems

In order to understand the accuracy of this selected transmission system, a belt driven mechanism model is built before implementing in CAD design of the workstation. The goal of the design is to determine the effect of the belt spring constant  $k$  and select appropriate



parameters for the system. A model of the belt-drive system as shown in Fig. 3.6 is determined and many of its parameters are selected.

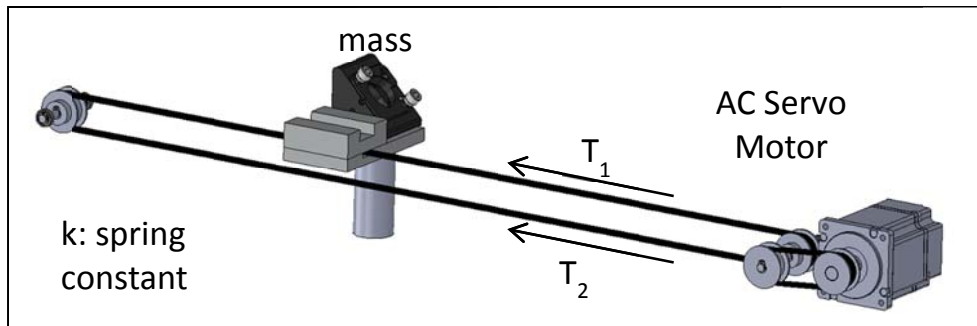


Figure 3.8 Lumped system model of belt-drive model

This model assumes that the spring constant of the belt is  $k$ , the radius of pulley is  $r$ , the angular rotation of the motor shaft is  $\theta$ , and the angular rotation of the right hand pulley is  $\theta_p$ . The mass of the moving component is  $m$ , and its position is  $y(t)$ . A linear encoder, which is used to measure  $y$  position, is able to use with Panasonic servo driver to obtain for Full Closed Loop Control of servo driver[29]. Therefore the positional inaccuracies due to the belt-driven nonlinearities would be compensated proportionally with the sensor resolution. Even the system will have full closed loop control the structural precautions should be included into the system and the belt-drive model must be investigated.

A moderate AC servo motor is planned to use in each axis. The inertia of the motor and pulley system is  $J = J_{motor} + J_{pulley}$ . The motor pulley friction is  $b=0.25$  Nms/rad. The radius of the pulley is  $r=0.0254$  m.

The equations of motion might be written for the system; note that  $y = r\theta_p$ . Then the tension from equilibrium  $T_1$  is,

$$T_1 = k(r\theta - r\theta_p) = k(r\theta - y) \quad [3.1]$$

The tension from equilibrium  $T_2$  is,

$$T_2 = k(y - r\theta) \quad [3.2]$$

From Eqs. [3.1] & [3.2], the net tension at the mass  $m$  is,

$$T_1 - T_2 = m \frac{d^2 y}{dt^2}$$

$$T_1 - T_2 = 2k(r\theta - y) = 2kx_1$$

Therefore the state variables are  $x_1 = r\theta_1 - y$ ,  $x_2 = \frac{dy}{dt}$

$$\frac{dx_1}{dt} = r \frac{d\theta}{dt} - \frac{dy}{dt} = rx_3 - x_2 \quad [3.3]$$

$$\frac{dx_2}{dt} = \frac{2kx_1}{m} \quad [3.4]$$

$$\frac{dx_3}{dt} = \frac{d^2\theta}{dt^2}$$

Hence,

$$\frac{dx_3}{dt} = \frac{T}{J} - \frac{b}{J}x_2 - 2krx_1 \quad [3.5]$$

The state space form this equations are

$$\begin{bmatrix} \dot{x}_1 \\ \dot{x}_2 \\ \dot{x}_3 \end{bmatrix} = \begin{bmatrix} 0 & -1 & r \\ 0 & 2k/m & 0 \\ -2kr & 0 & -b/J \end{bmatrix} \begin{bmatrix} x_1 \\ x_2 \\ x_3 \end{bmatrix} + \begin{bmatrix} 0 \\ 0 \\ 1 \end{bmatrix} T \text{ and } y = [1 \quad 0 \quad 0] \begin{bmatrix} x_1 \\ x_2 \\ x_3 \end{bmatrix}$$

By using this state space equation, the system response versus different stiffness and damping values would be compared.

### 3.4.2 Stiffness and Damping Outlook for Designed Workstation

The workstation requires sufficient stiffness in the structure between the moving axes so that the dynamic movement of flying optics or FDM head results in insignificant deflections. The entire structure isn't exposed to process loads while other types of loads may act on portions of the structural loop due to non-contact nature of laser processing. In addition, in the designed workstation, tool workpiece contacts do not occur as occurred in milling or turning. For example, the extruded material in the head flows out through nozzle and gently touches with the worktable by negligible force. Therefore, the dynamic

compliance calculations are not taken into consideration during designing stage. Except the dynamical movement of the flying optics, the quasi-static analysis (inertial loads from accelerating masses) act on the static compliance to generate position errors and resonant frequencies of the system will be examined during trial tests. Thus for high accuracy and minimum position errors the workstation requires low static compliance, well-damped resonances and high resonant frequencies. In short, the goal of design is achieving lower resonant peaks (indicating greater damping) and higher resonant frequencies to balance in smaller amplitudes, better finish, and allow greater servo stiffness.

For most large machine structures, the economics guide the design toward typical engineering materials such as steel, cast iron or aluminum. The specific modulus of cast iron is only 65% that of steel or aluminum yet it remains the preferred material for general-purpose outweigh its extra manufacturing cost. Aluminum castings are less expensive to manufacture but the material cost exceeds cast iron even though the weight required is less. On the other hand, especially in the prototyping stage of the machine design, there is an alternative to expensive casting procedure. Several machine companies and research laboratories are using extruded aluminum parts. However, there is several necessities while choosing these components such as dimensional accuracy of standard part and assembly. Even the usage of extruded aluminum profile is decreased the cost of design, the thermal expansion coefficient of aluminum is the main disadvantage to use in precision machinery applications. In order to solve this problem, a network of tubes can be cast in or the profiles internal channels could be used to provide internal passages to flow temperature controller water. In addition, aluminum can be used as matrix in a composite with ceramic fibers. The use of a structural ceramic such as aluminum oxide may have application for smaller components that have difficult design constraints. For example, a quill made of aluminum oxide would be 80% stiffer than steel for one-half weight.

Usually, the material selection has a relatively small role in the stiffness of a machine tool structure to the placement of the material. It is a matter of using the material most efficiently in the design. Obviously, the usage of structurally closed sections and favorable aspect ratios are priorities in the design of the machine. For each component, it is important that loads carried by a structural member be in plane to produce tension, compression or shear rather than bending. This is especially important in areas of concentrated loads such as bearing supports. For structures that see bending loads such as the machine base, the members in tension and compression must have adequate shear members connecting them. For structures that see torsional loads such as the column, all faces must support shear loads and should enclose the maximum volume. The open face of a bifurcated column requires a stiff perimeter frame around the opening to support the shear load. The shear load produces a bending moment in the frame that is maximum at the corners. The tension and compression members of the frame require extra support around the corners to prevent localized bending and the resulting loss of stiffness. In the designed layout, these physical aspects are taken into account in order to decrease the mechanical effects.

Therefore, finite element analysis (FEA) is the proper tool to provide visual and numerical information required to evaluate competing structural designs and/or to improve the design iterations. A plot of strain energy density is useful in optimizing the thicknesses of structural members by thickening high energy regions and thinning low energy regions, thus trying to achieve a uniform distribution. A sensitivity analysis, obtained by varying a design parameter and observing its effects on a figure of merit, is useful to assess the impact of a design change. A parameter study is similar except that it extends over a range that hopefully encompasses the optimum. These techniques are most applicable after the conceptual stage of design. Ideally, simple finite element models should be developed concurrently with the design concepts since much can be learned about the general behavior from simple models.

---

**3.4.3 Structural Stability**

Structural stability means that the metrology loop must remain robust through time to obtain error-free results either by mechanical compensation or software based pre-correction. A previously addressed thermal stability is another aspect of this requirement; therefore thermal analysis of the structure must be included in the analytical results. By including this and other aspects in to the design, we are concerned with eliminating variable loads on the metrology structures and/ or making those invariant structures to ones that are unavoidable. Transient response of the system from the short-term load sources are mobile and variable masses within the system, friction in rails, constraints between moving components, inertial and process loads. Long-term load sources result from movement in the foundation due to settling or hygroscopic action and whenever a friction joint slips and releases built-up stress.

The separation principle needs to be applied on structure to understand better the structural robustness of the system. This methodology will eliminate changing forces from the metrology loop; however, this is hard to apply to the workstation in the purest sense. Even a separate metrology frame and system of sensors is used, this frame become awkward for three or more axes and the expense is unwarranted for this level of accuracy. On the other hand, other approaches might be used as a principle. For example, the effect of a moving mass can be separated out through compensation if the mass is constant or if an exact model exists and the change in mass is measured. In applying, the separation principle, the first step is to identify the metrology loop and the parts within it. The parts list for the workstation includes the main structures (base, column, etc.), the linear guides, the laser guide, the extrusion head, the workpiece, and due to overconstraint, the foundation and 6 leveling caster with vibration dampers. The next step is to identify and classify the variable loads as separable, repeatable (or compensable) and non-repeatable. Large separable loads or ones that are easy to separate should be removed from the metrology loop while others

that are small relative to the process load may be ignored. Compensation can reduce the effects of repeatable loads but simply stiffening the structures may be the better solution since the effects of non-repeatable loads are also reduced.

The base is the primary metrology structure for the laser workstation like the most other machine tools. It supports and is influenced by the weight of moving and non-moving structures, the part weight and variable loads such as process and inertial loads as mentioned before. The undesirable influence from primary movement is mitigated by eliminating overconstraint in the machine support. The simplest approach is to use three support points aligned with gravity and incorporating elastic or viscoelastic interfaces to avoid frictional hysteresis. The number of supports can be increased up to six (the number required for exact constraint) to distribute more uniformly the weight of the machine but this requires the constraints to be angled appropriately. The additional support points will not affect the stiffness of the machine base but they may affect the mode shapes and the degree of damping that can be gained from viscoelastic supports. For considerably larger machines that may require multiple base sections each section should have exact constraint support relative to the foundation and adjacent sections so that movement coupled from the foundation is a detectable using sensor between sections. This information can be used to calculate compensation or to automatically level the machine with appropriately placed actuators.

The conceptual workstation will have a multi-piece base with a sufficient stiffness and damping (due to the effect of fasteners) so that non-compensable deflections are not so significant. The aluminum sigma profiles selected for this reason due to their high surface area far from neutral axis (important for bending) and their closed shaped inner structure (important for torsional effects). The jogging test of the servo driver shows that the upper machine base does not have sufficient stiffness to damp the movement of the y axis due to

the mass of this axis. Therefore, an additional bottom chassis is added in the structure as shown in Fig. 3.7.

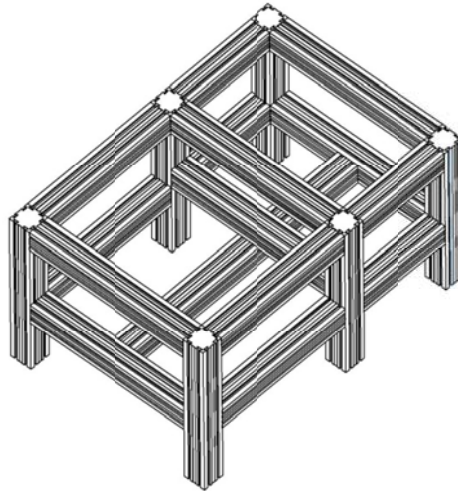


Figure 3.9 Bottom part of the chassis without vibration dampers

In addition to that, the placement of vibration damping supports for the base will minimize the deflections due to moving and variable masses that are not separable. This viscoelastic material incorporated in the mounts will provide passive damping for unwanted vibrational affects. These error compensation precautions will reduce the effect of manufacturing errors, deflections due to moving masses and variable part weight if necessary.

#### **3.4.5 Productivity and Manufacturability**

Several aspects have been addressed in the requirements and strategies for laser based manufacturing performance. The workstation will have ample power, axis speed for external laser power density adjustment and will have ample dynamic stiffness and axis force. The other issues left to address are associated with non-productive time such as powder feed, workpiece loading and optics cleaning. The non-productive time is especially important for advertisement of the designed industrial machine and creates difference with respect to other workstations. However, these are not our current concern in this design

stage. On the other hand, ergonomics is a critical factor for the machine operator to be productive or for the researcher to work longer hours. The dictionary definition of ergonomics is the intention to maximize productivity by reducing operator fatigue and discomfort. The ergonomics is more important concern than the other factors for productivity view and the main affects in order to estimate the boundary size of the machine. Except, conceptual size of that machine, the ergonomics point of view creates improvements that make the machine simpler, easier and flexible to use that will usually be valuable.

The minimum effort to build and qualify is required in order to design optimally manufacturable workstation. This design state has effects on the required number of labor to fabricate, machine, assemble and qualify the machine. In manufacturing of machined parts, the raw materials (e.g. aluminum) are bought from the local dealer cleaned the surfaces and machined according to the technical drawings, Fig. 3.10 gives example of the procedure. Afterwards, the parts are pre-assembled to check as if there is a manufacturing error. Finally they are combined on the main chassis.



(a)



(b)

Figure 3.10 (a) Cleaned surfaces of bought aluminum components (b) Pre-assembled parts after machining according to technical drawings

The cost of commercial components and raw materials, although not really a part of eliminate nonessentials, that is, only add parts or features that are required for the machine



to function or that simplify some other aspect of the machine. The principles of exact constraint provide guidance in determining the essential structural supports for and connections between components. The use of pre-qualified modules and subassemblies, while costing more per unit, reduces the time required to build the machine, reduces the chances of rework and increases the flexibility to reconfigure the machine for faster delivery or field retrofication. Therefore in the design stage, the workstation is designed by using standard parts and assemblies. In addition to that, the selection of the component builder companies is also important. The selected native company may have shorter delivery time and less cost with respect to competitive foreign companies, but the provided materials has dimensional inaccuracies up to 10 cm. The other important mistake is incorrect information of main CNC workspace which is given on the CNC machine label. The main CNC MAZAK FJV 200 has insufficient workspace on it so the main manufacturing is completed in universal milling machine of machine shop of the Koc University. The universal milling machine has inaccuracies up to 200  $\mu\text{m}$ . This leads also additional manufacturing problems.

Unfortunately, because of the aforementioned reasons, scraping, shimming and other fitting techniques are used and these decrease the manufacturing precision of the designed machine by means of main structure. On the other hand, at critical points such as main axes bearing locations, actuator flange plates etc. is manufactured in MAZAK FJV 200 CNC in high accuracies of this machine tool up to 50  $\mu\text{m}$ . In addition to that, this method may require in-process inspection of certain features and may become impractical if too many tolerances stack up in the design. This trial and error method may criticize by some people and seem as trivial but such cases require correction either through simple adjustments or software compensation. Therefore each manufactured parts are tested and required arrangements are completed.

### 3.5 Design Layouts

The development of the selected configuration is continued in this section for the conceptual design. The design-analysis is iterative procedure which starts with the selected configuration, the range drawing and actual or estimated envelopes for components like the galvanometric scanner or vacuum chamber, which would be implemented in future. In this study, the geometry was created first in 3D CAD software and then exported to a finite element analysis (FEA) program for analysis. A number of iterations occur to improve and/or simplify the design, but only the final and a couple of other versions are presented. Where available, past trends or future improvements will be discussed. In Table 3.1, the previous design studies are given in 3D model and finite element analysis shown in following sections give better definition for the selected construction. As a result, the gaps between linear bearings and the mounting surfaces may look strange. The CAD model also lacks ball screws, linear bearings, guarding and other details that would be time consuming for FEA to include, but ideas for them are studied.

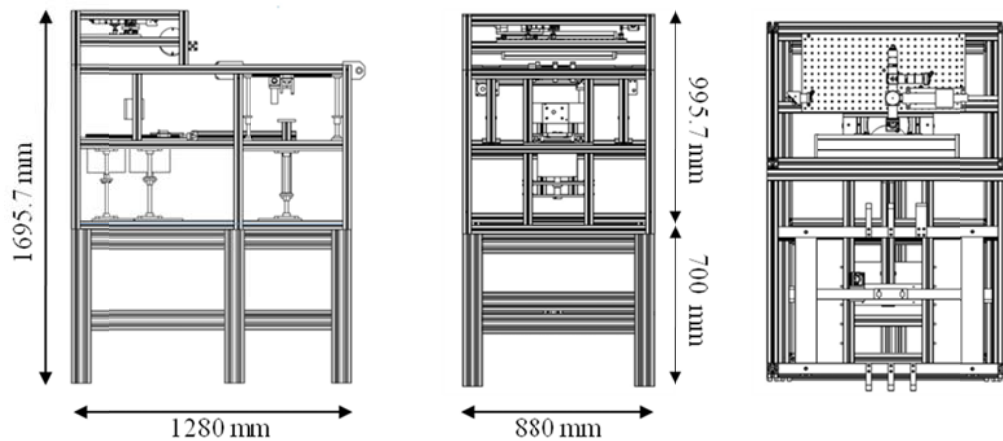


Figure 3.11 Final schematic of the designed laser workstation

This configuration leads naturally to design the column the front part of the machine which the dynamics effects are more effective on the structure. Then designing the base around the column and work table is followed by adding two bearings support to the laser head in a

centroid based arrangement. The main column in the front part not only supported by main chassis but also by the bifurcated 40x40 aluminum parts frame for shear stiffness at the moving axis plane. Six Z-axis bearings support the worktable and actuator ball screw are torsional coherent in an effort to release the planar constraint of six bearings. The moving axis is designed by aluminum plate which has interior belt pulling locations in order to increase tension in the timing belt. In addition to that in the X and Z axis locations, the actuator flange points have slotted holes in order to increase the tension in the timing belt. The modal analysis results show that the minimum mode is in 38.274 Hz according to the ANSYS Workbench results. The results seem true because the machine is actuated in that frequency and the similar dynamic behavior is examined. The other modes of the final design are given in Fig. 3.12. The carrier column is open at bottom to increase the productivity of the designed system which has good stiffness in planes, X-Y, Y-Z and X-Z.

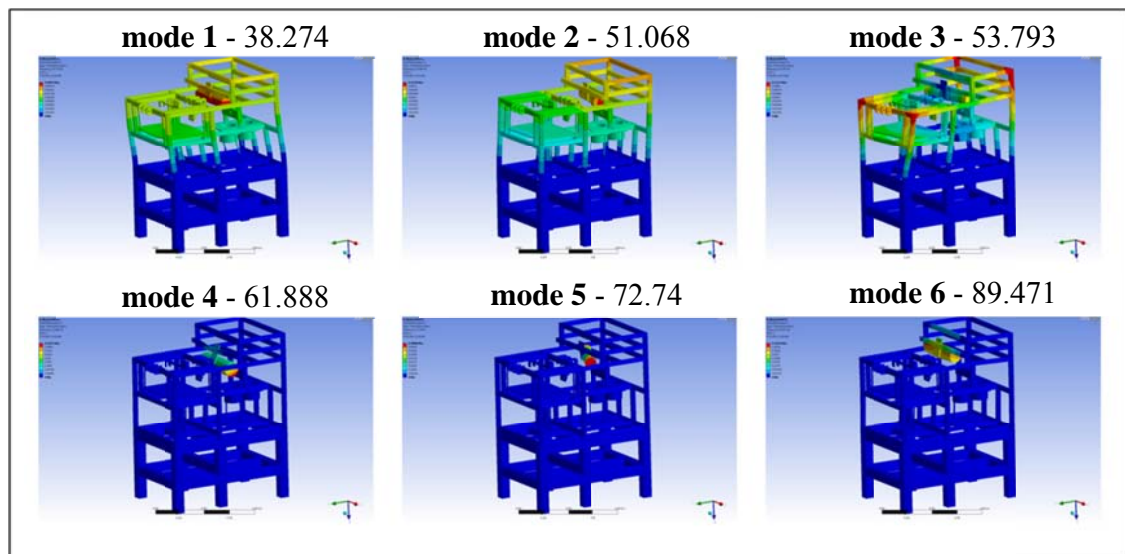


Figure 3.12 Modal analysis results of the final version of the machine

Instead of casting, the usage of aluminum profile would seem as a weak link in the system. However the principal compliances such as fasteners and bearings increase the damping of the system, which is also required by the workstation structure. Improvement to the

fastener locations is necessary and may require the additional connection such as long type nuts or connection strengthening plates.

The base has six supports to the floor but the two rear and two front supports have 90° angled chasis support in the Y-Z plane to form the structural constraint. The instant center of the structure is approximately 1320 mm above the floor and placed on the X-Z plane of symmetry. The node of the torsional mode (given in Fig 3.10 - 53.783 Hz) of the base typically lies close to the instant center as in Fig. 3.10. Placing the node nearer the centroid reduces the inertia of this mode and increases its frequency.

The two supports at the front of the base could also have constraints but it is more common to use flat pad air bearings, where friction provides the horizontal constraints. In either case, friction also causes over-constraint between the base and the floor and this over-constraining is good for static and dynamic stiffness. However, bad for precision, if air isolators are used in the lateral direction this over-constrained structure is no more a problem or a benefit. On the other hand, air isolators does not have very high viscous damping that a requirement for dynamical coupling from the base to the floor. A more practical and feasible approach for this machine is using a viscoelastic material its maximum damping in a range from 10 to 100 Hz. The viscoelastic components which are used for the mobility and leveling of the structure are used in order to damp the aforementioned frequency levels.

The guarding, operator control station and various utilities are not demonstrated in the figures. These are designed but in order to decrease the complexity of the system for the analysis is not included. The main effects of these components are mentioned in Productivity and Manufacturability part of this chapter. In the design strategy these equipment are supported from the base structure of the designed workstation. There will be reference features machined on the base to set up critical alignments. As mentioned before, the guarding is free standing on main chassis so as to be easily removed for transportation

or any major repairs or mobility requirement for the machine. Most utilities will be at the bottom part of the machine and have quickly disconnects from the machine.

Apart from the chassis or main structural components of the designed workstation some subassemblies are included such as laser-extrusion head (X-Y axes) stage, powder storage and feed cylinders and laser feedback structure.

The XY stage finalized after eight different designs. In the earlier design, the  $CO_2$  resonator is put on the XY stage and the fast movement is expected from that stage. This approach is useless due to the mass and dimensions of the  $CO_2$  resonator. In the other designs, the methodology is changed in to moving optic device but the question is the supplying the correct equipment which has high accuracy, speed and low inertia. The ball screw actuation mechanism is included in the later design, which is also not good idea to get rid of the required speed limitations. The rotating ball screw nut and stationary ball screw mechanism was thought to design but there is other transmission requirement for the rotation of ball screw nut is required. Therefore this design is also cancelled from the beginning. Finally, a belt system was included to the system. After that, different belt actuation systems were considered in the conceptual design stage. These design efforts are given in the following figures and the final design is already given separately in Fig. 3.9.

In powder based fusion processes, powder delivery is the most critical and mandatory topic. The designed system is based on the pneumatic actuated piston on a doctor blade to spread the powder from the main pool to the processing pool. The beauty of this design is possibility of conversion to the counter rotating roller mechanism from mentioned blade. The mechanism has several variables that influence the bed density, the linear speed of the blade, feed ratio, blade roughness, blade geometry and layer thickness. The feed ratio and the layer thickness are controlled by the movement of the feed side and part side cylinders. The feed ratio is the ratio of the inward movement of the feed side cylinder to the outward movement of the part side cylinder. To ensure full coverage on the part side the feed ratio

is the ratio of the inward movement of the feed side cylinder to the outward movement of the part side cylinder. To ensure full coverage on the part side the feed ratio is generally set generally at 2.0 in the commercial SLS machine[30].

Table 3-3 Design Iterations of the developed laser workstation

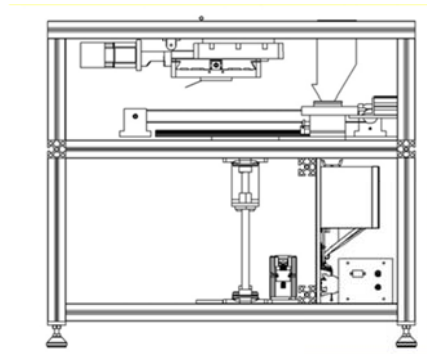
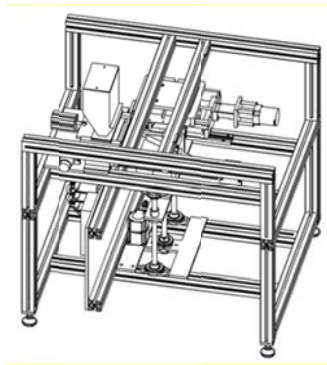
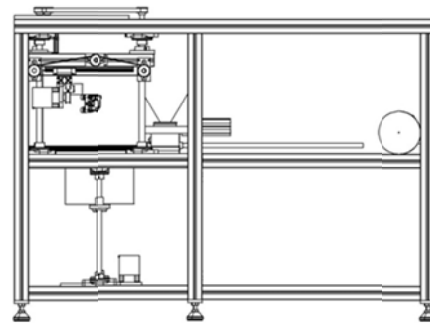
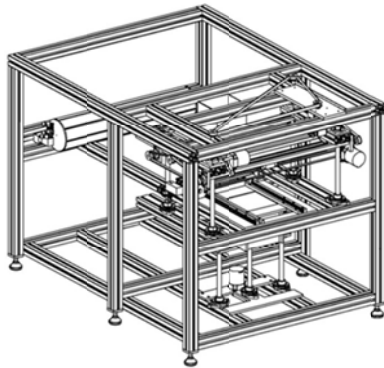
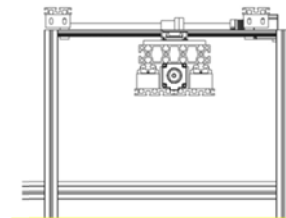
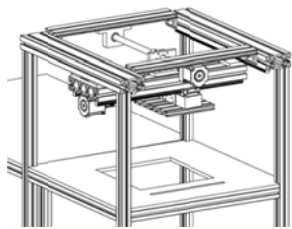
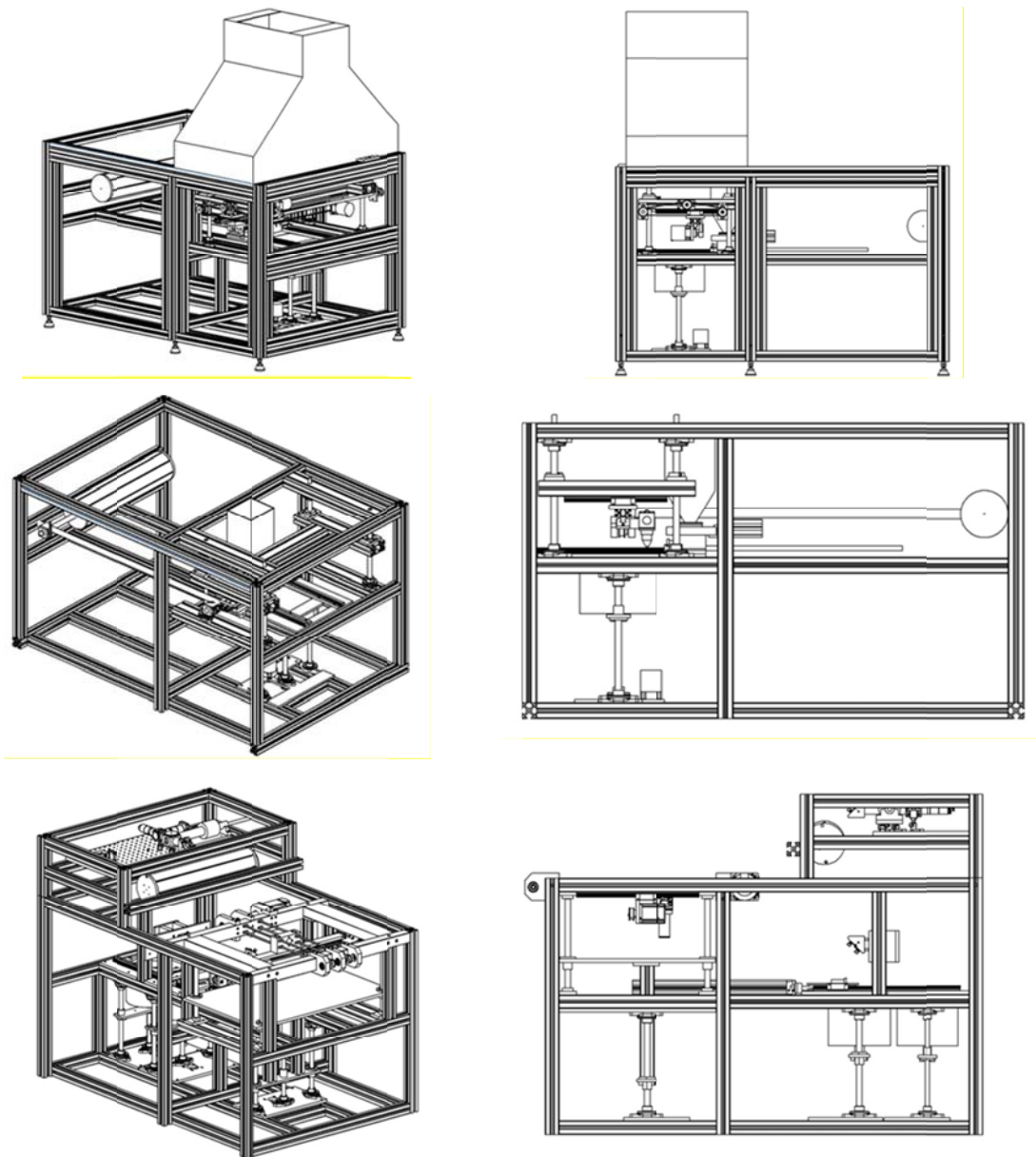


Table 3-4 Design Iterations of the developed laser workstation



It is easy to get the impression that this design is versatile and complex. Rather it is smaller and lighter than the equivalent designs in the industry. A key difference is the versatility and combined functions of the structure being long enough to support the other utilities. The Y axis is the heaviest part on that design. The decision to use a different actuation mechanism was considered carefully. On the other hand, its inertia and centroid base location will degrade these unwanted dynamic responses. In addition to that, the adaptive adjustment and created motion profile algorithm of the servo controller is also helped to get rid of with dynamic response problems.

Table 3-5 The masses of the given assemblies

| Laser Cutting Machine | mass (gram) |
|-----------------------|-------------|
| Main Chassis          | 98695.25    |
| Front Y-axis          | 2198.49     |
| Fly Optics X-axis     | 400.61      |
| Table Front Z-axis    | 11531.33    |
| Laser Feedback        | 3478.23     |
| Powder Piston         | 1712.71     |
| Powder Sinter         | 1066.33     |
| Powder Sinter Space   | 1066.33     |
| Bottom Chassis        | 36066.12    |
| Total                 | 156215.4    |

**3.6 Analytical Results**

In this analytical result part of this chapter, the simple test methodologies and the results will be given for X axis sub-assembly component in the order to understand the safe frequency zone for developed machine as in given Fig. 3.13. The results show that the first mode is far from the first mode of the chassis and beyond the working frequencies.



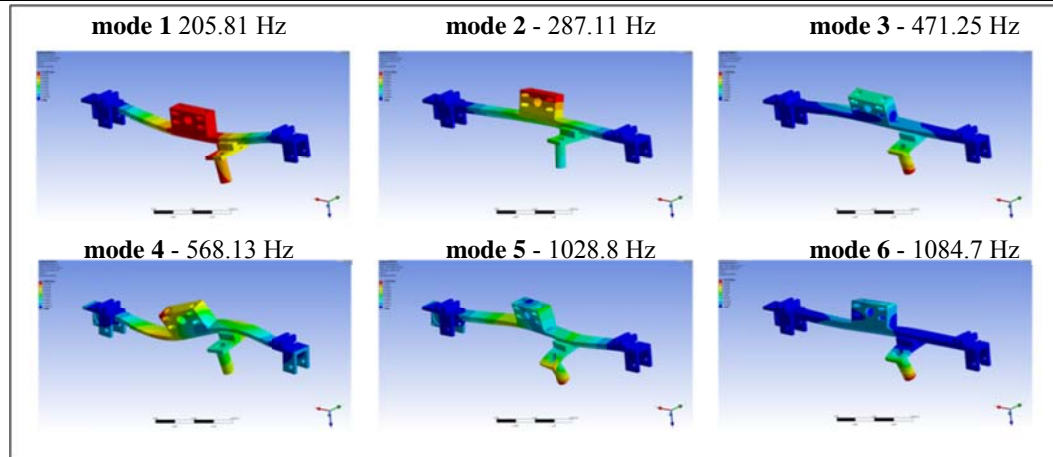


Figure 3.13 X axis sub-assembly modal analysis result

The machine base is a good example to present specific ideas on obtaining precision at reasonable cost. The primary requirement for the base is the ability to produce straight and parallel surfaces to support the rails. Therefore, the typical base carries the X, Y and Z the perpendicularity of the axes is mandatory. Perpendicularity may require an in-process inspection or pre-qualification of the workstation to achieve process control. A key aspect of the process is the proper support of the machine base so that the geometry is correct when the machine is assembled and used. If the machine base is designed to kinematic mount to its foundation, then the same mounting points should be used throughout manufacture to ensure consistency. In the following pictures an X-Y paralleling of the system is calculated by referencing the plane of the DEA CMM machine granite surface. A laboratory made two axes tilt sensor (i.e. in Fig. 3.12) is measured the surface parallelism. Then, the chassis is measured with that device at critical points and the results are as following Fig. 3.13 and Table 3.5.

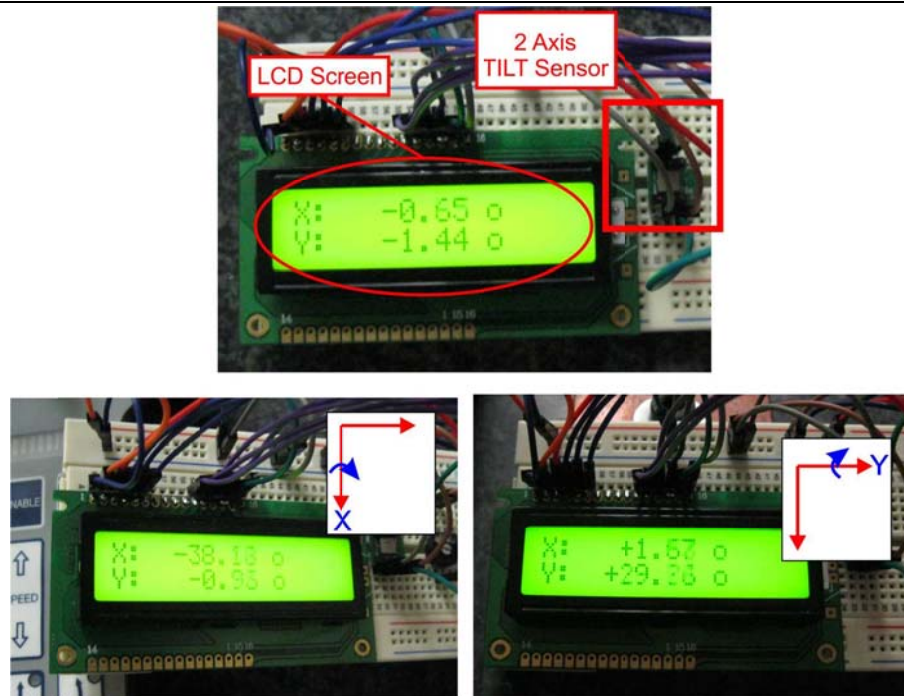


Figure 3.14 Implementation of sensor for measuring paralelity, offset calculation (top) and axes detection (bottom)

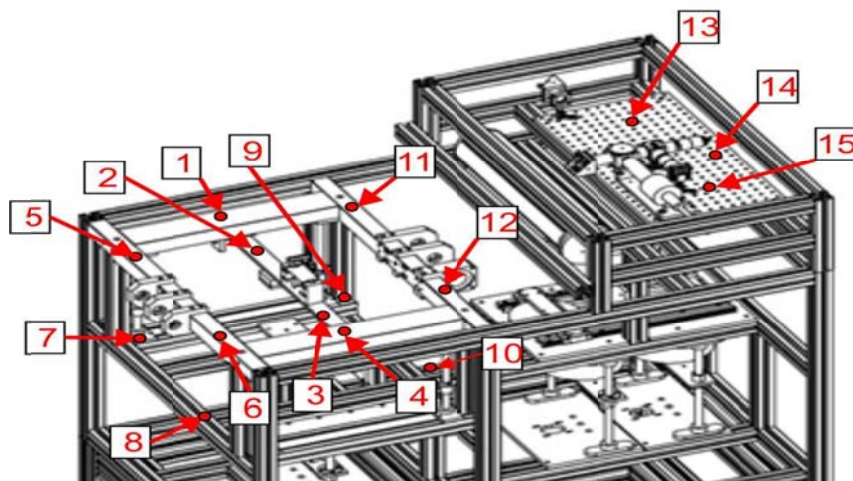


Figure 3.15 Measurement points of the machine

Table 3-6 Measurement results of the points in Fig. 3.12

|          | X [°] | Y [°] |           | X [°] | Y [°] |
|----------|-------|-------|-----------|-------|-------|
| <b>1</b> | -0.9  | -0.4  | <b>9</b>  | -1.5  | -0.1  |
| <b>2</b> | -0.5  | 0.2   | <b>10</b> | -1.6  | -0.1  |
| <b>3</b> | -0.5  | 0.2   | <b>11</b> | -0.1  | 0     |
| <b>4</b> | -0.9  | -0.4  | <b>12</b> | -0.1  | 0     |
| <b>5</b> | 0.2   | -0.1  | <b>13</b> | -0.2  | -0.3  |
| <b>6</b> | 0.2   | -0.1  | <b>14</b> | -0.2  | -0.2  |
| <b>7</b> | -1.6  | -0.1  | <b>15</b> | -0.3  | -0.3  |
| <b>8</b> | -1.4  | -0.2  |           |       |       |

The tensioning mechanism on the laser workstation is the belt itself. The belt is cut so that pulling the belt is possible at the disconnected parts which are fixed at the moving part of the X and Y axis centroid locations. In general, belts should be tight enough to minimize slack, but not so tight that they start placing a lot of stress on the motor shaft or pulleys. Once a belt is on, turn the motor pulley to gauge if there's too much resistance. If the belt makes an audible noise when it is plucked, it is too tight. The laser workstation operation should be nearly silent. In order to test if the belt is too loose, rotate the motor pulley back and forth. If the head moves back and forth in a synchronized manner with the AC servo motor rotation, then the tension will be okay. If there is a lag, the belt is too loose. A more quantitative test is to write a circle on the laser workstation. If any of the sides are flattened, then the belt on the corresponding axis is too loose. The results will be given in Chapter 5 – Conclusion Technological Demonstration.

There is another better way to measure these double axes inaccuracies such as laser interferometer, linear scale measurement or using robot arm probe etc. However, these methods require expensive infrastructures, which are out of the capabilities of the

laboratory. On the other hand, the following measurements are taken by using one axis of the laser workstation and laser displacement sensor is selected as measurement device.

As mentioned earlier in Design Layout part of the chapter, the powder mechanism has several features in it. Therefore, a couple of tests are required in order to estimate proper powder sweeping parameters. Thus, fragmented materials are placed in feeding cylinder and then the sweeping cycle is started. The sweeping speed and the leveling ratios are estimated according to supplied materials which is relevant to the layer thickness and the layer thickness is the amount the part cylinder is lowered after each scan. The typical value of layer thickness used for mesh powders (<100  $\mu\text{m}$ ) in SLS is approximately 150  $\mu\text{m}$ .

Unfortunately the designed pneumatic actuated system is not sufficient for this purpose. According to our applications, the reverse turnable cylindrical sweeper would be better. However, the electronic system and the code have compatible with any changes on that system. The user need to plug the new actuator into the solenoid I or solenoid II output of Arduino board and change the firmware PWM frequency from the given firmware.

On the other hand, the structural modal analysis results are promising. The first six modes of the designed workstation are given with bottom and without bottom chassis. The analysis shows that there isn't any significant change. The analysis is completed in ANSYS 12.0. The components which are given in Design Layout are sent from Solidworks to ANSYS in an assembly manner. Then the redundant details are decreased and the meshing (pre-processing) is completed in ICEM CFD. The used element geometry in modal analysis is in tetrahedral mixed (due to the 3D solid structure of the system). The boundary conditions are given in the following figures and the total deformations are also included in that figures for each mode.

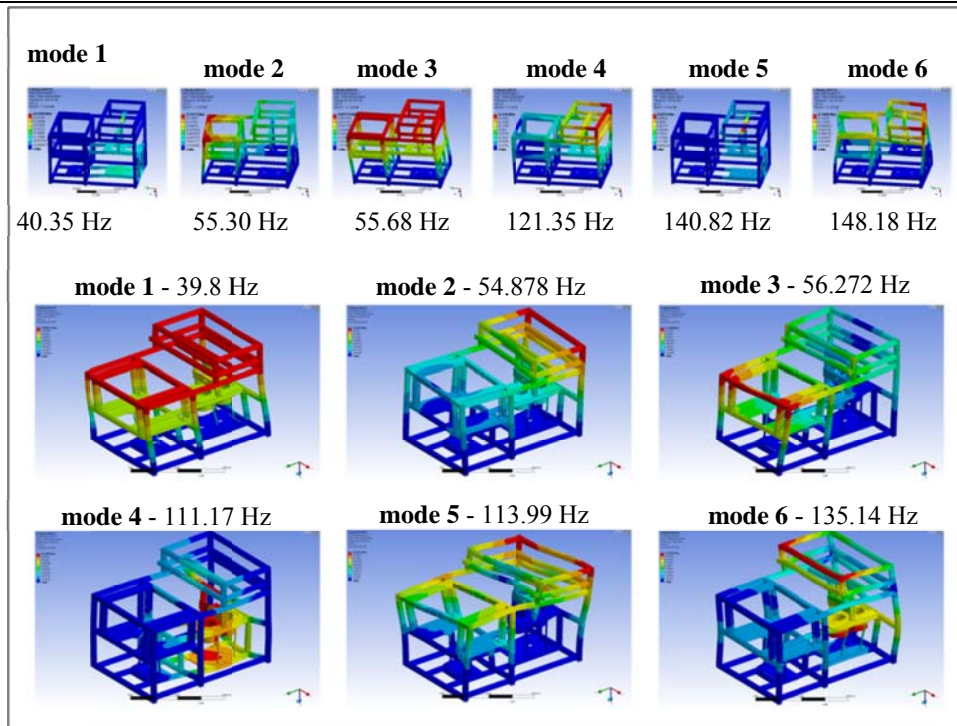


Figure 3.16 Top chassis modal analysis without bottom chassis

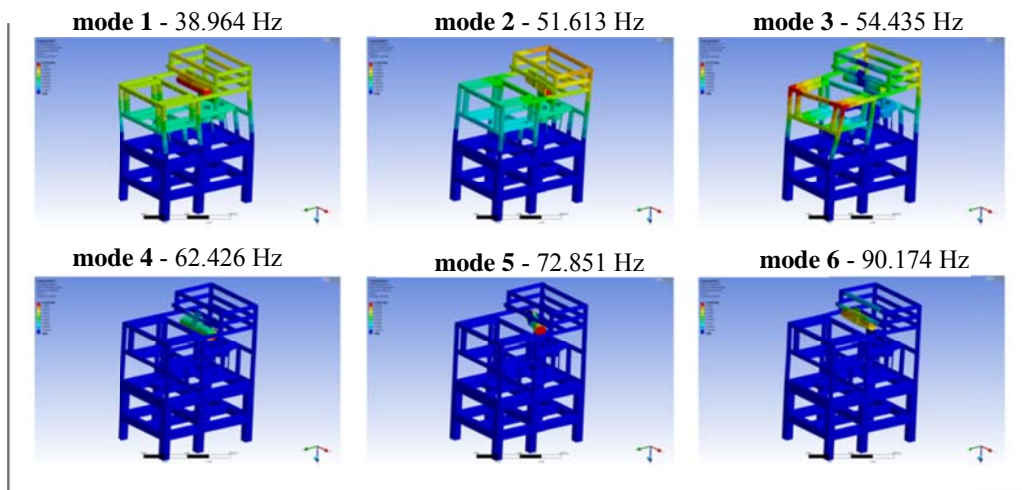


Figure 3.17 Total chassis modal analysis

---

**3.7 Recommendations for Design of Laser Workstation**

In this part of the thesis, the aim was to develop a conceptual design for a research and industrial purposed multi wavelength laser workstation. This conceptual design is deeply analyzed and manufactured in Manufacturing and Automation Research Center and Machine Shop, Koç University. The followings include a few remaining thoughts and hints on the design and the possible future steps required for workstation when they arise by means of funding and time.

- Especially a manufacturing method which uses thermal energy should be considered by adopting some strategies for thermal management. These may increase the costs but the results will be remarkable (i.e. using machinable ceramic base material in cylinders and plates on powder part). These changes create the possibility of sintering
- The placement of material in a structural design usually has the greatest impact on stiffness. These placements should be in the direction of tension, compression or shear except bending. Simple FEA might be useful in order to optimize the structural behavior.
- Special leveler/anti vibration casters might be used in order to damp the system. Thereby, that the system would have mobility by means of transportation of the system. Deeper impedance math between the structure and damping mechanism should be applied in order to understand the required (optimum) parameter.
- Design of Injector based System or Fused Deposition (FD) head: The developed front part of the machine is capable of using  $2^{1/2}$  type manufacturing. It is also possible to add robocasting system via injector exhaust system or fused deposition head. (i.e. in order to produce tissue engineering scaffolds, or other polymeric material manufacturing)
- Strategies for the conceptual design: A number of useful thoughts and ideas are given in design layout part. A timing belt is the final decision on that and included in this system. On the other hand, the servos full closed loop capability might be added into the system in

order to decrease the nonlinearities of this actuation mechanism. This linear encoders are not easy to find in such a speed (10 m/s) and accuracy ( $1 \mu m$ ) together.

-Several structural changes are applied based on FEA results and engineering intuition. However, none of the components thicknesses are optimized due to using the standard components. If the structural components will be fabricated, an optimization would be great in order to produce optimal structure. The total cost of this machine is included in the appendix by adding the equipment list. Thus the future designer may choose more efficient components from different dealers or the same dealers by making deeper analysis. The most important part would be the quality of the components that bought to use in structural components. This is the one of the key points in the design.

- Due to the curiosity during the design study one design change is completed and modal analyses have been completed. There are two modifications; first one thickened the middle Z sigma profit in the main chassis along the height of the machine; secondly redesigned the carbon-dioxide cavity holder to diminish the vibration on that component. (The design studies show that, modes are affected mainly on that component.)

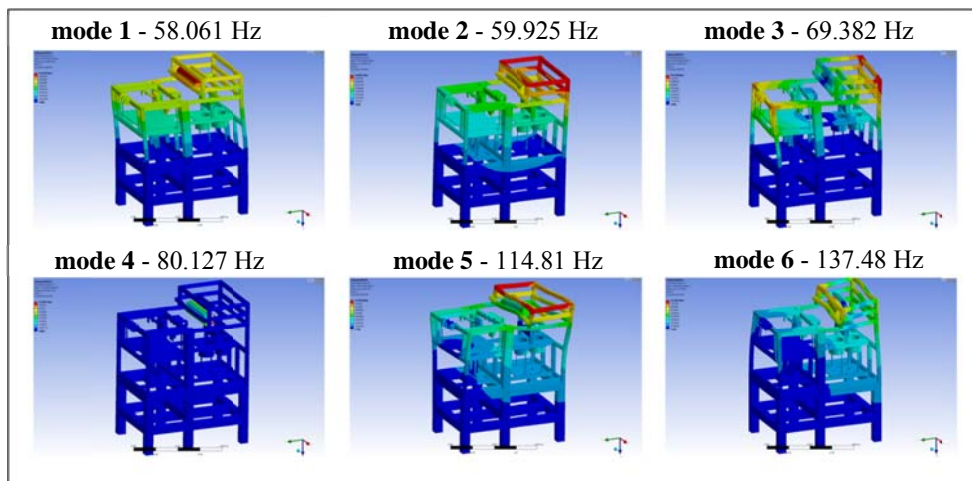


Figure 3.18 Modal analysis of recommended chasis design

**4. Development of Optic-Electronic Hardware and Computer Software for Laser Workstation**

**4.1 Introduction**

Many of the recent laser workstations involve automated devices for controlling the process, such as atmospheric, temperature, laser power, position and velocity control devices. These controlling efforts are due to the necessity of increasing the productivity in a manner of repeatability, accuracy and continuity of manufacturing. Therefore, almost all of the recent products are manufactured using automated processes which referred as automation. The basic elements of an automated system depend on the physics behind the production methodology, which would consist of optics, electronics, computer programming and mechanical design for this thesis. The mechanical design is already detailed in Chapter 3 Machine Design of this study. Herein, optical and electronic hardware and programming parts are deeply focused on.

In the software programming part of this study, the laser workstation instructions are calculated, that command the workstation how perform their specific function. The developed laser workstation can perform the same instruction over and over or it can be programmed to perform multiple jobs simultaneously by using the developed software, which is based on MATLAB and uses lots of its toolboxes.

Merely MATLAB software is not sufficient for commanding the instructions to the system. There is system specific electronic equipment that needs to be used to generate the required operations physically. These physical interactions between the software and the outer world are possible with basic electronic equipment such as microcontrollers, actuators, sensors, etc. An actuator conducts the required movement for the machine and basically, these would be the same like as workhorses of old-fashioned systems. In this thesis, in the front part (Module I) of the developed laser workstation, Alternative Current (AC) servo actuators are used and in the Module II galvanometric scanners and pneumatic piston are



#### **Chapter 4: Development of Optic-Electronic Hardware and Computer Software 81**

---

used in order to position the laser and supply new layer on the manufacturing cylinder, if the workstation is powder based manufacturing mode. In order to control the required movement in precise manner, sensors should be included in to the system. The aforementioned servo motors and galvano scanners have their own built in sensor to measure the movement that they completed. Except position control, the laser power could also be controlled by using the prepared optical/ electronic feedback mechanism, which measures the melt pool radiation and plan to adjust the laser power according to that parameter. The actuator movement and the sensors feedbacks are fed in the controller of the system. The developed laser workstation has a hierarchy in its control mechanism which might be concluded as upper controller (PC with MATLAB) lower controllers (FPGA and microcontrollers with its firmware). These upper and lower controllers control the motion and operation of the system components based on inputs from sensors or the pre-programmed instructions. Simply, a controller would be thought of as "the brain" of the laser workstation. It makes calculations and performs the particular action.

These calculations are mainly used in 2.5 axes based manufacturing. In 2.5 axes manufacturing, which could be solid freeform fabrication (SFF) or machining operation, objects are transformed from computer drawings into tangible objects in a specific axial movement order (X-Y axes and then Z axis). Currently, this methodology is popular due to the developments in digital fabrication and the link between computers and the machines using this technology is strengthening day by day. These technological developments involve some key points which are comprises by solving problems in each step such as importing the geometry, processing the geometry, create physical interaction between the digital and real world and manufacturing this virtual geometry. In importing and processing the geometry step, mainly depends on computer graphics. By using the former dedicated studies in this computer graphics, the stereo lithography file format (STL file) is selected for importing the geometry with its pros and cons which are explained in details in this

#### **Chapter 4: Development of Optic-Electronic Hardware and Computer Software 82**

---

chapter. In order to import the physical part into the virtual part, also a 3D scanner is developed. Both of the importing methods mainly served to the MATLAB software as STL.

The embodiment, which comes from computer aided design (CAD) programs to STL files, is used in prototyping and prototyping allows design engineers to share their work; the manufacturing engineers to estimate of the cost and difficulty of making the designed objects, thus completing a communication channel. Recently, prototypes are possibly manufactured mainly two different machines: computer numerical control (CNC) machine-tools and three dimensional printers (additive manufacturing or free-form fabrication machines). All of them create a physical object that may or may not allow being fully functional products and each has its place in the design and manufacturing process by additive or subtractive manner.

Both the subtractive and additive manufacturing made products which start as a rendering on the computer. CAD is the first step in this process, and the ability to render the three-dimensional physical part depends on the output of the CAD modeler (i.e. Solidworks, Unigraphics, Catia etc.) and on the user of the technology. The contention is developing a laser workstation which inserts a step between the CAD and the physical model.

The calculations mainly depends on importing a CAD neutral format STL as mention before and the solution of the calculations created in a neutral format G-code which is capable of open by the most basic text-read program such as Notepad, Textpad or Wordpad. The details are given in the following parts on G-code. Generated G-codes are sent to developed workstation line by line to control the process properly.

In the following paragraphs, the mentioned details are explained in details on laser optics, laser hardware interfaces and developed laser material processing software.

**4.2 Laser Beam Delivery**

The laser workstation is using two different type of the laser, an IPG YLP-1-120-50-50-HC Ytterbium fiber laser (50 Watt pulsed wave with Q-switching) and Teknofil  $CO_2$  (17 W continuous wave  $CO_2$  laser). The laser beam on IPG exits the cavity between 6 to 9 mm beam diameters with a beam quality [ $M^2$ ] of 1.5 to 2 [1]. The beam delivery system of Ytterbium Fiber laser initially consisted three coated mirrors, one dichroic mirror, Raylase SuperScan galvanometer and laser feedback system as given in Fig. 4.16. On the other hand, the  $CO_2$  laser is capable of used the same system by changing a suitable mirror which could reflect the far infrared wavelength but transparent to 900 -1000 nm. The scanning system consists of a pair of scan head instrumented with 15 mm clear aperture for Ytterbium Fiber [1064nm] and  $CO_2$  [10640 nm] wavelengths. The scan head communicate with and receive motion signals from an Altera FPGA and Motorola 32 bit microcontroller based Raylase SP-ICE 2 controller. The scan controller receives motion and laser switching commands from the software in MATLAB.

At the end of the IPG fiber there is a collimator which serves as the purpose of expanding or "up-collimating" the incident laser beam to a larger diameter collimated beam. Expanding the diameter of the beam incident on the focusing lens allows it to be focused to a smaller diameter at the focal plane. The diffraction limited spot size for a singlet lens can be estimated by the diameter of the first minimum of the Airy diffraction pattern in the focal plane and is given by,

$$d_{diff} = 2.44 \times \lambda \times \frac{f}{d_0} \quad [4.1]$$

where  $\lambda$  is the wavelength,  $f$  is the focal length and  $d_0$  is the diameter of the beam incident on the focusing lens. It is necessary to emphasize that Eqs. 4.1 predicts the theoretical spot size assuming the laser beam incident on the lens is perfectly collimated and composed of pure  $TEM_{00}$  mode. The diameter of a multimode  $TEM_{plq}$  beam is given by [2]

#### Chapter 4: Development of Optic-Electronic Hardware and Computer Software 84

---

$$d = 2.44\lambda \frac{f}{d_0} (2p + l + l) \quad [4.2]$$

In practice, industrial Ytterbium Fiber lasers always have a finite divergence and multiple modes. Multiple modes result in a larger beam diameter  $d > d_{diff}$ , typically increasing with input power (i.e. lamp current in the case of lamp excited solid state ytterbium fiber lasers) as higher order modes are emitted. Thus, rather than predicting the true focused beam diameter, Eqs. 4.2 merely serve as a lens selection guide. One method of maintaining beam quality across the input power range is to introduce a limiting aperture ahead of the laser cavity. The aperture only permits lower order modes to be transmitted at the expense of reduced peak power lost to the higher order modes.

Ytterbium fiber (  $1.06 \mu m$ ) laser beam exiting the laser cavity, at the end the collimator expands the beam for a diameter of 6 to 9 mm and pass through a 160 mm focal length lens, the diffraction limited spot size is around  $20 \mu m$ . Finer spot sizes would be desirable in laser material processing esp. on micro machining for better feature definition and increased laser energy density. An additional beam expander would be possible which is depending on the clear aperture size of the galvanometric scanner. If we roughly calculated, the maximum beam expanding factor is approximately 1.5. This means that the minimum laser spot diameter could be  $13.3 \mu m$  with this selected galvanometric scanner, which has 15 mm clear aperture. The expander allowed up-collimating the maximum 9 mm laser beam exiting the cavity to 13.5 mm. The existing focusing lens for Ytterbium Fiber having a 14.92 mm clear aperture was retained [3]. The  $CO_2$  lenses have also similar properties. These limitations prevented the usage of a larger expansion ratio over 15 mm by using beam expander and hence smaller spot size.

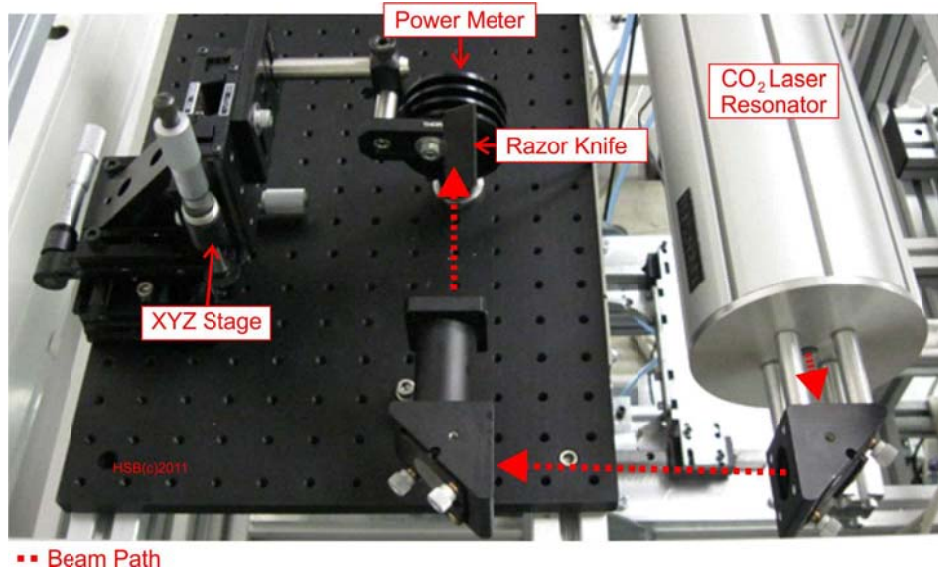


Figure 4.1 Knife edge test setup for  $CO_2$  laser

The optical characteristics of Ytterbium Fiber laser is given in IPG's product datasheet, however, the  $CO_2$  laser does not have any particular datasheet and the optical properties of  $CO_2$  laser is acquired with Foucault Knife Edge Test with a plano-convex lens as in Fig. 4.1 [4]. Thus, the laser beam exiting a  $CO_2$  laser cavity propagates this minimum diameter known as the waist and expands from there on, as shown in Fig. 4.2. The direct calculation of laser beam waist is redundant from exiting of the resonator for this survey, because the aim is not design a complete optical system. The aim is focusing the light by using  $f-\theta$  lens at the exit of galvanoscanner in order to process a material. However, in future applications if there is a necessity for smaller beam diameter, the divergence value could be calculated at the exit location of the resonator and fitted into a curve which is expected to get. Afterwards an optical design might be accomplished in order to decrease the spot diameter which is limited with the current clearance input of galvanometric scanner. In addition to that, current laser beam delivery and focusing optics were selected to accommodate a Teknofil  $CO_2$  laser. This laser has 20 Watts continuous wave (CW) power.  $CO_2$  Lasers

## Chapter 4: Development of Optic-Electronic Hardware and Computer Software 86

follow a Gaussian intensity profile and propagate hyperbolically. The beam quality of  $CO_2$  laser is characterized by  $M^2$  as it is shown in Ytterbium Fiber laser.

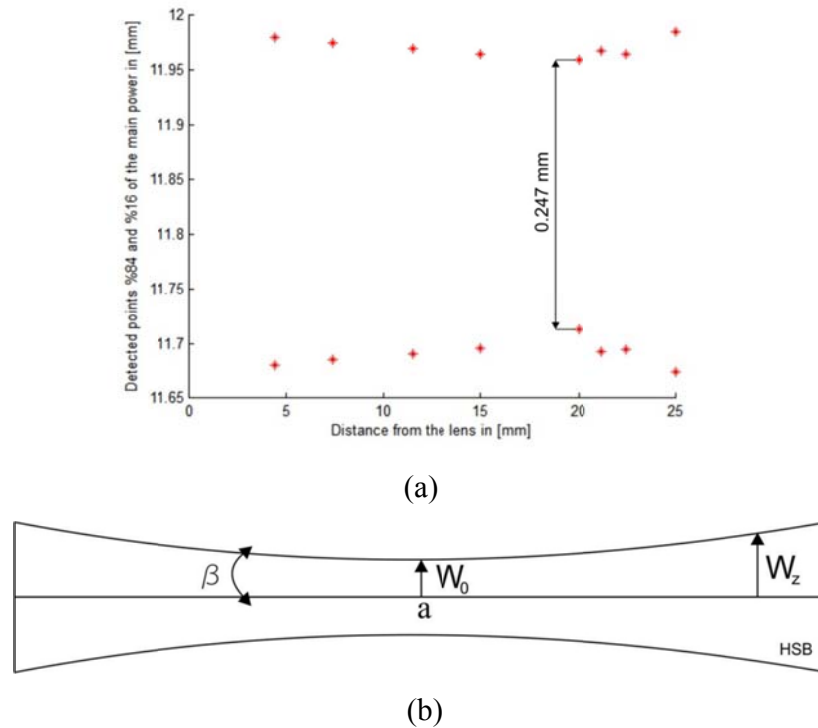


Figure 4.2 (a) Knife-edge test result, (b) Hyperbolic profile of  $CO_2$  laser beam propagation. This number determines the deviation of a laser beam's quality from that of an ideal, single mode  $TEM_{00}$  (transverse electromagnetic mode), pure Gaussian intensity distribution beam.  $M^2$  is defined as [5]

$$M^2 = \left(\frac{\pi}{4\lambda}\right) \times (2W_0 \times 2\beta) \quad [4.3]$$

where  $\lambda$  is the wavelength,  $2W_0$  is the beam diameter [mm] at the waist and  $2\beta$  is the total divergence angle (milliradian) of the beam. For a  $TEM_{00}$  beam,  $M^2=1$ , beam divergence is at its lowest and beam diameter is the smallest at all points along the path of propagation. Hence, for an industrial laser the closer its value of  $M^2$  is to 1, the higher its beam quality.

#### Chapter 4: Development of Optic-Electronic Hardware and Computer Software 87

With focusing optics and this quality is considering the fact that most industrial ytterbium fiber lasers have  $M^2$  typically one order of magnitude larger owing to the small wavelength. With known  $M^2$ , the hyperbolic relation for the beam radius ( $1/e^2$ ) as a function of distance from the laser's exit is defined by [5]

$$W(z) = W_0 \left\{ 1 + \left[ \lambda M^2 \frac{(z-a)}{\pi W_0^2} \right]^2 \right\}^{\frac{1}{2}} \quad [4.4]$$

where  $W(z)$  is the radius at a distance  $z$  from the laser exit and  $a$  is the distance of the waist from the laser exit. An approximation for the beam diameter at the focal plane of a focusing lens gives [5]

$$2W_f = \frac{4\lambda}{\pi} \frac{f}{2W_{lens}} M^2 \quad [4.5]$$

where  $2W_f$  is the beam diameter at the focal plane,  $f$  is the focal length of the focusing lens and  $2W_{lens}$  is the beam diameter incident on the focusing lens. Substituting equation 4.3 into equation 4.5 yields,

$$2W_f = \frac{f}{2W_{lens}} 2W_0 2\beta \quad [4.6]$$

From this equation 4.6, it is apparent that given a fixed focal length and a laser with fixed  $2W_0$  and  $2\beta$ , a larger diameter beam incident on the focusing lens results in a smaller diameter focused beam. The technique of obtaining this effect is to expand or up-collimate the beam via a beam expander prior to focusing it. If the beam is expanded, it is recommended that the expansion be done at the beam waist since the beam has the highest degree of collimation (minimum divergence) and hence least distortion at this point.

The distance between the present location of the laser cavity's exit and the location on the laser table where the feedback mirrors presented might be exactly the "exit to waist" distance for this particular laser. The laser beam exits the cavity at approximately 6 mm diameter ( $1/e^2$ ). A 2x beam expander might be used in a design to acquire smaller spot diameter as mentioned before and the same clearance parameter of the galvoscaner limits

## **Chapter 4: Development of Optic-Electronic Hardware and Computer Software 88**

the design of beam expander (max. 2.5X for this case). The measurements, calculations and design should be completed according the same criteria as in Ytterbium.

In order to provide a stable, flat, covered platform for laser beam delivery and optics, an optical breadboard implemented on the system. The table, made of 12.7mm of thick aluminum tooling plate flat to  $\pm 0.15$  mm over  $0.3 m^2$ . A number of M6 holes at 25.4 mm spacing were drilled and tapped to enable easy and flexible installation of optics as shown in Fig. 4.16. A combination of right angle kinematic mounts and laser tubes was assembled for the beam delivery of this table to allow the galvanometer scanners to redirect the beam into the fabricating piston. Since accumulation of dust on laser mirrors and lenses can lead to severe degradation, fans would be installed on the cover to provide continuous purging air flow over the optics.

Installation of the breadboard with associated chassis mounts resulted in an increase in the height of the scanners above the bed by a possible 170 mm to a total of 320 mm. The laser beam delivery configuration and experimental setup for monitoring the laser material processing is shown in Fig. 4.16. This setup is constructed on a breadboard for an in-house developed machine. Similar monitoring systems have been developed for other laser based production processes as laser cladding [6-8], laser beam welding [9-12], laser cutting [13], laser hardening [14] and selective laser melting [15]. In the developed setup, the laser source is deflected by means of a reflective mirror which transmits the visible spectrum.

### **4.3 Hardware Interfaces**

Generally, in the industry the feeding system, laser position and velocity, atmosphere and pistons are controlled by combinational work of the electronic components such as motor drivers, microcontrollers and computers. In this thesis, as parallel to the industry, the aforementioned properties such as feeding, laser position and velocity etc. are also automated. However, during the prototyping stage, in some manner the laser workstation is tested manually due to the tests of functionality. After doing proper tests the designed



#### **Chapter 4: Development of Optic-Electronic Hardware and Computer Software 89**

hardware for laser workstation will be compatible with fully automated system because the software algorithm is already written in order to do it.

The developed machine design is mentioned in the machine design chapter of this work. On the other hand, the electronic and software based issues are not considered before and will be given in this section. Functionally, by using with the proper head apparatus, the front (Module I) of the developed workstation might be used for laser cutting/ fused deposition modeling operation and the back (Module II) of the machine might be used for 3D laser engraving (machining) or powder sintering operations, as shown in Fig. 4.3.

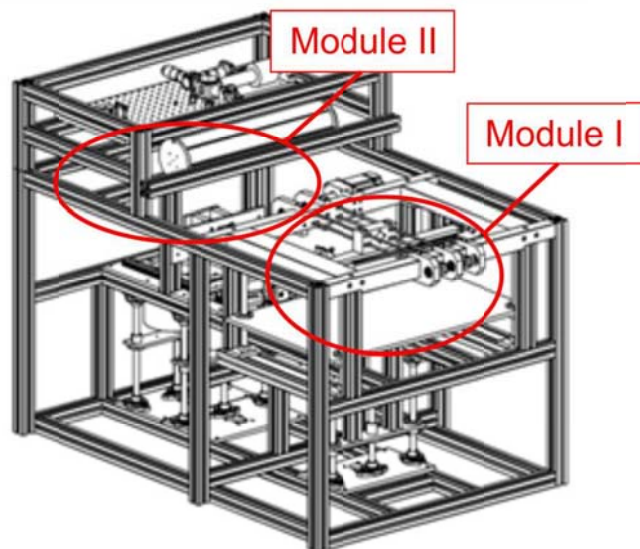


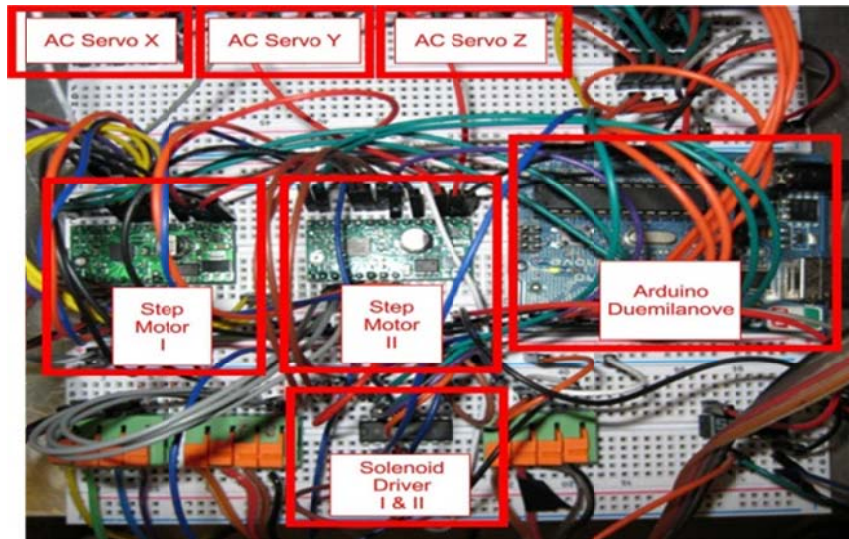
Figure 4.3 Modules of the designed laser workstation

The developed software is capable of generate the required signal to the outputs for additive and subtractive manner in G-Code format as given in the following sections.

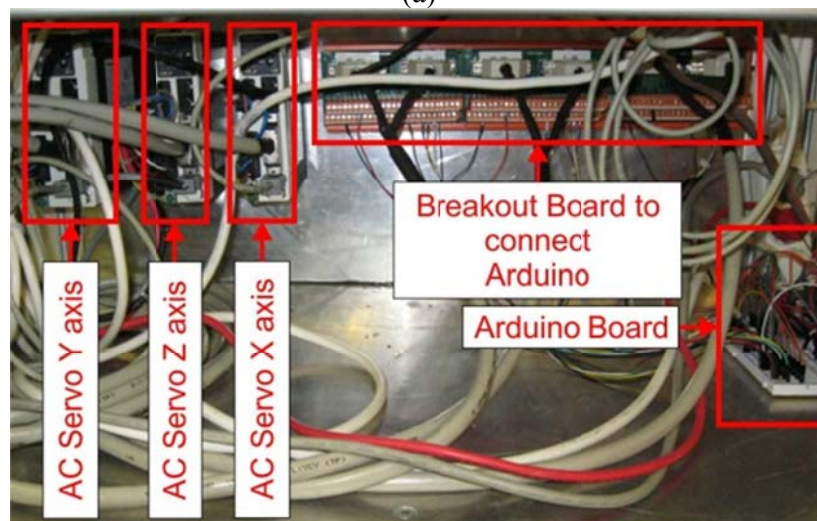
The powder delivery actuation is based on pneumatic linear sweeping motion. The used Dr. Blade method is controlled by pulsed signal given to the solenoid valves. The fabrication and storage cylinder pistons are driven by E-Minebea step motors. The Pololu A4983 step motor driver is used in order to get the highest resolution with a quite cheap solution, Fig.

## Chapter 4: Development of Optic-Electronic Hardware and Computer Software 90

4.5. Raylase SP-ICE 2, Raylase IPG Interface Card and Arduino 8 bit board is the main electronic components which are communicating with the developed MATLAB software.



(a)



(b)

Figure 4.4 The wiring of the developed electronic interface (a) Arduino Board (b) Electrical Panel

## Chapter 4: Development of Optic-Electronic Hardware and Computer Software 91

In this work, an alternative Xilinx Spartan 3 FPGA board is also developed with 32 bit PIC32MX microcontroller in order to control galvanometric scanner and laser power control, but this card is not included to this thesis due to some drawbacks. During research described in this thesis, several improvements are made to the hardware and software interfaces, especially in the areas of laser scanning and laser power control that resulted in huge advancements in the ability to process materials successfully. From a process control perspective, it is instructive to understand these improvements in the following section.

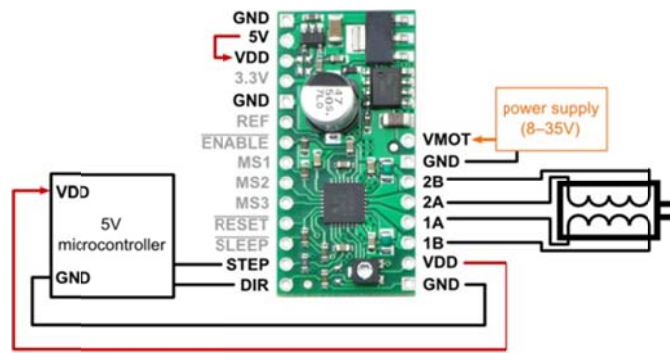


Figure 4.5 Pololu A4983 Step Motor Driver Wiring Schematic

### 4.3.1 Scan Control for Flying Optics (Module I) and Galvoscaner (Module II)

Two of the most important input parameters for laser scan control in direct laser material processing are laser scan speed and scan spacing as given in analytical model (Chapter 2). Therefore both of the modules of the designed machine have very high speed boundaries in the most precise condition (up to 10 m/s with changeable resolution). For positioning the laser beam by using galvanometric scanner for module II, the scan controller implements a rectangular grid coordinate system that is subdivided into 65536 ( $2^{16}$ ) points along each axis as seen in Fig. 4.5 [16]. The coordinates could be easily transformed in any type of units in the software before creating the G-Code. However, the software should be transforming the selected unit type into bits, as the Fig. 4.6, before sending through library functions of SP-ICE 2 card.



Figure 4.6 Scanning system field size and bit number relation

The X-Y scan heads have a  $\pm 20^\circ$  rotational freedom about their center positions. Hence, for each point located on the scan plane, there exists a transformation from scanner angular coordinates to scan field rectangular coordinates and this implemented to the MATLAB software while generating the G-code for module II. The resolution by means of linear motion for the scanner can execute along each coordinate axis is defined by,

$$LSB = \frac{1}{65536} \times Field\ Size \quad [4.7]$$

The field size is governed by R, the scan radius [mm], which is the distance from the axis of the final mirror to the center of the scan field area as shown in Fig. 4.7.

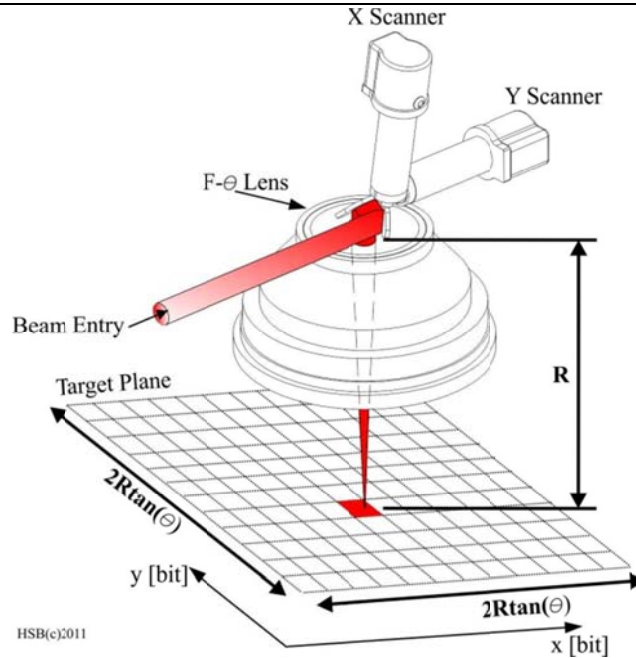


Figure 4.7 A Schematic of the Scan Field

For the  $f-\theta$  lenses, the field size is given by  $Field\ Size = 2R\tan\theta$  [mm] and therefore  $LSB = 2R\tan(\theta)/65536$  [mm].

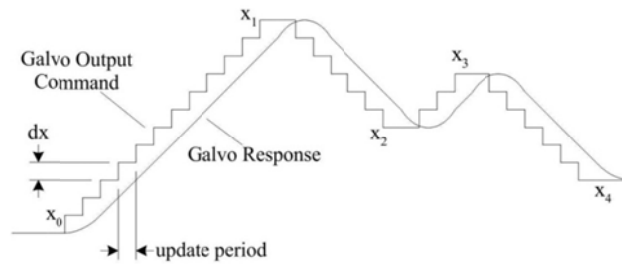


Figure 4.8 Micro-vector Operation

The galvoscaner divides each scan vector motion into a series of smaller segments or steps which is called micro-vectoring as shown in Figure 4.7. The magnitude of each step is determined by a user input parameter known as step size (SS). SS is a number indicating the size of each step in less significant bit (LSB) units. The step period (SP) is another user

#### **Chapter 4: Development of Optic-Electronic Hardware and Computer Software 94**

input parameter. SP is the time taken by the scanner to move the beam a length of SS LSB's. These SP and SS are also depends on the galvomotor drivers. For the developed system, the step period (SP) is expressed in  $\mu s$  and the allowed for SS is 1-32767 LSB's and for SP is 20-65534  $\mu s$ . Therefore, the scan speed is

$$V = \frac{SS \times LSB}{SP \times 10^{-6}} = \frac{2R \tan(\theta) \times 10^{-6} \times SS}{65536 \times SP} \quad [4.8]$$

$10^{-6}$  used in the formulae is for converting the seconds into microseconds. For uni-directional or bi-directional raster scanning, the scan spacing is the spacing between two successive scan vectors or the case of concentric contour scanning or spiral scanning, the scan spacing is the spacing between two successive  $360^\circ$  scan paths. For a given geometry, the smaller the scan spacing, the higher the number of scan vectors needed to "fill" the geometry. For processing a part, the scan spacing is a process parameter that is determined at the time of creation of the scanning geometry file that is derived from the sliced CAD file. The smallest scan spacing theoretically is LSB as given before. For the laser workstation, with the beam delivery set-up described before, the scan radius R is 160 mm. Hence, the smallest scan spacing available is optic dependent and for this case  $1.7 \mu m$ . For direct laser material processing of metals and cermets in general, fine spacing or order 127-5  $\mu m$  (0.005-0.0002 inches) are desirable for full density processing, superior surface finish and to avoid undesirable defects such as hot tearing and solidification cracking [17].

On the other hand, for the module I of the developed laser workstation, the workspace is 220 mm x 520 mm. The changeable head apparatus gives to chance to change the manufacturing type from laser cutting into fused deposition modeling as mentioned before. However, different from module II this part of the machine is using mm based scale and the measured tolerances are depends on the driver electronic gear ratio. The selected industrial servo drivers have the capability of working with the electronic gear ratio which mainly changing the gain from the driver. However, the higher gear ratio means higher velocities, but there is a tradeoff in resolution. In addition to that, if the selected gear ratio is beyond

## Chapter 4: Development of Optic-Electronic Hardware and Computer Software 95

the limits, an error is generated in the driver level and the drivers are not functional. The velocities of the module I is adjusted by using the G-Code command in each line as standard G-Code feedrate command F. Then, the microcontroller sets the pulse duration according to given F command and generate pulses related to the calculated feedrate delay and distance, the algorithm is given in Microcontroller G-Code Parser in Appendix 4.1. The wiring diagram of the designed system is given in the Fig. 4.9. The reader should understand the code and hardware before doing any changes.

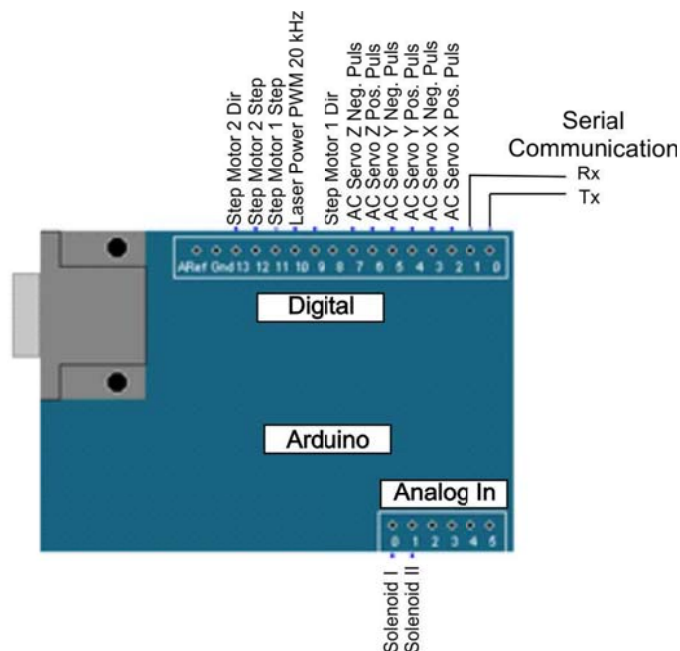


Figure 4.9 The wiring schematic of Arduino

### 4.3.2 Laser Power Control

In developed laser workstation, the laser power is changeable with power control signal of the Ytterbium (Bit 1-8 in DB25) and the low state duty cycle (DC) percentage of Teknofil  $CO_2$  laser. The details are given in this section of this study. In addition to that, the proper feedback mechanism makes sure the required power is given to the process according to selected thermal measurement method. It could be also keep constant during a layer scan or

#### **Chapter 4: Development of Optic-Electronic Hardware and Computer Software 96**

during entire part build. Studies, both theoretical [18] and experimental [19] have proposed real-time control of laser power for improved laser material processing. During literature survey, control of laser power was found to be utmost importance to eliminate a defect known as balling in powder based systems. Balling typically occurs at the starting point or starting vector of a scan and results in formation of clumps or agglomerates of the melted and resolidified material. These defects typically project out of the plane of the powder bed such that when powder delivery for the next layer takes place, the part being built is shifted owing to contact between the roller and the agglomerates. This results in unacceptable loss of geometry. During this literature survey, it was found that ramping the laser power from minimum to desired level across the first few scan vectors eliminates balling [17]. The proper adjustment in used dynamic link library and Arduino code it is possible to set the ramping. The first trials were done manually and these manual trials confirmed the necessity of a developed controlled laser power control system.

In order to implement computer control of laser power, a Raylase IPG interface card is selected as shown in Fig. 4.10. The details are given in Appendix 4.1 - Raylase IPG Interface Board on electronic wiring and computer program implementation.

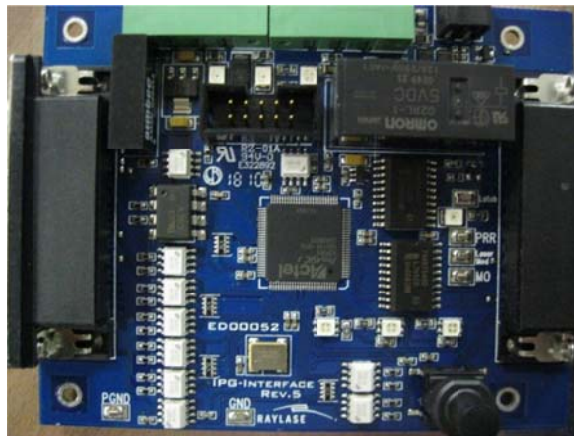


Figure 4.10 Actel FPGA Based Raylase IPG Interface Board



#### **Chapter 4: Development of Optic-Electronic Hardware and Computer Software 97**

---

Practically, the laser is controlled via signals applied to the DB-25 connector through Raylase IPG Interface Card. Please refer to the connector interface description table above for pin designation and operating levels. DB-25 is a standard output, which has 25 pins on it, from pin 1 to 8, the eight bit bus for the output power setting. Pin 1 is assumed as the least significant bit (LSB) and pin 8 is the most significant bit (MSB). This means that the 0...255 should be applied to these pins, which corresponds to the power tunability 0...100% of the specified nominal value. Pin 9 is the "Latch" control wire in order to store power settings into the laser. The data are stored in to the laser simultaneously with the rising (type B, B1) or falling (type B2) edge on the pin 9. Data on the pins 1-8 should be stable during the following time frames for type B: 500 ns before rising edge on pin 9, for type B1: 1us before and after rising edge on pin 9 and for type B2: 20 us after the falling edge on pin 9. IPG recommends supplying single positive pulse with duration longer than 2us to latch the data into the laser. Time interval between adjacent latching pulses should be longer than 100 us (latching frequency less than 10 kHz). The red guide option is beneficial property for the view of the material processing due to proper adjustment of the processed material. Therefore, Pin 17 is connected to 5+VDC power supply voltage for the guide laser. The red laser can operate independently of the main +24VDC supply. This ensures safe laser class 1 operation of the module, even in case of laser electronics malfunction. In order to control red guide laser Pin 22 is used. By applying HIGH to switch the guide laser ON and LOW to switch the guide laser OFF. The laser is activated the Master Oscillator (MO) and Booster modules of the resonator as shown in Figure 4.10. Pin 18 is the Master Oscillator (MO) ON/ OFF signal. The MO should be switched ON at least 7 ms before switching ON the Booster (BS). It can be switched OFF simultaneously with BS. After switching ON the MO, the laser starts to consume more electrical power and emits remnant power to the output even when BS pin 19 is LOW. The average optical power of the operating MO passes through the BS without amplification and its average value is

## Chapter 4: Development of Optic-Electronic Hardware and Computer Software 98

dependent on laser type (refer to the specification). For standard models it is less than 50 mW after the output collimator.

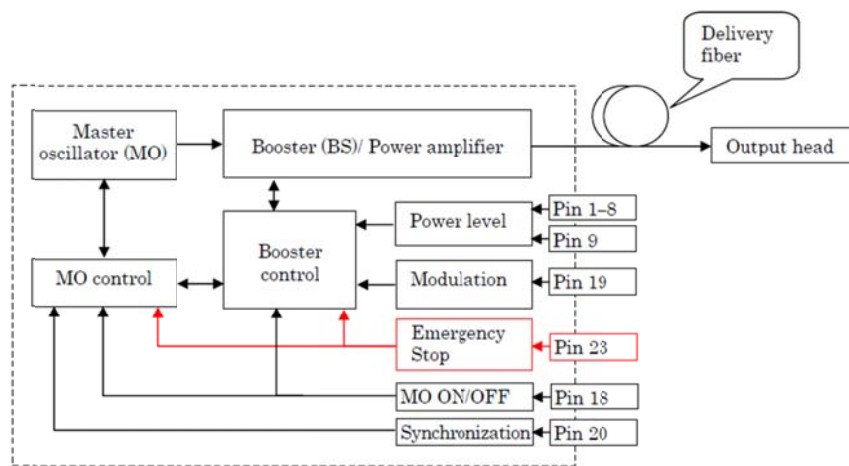


Figure 4.11 Interface Pin and Module Relations of IPG YLP-1-120-50-50-HC Ytterbium Fiber Laser

Note that, the MO should be switched ON at least 7 ms before switching ON the Booster. In case of switching ON BS while the MO is off, the laser does not start to emit. In case of switching ON the BS and later the MO, the laser starts to emit in range from 1 to 7 ms after switching ON the MO. The last two cases are not specified operating regimes and should be avoided during handling with the laser. BS is switching ON simultaneously with rising edge on the pin. If the HIGH level was applied to the pin before supplying the main voltage, the laser does not recognize that as the BS switching ON signal. The pin should be dropped and set to HIGH level again using described switching ON procedure. If the pin 18 was also in the HIGH state before supplying main +24VDC supply it should be also dropped to the LOW while pin 19 stays LOW. Pin 20 is used for the Synchronization, which combines Pulse repetition rate (PRR) within specified operating range (the optical specification should be examined for proper PRR limits). The laser emits pulses simultaneously with the rising edge of the signal.

#### **Chapter 4: Development of Optic-Electronic Hardware and Computer Software 99**

If the supplied PRR is out of the specified range (or missing the signal) the laser safety circuit will substitute missing pulses or limit the PRR. The laser emission is not allowed simultaneously with the guide laser operation. This means that BS is blocked internally during the guide laser operation. If the Emission Modulation (pin 19) was set to HIGH level during guide laser operation, the laser will not emit power, and will not start to emit even after switching OFF the guide laser. In order to reactivate the laser emission (emission modulation) the pin should be reset. It is allowable to switch ON and OFF MO during guide laser operation. As any type of industrial machine, emergency stop is mandatory specification of the laser system; therefore, Pin 23 is used. It should be set to HIGH for normal operation. In case of dropping this pin to LOW state (even for a short period) the laser automatically switches OFF (similar state when both MO and BS pins are OFF) independently of other control signals. It is necessary to drop both MO and BS pins (if they were in HIGH state) to restart laser operation. For laser operation pin 23 should be set to HIGH at least 2 $\mu$ s before supplying ON signals to MO and BS.

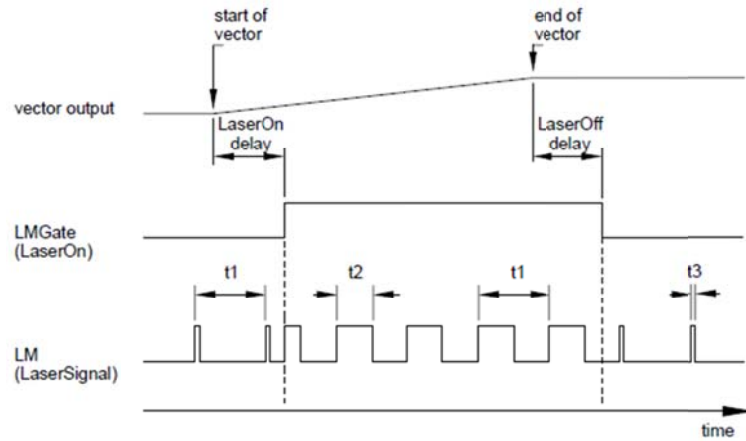
This simple procedure is used in order to use the laser in required power. The purchased Ytterbium laser resonator equipment is very expensive and maybe redundant for a starting project like this research. However, this expense is made sure that the laser has robust and stable laser output for using in material processing and this laser is useless without the developed computer software by means of position, velocity and power settings adjustments. Therefore, MATLAB software is used to control the process and give proper calculations. The developed process control software was written in MATLAB (Windows 7 operating system). MATLAB software sends the coordinates and commands for scanning to the SP-ICE 2 controller, laser scanning is initiated only after all the coordinates has been downloaded into the scan controller's vector table. The time taken to load list of vectors is increased as the number of vectors is increased. Thus, the time delay between starting a vector list's load operation and initiation of scanning is variable. In addition, the Raylase

#### **Chapter 4: Development of Optic-Electronic Hardware and Computer Software 100**

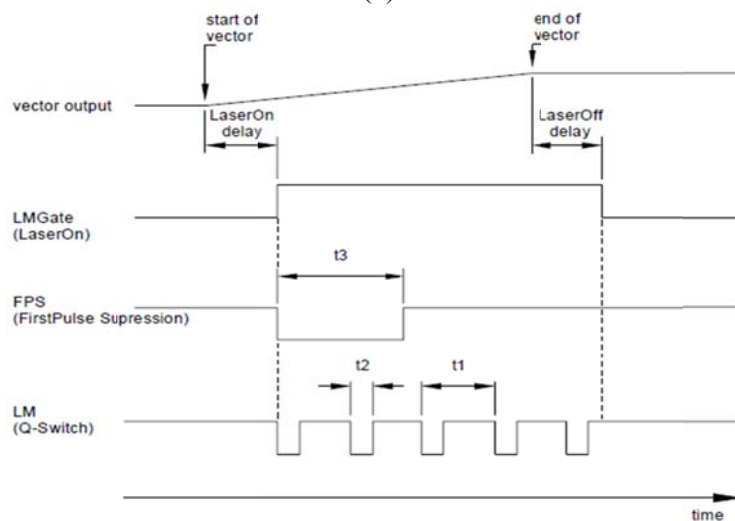
SP-ICE 2 supports double buffering; this provides the ability to load a vector list ahead of manufacturing time. Each buffer has a job limit as 500000, which is well enough for the workspace used in the processing operation.

On the other hand, for Teknofil  $CO_2$ , the duty cycle of the LOW Pulse Width Modulation (PWM) signal is used to control the power. Except the SP-ICE 2 card, the  $CO_2$  laser is also controlled through the Arduino based microcontroller (i.e. for the Module I of the designed machine). This electronic hardware and its firmware is explained in relevant section by details. It is also to initiate the emission by using multiple revolutive potentiometer and start button. However, this is not guarantee robust and repeatable process parameters due to the manual operation.

The mentioned laser power synchronization with the laser position is an obligatory specification of this system for  $CO_2$  and Ytterbium fiber laser. In order to understand the synchronization of laser scanning for a particular layer with the start of the laser power control, it was necessary to have a timing diagram according to the working mode of the selected laser as in Fig. 4.12. On the other hand, the power control of the  $CO_2$  laser is manipulated with low state duty cycle (DC) of 20 kHz PWM signal. The BNC input of the power supply for resonator is the physical input for that purpose. This hardware is controlled in Module I via Timer 2 of the Arduino and Port C laser I/O interface. In order to turn off laser, DC should be 100 % (like continuous 5V) and for 50% power output DC should be 50% LOW.



(a)



(b)

Figure 4.12 Laser Power Control Signals (a) Mode 0 – ( $CO_2$ ), (b) Mode 1- (Ytterbium)

Two alternate methods were implemented to prevent overexposure due to finite time delay for laser power ramp-down at the end of a scan. Generally in the literature, the first method comprises electronically closing the mechanical shutter placed between the laser cavity and front laser mirror upon receiving the turn off signal. The second method is to adjusting the proper delays before and after laser on. In the latter case, the power ramp down takes place

## **Chapter 4: Development of Optic-Electronic Hardware and Computer Software 102**

via software, therefore need proper adjustments before using it. Table 4.2 illustrates this synchronization capability of the motion comes from the delays.

### **4.3.3 Optical Feedback System**

Even in the process modeling part a system model is given, there are lots of boundary conditions and assumptions in order to calculate the system response. These assumptions simplify the system, but also alienate from the real process and estimating with an error. In literature, tons of other modeling approaches beyond the given in Chapter 2 are available such as [13, 20, 21] Some of the given methods depends on the “black box modeling” (via system identification) of the process and controlling according to that identified system. In addition to that, the feedback system is also preferred method for validating the calculations of given system model.

Basically, the feedback systems are the part of the control systems which has inputs and outputs. The changes of input parameter are used to hold the system in a requested state. On the other hand the system response of the given input is referred as output which gives a measure of the state of the process and its quality. The feedback system should be measure processing inputs such as beam power, size and velocity (secondary outputs). Other process parameters are detailed in several sections such as software details, process modeling etc.

Real time measurement of the primary outputs of the system is difficult to detect directly and extremely important, while the process is in progress. These primary outputs would be penetration depth, bead width, reinforcement, heat affected zone (HAZ) size, microstructure, mechanical properties (hardness and strength), residual stresses and defects (such as porosity, inclusions, cracks , undercut etc.) whose require destroying the part to measure. Oppositely, the secondary outputs of laser processing which are temperatures (temperature distribution, peak temperatures, cooling rate), melt pool behavior and acoustic emission are easier to measure.

## Chapter 4: Development of Optic-Electronic Hardware and Computer Software 103

In addition to that, ensuring the process quality is necessary by measuring the outputs of interest. The process outputs, however, often need special detecting devices. Theoretically, these devices have to be robust in hostile environment, repeatable, reliable and inexpensive. In this section of the chapter, some of the sensor and sensing technologies, which are commonly used during laser material processing, are explained.

The most commonly used sensors for real-time monitoring are acoustic emission, audible sound (acoustic sensing) and infrared/ ultraviolet detectors. These sensors are generally used for measurement of secondary outputs as shown in Fig. 4.13.

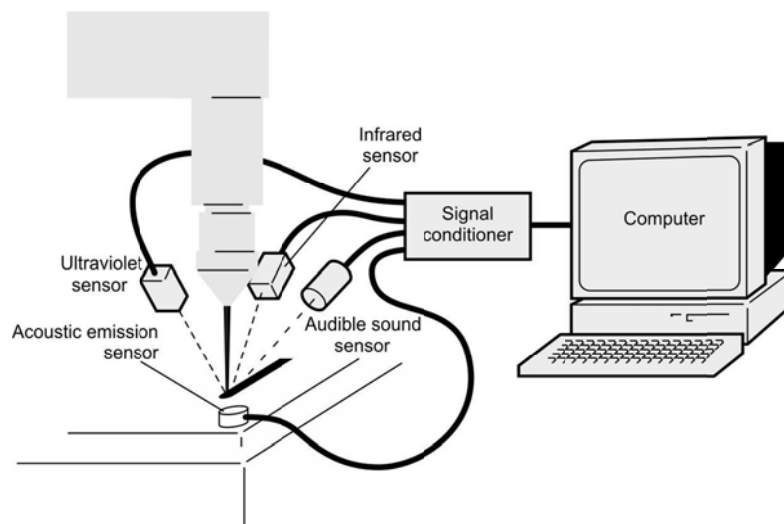


Figure 4.13 Audible sound, acoustic emission, infrared and ultraviolet sensing feedback system

Herein, the rapid release of elastic strain energy within a material is caused due to the stress waves. These waves are measured through sensors referred as Acoustic Emission (AE) transducers which are linearly change the small displacements into electrical signals.

The low frequency sound would be detected with audible sound emission method. During laser processing between 15 Hz to 20 kHz acoustic signals are generated. The source of the generated acoustic is the pressure variations at the process source; this sound is acquired by using a microphone. The measurement method is using pressure and velocity of the fluid at

#### **Chapter 4: Development of Optic-Electronic Hardware and Computer Software 104**

the source and from the resonant frequency of the detected signal the cutting front geometry especially kerf width and depth of the cut.

Except acoustic emission and audible sound sensing, the IR/ UV radiation measurement is other possibility for getting feedback from laser material processing. A relation is inevitable by its nature between high-temperature plasma and emitted ultraviolet radiation which would provide a predictive indication of laser processing. In addition to that, the changes in the infrared signal also give on variations in the melt pool. Generally, the infrared radiation is measured with a germanium photodiode fitted with silicone filter with a spectral range from 1.0 to 1.9  $\mu m$  which is similar with the used one in this thesis. Other essential measurement is detected with gallium phosphide (GaP) photodiode which has spectral range 0.19 to 0.52  $\mu m$ . The generated laser power is proportional with the signal intensities which easily affected by atmospheric conditions. The Fig. 4.16 shows for the possible setup which is not suitable for this study. However, in order to develop better feedback system the former studies should be understood with the physics behind it.

In the literature, especially in the heat transfer books, the fundamentals of radiations are given [22]. Thus, it is good to know about these physical phenomena “radiation” for the future developments of the laser feedback system. Physically, above the temperature of absolute zero (0 K), all objects emit infrared radiation, which is part of the electromagnetic spectrum from 0.75 to  $10^3 \mu m$ . The ratio of the radiant energy with compare to the blackbody at the same temperature is defined as emissivity. Emissivity is also depends in which direction of the incident radiation came and is highest in the normal direction (proportional with cosine). The infrared radiated bodies would be classified into three types related to the spectral characteristics of radiation; Blackbody radiation, emitted from a body with an emissivity of one. Theoretically, this body absorbs all incident radiation but reflects none. Graybody radiation may be defined as one for which  $\alpha_\lambda$  and  $\varepsilon_\lambda$  are independent of  $\lambda$  over the spectral regions of irradiation and the surface emission. In selective body (non-



**Chapter 4: Development of Optic-Electronic Hardware and Computer Software 105**

gray body), the emissivity varies with wavelength. The radiated power [ $W/mm^2$ ] depends on the temperature of the body and the wavelength. For example, according to Planck's Law, for blackbody case the intensity would be,

$$I_\lambda = c_1 \lambda^{-5} / (e^{\frac{c_2}{\lambda T}} - 1) \tag{4.9}$$

Here,  $c_1 = 2\pi c_0^2 h_p = 3.74 \times 10^{-16} Jm^2/s$   $c_2 = \frac{c_0 h_p}{k_B} = 1.44 \times 10^{-2} mK$  and  $I_\lambda$  is the amplitude of radiant energy at a given wavelength  $\lambda$ , at temperature T, per -unit wavelength interval, unit time, unit solid angle, unit area– .

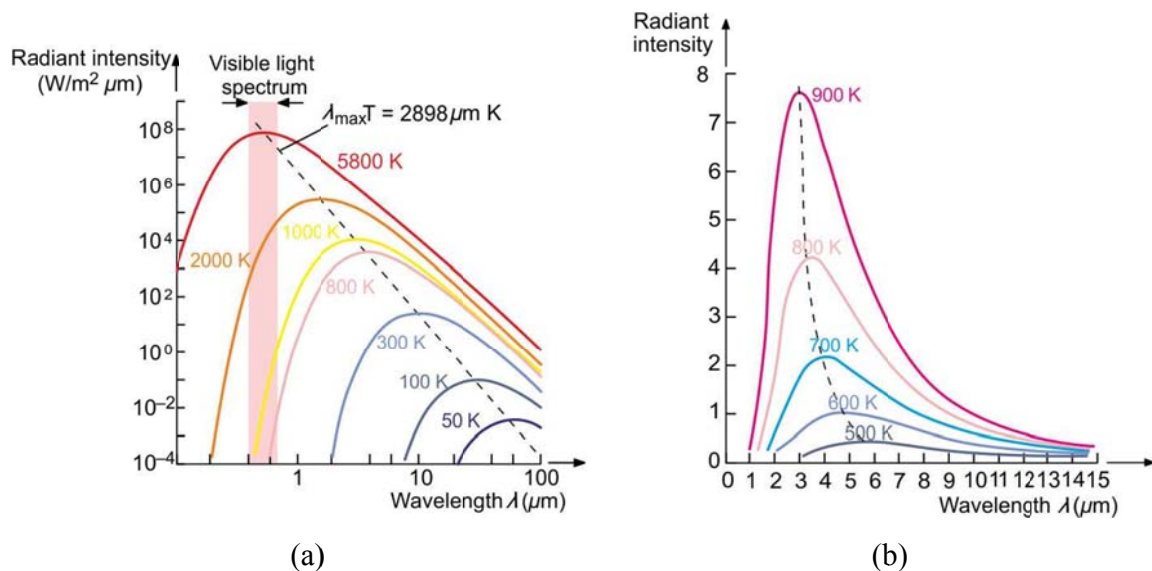


Figure 4.14 Blackbody energy distribution (a) log scale (b) linear scale [23]

The energy distributions for a blackbody are shown in Fig. 4.14 on log-log (a) and linear plots (b), respectively. In other cases, for a graybody and non-graybody (selective body) are given in Fig. 4.15.

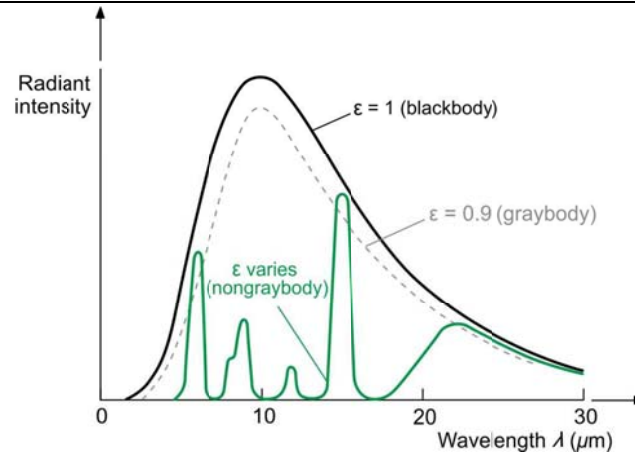


Figure 4.15 A graybody and non-graybody energy distribution [23]

From the Eqs. 4.9, each temperature has a specific curve which increases instantly from zero intensity at zero wavelength to a maximum, then gradually decreases asymptotically toward zero at long wavelengths. The Wien's law ( $\lambda_m T = \text{constant}$ ) states that, the wavelength  $\lambda_m$  is proportional to the temperature for peak intensity as shown with a dotted line in Fig. 4.14.

By integrating the equation of Planck's law, the total hemispherical radiation  $I$  per unit area and time is calculated by the area under the distribution curve for that temperature. This referred as Stefan-Boltzmann law

$$I = \int_0^{\infty} I_{\lambda} d\lambda = \sigma_B (T^4 - T_0^4) \quad [4.10]$$

where  $\sigma_B = 5.6704 \times 10^{-8} W/m^2 K^4$  is Stefan-Boltzman Constant. On the other hand, for a graybody, the production of the blackbody and the emissivity of the body in question give the total radiation. The material and its surface conditions are designated the emissivity. From these points, just by measuring the radiance of the processing condition, the temperature of a graybody could be calculated.

In order to measure the temperature and radiation on the surface due to the infrared radiation, two stepped measurement methodology might be used such as thermal detectors

#### **Chapter 4: Development of Optic-Electronic Hardware and Computer Software 107**

(i.e. Pyroelectric Devices, Thermocouples etc.) or photon detectors (i.e. photoconductive detectors, photo-resistive detectors, photo-emissive detectors or photovoltaic detectors etc.). In temperature sensors, the lattice heating is generated because of absorbed radiation, which also changes the electrical properties of the transducer. On the other hand, with photon detectors, absorbed radiation directly produces a change in the electrical properties of the detector; therefore these sensors have faster responses.

The detection scheme also an important factor in order to collect the information correctly. Single type, linear type or array scheme creates possibility to detect the signals according to the usage of the sensors.

In addition to the collecting the surface temperature information, imaging methods would improve the quality of feedback mechanism by concluding the relation between the captured image and collected temperature data. The image processing for online laser material processing is expensive by all manners. Especially, if the case is thermal imaging, the cost of the acquisition equipment and the complexity of programming are high with compare to the optical imaging and its processing. However, an imaging methodology would add great advantages such as estimating molten pool geometry, kerf size. The required equipment would be high speed camera, high sampling rate data acquisition system, powerful computer processor etc. and in programming perspective the image processing algorithms could be complex.

In this thesis, the aforementioned topics are studied carefully and later on the sensors are selected according to the planned applications of the developed system. In the preferred design, the laser is deflected by means of semi-reflective mirror through galvoscaner with  $f-\theta$  focusing lens. The focusing lens has a focal length of 160 mm. The radiation from the melt pool is transmitted through the  $f-\theta$  lens, scan head and dichroic mirror to beam splitter.

## Chapter 4: Development of Optic-Electronic Hardware and Computer Software 108

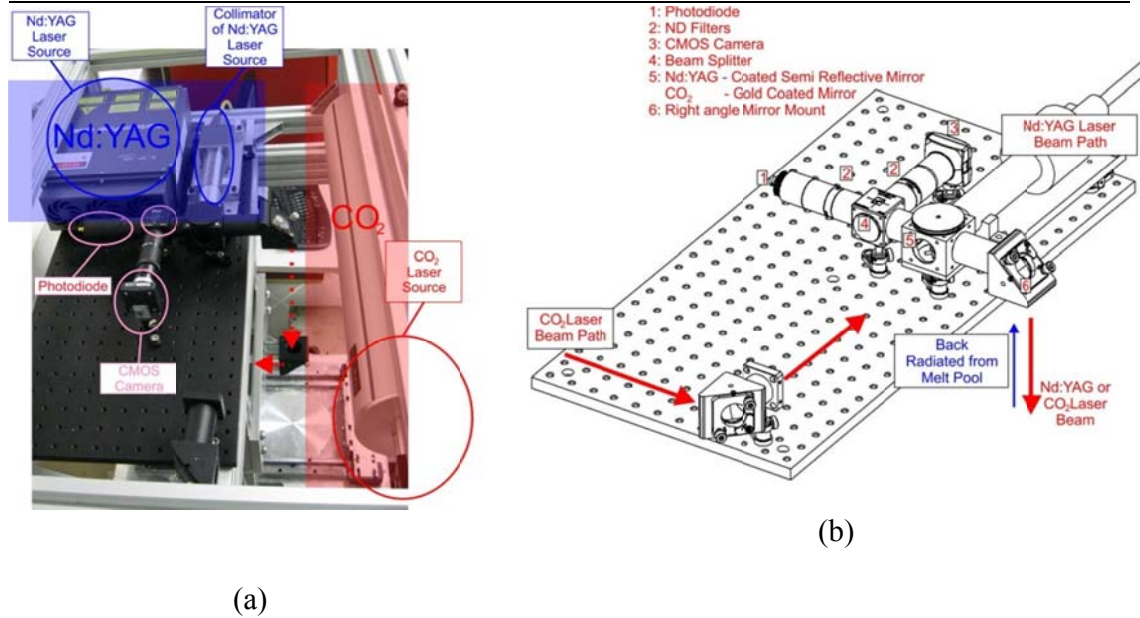


Figure 4.16 Developed Laser Feedback System Schematic (a) Final optical system (b) Designed Optical System

As stated before, while the processed metal is melting around 1500K, the radiation energy should be highest in the near infrared region around 1000nm according to Planck's Law. The selected semi-reflective mirror (Fig. 4.16 (b) Equipment 5) which is coated for 50% Transmission/Reflection at 1000 nm is capable of reflecting nearly 100% at 1064 nm Ytterbium Fiber laser wavelength. In addition to that it will transmit nearly 100% under 950 nm. On the other hand, the lower bound of the system-wavelength should be higher than 700 nm in order to avoid visible light from illumination in the process chamber. Sectioned radiation from the beam splitter focused on the Complementary Metal Oxide Semiconductor (CMOS) camera and photodiode through the lenses that placed before the photodiode and CMOS camera.

The CMOS camera is not a thermal camera and only outputs a 8-bit grey value image. The grey values given by the camera can be related to temperature and a correlation between the melt temperature of the used material and so called melt grey value can be derived.

#### **Chapter 4: Development of Optic-Electronic Hardware and Computer Software 109**

However, the objective of the usage is to understand the relation between the camera image and the simultaneously captured photodiode signal. In other words, the camera is used for calibration of the real time photodiode sensor. The CMOS-photodiode couple could also compensate the region of the captured signal. CMOS detects local radiation intensity; on the other hand photodiode collects global radiation intensity between the selected bandwidth.

The selected feedback mechanism brings the problems with it due to the sensing technology. The most important problems that photodiode would have the plasma interference and requiring the emissivity data of the processed material. For reliable monitoring without plasma interference, the incoming spikes due to that should be differentiated (by using additional UV sensors or proper filter selection). This differentiation would increase the detecting signal-to-noise ratio.

There should be taken couple of precautions for protecting the system and acquiring proper data against the explained problem. First of all, the sensor must be selected according to the proper central bandwidth that the system is designed to. In order to guarantee the wavelength range, couple of optical filters is implemented into the system. In addition to that focused beam would damage the sensor due to the higher intensity that the radiation has. Natural density (ND) filters are added into the system to protect the sensors against the possible overexposure. Moreover, the captured images would also filter for properly detection of required feedback. In Image Processing Toolbox, lots of already prepared function is available for that reason. For example, in order to identify molten pool library edge detection algorithm would be useful.

The mentioned case is sufficient, if the monitoring is required in order to collect isotherms or temperature gradients with photodiode-CMOS couple (knowledge of the emissivity is not essential) and some estimation is also possible using single scan track on a test plate, which will be mentioned in Chapter 5 Technological Demonstration. On the other hand, for

## **Chapter 4: Development of Optic-Electronic Hardware and Computer Software 110**

precise determination of the temperature, the emissivity value for the section of interest needs to be added.

Before finalizing this section some of the optical based setup requirements are given such as cleaning the dust on the optical equipment, match the image grabber resolution with camera resolution (to avoid image digitization noise), CMOS camera offset noise etc. The feedback system should have test and validated.

### **4.4 Developed Laser Processing Software**

Most of laser material processing software includes three parts: (i) interface software; (ii) data processing software, and (iii) model creation software. The developed MATLAB program supports IGES, STL and G-Code file formats. Design models can be created by any computer aided design (CAD) systems and then translated to the STL format. The optimal path orientation should be given to the data processing software for part building and to slice the CAD model in the required layer thickness. The software allows the user to view the sliced data in geometry window. The model creation software is used to control the part-building process. Operating parameters must be appropriately defined within the program in order to create a part accurately. Model scaling is also supported by the program sub-functions. Some of the important process parameters included in the laser processing software will be described later.

The developed software is using basic principle rapid prototyping algorithms such as slicing, which is novel for Manufacturing and Automation and Research Center. The geometries are initially generated using a three-dimensional CAD system, can be fabricated directly without the need for process planning or computer aided manufacturing (CAM) background. In addition using the STL or IGES file types, the software is capable of processing the pictures taken by the developed 3D Scanner. The laser workstation software needs to be capable of generating laser path for additive or subtractive manner to send the

## **Chapter 4: Development of Optic-Electronic Hardware and Computer Software 111**

generated commands to the related controller/ actuator. The details of the algorithm are presented in the following sections.

### **4.4.1 Importing Geometry by Reverse Engineering**

The external shape features of arbitrary objects have been widely scanned by using 3D scanning systems. This technology is used for many years in industry in reverse engineering part inspection and automated design. The decrease in the cost of this scanner equipment has led to its increase usage for other applications such as rapid prototyping, video gaming [24], e-commerce, apparel industry [25], digitizing of cultural heritage artifacts [26] and in the biomedical field. The motivation to develop a 3D scanner is due to the relation of this thesis with some this application list. In addition to that, the newly entered biomedical applications are another cause to develop these system algorithms. Especially in biomedical engineering, 3D scanning is used by including anatomical part reconstruction [27], orthodontic treatment planning [28], cranial deformation research [29] cartilage morphology study [30], anthropometric data collection [31] and various forms of surgery (plastic and maxilla-facial for example [32]. Beyond that surgical based biomedical applications, by using this technology prosthesis or handicapped equipment would be easily manufactured [33].

Different techniques are available in the literature for 3D model of object digitization. Each of which has wide range of equipment cost, different level of achievable accuracy and details. Time-of-flight range finders, stereoscopic image-based techniques [34], shape-form-silhouette algorithms, structured light techniques [35] and laser light sectioning methods [36] are some of the methods which are studied recently.

The advancements in camera technology and computing power brings the possibility for 3D scanner as economic and application specific. For this application, the overall objective is the development of a simple 3D scanning system and algorithms for laser workstation applications with underlying goals of cost effectiveness and versatility as designed

#### **Chapter 4: Development of Optic-Electronic Hardware and Computer Software 112**

machine. Laser-light-sectioning technique is accepted as main digitizing method because easier to atomize and write the algorithms. During the development of 3D scanning process, calibration, image and data processing and surface construction topics are covered. The demonstration of the system was also an objective and testing this system on multiple tests.

Different methods for accomplishing various stages of scanning process have been examined with their advantage and disadvantages. Due to the feasibility, the laser light sectioning technique is applied and this technique might be used in several areas of reverse engineering.

The calibration procedure is simple and open to the development, the transformation matrix is acquired by using a dimensionally-known geometry. The secondary scan is normalized by this transformation matrix. This approach is similar with Direct Linear Transformation (DLT) algorithm with least squares (LS). Automated laser light movement, image taking and image pre-post processing is supported by Laser Workstation software.

In this section of this thesis, an overview of 3D scanning technology and current literature is also given on that topic. As mentioned before, there are different technologies for digitizing 3D models of objects with hardware cost, accuracy level and detail in the virtual models. In the literature, [1, 2, 19] high-level reviews of 3D scanning techniques are possible with numerical representations.

In Manufacturing and Automation Research Center, contact-based 3D measurement system is available (Coordinate Measuring Machine – DEA). Generally contact-based 3D measurement equipments are very precise with specific configuration, which requires climate controlling environment due to mechanical system that the device has. On the other hand, the main disadvantages are slowness, expensive and not easily automated for scanning complex shapes (i.e. machining tool helix scanning, machine surface scanning est. 3 days to scan) In CMM, the coordinates of a probe are recorded when it is physically



#### **Chapter 4: Development of Optic-Electronic Hardware and Computer Software 113**

brought in contact with the object; this tends to be a very manual process [33]. Therefore, this contact based systems are very useful for checking the manufactured geometries (i.e. checking the boring tolerances such as diameter or cylindricity of an automobile engine) with a conditioned environment as mentioned before. This device is not useful for rapid manufacturing based reverse engineering and also has Cartesian coordinate constraints.

The proposed method is a basically non-contact 2.5 D active system to measure 3D surface information. The active scanners actively emit some kind of radiation or light, sometimes using textures and masks. Then detect the light's reflection of the object's surface using an appropriate sensor [33]. The illumination sources could be different from device to other device, such as coherent light (laser) or incoherent light (white light), with varying wavelengths or bandwidths [33]. The computational costs of the active systems are less with more accurate results.

In the proposed algorithm, laser light sections are used to derive data coordinates (point cloud) via optical triangulation approach. Laser light is used as the illumination source. The principle behind optical triangulation is follows. A focused light beam of light illuminates a line on the surface of an object. The sensors collected the reflected light beam and the center location of the spot is processing afterwards by filtering and noise cancelation. If the illuminated point on a line is traced back to the source, the point on the surface of the object could be revealed as shown in Fig. 4.17. This location, the camera's line-of-sight and laser beam form a triangle which has the following geometrical relationship. Spot location on the sensor  $u$ , the triangulation distance  $b$ , the angle between the laser beam and the camera  $\alpha$  and camera's focal length of  $f$ , from this given parameters the coordinate point of cloud might be calculated from,

$$x = \frac{b \times u}{f \times \cot(\alpha) - u} \quad [4.11]$$

$$z = \frac{b \times f}{f \times \cot(\alpha) - u} \quad [4.12]$$

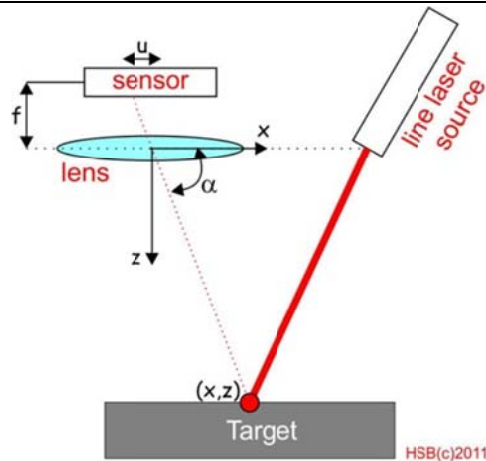


Figure 4.17 Optic Triangulation Schematic

Over the years to facilitate the scanning of an entire object's surface, many variations of this basic setup have been studied [37, 38].

In order to collect coordinate points in a given equations, the light source should have tightly focusable and narrow radiation spectrum. The tighter the light source is the better resolution that the system would have. Moreover the narrow radiation spectrum could be easily filtered by digitally or directly and is less susceptible from ambient light source. In 3D scanning applications the laser light is a natural choice due to these reputed properties. On the other hand, one of the biggest disadvantages of laser technology in 3D scanning is requirement of clear view between the scanned surface, laser source and sensor.

As stated before, in order to decrease the cost of the system a CCD based web camera is used for laser light detection. Thanks to the MATLAB and its Image Processing Toolbox, this approach easier to implement by means of hardware and software.

Except the applied laser sectioning method, structured light and time-of-flight distance measurement systems are also applied methodologies in order to digitize geometries. In structured light method the mathematics (i.e. optical triangulation formulas) is the same as in laser light sectioning method. However, the light is sent with grids or line striped

#### **Chapter 4: Development of Optic-Electronic Hardware and Computer Software 115**

---

patterns on scanned surface. This multi-point calculation has a couple of drawbacks such as requirement of complex algorithms in order to separate the adjacent point location from each other or light combination which harden to filter the reflected light on scanned surface. Hence, Multi-stripe Laser Technology or spectral grid generation techniques help to eliminate these drawbacks. Steinbichler, Inspek and 3DMD are some companies that use this technology. The final time-of-flight based devices are also using laser light to detect the distance from the reflected surface, since the speed of light is approximately known. The accuracy of the measurements depends on how accurately the speed of pulse actually measured. The speed of light would be effected any physical change of the environment and therefore this method should be carefully calibrated (environmental light detectors, temperature sensors etc.) before any usage.

Depending on the technology used in the scanning, the returning data type can come in different forms. Most of the 2.5D systems take pictures what is named as a range image. This is similar to take pictures from a web based camera, except rather than each pixel storing RGB color data (i.e. MATLAB Image Processing Toolbox). Multiple range images are processed and then merged in order to create (x, y, z) points in 3D space, referred generally as a point cloud. A 3D model is generated by connecting these data points with their adjacent points to form a tessellated, polygonal or NURBS based surface.

After post processing of this point clouds, it might be used for a number of industrial applications including part inspection, rapid prototyping or reverse engineering.

Reverse engineering is the process of creating processable parts via Computer Aided Design (CAD) tools so that it can be copied and re-manufactured. After reverse engineering process, the geometries could be manufactured for functional product or prototyping by using stereolithography methods 3D Printing or SLS. The video gaming market has also great influence on 3D scanning industry, the requirement of artistic rendering images and movements create great funding in that area of research.

#### **Chapter 4: Development of Optic-Electronic Hardware and Computer Software 116**

In this thesis, the geometric construction and its re-manufacturing is important rather than the system by itself.

However, the methodology, fundamentals behind it is given so far. Some industrial search would be helpful in order to increase the chance of future development and therefore Table 4.1 is given. Beyond the literature and application of 3D scanner, this 3D scanner is developed in order to acquire geometries for Laser Workstation software. None of the current laser workstation software available in the literature has such a property combined with the 3D scanning. However, the biggest missing part is the requirement of post-processing in scanning process.

Table 4-1 Commercial 3D Scanners

| <b>Company</b>   | <b>Scanner</b>     | <b>Type of technology</b>              |
|------------------|--------------------|--|
| Konica Minolta   | Vivid 700 and 910  | Laser Light Stripe                     |
| Cyberware        | WB4, WBX           | Laser Light Stripe                     |
| Metris           | ModelMaker         | Laser Light Stripe with digitizing arm |
| Polhemus         | FastScan           | Handheld laser light stripe            |
| Shape-Grabber    | Ai310, Ai810       | Laser light strip                      |
| Next-Engine      | Desktop 3D Scanner | Multistripe Laser Technology           |
| 3D Digital Corp. | EScan              | Laser Light Stripe                     |
| Vitronic         | Vitus              | Laser Light Stripe                     |
| Creaform         | ERGOScan           | Handheld laser light stripe            |
| 3DMD             | 3dMDface           | Active stereophotogrammetry            |

Beyond the literature and application of 3D scanner, this 3D scanner is developed in order to acquire geometries for Laser Workstation software. None of the current software has

#### Chapter 4: Development of Optic-Electronic Hardware and Computer Software 117

such a property combined with the 3D scanning. However, this point clouds must be processed after scanning process.

Up to this point, the designed system is not given in the following paragraphs, the designed 3D scanner is explained by details with calibration, image acquisition, image processing data manipulation and finalizing of object construction. The designed laser scanning system is given in Fig. 4.18. The provided figure is the second generation which has different calibration approach with the provided algorithms. In the provided algorithms, the scanner is calibrated through a calibration box. On the other hand, in v. 2.0 the calibration is completed through center catching algorithm by some defects. Therefore it is not included in this thesis.

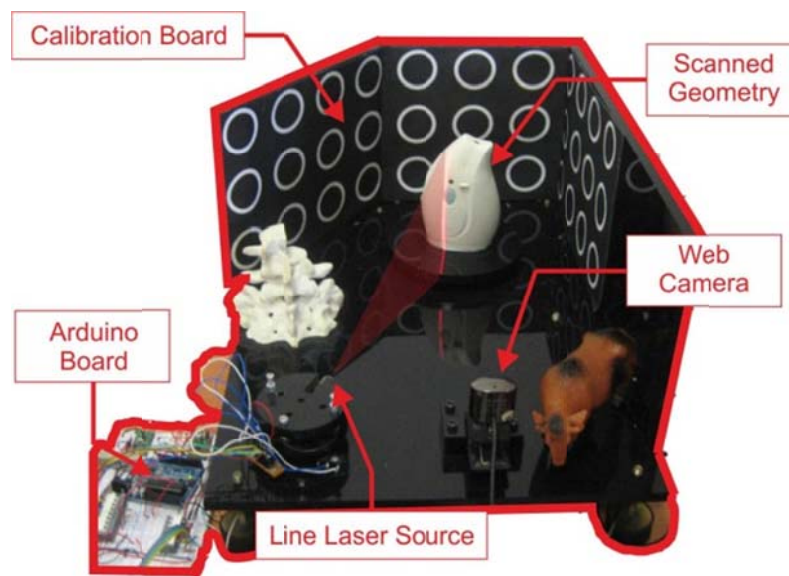


Figure 4.18 System Design Overview v.2.0

Laser light sectioning technique applied typical system would have the following setup equipment. A laser source fitted with line optics creates a vertical light plane the trace of which should be visible when pointed on the interested geometry. The taken image of this trace is recorded with a CCD based web camera, which is inclined at a fixed angle  $\alpha$ ,

#### **Chapter 4: Development of Optic-Electronic Hardware and Computer Software 118**

relative to laser line plane. Each segment is captured by using camera until the trace is moving on the complete range image closed geometry. Multiple sections of the images are obtained by rotating the geometry and yielding a complete planar cross-section. Multiple 360° planar sections are stacked until the data points giving the construction of the geometry.

In the light of the forgoing points, this presented system herein consist a 10 megapixel web cam, a focusable line laser, two E-Minebea step motor (1.8° nominal step), step motor drivers(with microstepping) and Arduino board. The microcontroller send signal to motor controller in order to rotate the table and laser. At each rotation of the laser the MATLAB program is taken picture. After finishing each segment the part motor is changing the view by using main part step motor. The device is calibrated by using the pre-defined geometry (calibration box) scan. However, after a couple debugging of v2.0, it is possible to add this feature in the system. Therefore a center catching algorithm is written and a proper calibration paper is attached on system.

The laser is starting at 15° to take picture and turns approximately 90°. Between 15° to 90°, a lot of redundant pictures are unnecessarily captured. The user might delete them by using the developed software in order to process necessary pictures. The captured images are filtered in software before calculating the points.

In this setup, one of the most important design decisions comes from the hardware setup which is the angle at which to locate the web cam. The triangulation angle is mainly depends on the measurement range and resolution of the system in which the plane of the laser line and optical axis of the web camera are reasons for that dependence [39] The larger this angle, the larger the observed displacement of the line, which means more details would be scanned. If the object has variable surface topography, a smaller triangulation angle must be used with the trade-off in poorer details. Therefore in the designed system this angle would be changeable within a limit before scanning any object.

#### **Chapter 4: Development of Optic-Electronic Hardware and Computer Software 119**

After applying these steps in order to collect surface data points, the set of coordinates are mapped to the Cartesian plane using the transformation matrix obtained from calibration box data. Some regions from the captured images tend to be affected with noise, showing excessive steep slopes and frequent outliers. This is due to the quality of light signal where it intersects the edges of the scanned geometry. Therefore, some point cloud coordinates should be neglected in the post processing of those points.

Micro-movement of the laser motor enhances the resolution of the surface scan. In addition to that movement based fine tuning; the sample overlapping is also suggested to increase actual surface points. Therefore, the residual error would be also dealt with. Another tuning algorithm is adding curve fitting algorithm to the software. The software will fit a curve to the points that it processed. From the assumption of the smooth point collection the curve fitting technique would increase the minor fluctuations from the collected data.

The captured images or point clouds produced by 3D scanners are typically not used directly as stated before. In order to use scanned data, a 3D model is required. The part of converting a point cloud into a 3D model is referred as geometry reconstruction. In this reconstruction process, all of the range data precisely registered into a common reference system and connecting adjacent points in order to combine the data into a single continuous geometry. A lot of research conducted in the area of geometry construction. A review of these construction methods can be found in [40]. Some these solutions use the original structure of the scanned data. The researcher work on range images which have been registered into a common reference system (as described above), process them as surfaces and fuse those geometries together. This is referred as integration. Although the captured images may be collected continuously, they are still not combined into one surface after processing. The area of captured image integration may be found [41, 42]. Unfortunately, like captured image collection itself, 3D stitching is quite complex, computationally

## Chapter 4: Development of Optic-Electronic Hardware and Computer Software 120

expensive and there isn't any full automated software available in the literature for all type of the geometries.

Possible software applications capable of converting point clouds into triangular meshes include: VRMesh (Seattle, WA), Geomagic (Research Triangle Park, NC), Meshlab (Pisa Italy), Cycloes by Leica Geosystems (Heerburg, Switzerland) and Polyworks by Innovmetric (Quebec, QC).

It should be noted 3D Scanner Design was not the main focus of this thesis and therefore couple of software is used to construct surfaces. However, the implemented 3D scanner has promising results and ready to any improvement. Some of the scanned geometries and their point clouds are given in the Fig. 4.19.

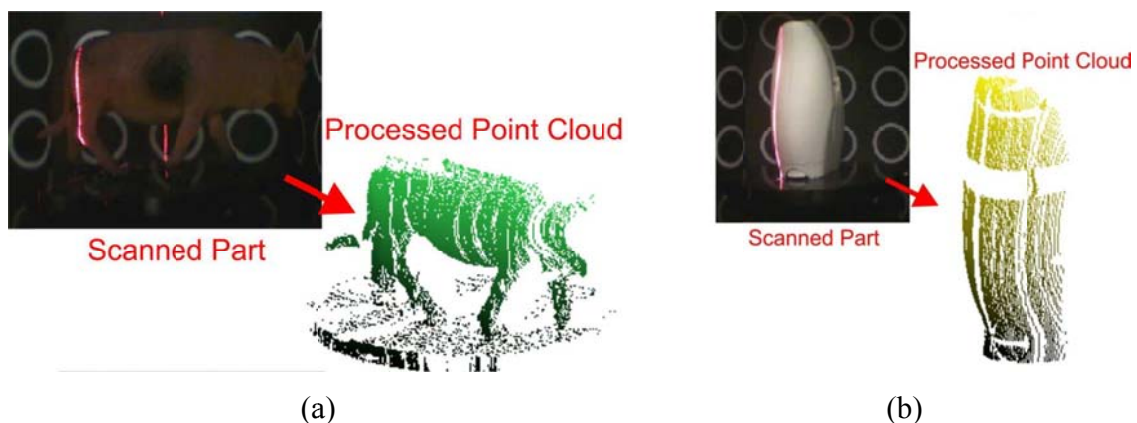


Figure 4.19 Scanned free-form geometries of (a) cow sculpture and (b) air-wick

### 4.4.2 Geometry Importing and Processing

The computer software should cover number of steps from the virtual CAD description to the physical result. These steps could be generalized as generating CAD data, STL file conversion, slicing, path generation, transferring the files to the machine and processing of generated geometry in machine.

For the first step Unigraphics NX 7.5 would be used and the designed geometry will be easily changed to STL or IGES file format. In addition to that a 3D scanner is also added to



#### **Chapter 4: Development of Optic-Electronic Hardware and Computer Software 121**

the system in order to digitize the geometric information of already generated geometries. The digitized or created geometries should be converted to STL file format or IGES as stated before. This has become a de facto standard and has its own advantages or disadvantages. Some of the advantages regarding to STL file format is its platform free format, easy to generate, possible to create supporting material toolpath (by using normal vector method). On the other hand, some of disadvantages are inconsistency problems such as incorrect normal vector [43, 44], second malformation problems such as cracks and holes that exist; and illegal overlaps in the STL geometries. The drawbacks of the developed software are counted in disadvantages due to the input geometry type and there are measures to take in. However, in this study the STL files are assumed as defect free and faultless. Even this is the case; the geometries should be checked before slicing operation carefully with software programs such as MAGICS (from Materialize, Spin-off Company of Technische Universitaet Leuven). This software is capable of repairing STL files and showing defects on the selected geometries.

STL files can be output as either binary or ASCII (text) format. In the developed software, ASCII compatible STL files are used. This format is less common than binary format due to giving every detail explicitly. On the other hand, ASCII format is easier to understand and implement into any code. An STL file consists of list of triangular facets which are created during tessellation. Each triangular facet should be uniquely identified by a unit normal vector and three vertices or corners without any overlap as stated before. The unit normal vector is a line that is perpendicular to the triangle facet and has a length equal to 1.0. This unit vector also useful while creating the toolpath for support material as stated before. The STL file does not include any unit only the numerical vertex points are represented. Therefore, the operator should know whether the main unit is mm, inches or some other unit. Each triangle has twelve numbers by each three numbers showing one vertex.

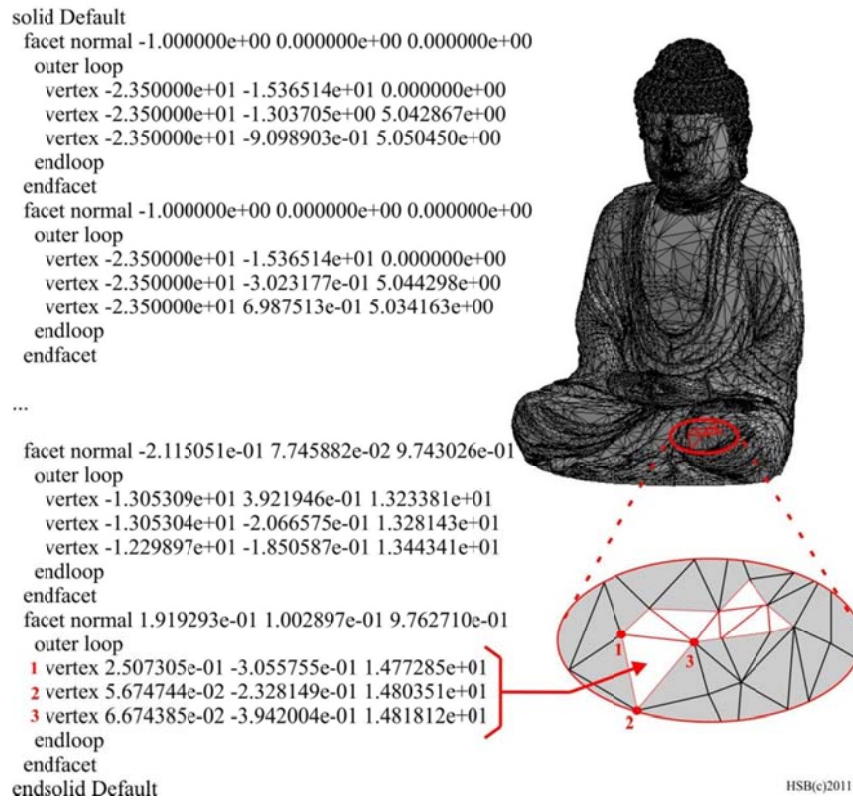


Figure 4.20 ASCII STL geometry file

Except the coordinate points the ASCII file also includes some template words such as "object name" delimited with "solid", "outer loop" and "endloop". The order of the vertex could be understood easily using right hand rule approach. A binary STL file can be described in, an 80 byte header that can be used to describe the part; 4 byte unsigned integer that indicates the number of facets in the object and a list of facet records, each 50 bytes long.

The record of the 50 byte face includes 3 floating values of 4 bytes each to describe the normal vector, 3 floating values of 4 bytes each to describe the first vertex, 3 floating values of 4 bytes each to describe the second vertex, 3 floating values of 4 bytes each to

## Chapter 4: Development of Optic-Electronic Hardware and Computer Software 123

describe the third vertex, one unsigned integer of 2 bytes which should be zero for checking purposes.

The ASCII type STL is given in Fig. 4.20. After loading the error-free CAD data, it will be sliced by the algorithm which has a flowchart as in the Fig. 4.21.

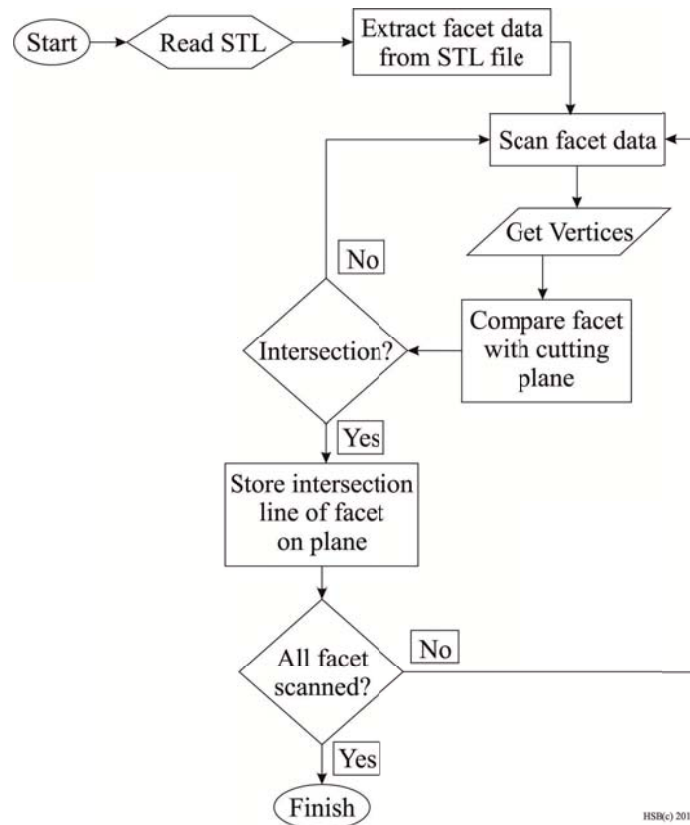


Figure 4.21 The flowchart for plane triangle intersection algorithm

The slicing algorithm could be used for freeform surfaces which has multiple contours in each layer. The geometry size and the number of contours are limited with the capacity of the computer that the software is installed. In order to slice the geometry properly, the powder diameter should be measured and thus, the slice thickness should be estimated according to that physical quantity. Moreover, this iterative procedure requires knowledge

**Chapter 4: Development of Optic-Electronic Hardware and Computer Software 124**

comes from some testing and calibration. Some of the sliced geometries are given in the Fig. 4.22. In order to show exact slicing operation the slice thickness are kept high and there is not any slice thickness limitation in proposed algorithm. Unfortunately, this is the first fully working algorithm since 2008 in Manufacturing and Automation Research Center.

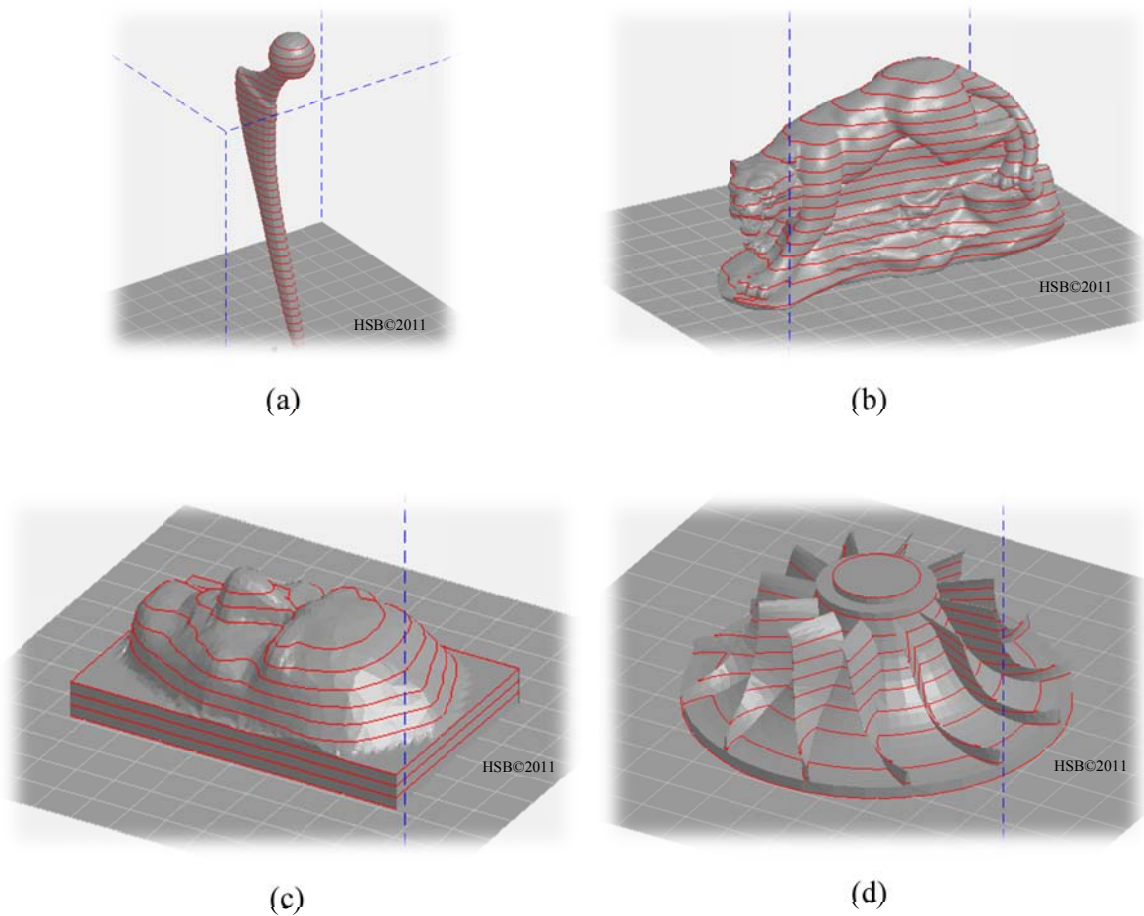
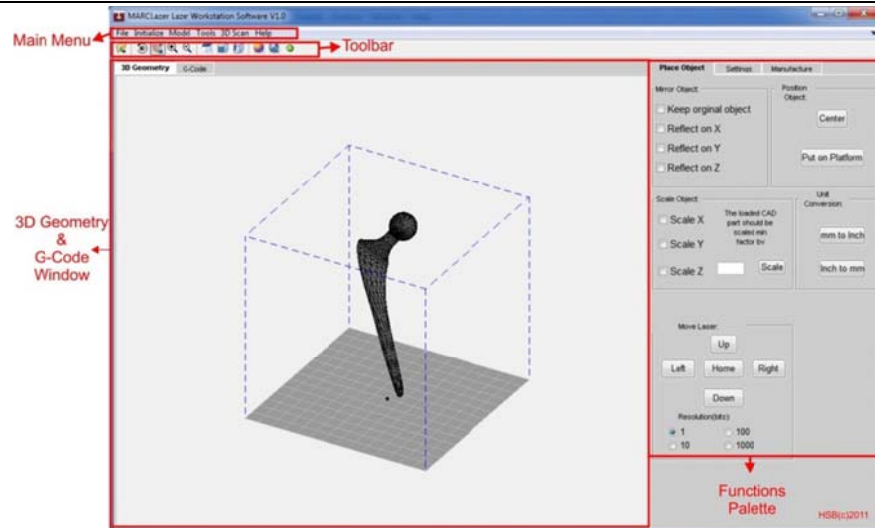
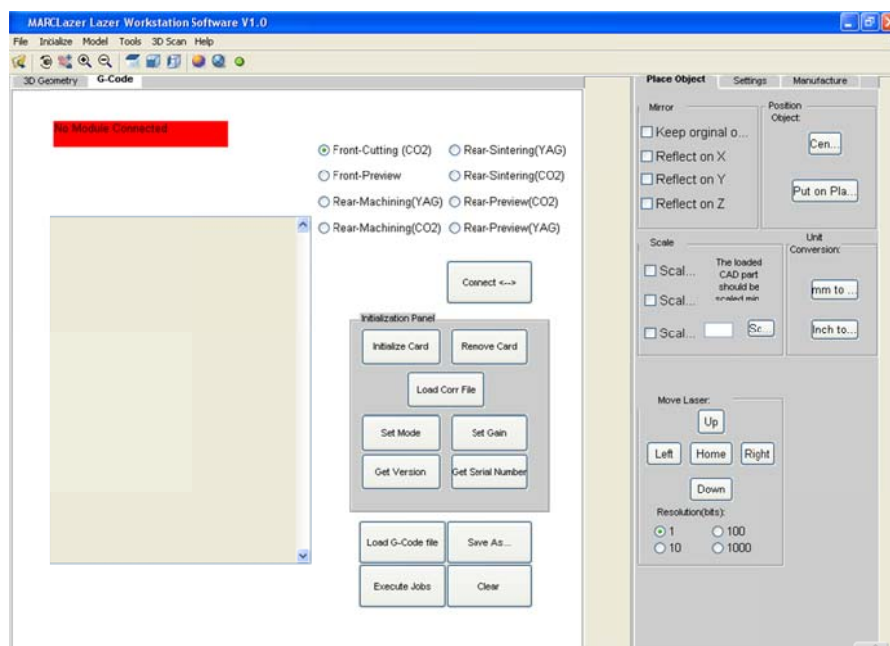


Figure 4.22 Sliced geometry examples, Slice Thickness 3mm a) Hip Implant b) Tiger  
Figure c) Ataturk Mask (Multi contour example) d) Impeller (Flat start point example) [The Ataturk mask and impeller blade is created by HSB©2011]



(a)



(b)

Figure 4.23 Developed Lazer Workstation Software GUI (a) 3D Geometry Panel (b) G-Code Panel

#### **Chapter 4: Development of Optic-Electronic Hardware and Computer Software 126**

In order to understand the capability of the developed algorithm, detailed software benchmarking is studied between several programs such as 3D Lightyear, Buildstation, EzMark, WeldMarkt etc. The reason behind that is simple, the capability of this machine is basically comes from the capability of the used software. First of all, there is huge difference between the subtractive based software and additive based software. The commercially available subtractive software (marking or engraving software EzMark or WeldMarkt) are working only in two dimensional (2D). However, the developed Laser Workstation Software is capable of working in 2D plane or three dimensional (3D) space even there isn't any 3D galvoscaner. In addition, none of the current laser workstations accept any G-Code command in order to increase the dependability of their software. However, in Laser Workstation software (Fig. 4.23), the user might write with a standard notepad and send to the workstation for 2D applications. In any case, it is recommended to check the toolpath with the commercial G-code checking software such as CIMCO to avoid any errors prior to processing.

The main menu includes File, Initialize, Model, Tools, 3D Scan and Help as main menu. In order to load the geometry File>Load STL file should be selected. The loaded 3D geometry would be rotated, zoomed in and out, panned by using toolbar. Moreover, the toolbar is also change the style of loaded geometries such as shaded view, no-shaded view and turns the 3D model on or off. After slicing the geometry properly or generating the toolpath, the model off button is useful to check the contours and the laser on-off points (G1-G0) respectively.

The slicing and toolpath generation settings are in the functions palette tab Manufacture. The software might slice in X-Y-Z axes. However, for this laser workstation only slicing along Z-axis is sufficient. In order to generate the tool path, the contours must be ordered. Therefore, an algorithm is used in the software to order the intersection points. The flowchart of this function is given in Fig. 4.24.

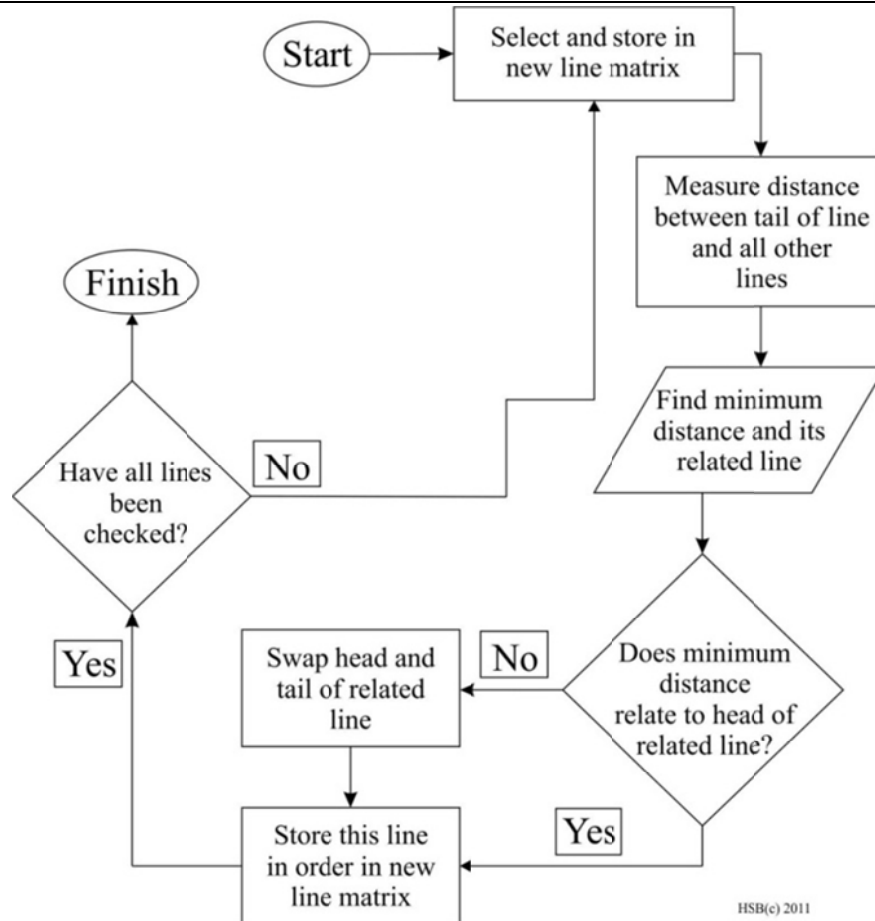


Figure 4.24 The flowchart for ordering the line intersections into complete outlines

In commercial CAM packages there is a lot of possibility for creating toolpaths. As stated before, in laser material processing, raster-scanning (zig, zig-zag toolpaths) and continuous vector scanning are commonly used. In addition to that there are other intelligent scanning strategies in order to avoid part shrinkage and warpage by using toolpath selection [45]. The algorithm to generate of Zig and Zig-Zag type toolpaths are demonstrated in Fig. 4.26.

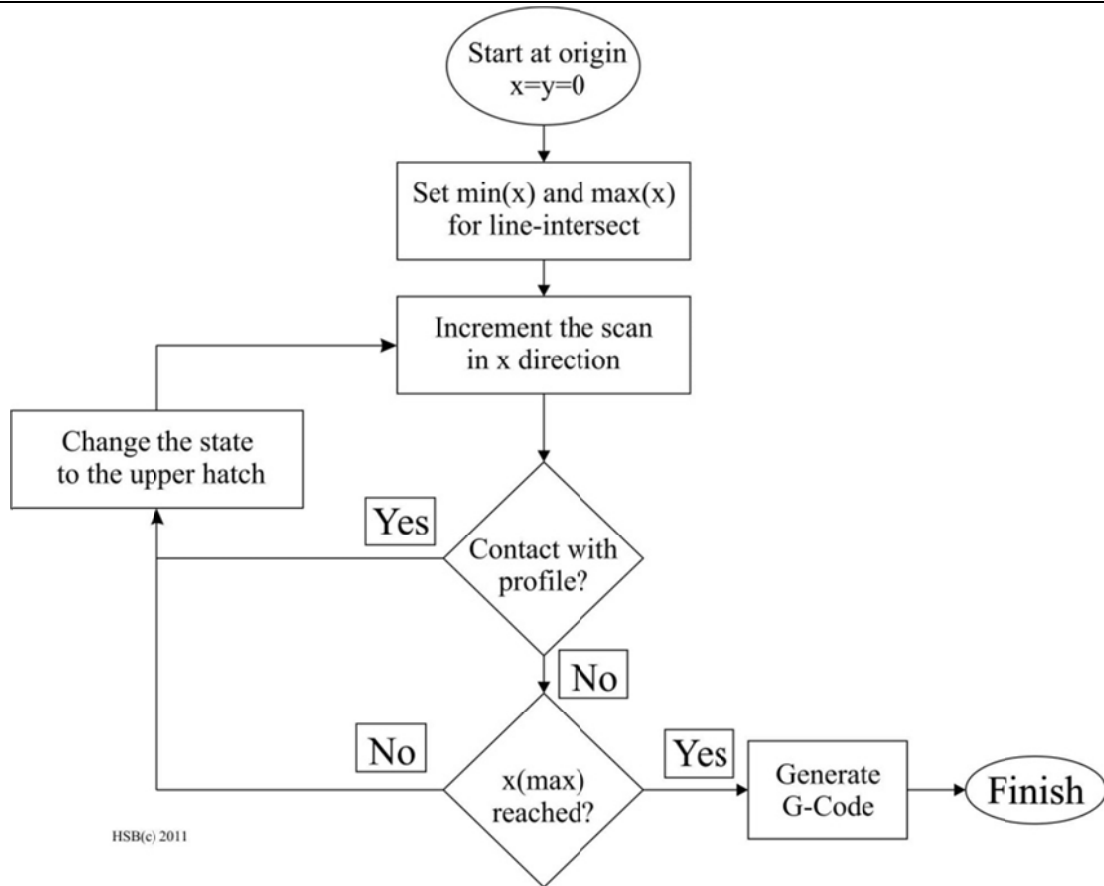


Figure 4.25 The flowchart of raster-scanning to generate G-code for Module I or Module II

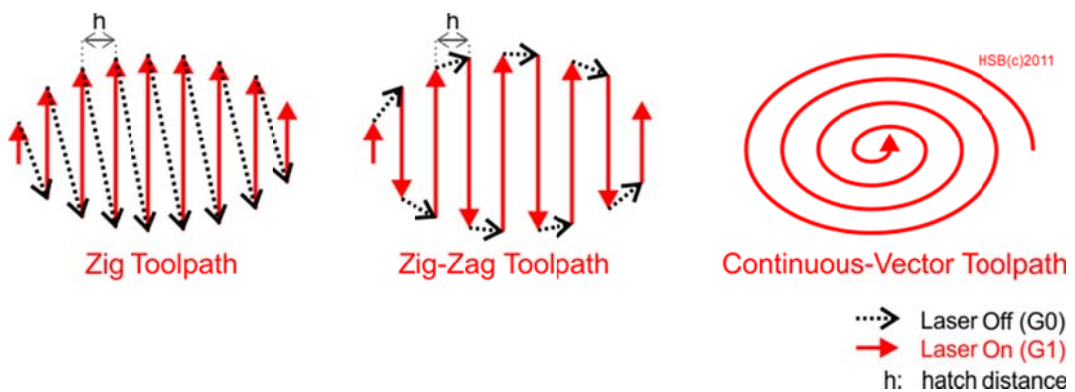


Figure 4.26 The output of the selected algorithms for laser material processing



## **Chapter 4: Development of Optic-Electronic Hardware and Computer Software 129**

---

The communication with scan card and interface card is occurs by using sub functions under the initialize menu. The Initialize Scan Card connects the card to main software; by the name implies the Remove Scan Card closes the communication between scan card and software (If the user want to use the scan card with different software such as Weldmarkt, she/ he has to close the communication with the active software.)

While initialization of the scan card into the system SP-ICE 2 is asking for grid correction files. Grid correction is needed to compensate for optical errors induced by all two axis laser beam systems. These optical distortions are caused by the distance between each mirror, the distance between image field and mirrors and type of lens used in the laser for focusing of the laser beam. Some of the distortions are pincushion distortion which is caused by 2 axis galvano scanner system. The distortion in the X axis is proportional to the tangent of the angle of the Y axis mirror and the distance from Y mirror to the focal plane. Second distortion type is the F-theta objective induced distortion, the other major type of distortion is caused by the addition of an f-theta objective to an X-Y galvano scanner system. F-theta objective lenses, like all optical lenses, are not perfect and induce their own projection field distortions. This type of distortion is also called pillow distortion for what it does to a square image as in Fig. 4.27. The correction methodology is based on the correction of composite distortion. Correction tables represent a 65x65 element grid covering the full addressable projection range of the system. Each grid element contains three components: one each for the X, Y and Z axes. The components represent an offset that if added to an ideal position command for that point, would alter the galvano scanner positions such that the resulting projected point would fall onto a "perfect" grid. Then the image would be corrected. In the developed algorithm the correction table of the Raylase company is used and the tables are loaded through the menu of Initialize > Load Correction File.

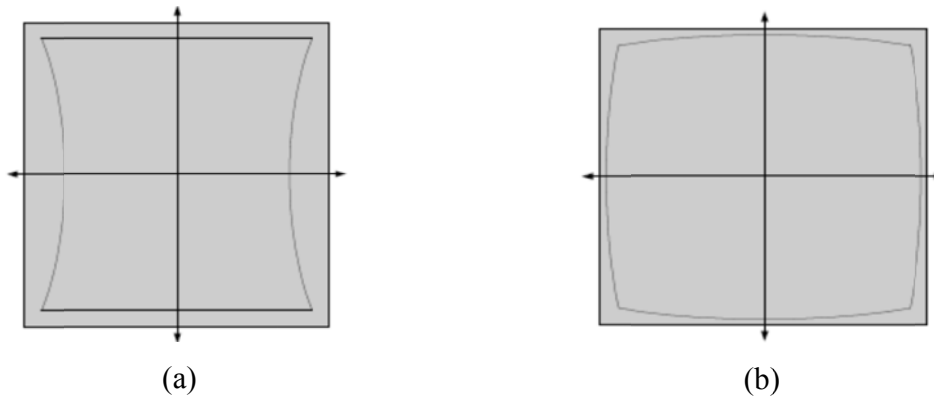


Figure 4.27 The galvoscan outputs without grid compensation (a) Pincushion Distortion  
(b) Pillow Distortion

As stated before in Chapter 2, the estimation of the thermal field is important subject in order to anticipate the penetration depth of the laser. The details of model are already given and the MATLAB code is written on Appendix 2.1 and 2.2. The user can create a custom material in the software via Model > Save Material As and is able to call this material property by load material file by Model > Load Material As. The point source model and line source model is available as function. The user can select the appropriate function by clicking on it. Afterwards, the model temperature gradient is plotted on the screen in a different plot.

In the 3D scan part of the software, a formerly taken picture for 3D scan is used and the surface points are calculated with a 150-200 micron resolution which depends on the laser intensity on the scanned part as mentioned before.

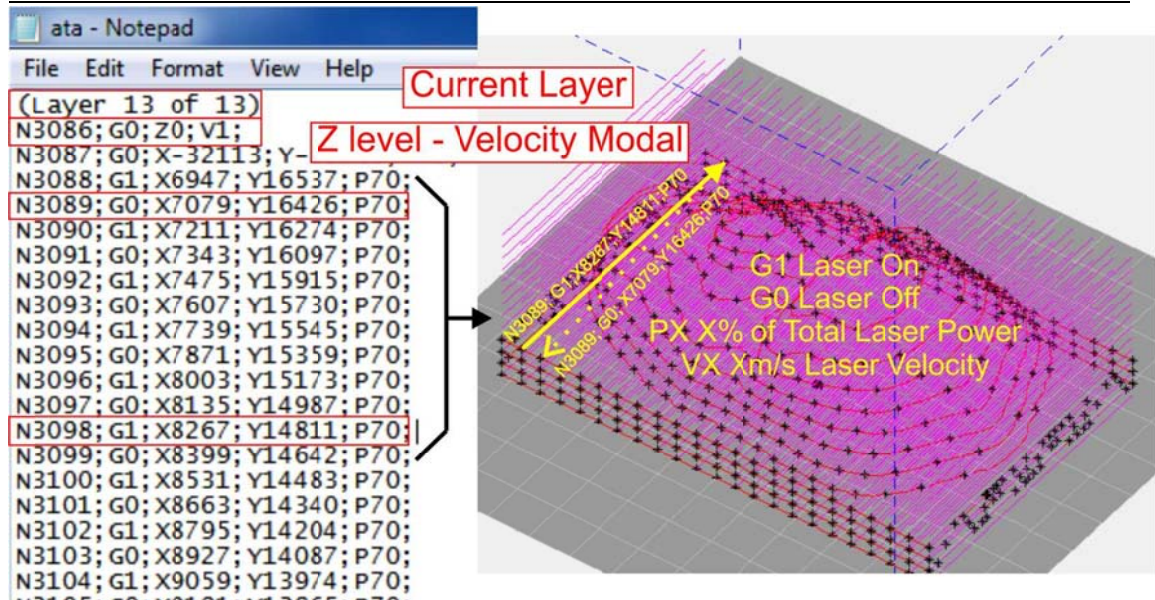


Figure 4.28 G-code file for the developed system

The G-Code standard is similar to one in used for CNC machines. However, for Module II the unit system is based on bit which is the standard unit for galvano scanners. For Module I, G0: Rapid motion; G1: Moving with action; G2-G3: Circular motion; G20: Inch unit; G21: Millimeters as unit; G28: Go home; G90: Absolute positioning; G91: Incremental positioning. The arguments for Module I is X, Y, Z position coordinates in selected unit system; M: Registered machine action code; F: Feedrate; I: Arc data X axis; J: Arc data Y axis. The Module II is working similar manner. In the final version of the G-code generator for Module II is G0: Jump to given coordinate; G1: Mark to the given location; ‘(‘: shows the starting point of comment; V-X-: the galvoscaner speed in m/s and P-X-: X% of total laser power as given in Fig. 4.27. Before sending the G-code command through the main window G-Code tab the code must be checked proper simulation software such as CIMCO. After properly check the convenient Module should be chosen according to desired manufacturing and the calculated commands will be send to the machine after pressing execute button.

**4.4.3 Software Process Parameters**

The Raylase SuperScan galvano scanner system (Module II) and developed flying optics (Module I) installed on laser workstation is capable of move based on the reference that it receives from the software bit coordinates (Module II) or millimetric dimensions (Module I) according to G-code. Both of the modules are capable of moving in two modes. The first more commonly used mode known as vector scanning is a mode in which each pair of coordinates is treated by the scan controller as an individual motion segment. In this mode, a coordinate point either a jump point (laser off - G0 command) or a move point (laser on – G1 command). Thus, an arbitrary sequence of line vectors may be drawn with the laser on or off. However, each move to a jump or next point has an associated time delay to allow for settling of scanners. This typically leads to laser over-exposure or "blooming" at vector end-points, therefore laser on delay and laser off delay are described in the job lists function as in Table 4.2. Traditionally in laser material processing, vector scanning mode is used for parallel (or anti-parallel) raster scanning. This is akin to filling an arbitrary shape with parallel lines as shown in Figure 4.28.

The second scanning mode known as continuous vector (CV) mode allows each individual motion segment to take place in an arbitrary direction but treats successive segments as part of a continuous path and hence eliminates the inter-segment delays experienced in vector scanning mode. An example of this mode is shown in Figure 4.26. Upon encountering this keyword, the scan controller gates the laser on (G1) and keeps it on for all successive coordinate point motions until it encounters the a specific keyword, at which point the laser is gated off (G0).

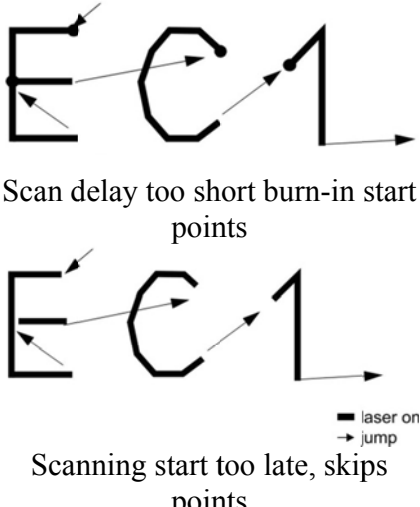
The CV mode is useful for tracing smooth curved paths or outlines of shapes. The CV mode is especially useful for full density direct laser processing where maintaining continuity of the solid-liquid interface is of utmost importance to obtain defect free features. A major advantage of using the CV mode for curved paths is that the coordinate

**Chapter 4: Development of Optic-Electronic Hardware and Computer Software 133**

points for scanning may be generated by evaluating the parametric equation of a curve at regular (or irregular) parameter values. Modifications were incorporated into the existing process control software to enable the use of CV mode.

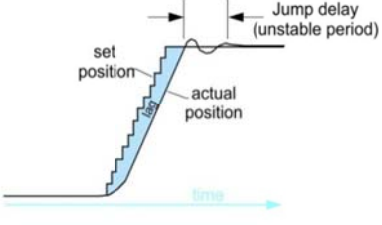
It has been reported that there are as many as 30 parameters affecting the laser material processing [46]. However, a recent study conducted by Schaub et al. [47] reported that more than 50 process parameters affecting the accuracy of the built part and some of them are shown in Table 4.2.

Table 4-2 List of important laser material processing parameters

|            | <b>Parameters</b>  | <b>Function</b>   |
|------------|--|---|
| Step Size  |  | Controls the speed of laser scanning                                |
| Jump Size  |  | Controls the speed of the laser movement when not drawing           |
| Scan Delay |  <p>Scan delay too short burn-in start points</p> <p>Scanning start too late, skips points</p> <p>— laser on<br/>→ jump</p> | Specifies the time the scanner waits before drawing the next vector |

## Chapter 4: Development of Optic-Electronic Hardware and Computer Software 134

Table 4-3 List of important laser material processing parameters

|             |   |   |
|-------------|---|---|
| Jump Delay  |  | Specifies the settling time for the scanner after executing a jump (laser starts before mirrors properly settle shown left) |
| Laser Off   |   | Synchronizes the laser to the phase delay of the scanner for precise line ending  |
| Laser On    |   | Synchronizes the laser to the phase delay of the scanner for precise commencement of scanning                               |
| Scan Pitch  |   | Control the distance between adjacent lines of scan   |
| Scan Offset |   | Compensates for the laser beam size at the boundaries of the scanned sections   |
| Step Period |   | The time required for the scanner to move the specified step size   |
| Layer Pitch |   | Specifies the layer incremental distance during part building   |

As stated several times, among these parameters, the laser power, hatch distance and scan pitch parameters has great influence on the mechanical properties of the part built significantly [48, 49]. Unfortunately, in Turkey there isn't any research except this mentioned parameter influence based research. However, in the Manufacturing and Automation Research Center the focus is on how to build this workstation and the details about it, later on the mechanical influences and other material based optimization would be investigated more freely due to the know-how on the developed system. More than mechanical aspects of the process, accuracy of the built part is analyzed deeply [50]. The other parameters than the Table 4.2 are as follows:

#### **Chapter 4: Development of Optic-Electronic Hardware and Computer Software 135**

*Accuracy and Integrity of STL CAD Data:* The CAD model to STL format conversion would show errors as mentioned before, due to the tessellation error. The accuracy of built part is determined by chosen size of the facets [51, 52].

*Flatness of the Building Platform:* Due to the layer-by-layer manufacturing of the stage, any deviation of the stage would create inaccuracies in the part. Unfortunately, the developed system has kind a problem, which needs correction by the mechanical technician.

*Initial Position of Stage:* The laser beam is positioned at a fixed distance according to the focal length of the lens from free processing surface to produce accurate X-Y processing. The beam is positioned by using red guide of the system. However, if the initial position of the stage is above the material surface, it would result in error in the Z direction (vertical) of the model.

*Laser characteristics:* The laser beam diameter may change slightly as the laser tube ages. There may also be shift in the optical alignment due to small temperature variations and the mode structure of the laser may be altered. This would in turn alter the processed material characteristics.

*Changes in Processed Material Properties:* In the normal course of part building, the material characteristics may vary upon refilling of the material with a different lot. Also, material properties may vary with aging due to atmospheric (i.e. oxidation, humidity) or temperature based conditions.

*Variation of Laser Beam Size across Surface:* The shape and diameter of the laser beam spot change from the center to the outer edge. The laser beam spot changes from a perfect circular spot at the center to an elliptical spot at the extreme position. In addition, the beam will also move out of focus as the angle increases. Unless these changes are dynamically compensated by the software resulting errors may be significant [53]. Thanks to the

#### **Chapter 4: Development of Optic-Electronic Hardware and Computer Software 136**

Raylase SP-ICE 2 the correction tables provides better laser light on the surface with minimum error.

*Settling Time (Z-Wait) before Scanning:* Once the platform has moved to the required position, in principle, the powder on the top of the previous layer should cover seamlessly with the free surface after the action of the squeegee (Dr Blade). The relaxation time is dependent upon the rise time and sweeping process completion.

*Changes in Material Level during Building:* The surface level must be maintained at the correct Z-level for optimal laser focus. However, during sintering, the polymer undergoes a volumetric shrinkage. Because of this, polymer surface level will deviate from the optimal level during fabrication, thereby affecting the laser focus.

*Accuracy of doctor blade (Squeegee):* For accurate building, the lower edge of squeegee should be leveled with the free surface of the material.

The other parameters which would affect the system are dimension changes due to shrinkage, distortion during building, post-cure distortion, delamination, entrapped bubbles, trapped volume effect, swelling effects, distortion after support removal[54].



## **5. Conclusion: Technological Demonstration**

### **5.1 Introduction**

The task of technology demonstration for developed laser workstation is crucial to prove the capabilities of the current machine. The goal was to fabricate demonstration components in the suitable materials by confirming the dimensions and proving of the conceptual functionality of the workstation. As it was indicated in previous chapters, the components selected for technology demonstration are the scaffolds generated in former open-architecture rapid prototyping system (to prove that the proposed algorithm is a general solution), the cut laser parts in current developed system (in Module I), polymeric powder sintered freeform and primitive geometric components and laser engraved silicon parts (in Module II). All of these examples are given for validating the algorithm and machine interactions while seeing the results of laser material processing. The geometries are given on each section and the dimensional tolerances are also included presented sections. Microstructural, chemical and mechanical properties are not included in this dissertation.

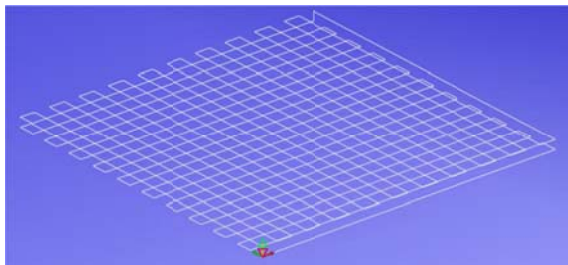
### **5.2 General solution from the plan into the motion G-code Approach**

#### **5.2.1 Scaffold production**

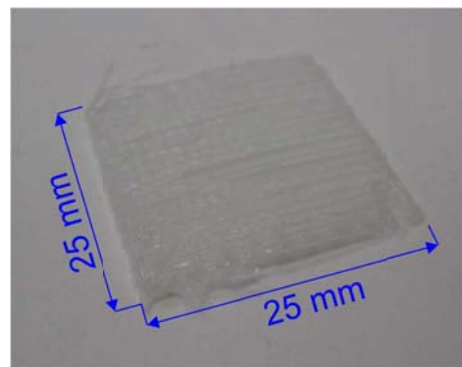
The scaffolds are manufactured in three-dimensional manner. Therefore the operator requires including few data about scaffold, which are the distance between each line (increment) and dimensions of a scaffold in X, Y and Z directions. This information is going to repeated according to rotating manner. This increase the pores and strength of fiber in X and Y directions. The proposed algorithm is not only capable of sending signals for primitive meshed scaffold structures. It is capable of sending any type of  $2\frac{1}{2}$  and 3 axes commands to servo drivers simultaneously.

The figure given below shows the required dimensions and produced dimensions in the first generation open architecture rapid prototyping machine.

The biggest advantage of this G programming approach is writing the required scaffold geometries easily in any notepad program and testing in simulation software such as CIMCO to see the result. On the other hand, without developed MATLAB program it is hard to generate complex geometries.



(a)



(b)

Figure 5.1 G programming output of Open-Architecture Rapid Prototyping Machine V.1  
(a) CIMCO Software Simulation (b) Manufactured scaffold example

In the demonstrated Fig. 5.1, the G-code command is 25 mm x 25 mm and the hatch distance between the adjacent lines is 1 mm. For that purpose the required G-Code commands are given in Table 5.1,

Table 5-1 The given G-code, in order to produce the scaffolds in Fig. 5.1

|                        |                      |                      |
|------------------------|----------------------|----------------------|
| G21 (Metric)           | G01 X0 Y13 Z0 F21    | G01 X11 Y0 Z0.6 F20  |
| G90 (Abs. positioning) | G01 X0 Y14 Z0 F21    | G01 X11 Y20 Z0.6 F20 |
| G92 (Set home)         | G01 X20 Y14 Z0 F21   | G01 X10 Y20 Z0.6 F20 |
| G01 X25 Y-5 Z0 F2      | G01 X20 Y15 Z0 F21   | G01 X10 Y0 Z0.6 F20  |
| G01 X25 Y25 Z0 F2      | G01 X0 Y15 Z0 F21    | G01 X9 Y0 Z0.6 F20   |
| G01 X-5 Y25 Z0 F2      | G01 X0 Y16 Z0 F21    | G01 X9 Y20 Z0.6 F20  |
| G01 X-5 Y-5 Z0 F2      | G01 X20 Y16 Z0 F21   | G01 X8 Y20 Z0.6 F20  |
| G01 x25 Y-5 Z0 F4      | G01 X20 Y17 Z0 F21   | G01 X8 Y0 Z0.6 F20   |
| G01 X0 Y0 Z0 F21       | G01 X0 Y17 Z0 F21    | G01 X7 Y0 Z0.6 F20   |
| G01 X20 Y0 Z0 F21      | G01 X0 Y18 Z0 F21    | G01 X7 Y20 Z0.6 F20  |
| G01 X20 Y1 Z0 F21      | G01 X20 Y18 Z0 F21   | G01 X6 Y20 Z0.6 F20  |
| G01 X0 Y1 Z0 F21       | G01 X20 Y19 Z0 F21   | G01 X6 Y0 Z0.6 F20   |
| G01 X0 Y2 Z0 F21       | G01 X0 Y19 Z0 F21    | G01 X5 Y0 Z0.6 F20   |
| G01 X20 Y2 Z0 F21      | G01 X0 Y20 Z0 F21    | G01 X5 Y20 Z0.6 F20  |
| G01 X20 Y3 Z0 F21      | G01 X20 Y20 Z0 F21   | G01 X4 Y20 Z0.6 F20  |
| G01 X0 Y3 Z0 F21       | G01 X20 Y20 Z0.6 F20 | G01 X4 Y0 Z0.6 F20   |
| G01 X0 Y4 Z0 F21       | G01 X20 Y0 Z0.6 F20  | G01 X3 Y20 Z0.6 F20  |
| G01 X20 Y4 Z0 F21      | G01 X20 Y0 Z0.6 F20  | G01 X2 Y20 Z0.6 F20  |
| G01 X20 Y5 Z0 F21      | G01 X19 Y0 Z0.6 F20  | G01 X2 Y0 Z0.6 F20   |
| G01 X0 Y5 Z0 F21       | G01 X19 Y20 Z0.6 F20 | G01 X1 Y0 Z0.6 F20   |
| G01 X0 Y6 Z0 F21       | G01 X18 Y20 Z0.6 F20 | G01 X1 Y20 Z0.6 F20  |
| G01 X20 Y6 Z0 F21      | G01 X18 Y0 Z0.6 F20  | G01 X0 Y20 Z0.6 F20  |
| G01 X20 Y7 Z0 F21      | G01 X17 Y0 Z0.6 F20  | G01 X0 Y0 Z0.6 F20   |
| G01 X0 Y7 Z0 F21       | G01 X17 Y20 Z0.6 F20 | G01 X25 Y-15 Z5 F16  |
| G01 X0 Y8 Z0 F21       | G01 X16 Y20 Z0.6 F20 |                      |
| G01 X20 Y8 Z0 F21      | G01 X16 Y0 Z0.6 F20  |                      |
| G01 X20 Y9 Z0 F21      | G01 X15 Y0 Z0.6 F20  |                      |
| G01 X0 Y9 Z0 F21       | G01 X15 Y20 Z0.6 F20 |                      |
| G01 X0 Y10 Z0 F21      | G01 X14 Y20 Z0.6 F20 |                      |
| G01 X20 Y10 Z0 F21     | G01 X14 Y0 Z0.6 F20  |                      |
| G01 X20 Y11 Z0 F21     | G01 X13 Y0 Z0.6 F20  |                      |
| G01 X0 Y11 Z0 F21      | G01 X13 Y20 Z0.6 F20 |                      |
| G01 X0 Y12 Z0 F21      | G01 X12 Y20 Z0.6 F20 |                      |
| G01 X20 Y12 Z0 F21     | G01 X12 Y0 Z0.6 F20  |                      |
| G01 X20 Y13 Z0 F21     |                      |                      |

### 5.2.2 Laser cutting operation

Same algorithm would be used in laser cutting operation as it used in the fused deposition method. Instead of injector as in the former section, there is a flying optics which is

focused on a planned to processed material and  $CO_2$  laser source is used for that operation. Details of the hardware are already given in the previous chapters.

On the other hand, there are slight differences between the applied G-code commands to Module I and II. In module I, the operation needs the parameters which are given below

*N0 G0 X(Coordinate Point) Y(Coordinate Point) Z(Coordinate Point) F(mm/sec)*

*N0 G01 X(Coordinate Point) Y(Coordinate Point) Z(Coordinate Point) F(mm/sec) P(Laser Power)*

*N0 G02 X(Start. Coord. Point) Y (Start. Coord. Point) I(Fin. Coordinate X) J(Fin. Coord. Y.) P (Laser Pow.)*

In order to check the geometrical tolerances in the developed system diamond, circle, square and several lines are processed in the developed machine.

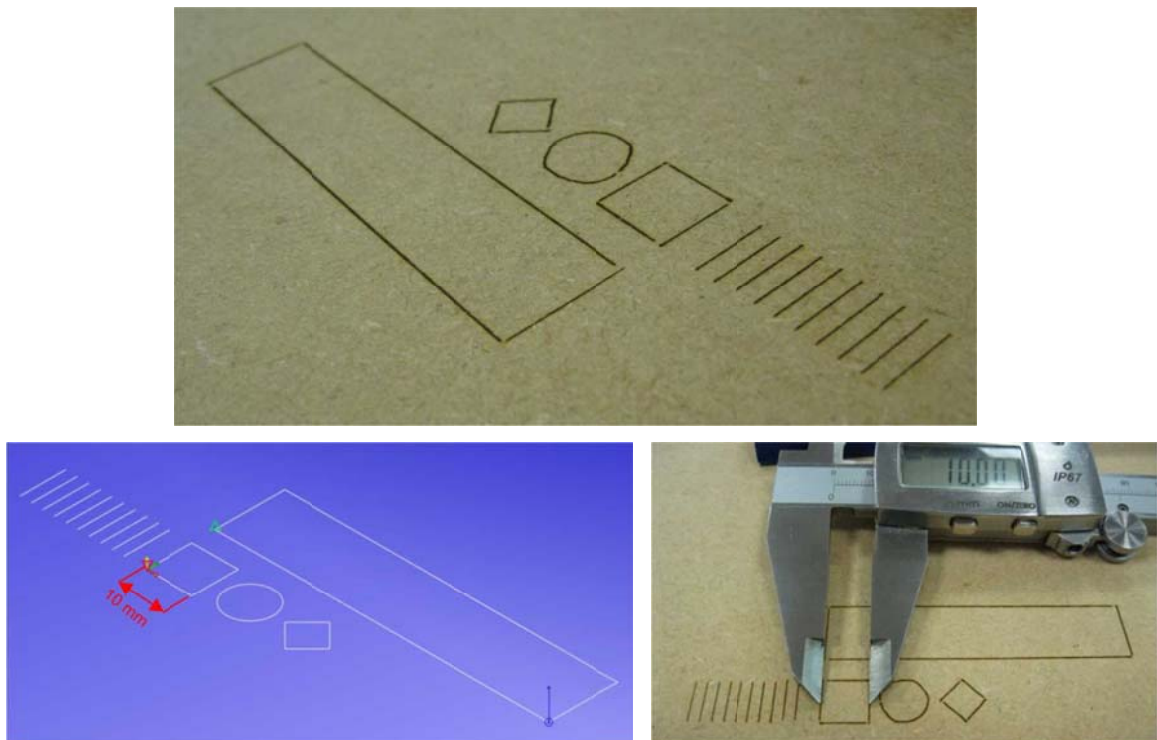


Figure 5.2 Test pattern for the Module I of the developed laser workstation

The G-Code commands for the Module I are given in Table 5.2. The given G-Code commands have line length 10 mm x 10 lines; 10mm x 10mm square; 10mm diameter circle and a diamond shape with  $5\sqrt{2}$ mm edge length.

Table 5-2 G-Code Command for the given test pattern of front part

|                        |                        |
|------------------------|------------------------|
| G21 (Metric units)     | G0 X-17.5 Y0 F100      |
| G90 (Abs. positioning) | G1 X-17.5 Y10 F100     |
| G92 (Set home)         | G0 X-20 Y0 F100        |
| (Layer 1 of 3)         | G1 X-20 Y10 F100       |
| G0 X0 Y0 F100          | G0 X-22.5 Y0 F100      |
| G1 X10 Y0 F100         | G1 X-22.5 Y10 F100     |
| G1 X10 Y10 F100        | G0 X-25 Y0 F100        |
| G1 X0 Y10 F100         | G1 X-25 Y10 F100       |
| G1 X0 Y0 F100          | G0 X-27.5 Y0 F100      |
| G0 X-5 Y10 F100        | G1 X-27.5 Y10 F100     |
| G1 X-5 Y0 F100         | G0 X12.5 Y5 F100       |
| G0 X-7.5 Y10 F100      | G2 X12.5 Y5 I5 J0 F100 |
| G1 X-7.5 Y0 F100       | G0 X25 Y5 F100         |
| G0 X-10 Y0 F100        | G1 X30 Y10 F100        |
| G1 X-10 Y10 F100       | G1 X35 Y5 F100         |
| G0 X-12.5 Y0 F100      | G1 X30 Y0 F100         |
| G1 X-12.5 Y10 F100     | G1 X25 Y5 F100         |
| G0 X-15 Y0 F100        | (END)                  |
| G1 X-15 Y10 F100       |                        |

### 5.3 Three-dimensional (3D) Applications of Developed Laser Workstation

The designed workstation built up by two modules as mentioned before. Hereafter, second module examples are given. In order to avoid the confusion between G-Code of the Modules, the G-Code output of the three-dimensional software part differs from the processed G-Code of Module I. However, due to the open architecture format of the system the module II algorithm would be used in first and vice versa. In any case, in this thesis, the given G-code format is used as default. In addition to that, instead of flying optics herein (Module II) galvanometric scanner is used to guide the laser light.

The process is simple; first the geometry is loaded to developed software. Afterwards, the slicing and toolpath generation steps are completed and coordinate points are generated with input parameters. This created file could be checked via CIMCO as stated before.

### 5.3.1 Powder Sintering Applications

In order to understand the laser material interaction, one line laser tracking is applied on the powders which placed on single and multi-contour wells. The material properties are given in Appendix 5.1. The wells are demonstrated in the Fig. 5.3,

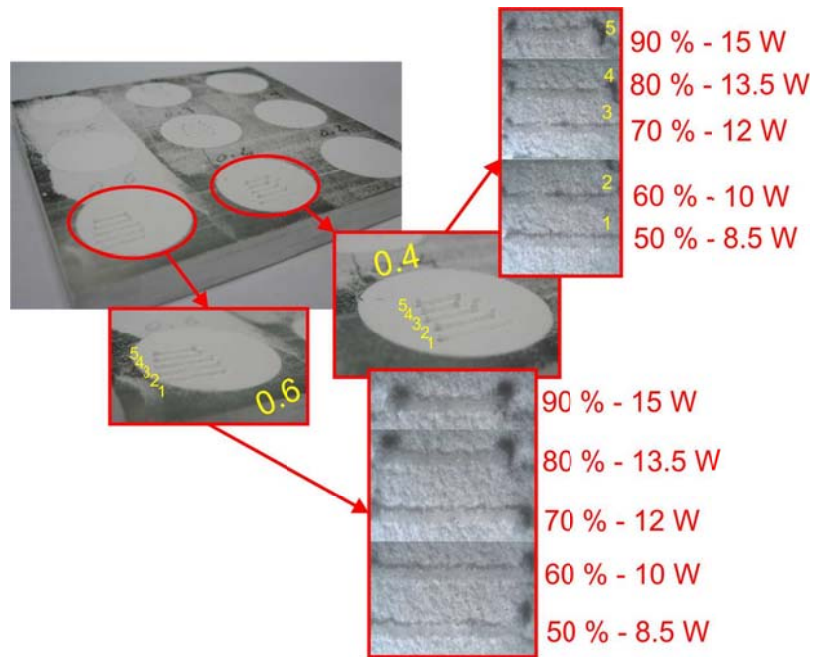


Figure 5.3 Single track testing wells for depth 0.4 [mm] and 0.6 [mm]

The experiments show that the warping is the most important problem in this process. In order to obstruct this problem, some pre-heating operations would be useful on fabrication cylinder. In literature, there are similar solutions like pre-heating this area. Even this method prevent the warpage, the powder is change its structure and hard to recycle with new powder.

The macroscope and microscope examinations (i.e. Fig. 5.4) show that there is also a relation between the given laser power and sintered line diameter as expected. In addition to that, especially in examples 5 the sintering is better with respect to examples 4 or 3. The reason behind that is the laser power is sufficient to melt up to the edges of the powder

layer and creates requested sintered line. The requirement in the sintered geometries is less porosity or solid stated polymers, which would cause mechanical defects in the manufactured components. However, for this example warping need to be impeded.

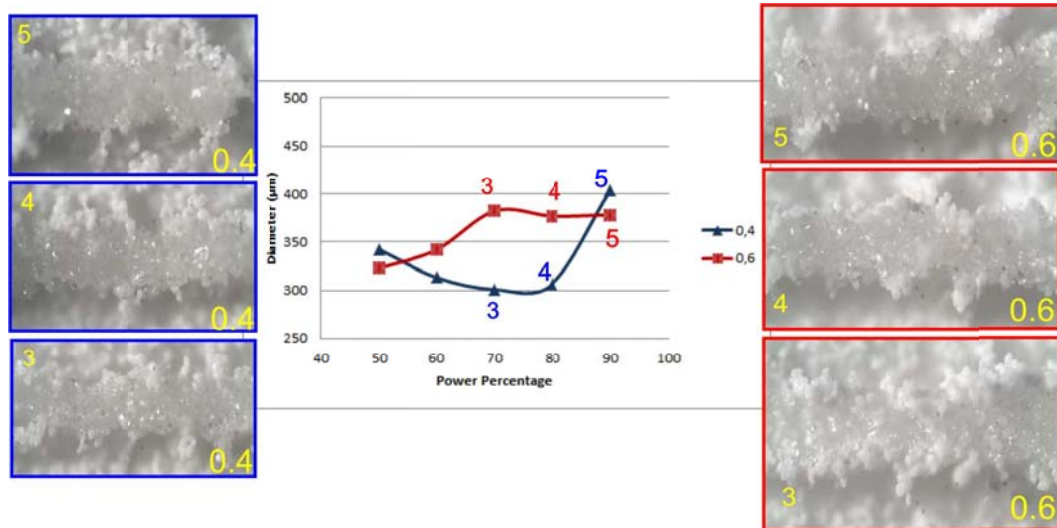
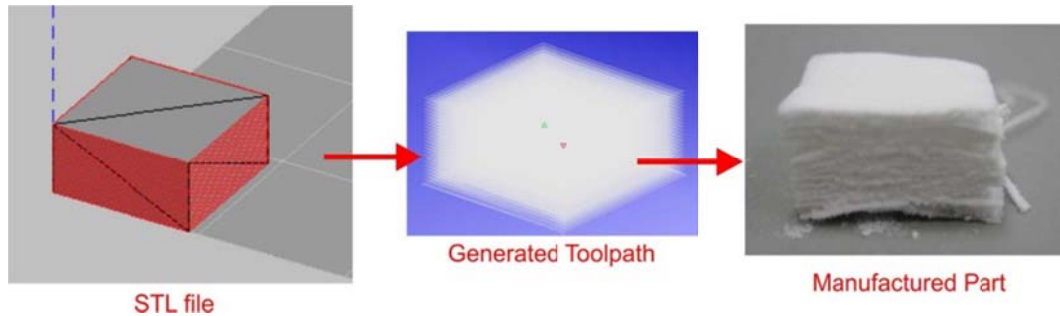
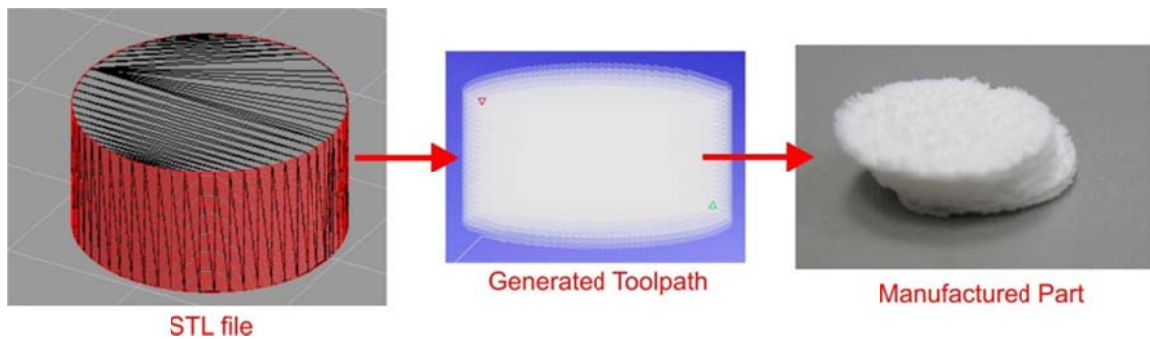


Figure 5.4 Single scan track results with microscopic pictures 0.4 [mm] and 0.6 [mm]

After completing the single line track, some process parameters could be selected as 80 % laser power (to avoid warping), 1 m/s track speed and 200 µm layer thickness (the effective depth is between 150-200 µm). The test geometries given in the following cube (single/ multi layered), cylinder (single/ multi layered), freeform geometry example (fish), complex geometry example (5 axis impeller blade) for powder sintering. In the first step, dimensional accuracies are not considered in three-dimensional geometries because of material based problem should be investigated first. The first easily detected problem is, the interlayer bindings between layers. These bindings are weak and therefore, the layers are split up from each other lightly. This could be seen in Fig. 5.5 (a) in 3D-cube example.



(a)



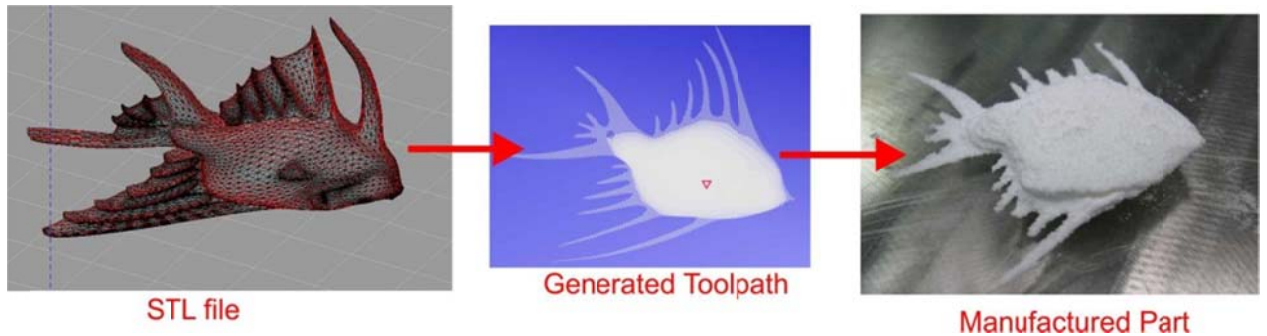
(b)

Figure 5.5 Example geometries, toolpath and manufactured parts

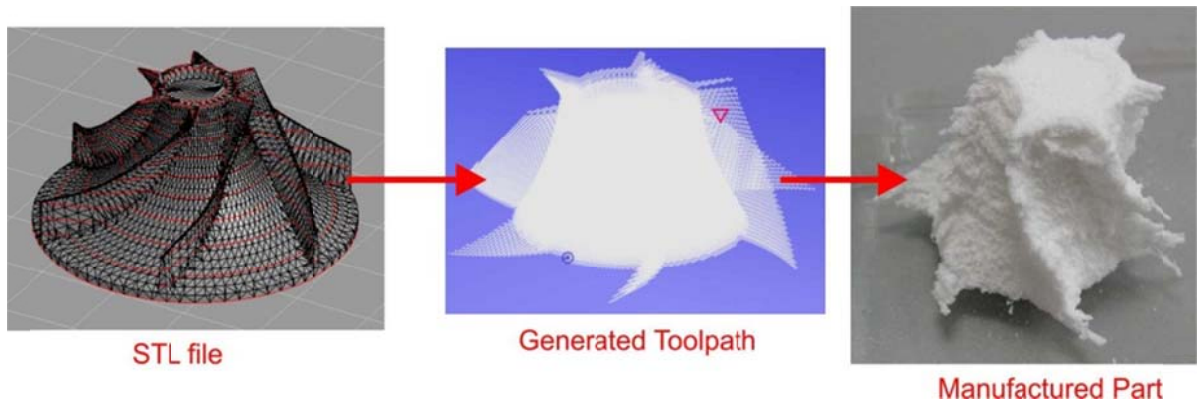
Regarding to the machine and process relation, the powder sweeper is not sufficient for that process as mentioned before. Doctor blade should be change with a cylindrical sweeper which is rotation counter direction with respect to the translation. Doctor blade applied large shear stress on powder bed and the powder sweep is not homogenous with compare to cylindrical sweepers.

Moreover, as given in Fig. 5.5 (b), the sweep action would also shift the manufactured geometry. In addition to that, different than the proposed cylindrical powder feed and sweeping systems could also added in to this system without paramount change in the current electronic hardware and firmware.





(a)



(b)

Figure 5.6 Example geometries, toolpath and manufactured parts

The temperature control of the powder bed should be included to the processing zone. Electrical or infrared heaters will give better results by means of interlayer bonding and warping avoidance. The reason behind that is radiation has faster response to the control signal and more controllable on the confined powder surface.

On the other hand, the dimensions of the manufactured parts are investigated in two-dimensional parts, as given in Fig. 5.7. Moreover, if the three-dimensional parts were manufactured properly, their dimensions have promising results. The square and the

circular part dimensions are 12.5 [mm]. The manufactured part dimensions are given with respect to caliper. The circularity of the designed geometries is not inspected. For future studies roundedness and paralleling check should be completed with the precise measurement of the manufactured parts.

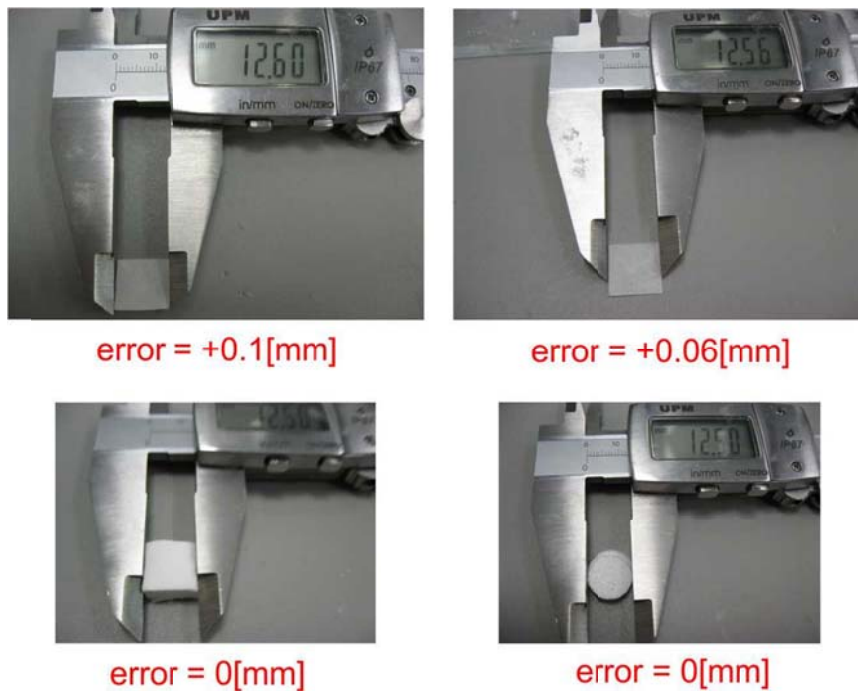


Figure 5.7 Vernier caliper measurements of the manufactured two-dimensional and three-dimensional parts

Appendix 2.1 – Mathematical Derivation of Analytical Model

A.2.1.1 The Point Source Solution

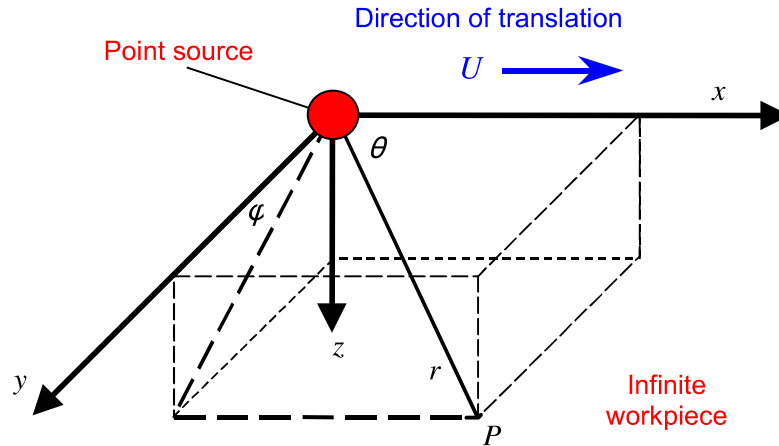


Figure A2.1 Schematic for point source solution

If it is assumed that the workpiece is in steady motion parallel to the x-axis with velocity  $U$  and that all the material parameters are constant with respect to time. The equation,

$$\rho c_p U \frac{\partial T}{\partial x} = \lambda \left( \frac{\partial^2 T}{\partial x^2} + \frac{\partial^2 T}{\partial y^2} + \frac{\partial^2 T}{\partial z^2} \right) + q \quad [A2.1]$$

becomes into

$$U \frac{\partial T}{\partial x} = \kappa \left( \frac{\partial^2 T}{\partial x^2} + \frac{\partial^2 T}{\partial y^2} + \frac{\partial^2 T}{\partial z^2} \right) \quad [A2.2]$$

The parameter  $\kappa$  is the thermal diffusivity (the variables given in Nomenclature of this work) and the schematic of geometry and coordinate system are given in the Fig. A2.1.

The point and line source models are two special solutions of Equation A2.2. That can be obtained as follows. If the transformation,

$$T = T_0 + S e^{\frac{Ux}{2\kappa}} \quad [A2.3]$$

is implemented, where  $T_0$  is the environment temperature, Equation 2.2 reduces to

$$\frac{\partial^2 S}{\partial x^2} + \frac{\partial^2 S}{\partial y^2} + \frac{\partial^2 S}{\partial z^2} = \frac{U^2}{4\kappa^2} S \quad [A2.4]$$

By using  $r = \sqrt{x^2 + y^2 + z^2}$  a solution for S that depends only on the radial distance from the origin is possible. The chain rule shows that

$$\frac{\partial S}{\partial x} = \frac{1}{r} \frac{\partial S}{\partial x} + \frac{x^2}{r} \frac{d}{dr} \left( \frac{1}{r} \frac{dS}{dr} \right) = \frac{1}{r} \frac{dS}{dr} + \frac{x^2}{r^2} \frac{d^2 S}{dx^2} - \frac{x^2}{r^3} \frac{dS}{dr}$$

The second derivatives of S with respect to y and z are identical as x, except x is replaced by y for  $\frac{\partial^2 S}{\partial y^2}$  and by z for  $\frac{\partial^2 S}{\partial z^2}$ . Addition of these derivatives will give

$$\frac{d^2 S}{dr^2} + \frac{2}{r} \frac{dS}{dr} = \frac{U^2}{4\kappa^2} S$$

The explicit form of S in general solution is written [67],

$$S = \frac{A}{r} e^{-\frac{Ur}{\kappa}} + \frac{B}{r} e^{\frac{Ur}{2\kappa}}$$

Combination of these given equations with the definition of S given in (A2.3) shows that

$$T = T_0 + \frac{A}{r} e^{\left\{ \frac{U}{2\kappa}(x-r) \right\}} + \frac{B}{r} e^{\left\{ \frac{U}{2\kappa}(x+r) \right\}} \quad [\text{A2.5}]$$

In the theory of material processing, there is no additional heat input. The remainder of the workpiece acts as a heat sink and the value far from the origin is converges to  $T_0$ . The exponential multiplier B, if  $x > 0$  then the  $x+r > 0$  and so that the coefficient of B tends to converge infinity as x tends to, far heat flow of the heat source. Due to this inconsistency the coefficient must be zero.

In the equation 2.5, there is a necessity to explain the coefficient A. This explanation depends on where the origin of the point source assumed at the surface of a workpiece or in the interior. In this study the point heat source assumed to be in the interior of the small sphere  $\Sigma$  of radius  $a$  centered on the origin and estimated the flux of heat out of the surface of the sphere shown in Fig. 2.3. As long as the thermal energy flows in the sphere across its boundaries and flows out across them. Hence, the Fourier's Law is the only contributor due to the assumption that we have made and this is summed over the surface of the sphere. This means that the total power flows across the surface is

$$\int_{\Sigma} \left( -\lambda \frac{\partial T}{\partial r} \right) d\Sigma = -\lambda A \int_{\Sigma} \frac{\partial}{\partial r} \left\{ \frac{1}{r} e^{\left[ \frac{U r}{2\kappa} (\cos\theta - 1) \right]} \right\} d\Sigma$$

In this equation the coordinate substitution  $x = r \cos\theta$  has been used because of the heat source assumed as sphere. After the differentiation, the  $r$  can be set equal to a

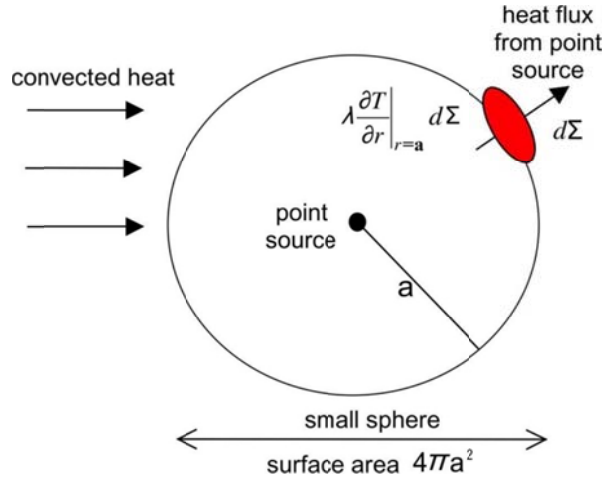


Figure A2.2 On the origin centered sphere (radius  $a$ ), heat flux schematic

The right-hand side of the equation is equal to

$$\lambda A \int_{\Sigma} \left\{ \frac{1}{a^2} e^{\left[ \frac{U a}{2\kappa} (\cos\theta - 1) \right]} + O\left(\frac{1}{a}\right) \right\} d\Sigma$$

The notation  $O\left(\frac{1}{a}\right)$  is neglected compared to the other terms in the equation. These terms are only as big as  $\frac{1}{a}$  if  $a$  is small, and can therefore, as  $a$  is taken to be progressively smaller. For that reason, the exponent is almost zero as well as  $a$  gets smaller. The integrand therefore becomes like  $\frac{1}{a^2}$ , which is a constant on the surface  $\Sigma$ . The value of the integral is simply the surface area of the sphere,  $4\pi a^2$ , multiplied by  $\frac{\lambda A}{a^2}$ . Consequently, if the power supplied by the point source is  $P(W)$ .

$$P = \frac{\lambda A}{a^2} \times 4\pi a^2 = 4\pi \lambda A$$

Giving

$$A = \frac{P}{4\pi\lambda}$$

The point source whose power is P in the interior of an unbounded workpiece, whose temperature far away is  $T_0$ , gives rise to a temperature distribution given by

$$T = T_0 + \frac{P}{4\pi\lambda r} e^{\left\{\frac{U}{2\kappa}(x-r)\right\}} \quad [\text{A2.6}]$$

In which r is radial distance from the point source Fig. A2.6 shows the isotherms corresponding to such a point source embedded in an infinite medium. They are cylindrically symmetric about the x-axis. The diagram has been plotted in dimensionless form so that  $T - T_0$  is scaled with  $PU/k\kappa$ , and the lengths x and r with  $2\kappa/U$  so that

$$T = T_0 + \frac{PU}{2\kappa\lambda} I_p \left( \frac{U_x}{2\kappa} \frac{U_y}{2\kappa} \frac{U_z}{2\kappa} \right)$$

with

$$I_p(x', y', z') = \frac{1}{4\pi} \frac{e^{x' - \sqrt{x'^2 + y'^2 + z'^2}}}{\sqrt{x'^2 + y'^2 + z'^2}} \quad [\text{A2.7}]$$

and

$$x' = \frac{Ux}{2\kappa}, \quad r' = \frac{Ur}{2\kappa}$$

It can be helpful to define the function  $I_p$  in a way that is independent of the specific coordinate system in use; one way of doing so is to define

$$I_p(r', \hat{u}) = \frac{1}{4\pi} \frac{e^{(r'\hat{u} - |r'|)}}{|r'|} \quad [\text{A2.8}]$$

The second argument in this generalized notation for  $I_p$ , written here as  $\hat{u}$ , is a unit vector in the direction of translation and can usually be omitted since, in any given problem, it will always be the same.

There is a difference, however, if the point source is at the surface of a semi-infinite workpiece defined only in  $z \geq 0$ .

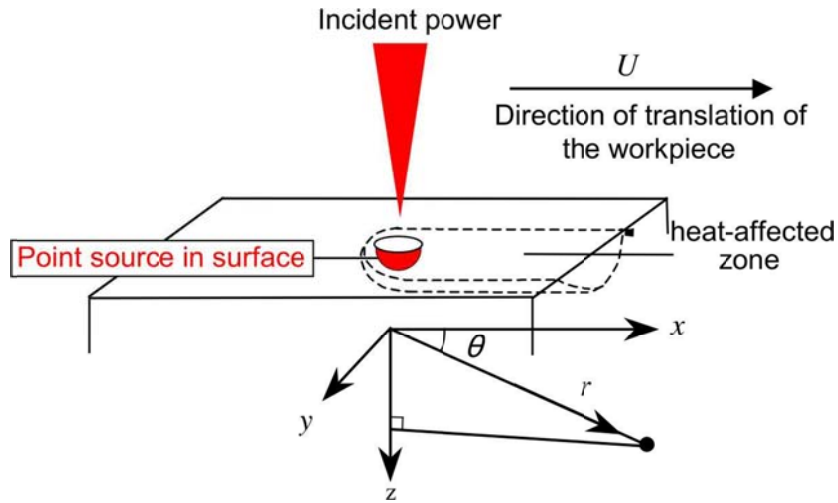


Figure A2.3 Point source on the surface of a workpiece

The solution is still a valid temperature distribution so long as it is assumed that there is no heat loss by radiation, conduction, or any other means across the surface  $z=0$ . By symmetry, the isotherms are perpendicular to the surface, thus ensuring that  $-\lambda \frac{\partial T}{\partial z} |_{z=0} = 0$ . However, all the power now flows into the region  $z \geq 0$ , whereas before only half of it did, the rest flowing into  $z < 0$ . The departure of the temperature from  $T_0$  is therefore double that given by (2.4), resulting in the temperature field

$$T = T_0 + \frac{P}{2\pi\lambda r} e^{\left\{\frac{U}{2\kappa}(x-r)\right\}}$$

which can also be written

$$T = T_0 + \frac{PU}{\kappa\lambda} I_p(x', y', z') \tag{A2.9}$$

for point source of power  $P$  at the surface of a semi-infinite slab. Fig. A.2.4 shows the isotherms corresponding to such a point source embedded in an infinite medium.

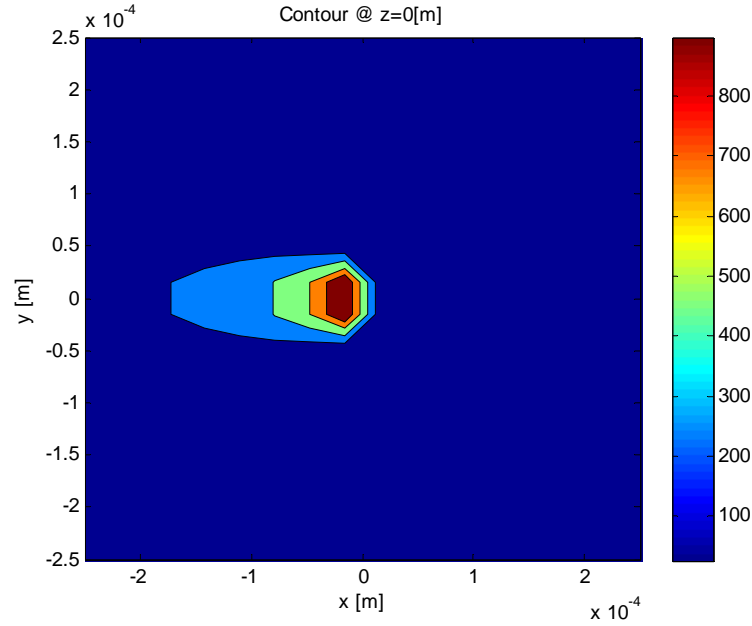


Figure A2.4 Contours of  $I_p(x', y', 0)$ , the contours are at min grid size of 0.03125 [mm] from written MATLAB algorithm of analytical model

**A.2.1.2 Applications of the point source solution**

If there is a specified incident intensity distribution, the point source solution can be very useful in the construction of solutions to problems. The heat conduction equation is not given explicitly as x, y and z;

$$I_p\left(\frac{U}{2\kappa}(x - x_1), \frac{U}{2\kappa}(y - y_1), \frac{U}{2\kappa}(z - z_1)\right)$$

is a solution of the equation, and corresponds to a point source of unit strength located at  $(x_1, y_1, z_1)$ .

Assume that the power absorbed is  $I_a(r_1)\delta S$  over an area  $\delta S$  centered on the point  $r_1 = (x_1, y_1, 0)$  in the surface of the workpiece. Then

$$\frac{I_a(r_1)U}{\lambda\kappa} \text{point} \left( \frac{U(r - r_1)}{2\kappa} \right) \delta S$$

is the added temperature at point r for this particular element. The factor 2 comes from the fact that the power is absorbed in the surface of the workpiece, not its interior. See Eqs.



A2.9. The linearity of the equation of heat conduction (when the coefficients are all constants) is used to add the individual values together for each such small element of area in the surface, giving a temperature distribution that is approximately

$$T = T_0 + \sum_{\text{all } \delta S} \frac{I_a(r_1)U}{\lambda\kappa} I_p \left( \frac{U(r-r_1)}{2\kappa} \right) \delta S$$

In the limit, as the diameter of every element in the surface tends to zero (which is the one of the biggest disadvantages of the analytic models), this becomes an integral over the surface S of the workpiece, so that

$$T(r) = T_0 + \int_{r_1 \in S} \frac{I_a(r_1)U}{\lambda\kappa} I_p \left( \frac{U(r-r_1)}{2\kappa} \right) dS \quad [\text{A2.10}]$$

or

$$T(x, y, z) = T_0 + \frac{1}{2\pi\lambda} \int_{x_1=-\infty}^{\infty} \int_{x_2=-\infty}^{\infty} I_a(x_1, y_1) \times \frac{e^{\left[ \frac{U}{2\kappa}(x-x_1) - \sqrt{(x-x_1)^2 + (y-y_1)^2 + z^2} \right]}}{\sqrt{(x-x_1)^2 + (y-y_1)^2 + z^2}} dy_1 dx_1$$

in which  $I_a(x, y)$  is the absorbed intensity distribution falling on the surface of the workpiece. Normally it is calculated from the relation

$$I_a(x, y) = (1 - \mathcal{R})I(x, y)$$

$I$  is the actual incident intensity and  $\mathcal{R}$  is a suitably chosen reflection coefficient. These coefficients are already given in Table 2.4-2.5 as initial conditions. An alternative way of expressing temperature gradient on the surface of the workpiece is to make the substitution  $x_1 = x - x_2, y_1 = y - y_2$ . In that case, the alternative form of the integral is

$$T(x, y, z) = T_0 + \frac{1}{2\pi\lambda} \int_{x_1=-\infty}^{\infty} \int_{x_2=-\infty}^{\infty} I_a(x - x_2, y - y_2) \times \frac{e^{\left[ \frac{U}{2\kappa}(x_2 - \sqrt{x_2^2 + y_2^2 + z^2}) \right]}}{\sqrt{x_2^2 + y_2^2 + z^2}} dy_2 dx_2$$

Either of these forms could be used with the following two cases as specially-shaped distributions of surface intensity.

The only examined case of a Gaussian beam of radius  $a$  centered on the origin for which,

$$I(x, y) = \frac{P}{2\pi a^2} e^{-\frac{x^2 + y^2}{2a^2}} \quad [2.12]$$

The total power in Gaussian beam case is  $P$ . Fig. A2.5 shows graph of the intensity with the corresponding surface map. In general, the integrations will have to be performed numerically to find the temperature below the surface of the intensity region.

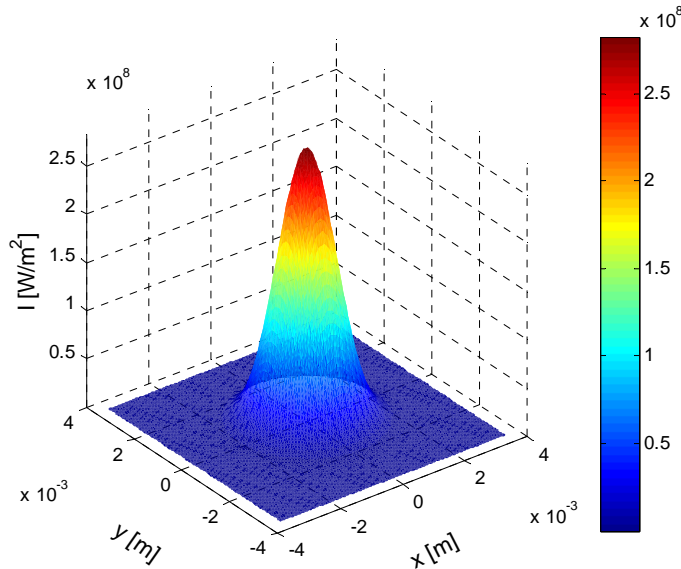


Figure A2.5 The Gaussian source is shown as a surface plot  $P=1\text{kW}$ ,  $I_{max} = 0.28 \text{ GW}/\text{m}^2$  Equation A2.12 might be used to study the effect of other shapes into Equation A2.11 by integrating it over the required shape using the same power for each individual elementary Gaussian source. The discontinuities at the peak position of the Gaussian source should be taken care of as the following partial function,

$$I(x, y) = \begin{cases} P/\pi a^2 & \sqrt{x^2 + y^2} < a \\ 0 & \text{otherwise} \end{cases} \quad \text{[A2.13]}$$

The Equation A2.11 would be converted into polar instead of cartesian one. This would be easier in order to get temperature distribution due to the elimination of the double integral. Beyond these calculations a mathematical approximation is sometimes available and worthwhile to try. If the intensity distribution is characterized by a length scale  $a$ , so that outside a distance from the origin of this order,  $I_a$  is effectively zero. In that case, there is a Péclet number  $Pe = Ua/2\kappa$  and this determined the relative dominance of the exponential

term. The exponential falls very rapidly from the maximum value as  $\theta$  from zero and the integrand is effectively zero, if the Péclet number is large. What this means is that if  $\cos\theta$  is replaced by its local approximation,  $1 - \frac{1}{2}\theta^2$ , the error introduced will be very small indeed. Furthermore, the range of integration can even be extended (purely for convenience) to  $-\infty < \theta < \infty$  without significant additional error. The contribution from the intensity can then be approximated by the value local to  $\theta = 0$ . It does not vary rapidly on the length-scale  $a$ , unlike the exponential, so it will not have changed significantly by the time the exponential has become very small.

### A2.1.3 Line Source Solution

The line source solution can be obtained in essentially the same way as the point source. The difference is that a solution is sought that depends only on the coordinate in the direction of translation and distance from z-axis, but is independent of distance in the z direction. As before, it is assumed that the workpiece is moving steadily parallel to the x-axis with velocity  $U$ , and that all the material parameters are constants. Consequently, the temperature satisfies Equation (A2.2). Figure A2.6 shows the relative geometry and the coordinate system. Once again, look for a solution of the form given by Equation (A2.3) so that  $S$  is given by (A2.3).

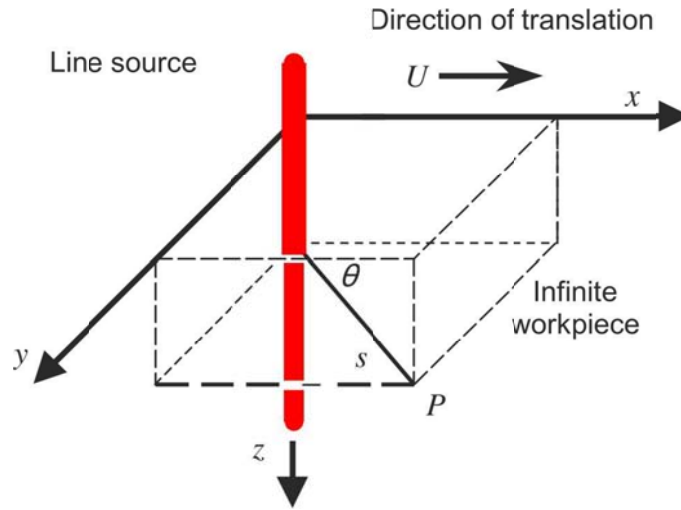


Figure A2.6 The line source schematic, the relative geometry and the coordinate system implementation

For the sake of the complexities the coordinate transformation would be better for this analytical model as stated at the end of point source model. Meanwhile, this transformation could also be used point source solution. The solution for S that depends only on distance s from the z-axis,  $s = \sqrt{x^2 + y^2}$ . (As a reminder, the usage of r to mean both radial distance from the origin of spherical polar coordinates and the distance from the axis in cylindrical coordinates is very common. This is not standard and used only for avoiding confusion.)

The equation,

$$\frac{\partial S}{\partial x} = \frac{\partial s}{\partial x} \frac{dS}{ds} = \frac{x}{s} \frac{dS}{ds}$$

Consequently,

$$\frac{\partial^2 S}{\partial x^2} = \frac{1}{s} \frac{dS}{ds} + \frac{x^2}{s^2} \frac{d^2 S}{ds^2} - \frac{x^2}{s^3} \frac{dS}{ds}$$

and similarly for the second derivative of S with respect to z. The second derivative with respect to z is unaltered in form. Adding together shows that,

$$\frac{d^2 S}{ds^2} + \frac{1}{s} \frac{dS}{ds} - \frac{U^2}{4\kappa^2} S = 0$$

As stated also in Abramowitz and Stegun [68], the general solution of this equation is,

$$S = AI_0\left(\frac{U_s}{2\kappa}\right) + BK_0\left(\frac{U_s}{2\kappa}\right)$$

where  $I_0$  and  $K_0$  are the modified Bessel functions of order 0. In order to understand use of this solution, it is helpful to show the behavior of the two functions  $I_0$  and  $K_0$ . Figure A2.7 demonstrates the graphs of each of them on the same axis. [68] The most important points to notice are the following.

- $I_0$  increases indefinitely as  $s'$  increases;
- $K_0$  tends to zero as  $s'$  increases;
- $K_0$  is unbounded (tends to infinity) as  $s'$  tends to zero.

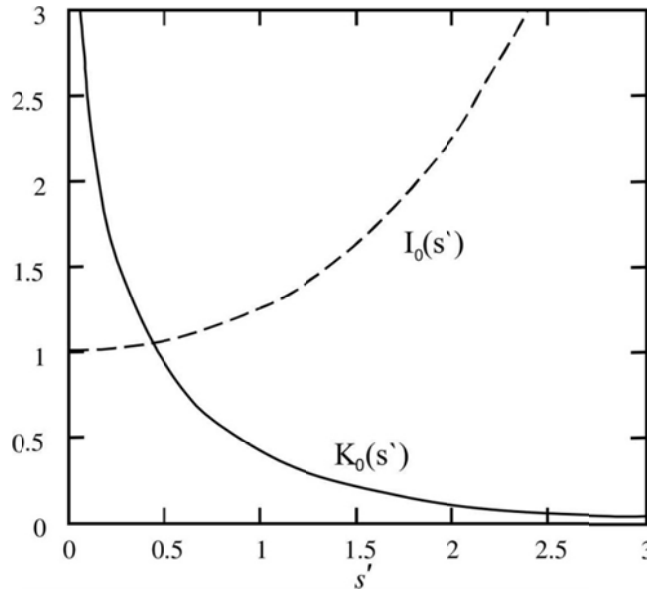


Figure A2.7 The  $K_0(s')$  (solid line) and  $I_0(s')$  (broken Line)

Suppose the combination of the given definition of S in (2.3) and this solution of S, it follows that

$$T = T_0 + Ae_0^{\left(\frac{U}{2\kappa}x\right)} I_0\left(\frac{US}{2\kappa}\right) + Be^{\frac{U}{2\kappa}} K_0\left(\frac{US}{2\kappa}\right)$$

Once again imposes a restriction on the coefficients A and B as stated in point source solution, the condition that there is no additional heat input to the remainder of the workpiece (acts as a heat sink). For large value of s the asymptotic forms of the Bessel functions show that

$$T \sim T_0 + A \sqrt{\left(\frac{\kappa}{\pi U s}\right)} e^{\left\{\frac{U}{2\kappa}(x+s)\right\}} + B \sqrt{\frac{\pi\kappa}{U s}} e^{\left\{\frac{U}{2\kappa}(x-s)\right\}}$$

For the coefficient A,  $x + s > 0$  if  $x > 0$ , so that the multiple of A tends to infinity as  $x$  tends to infinity far from the heat source; consequently, the coefficient A must be zero.

An explanation of B is valid in the same manner as before; once again some attention is required depending on the position of the z-axis whether in interior or on the surface of a semi-infinite workpiece. In this study z will be assumed in the interior.

Instead of the spherical heat flux model, here cylindrical one will be taken for heat flux approximation. The consideration based on a small cylinder (radius a) centered on the axis and the flux will be estimated from its surface per unit length as in Figure A2.8. As much thermal energy flows into the cylinder across its boundaries as flows out across them. The only contribution to the flux is the part due to Fourier's law, and this has to be summed over the surface of the cylinder; i.e., the total power flowing across the surface per unit length is

$$\int_C \left(-\lambda \frac{\partial T}{\partial s}\right) dC = -\lambda B \int_C \left\{ e^{\frac{U}{2\kappa} s \cos\theta} K_0\left(\frac{U s}{2\kappa}\right) \right\} dC \quad [A2.14]$$

where the polar coordinate substitution  $x = s \cos\theta$  has been used. It should be remembered that after the differentiation has been performed, s can be set equal a.

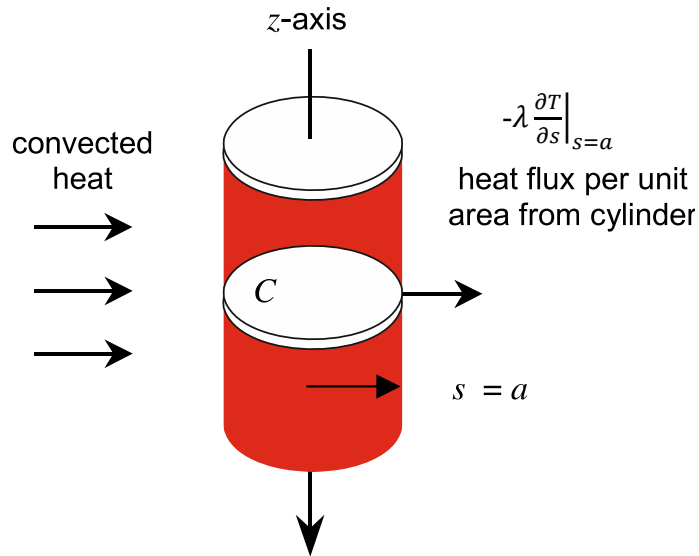


Figure A2.8 Heat flux out of a cylinder of a radius a

By using Euler-Mascheroni coefficient ( $\gamma = 0.57 \dots$ ), the  $K_0(s')$  will be

$$K_0(s') = - \left\{ \ln \frac{1}{2} s' + \gamma \right\} O(s'^2)$$

and the derivation is

$$\frac{\partial}{\partial s} \left\{ \exp \left( \frac{U}{2\kappa} s \cos \theta \right) K_0 \left( \frac{Us}{2\kappa} \right) \right\} = \frac{\partial}{\partial s} \left\{ e^{\frac{U}{2\kappa} s \cos \theta} \left[ - \ln \frac{1}{2} s - \gamma + O(s'^2) \right] \right\} = - \frac{1}{s} + O(\ln s)$$

The right-hand side of equation (A2.14) is equal to,

$$- \lambda B \int_C \left\{ - \frac{1}{a} + O(\ln a) \right\} dC$$

As used in the section of point source solution, the notation  $O(X)$  is capable of big as  $X$ . Due to that, the integrand will be progressively like  $1/a$  since  $a \ln a \rightarrow 0$  as  $a \rightarrow 0$ , and therefore coefficient on the surface of  $C$  for sufficiently small  $a$ . In conclusion, the integral is just as the length of the circumference of the circle,  $2\pi a$ , which multiplied by  $\frac{\lambda B}{a}$ . If the power given by the line source per unit length is  $Q$ ,

$$Q = \frac{\lambda B}{a} \times 2\pi a = 2\pi \lambda B$$

and

$$B = \frac{Q}{2\pi\lambda}$$

Therefore, the  $Q(W/m)$  powered line source with the interior of an unbounded workpiece whose ambient temperature is  $T_0$  brings the increment to a temperature distribution given by equation

$$T = T_0 + \frac{Q}{2\pi\lambda} e^{\frac{Ux}{2\kappa}} K_0\left(\frac{Us}{2\kappa}\right) \tag{A2.15}$$

$s$  is the distance from the source.

Figure A2.9 shows the temperature profile corresponding to such a line source embedded in an infinite medium (material properties are given in Appendix 2.4). The diagram has been plotted in dimensionless form so that  $T - T_0$  is scaled with  $QU/\lambda\kappa$  and the lengths  $x$  and  $r$  with  $2\kappa/U$  so that

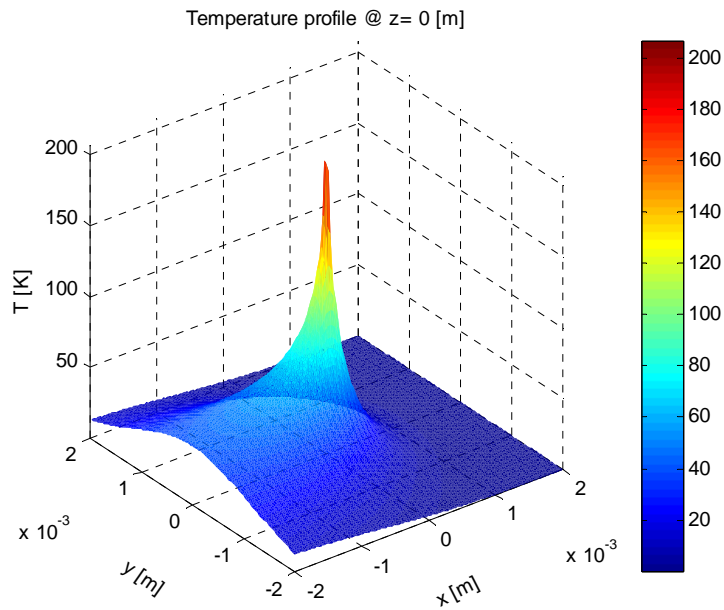


Figure A2.9 Temperature profile for thin steel plate ( $P=50W$ ,  $\lambda = 73W/K$ ,  $C_p = 472 J/kgK$ ,  $v=50mm/s$ ,  $\rho = 7870kg/m^3$ )

$$T = T_0 + \frac{Q}{\lambda} I_0(x', y')$$



and

$$I_l(x', z') = \frac{1}{2\pi} e^{x'} K_0 \sqrt{x'^2 + y'^2} \quad [A2.16]$$

with

$$x' = \frac{Ux}{2\kappa}, y' = \frac{Uy}{2\kappa}$$

If  $I_l$  can be defined in coordinate free, it might be useful as,

$$I_l(\mathbf{s}', \hat{\mathbf{u}}) = \frac{1}{2\pi} e^{s' \cdot \hat{\mathbf{u}}} K_0(s') \quad [A2.17]$$

$\hat{\mathbf{u}}$  is a unit vector in the direction of translation and can often be left out. As given in the Fig. A2.6, the vector  $s'$  is the vector perpendicular to the line source to the point P in space given by the position vector  $r'$ . It is related to  $r'$  by perpendicular to the direction of translation, so that  $\hat{\mathbf{u}} \cdot \mathbf{k} = 0$ . Fig. A2.12 shows the difference, if the line source lies along the y-axis in the surface of a semi-infinite workpiece defined only in  $z \geq 0$ .

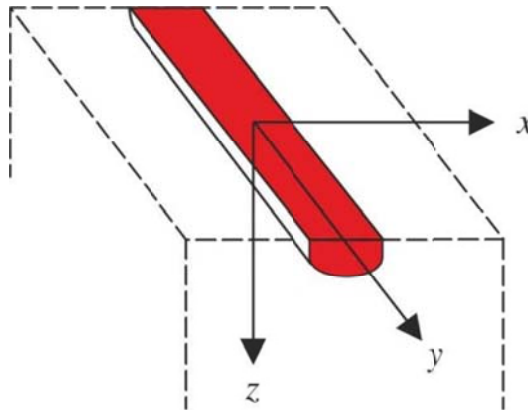


Figure A2.10 The source on the surface of a workpiece

Across the surface  $z=0$ , there is no heat loss by radiation, convective cooling, or any other effects which may corrupt the symmetry of the isotherms. The condition  $-\lambda \frac{\partial T}{\partial z} \Big|_{z=0} = 0$  is obtained due to the perpendicularity of the isotherms to the surface and therefore this solution is compatible with the assumption of no heat loss on the boundary. The result in the temperature distribution is double with respect to the equation 2.15.

$$\begin{aligned}
 T &= T_0 + \frac{Q}{\pi\lambda} e^{\frac{Ux}{2\kappa}} K_0\left(\frac{U}{2\kappa} \sqrt{x^2 + z^2}\right) \\
 &= T_0 + 2\frac{Q}{\lambda} I_l(x', z')
 \end{aligned}
 \tag{A2.18}$$

Just as the point source solution can be used to construct further solution by adding together individual solutions or, in the limit, integrating over them, so, too, the line source solution can be used in exactly the same way. Suppose it is desired to find the temperature distribution in a semi-infinite block whose surface  $z = 0$  is subject to an incident intensity, whose absorbed value is  $I_a(x)[W/m^2]$ , and is independent of the lateral coordinate  $y$ . If we consider just the effect due to absorption in a strip of width  $\delta x_1$  in the surface at  $x = x_1$ , the rise in the temperature at the point  $(x, z)$  caused by absorption in the strip is

$$\delta T = 2 \frac{I_a(x_1) \delta x_1}{\lambda} I_l\left(\frac{U(x-x_1)}{2\kappa}, \frac{Uz}{2\kappa}\right)$$

In order to find the rise in temperature caused by all of these small strips it is only necessary to add them all together or, in the limit, to use integration. The result is that

$$T = T_0 + \frac{2}{\lambda} \int_{x_1=-\infty}^{\infty} I_a(x_1) I_l\left(\frac{U(x-x_1)}{2\kappa}, \frac{Uz}{2\kappa}\right) dx_1
 \tag{A2.19}$$

Alternatively, the substitution  $x_1 = x - x_2$  can be made so that the temperature distribution is given by

$$T = T_0 + \frac{2}{\lambda} \int_{x_2=-\infty}^{\infty} I_a(x - x_2) I_l\left(\frac{Ux_2}{2\kappa}, \frac{Uz}{2\kappa}\right) dx_2
 \tag{A2.20}$$

These formulae can be applied for example to the one-dimensional Gaussian distribution

$$I(x) = Q \frac{e^{-\frac{x^2}{2a^2}}}{a\sqrt{2\pi}}
 \tag{A2.21}$$

and one-dimensional ‘‘top-hat’’ distribution

$$I(x) = \frac{Q}{2a} \mathbf{H}(a - |x|) = \begin{cases} 0 & x < -a \\ Q/2a & -a < x < a \\ 0 & x > a \end{cases}
 \tag{A2.22}$$

in which  $\mathbf{H}(\mathbf{x})$  is the Heaviside step function whose value is zero when its argument is negative, and 1 when it is positive. In the problems considered, its value at the point of discontinuity is irrelevant provided, in practice, the intensity distribution is not

characterized by a sharp spike at these points. In each case  $Q$  is the absorbed power per unit width of the workpiece and  $2a$  is the beam width. Either formula can be used, but in the case of the top-hat distribution, care is needed with (A2.20), as the integral is over a finite range from  $x - a$  to  $x + a$ .

If Equation (A2.20) is used, the problem with the top-hat distribution has a solution that can be written [53]. Note that the solution given there is for a line source moving through the interior of an infinite medium, and their symbol  $Q$  is the quantity used here divided by  $2a$ ;  $a$  is  $b$  in their notation.)

$$T = T_0 + \frac{Q}{2\pi\lambda a} \int_{x_1=x-a}^{x+a} e_0^{\left(\frac{Ux_1}{2\kappa}\right)} K_0 \left( \frac{U}{2\kappa} \sqrt{x_1^2 + z^2} \right) dx_1$$

it can also be written as

$$T = T_0 + \frac{Q}{2\pi\lambda} f\left(\frac{Ux}{2\kappa}, \frac{Uz}{2\kappa}, \frac{Ua}{2\kappa}\right) \quad [\text{A2.23}]$$

with

$$f(x', z', Pe) = \frac{1}{Pe} \int_{x'_1=x-Pe}^{x'+Pe} e^{x'_1} K_0 \left( \sqrt{x'^2_1 + z'^2} \right) dx'_1 \quad [\text{A2.24}]$$

The form for  $f$  is obtained by means of the substitutions  $x' = Ux/2\kappa$ ,  $x'_1 = Ux_1/2\kappa$ ,  $z' = Uz/2\kappa$  and  $Pe = Ua/2\kappa$ . Note the way in which the maximum temperature and the thickness of the layer affected both decrease as the Péclet number increases. The maximum temperature always occurs on the surface.

**Appendix 2.2 Thermal Model Codes**

```
function T=PointSrcCal(mat,P,v,x,y,z)
errorCheck=1e-12;
s=size(x);

if prod(s)>max(s)
    error('x shall be a row vector.');
```

---

```
end;
if s(1,1)>1
    x=x';
end;
s=size(y);
if prod(s)>max(s)
    error('y shall be a row vector.');
```

---

```
end;
if s(1,1)>1
    y=y';
end;

LK1=P/2/pi/mat.K;
LK2=abs(v)/2/mat.kappa;

[X Y]=meshgrid(x,y);

T.name='TempPointSrc';
T.x=x;
T.y=y;
T.z=z;

for m=1:length(z)
    R=sqrt(Y.^2+X.^2+z(m)^2);
    if min(min(R))==0
        R=R+errorCheck;
    end
    T.Txyz(:, :, m)=LK1*exp(-LK2*(X+R))./R;
end;
```

---

```

function T=TempLineSrc(mat,P,v,x,y,z)

s=size(x);

if prod(s)>max(s)
    error('x shall be a row vector.');
```

end;

```
if s(1,1)>1
    x=x';
end;
s=size(y);
if prod(s)>max(s)
    error('y shall be a row vector.');
```

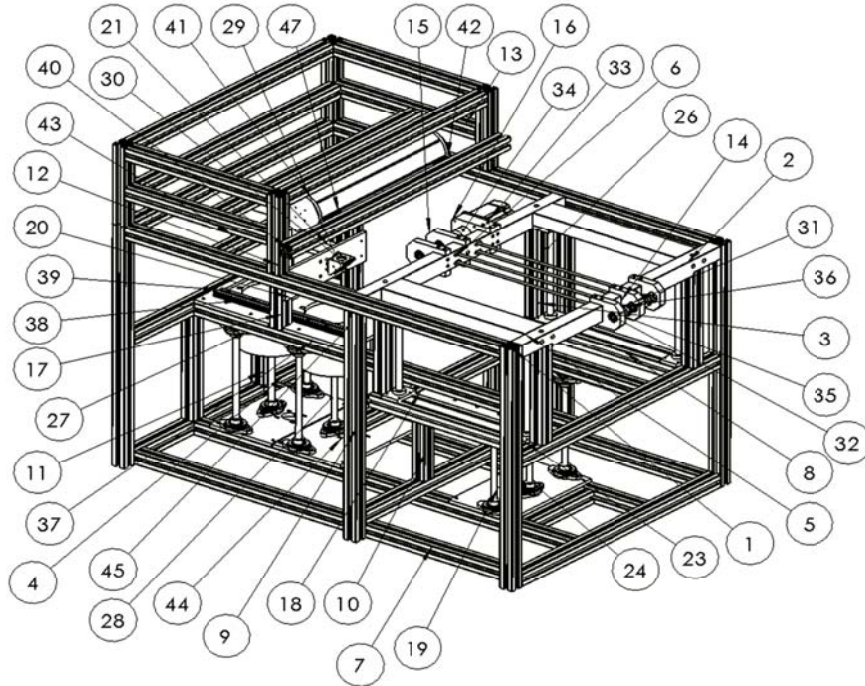
end;

```
if s(1,1)>1
    y=y';
end;
LK1=Q/(2*pi*mat.Ti);
LK2=v/(2*mat.Ti);
[X Y]=meshgrid(x,y);
R=sqrt(Y.^2+X.^2);
t=LK1*exp(-LK2*X).*besselk(0,LK2*R);
T.x=x;
T.y=y;
T.Txyz(:,:,1)=t;

n=max(size(T));
N=4;

for j=1:n
    [cs,h]=contourf(T(j).x,T(j).y,T(j).Txyz(:,:,1),N);
    colorbar;
    xlabel('x [m]');
    ylabel('y [m]');
    s='Contour';
    if isfield(T(j),'z')
        s=[s ' @ z=' num2str(T(j).z(1)) '[m]'];
    end
    if n>1
        s=[ 't=' num2str(T(j).t) '[s], ' s ];
    end
    title(s);
    axis([-0.25e-3 0.25e-3 -0.25e-3 0.25e-3]);
end
```

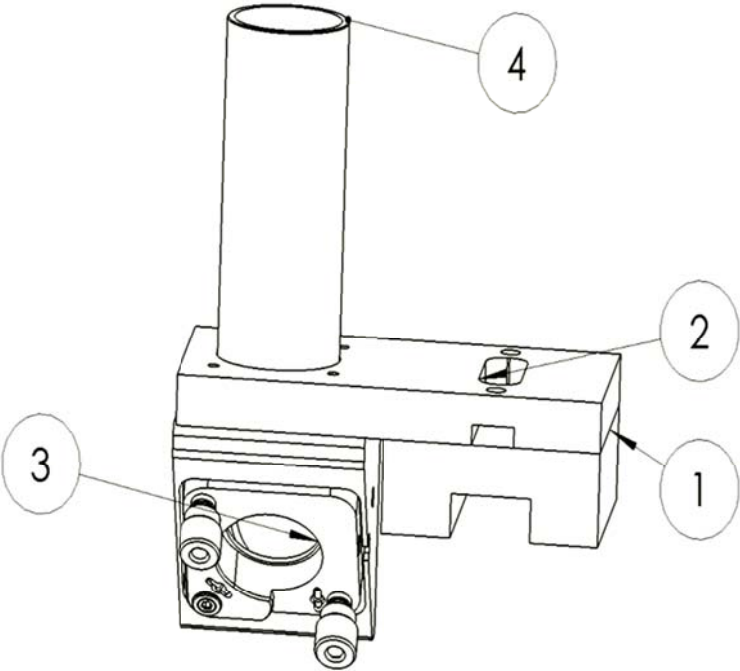
A3.1.1 Chassis Assembly



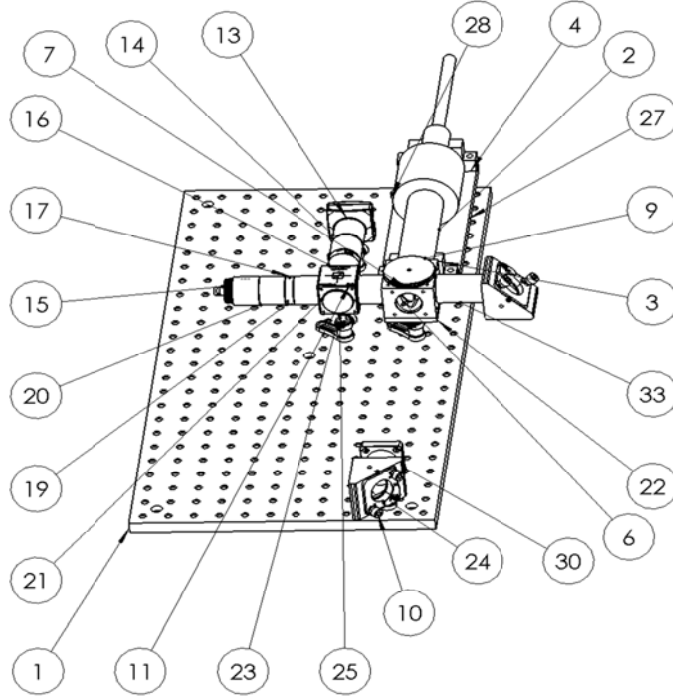
| ITEM NO. | PART NUMBER               | QTY. | ITEM NO. | PART NUMBER          | QTY. |
|----------|---------------------------|------|----------|----------------------|------|
| 1        | 765040040_750             | 4    | 37       | BackPlate            | 1    |
| 2        | xyFront                   | 1    | 38       | LinearGuide          | 2    |
| 3        | 765040040_ddd             | 4    | 39       | backPlate1           | 2    |
| 4        | 765040040_800             | 12   | 40       | 765040040_880        | 1    |
| 5        | xyFrontMiddle             | 2    | 41       | laser_cavity         | 2    |
| 6        | xyBack                    | 1    | 42       | laserKapak           | 4    |
| 7        | 765040040_1100            | 8    | 43       | galvo2               | 1    |
| 8        | 765040080_500             | 2    | 44       | servo_powder_flange3 | 1    |
| 9        | 765040040_750_2           | 2    | 45       | PowderDepot          | 2    |
| 10       | 765040040_2492            | 2    | 46       | Chasis Base          | 1    |
| 11       | 765040040_2492_2          | 2    | 47       | Laser Plate          | 1    |
| 12       | 765040040_245             | 5    | 48       | Part4^Chasis         | 1    |
| 13       | 765040040_45447           | 4    |          |                      |      |
| 14       | FrontActFlange            | 3    |          |                      |      |
| 15       | 750WFlange                | 2    |          |                      |      |
| 16       | ServoFlange               | 1    |          |                      |      |
| 17       | 765040040_3015            | 2    |          |                      |      |
| 18       | OnKapak                   | 2    |          |                      |      |
| 19       | servo_powder_flange       | 2    |          |                      |      |
| 20       | GalvoFlange1              | 1    |          |                      |      |
| 21       | GalvoFlange2              | 2    |          |                      |      |
| 22       | GalvoFlange3              | 1    |          |                      |      |
| 23       | LinearGuideEnd            | 8    |          |                      |      |
| 24       | inafagBearing             | 15   |          |                      |      |
| 25       | powder_linear_rail_ust    | 2    |          |                      |      |
| 26       | FrontChasisLinearGuide    | 4    |          |                      |      |
| 27       | powder_z_linear_rail      | 6    |          |                      |      |
| 28       | powder_z_linear_screw     | 3    |          |                      |      |
| 29       | 13038-E0W                 | 1    |          |                      |      |
| 30       | 8572-E0W                  | 4    |          |                      |      |
| 31       | SKF - 6200 - 8,SI,NC,8_68 | 7    |          |                      |      |
| 32       | Circlip DIN 471 - 10 x 1  | 11   |          |                      |      |
| 33       | 750W                      | 1    |          |                      |      |
| 34       | Part3^Chasis              | 1    |          |                      |      |
| 35       | pulleyPhi12               | 4    |          |                      |      |
| 36       | BeltY                     | 2    |          |                      |      |

A3.1.2 Fly-optics X-axis

| ITEM NO. | PART NUMBER     | QTY. |
|----------|-----------------|------|
| 1        | Xaxis           | 1    |
| 2        | Xaxis2          | 1    |
| 3        | 13038-E0W-Xaxis | 1    |
| 4        | 0209-E0W-Xaxis  | 1    |



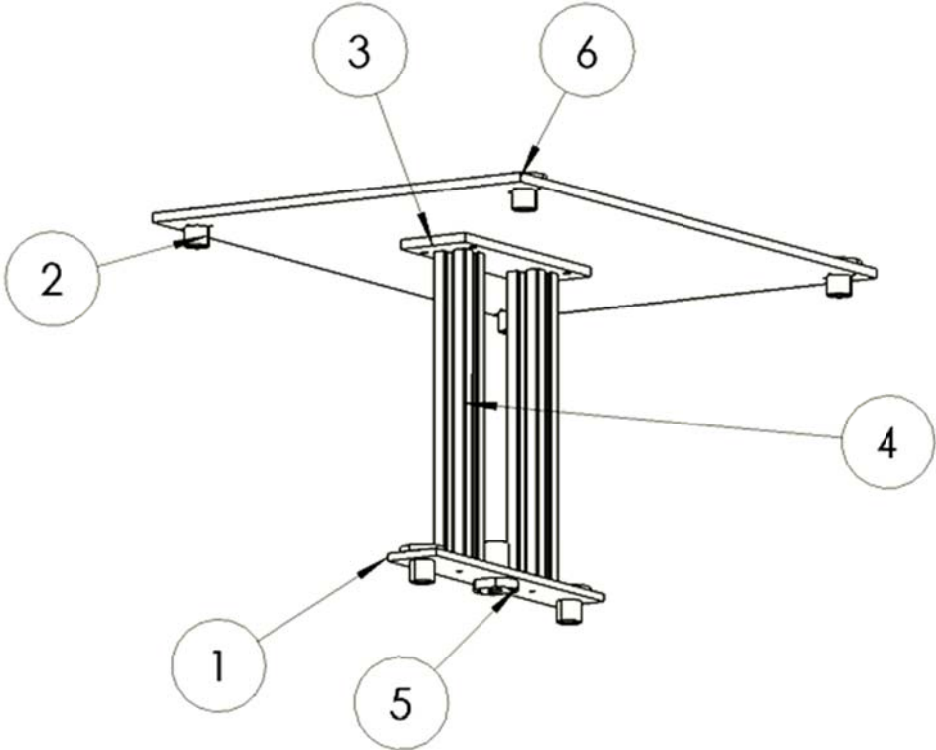
A3.1.3 Laser Feedback Assembly



| ITEM NO. | PART NUMBER         | QTY. |
|----------|---------------------|------|
| 1        | 6281-E0W            | 1    |
| 2        | laser_head          | 1    |
| 3        | Part15_2            | 1    |
| 4        | Part15              | 1    |
| 5        | 20731-E0W           | 1    |
| 6        | 1296-E0W            | 1    |
| 7        | 0198-E0Wb           | 1    |
| 8        | Part2^Assem1        | 1    |
| 9        | 1181-E0W            | 1    |
| 10       | 13038-E0W           | 3    |
| 11       | 20404-E0W           | 1    |
| 12       | 7703-E0W            | 1    |
| 13       | 19418-E0W           | 1    |
| 14       | lens                | 1    |
| 15       | 14182-E01           | 1    |
| 16       | 21444-E0W           | 5    |
| 17       | 2157-E0W            | 2    |
| 18       | 4488-E0W            | 1    |
| 19       | 18672-E0W           | 1    |
| 20       | 0371-E0W            | 2    |
| 21       | 0757-E0W            | 1    |
| 22       | 0762-E0W            | 1    |
| 23       | 11899-E0W           | 2    |
| 24       | 8583-E0W            | 5    |
| 25       | 8574-E0W            | 8    |
| 26       | 11900-E0W           | 1    |
| 27       | Part6^Laserfb       | 1    |
| 28       | 7271-E0W            | 4    |
| 29       | 8572-E0W            | 1    |
| 30       | 0440-E0W            | 2    |
| 31       | Part15^machine1     | 1    |
| 32       | Part22^machine1     | 1    |
| 33       | 21445-E0W           | 1    |
| 34       | Part1^Laserfeedback | 1    |

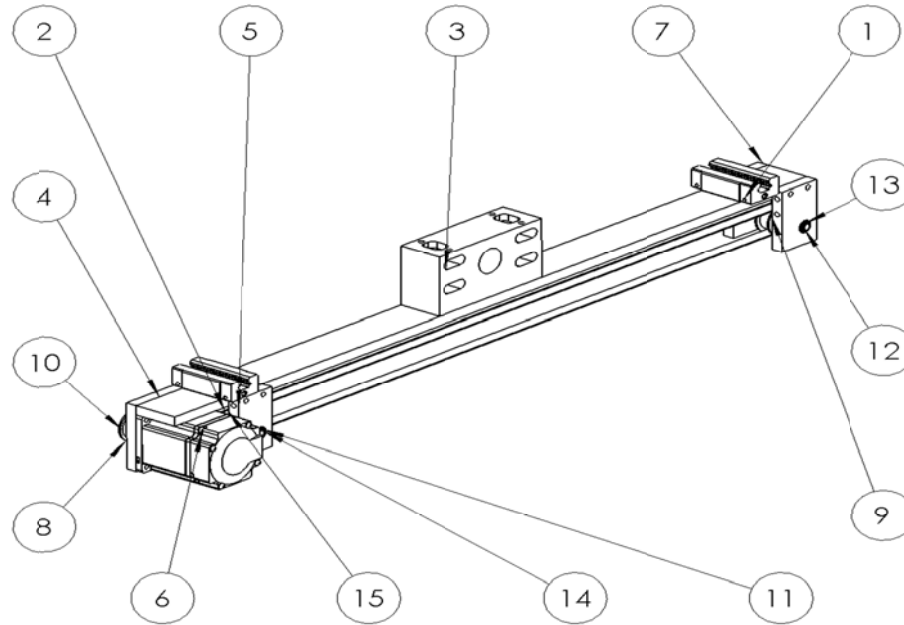


A3.1.4 Work Table (Module I) Assembly



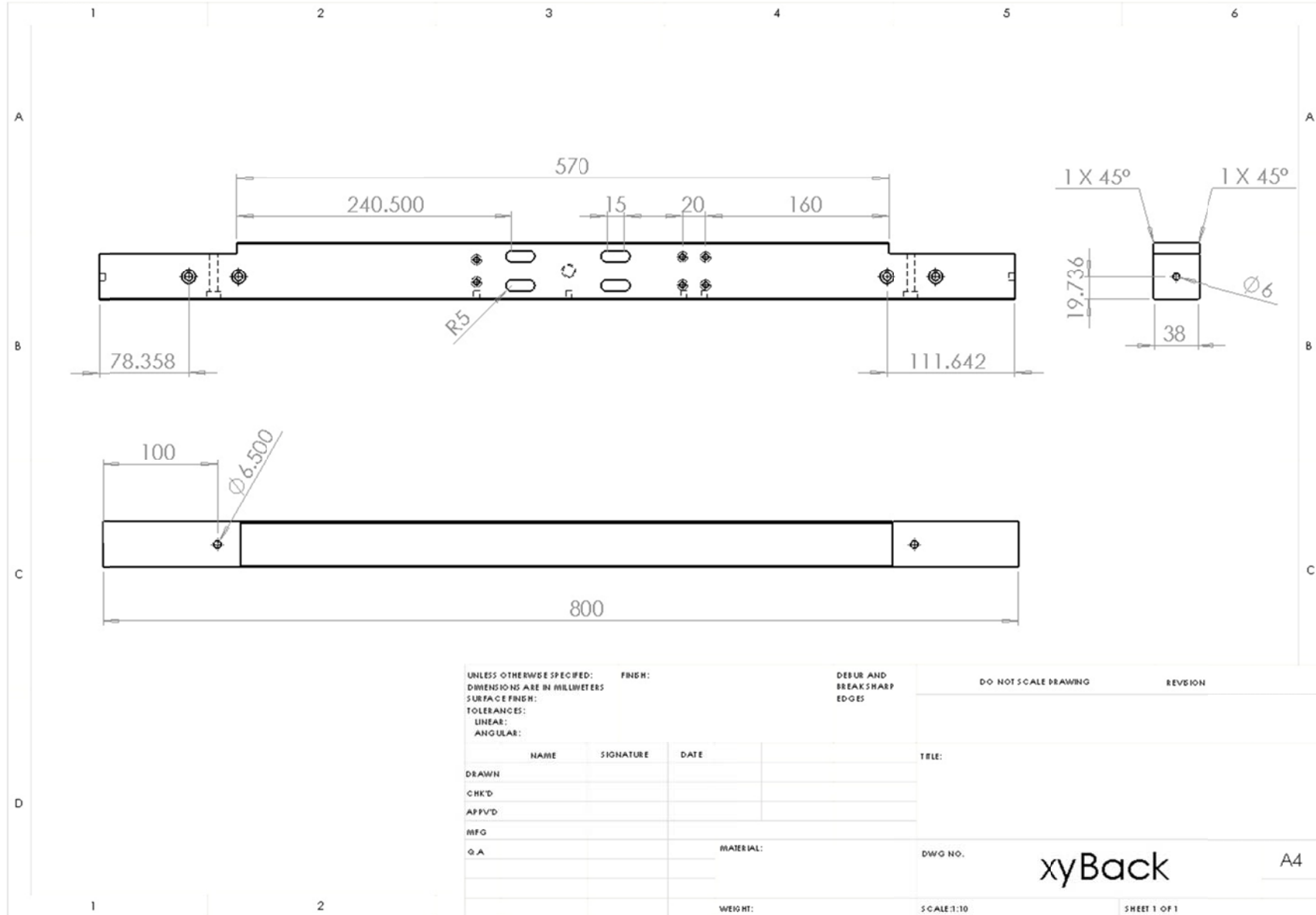
| ITEM NO. | PART NUMBER        | QTY. |
|----------|--------------------|------|
| 1        | Part8              | 1    |
| 2        | powder_z_lin_bear2 | 6    |
| 3        | TableSupport       | 1    |
| 4        | z_ara              | 2    |
| 5        | powder_z_ball_nut  | 1    |
| 6        | TableZ             | 1    |

**A3.1.5 Y Axis (Module I) Assembly**

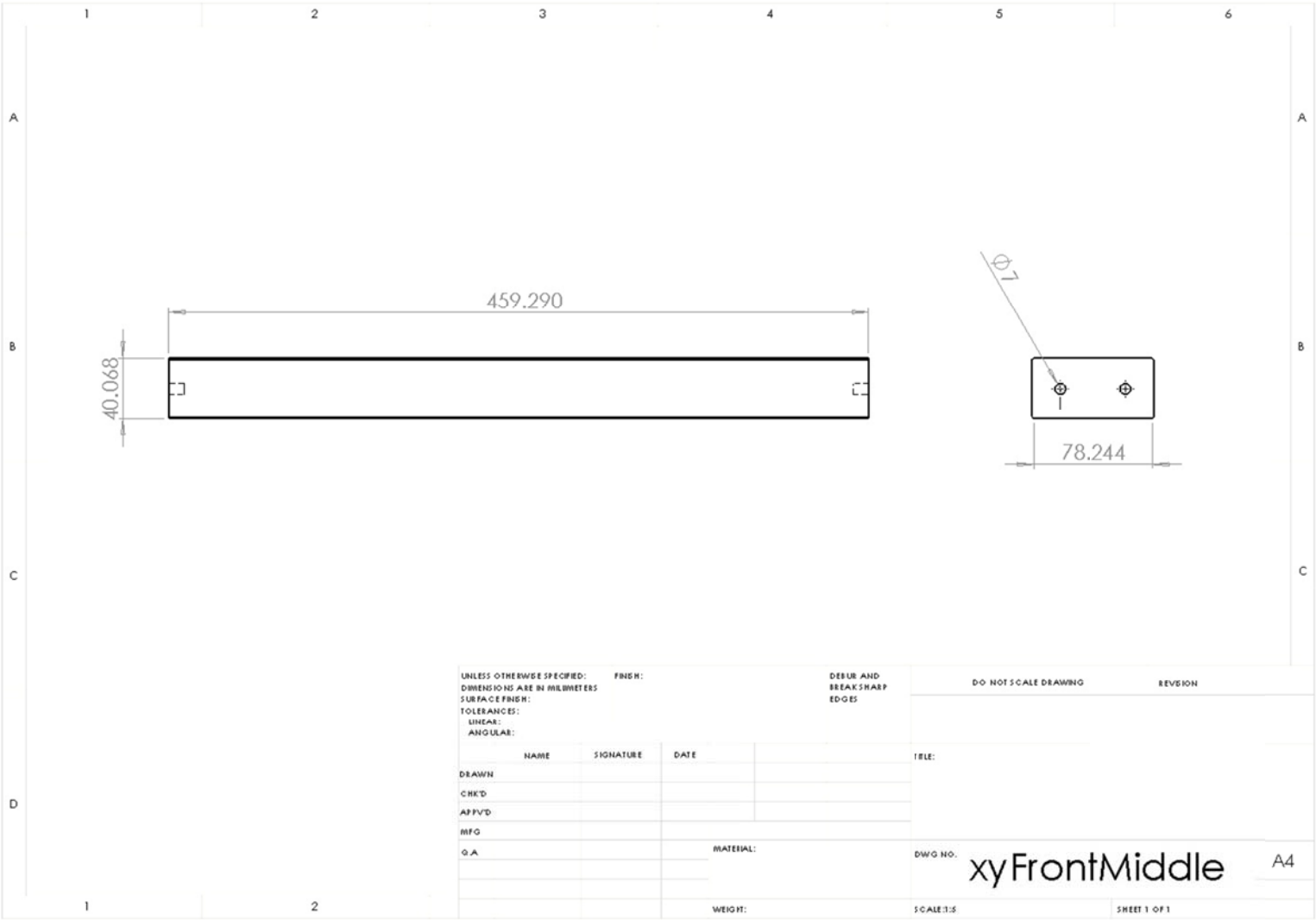


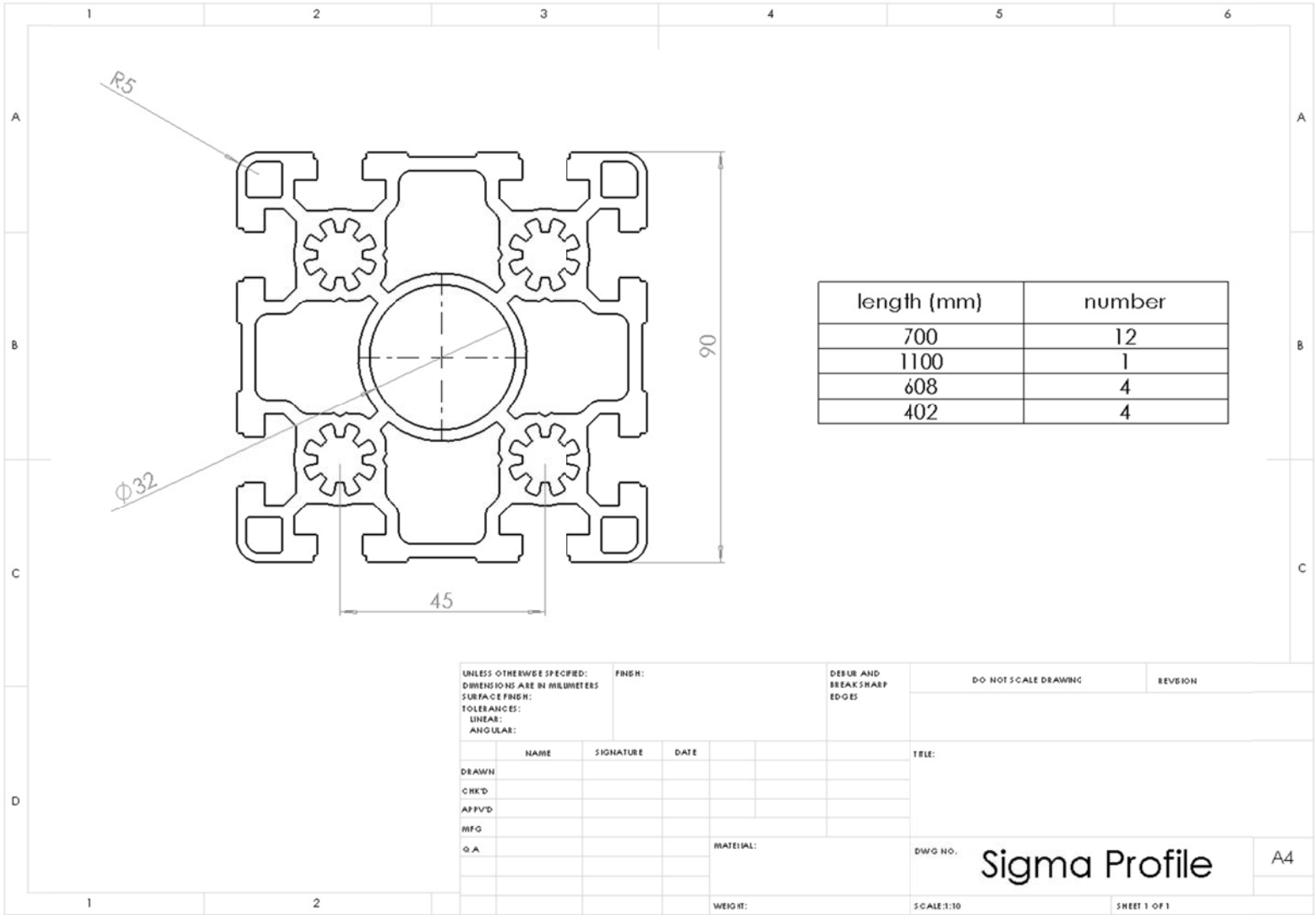
| ITEM NO. | PART NUMBER                  | QTY. |
|----------|------------------------------|------|
| 1        | hiwinHGR                     | 2    |
| 2        | Yaxis                        | 1    |
| 3        | UstBagOn                     | 1    |
| 4        | MotorFlange                  | 1    |
| 5        | MirrorConnect1               | 2    |
| 6        | ACmotor200W                  | 1    |
| 7        | Xmount                       | 1    |
| 8        | pulleyPhi109                 | 1    |
| 9        | pulleyPhi6                   | 3    |
| 10       | Belt200W                     | 1    |
| 11       | SKF - 618-6 - 10,SI,NC,10_68 | 4    |
| 12       | Phi6Shaft                    | 1    |
| 13       | Circlip DIN 471 - 6 x 0.7    | 9    |
| 14       | Phi6Shaft200W                | 1    |
| 15       | BeltXaxis                    | 1    |



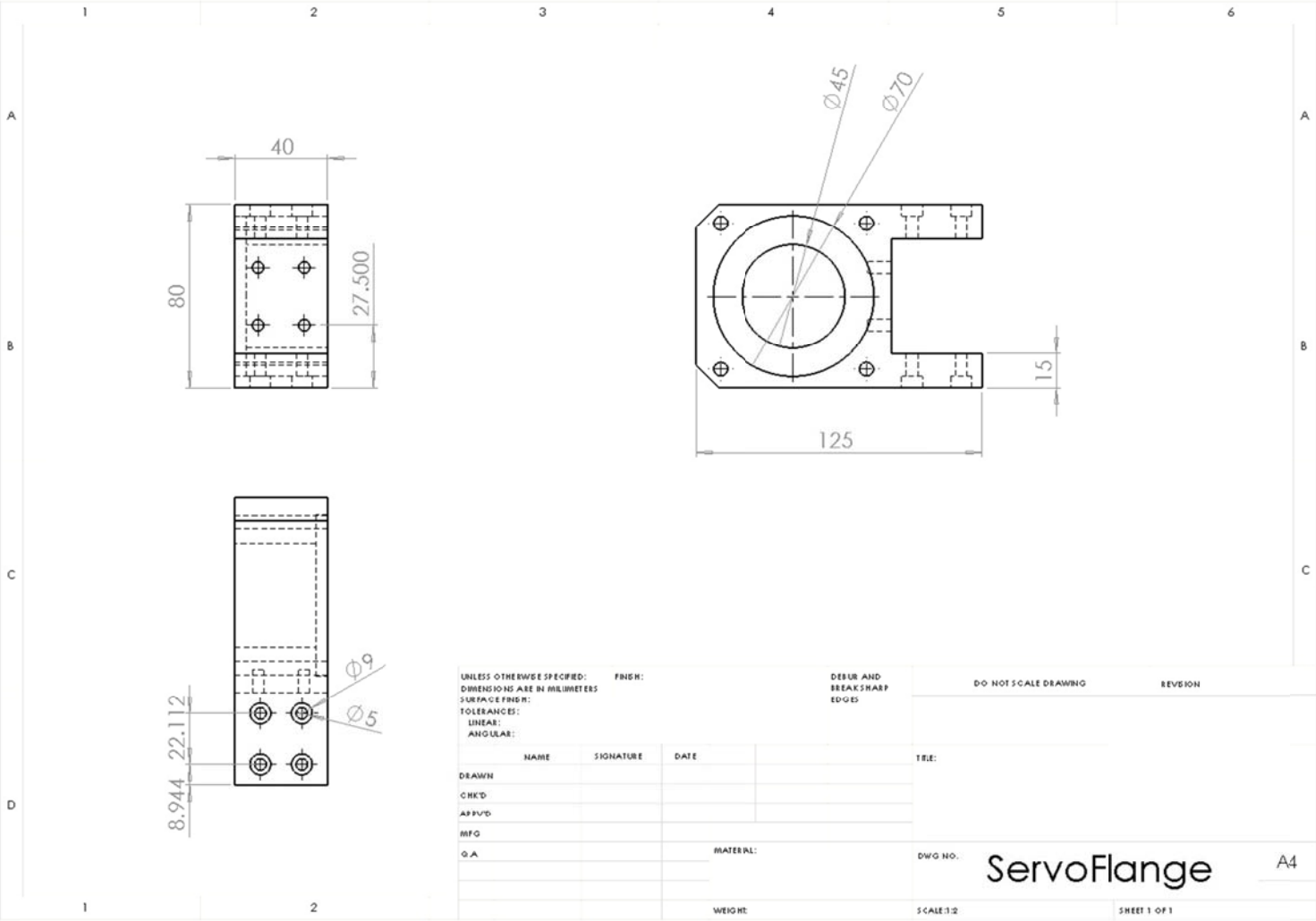


|                               |           |         |                             |             |                      |          |
|-------------------------------|-----------|---------|-----------------------------|-------------|----------------------|----------|
| UNLESS OTHERWISE SPECIFIED:   |           | FINISH: | DEBUR AND BREAK SHARP EDGES |             | DO NOT SCALE DRAWING | REVISION |
| DIMENSIONS ARE IN MILLIMETERS |           |         |                             |             |                      |          |
| SURFACE FINISH:               |           |         |                             |             |                      |          |
| TOLERANCES:                   |           |         |                             |             |                      |          |
| LINEAR:                       |           |         |                             |             |                      |          |
| ANGULAR:                      |           |         |                             |             |                      |          |
| NAME                          | SIGNATURE | DATE    | TITLE:                      |             |                      |          |
| DRAWN                         |           |         |                             |             |                      |          |
| CHK'D                         |           |         |                             |             |                      |          |
| APP'VD                        |           |         |                             |             |                      |          |
| MFG                           |           |         |                             |             |                      |          |
| Q.A.                          |           |         | MATERIAL:                   | DWG NO.     | xyBack A4            |          |
|                               |           |         |                             |             |                      |          |
|                               |           |         | WEIGHT:                     | SCALE: 1:10 | SHEET 1 OF 1         |          |



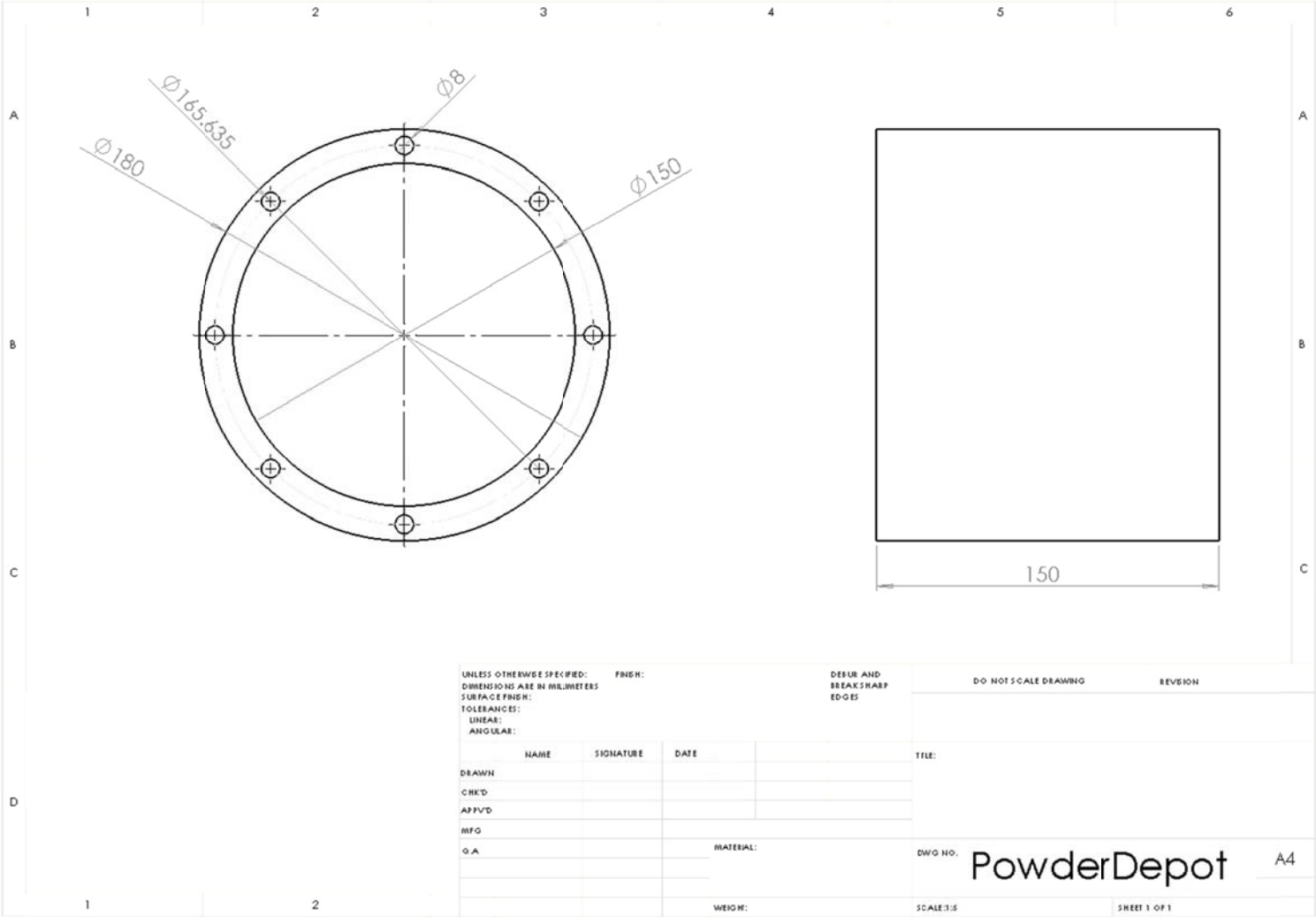


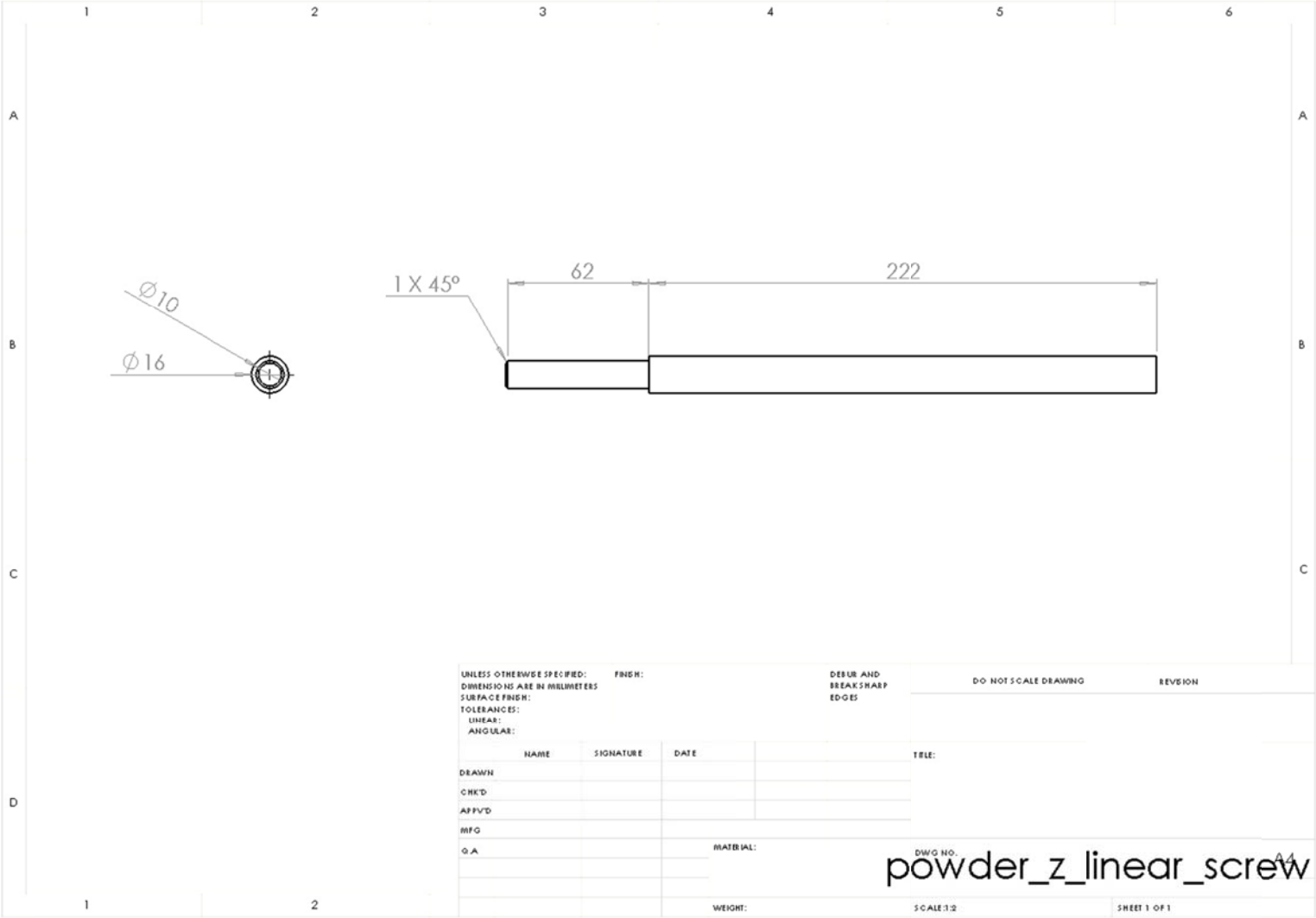
|   |      |           |         |                                   |                        |                      |
|---|------|-----------|---------|-----------------------------------|------------------------|----------------------|
| UNLESS OTHERWISE SPECIFIED:<br>DIMENSIONS ARE IN MILLIMETERS<br>SURFACE FINISH:<br>TOLERANCES:<br>LINEAR:<br>ANGULAR: |      |           | FINISH: | DEBUR AND<br>BREAK SHARP<br>EDGES | D.O. NOT SCALE DRAWING | REVISION             |
| DRAWN   | NAME | SIGNATURE | DATE    |                                   | TITLE:                 |                      |
| CHK'D   |      |           |         |                                   |                        |                      |
| APP'VD  |      |           |         |                                   |                        |                      |
| MFG   |      |           |         |                                   |                        |                      |
| Q.A.  |      |           |         | MATERIAL:                         | DWG NO.                | <b>Sigma Profile</b> |
|   |      |           |         |                                   |                        | A4                   |
|   |      |           |         | WEIGHT:                           | SCALE:1:10             | SHEET 1 OF 1         |

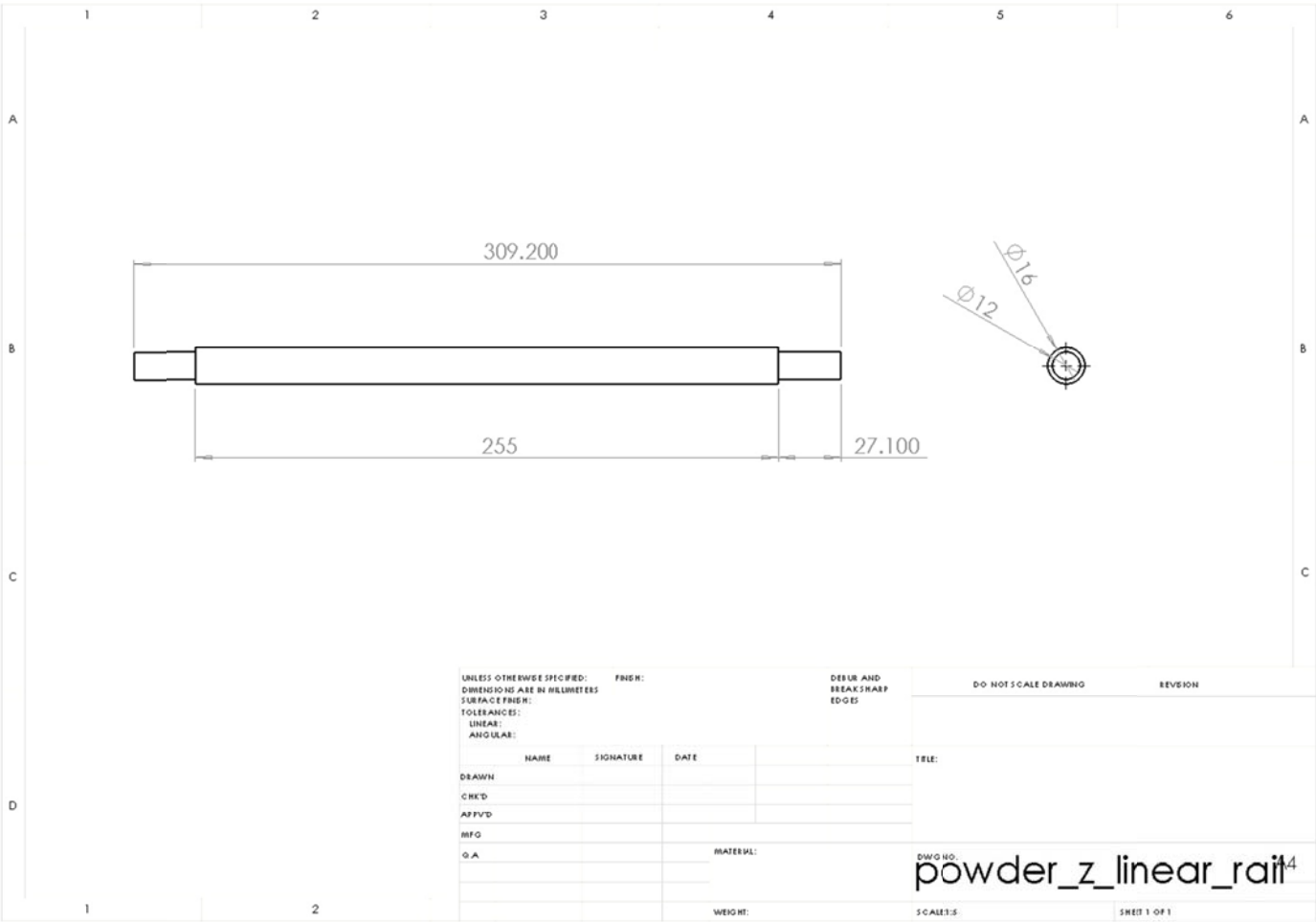


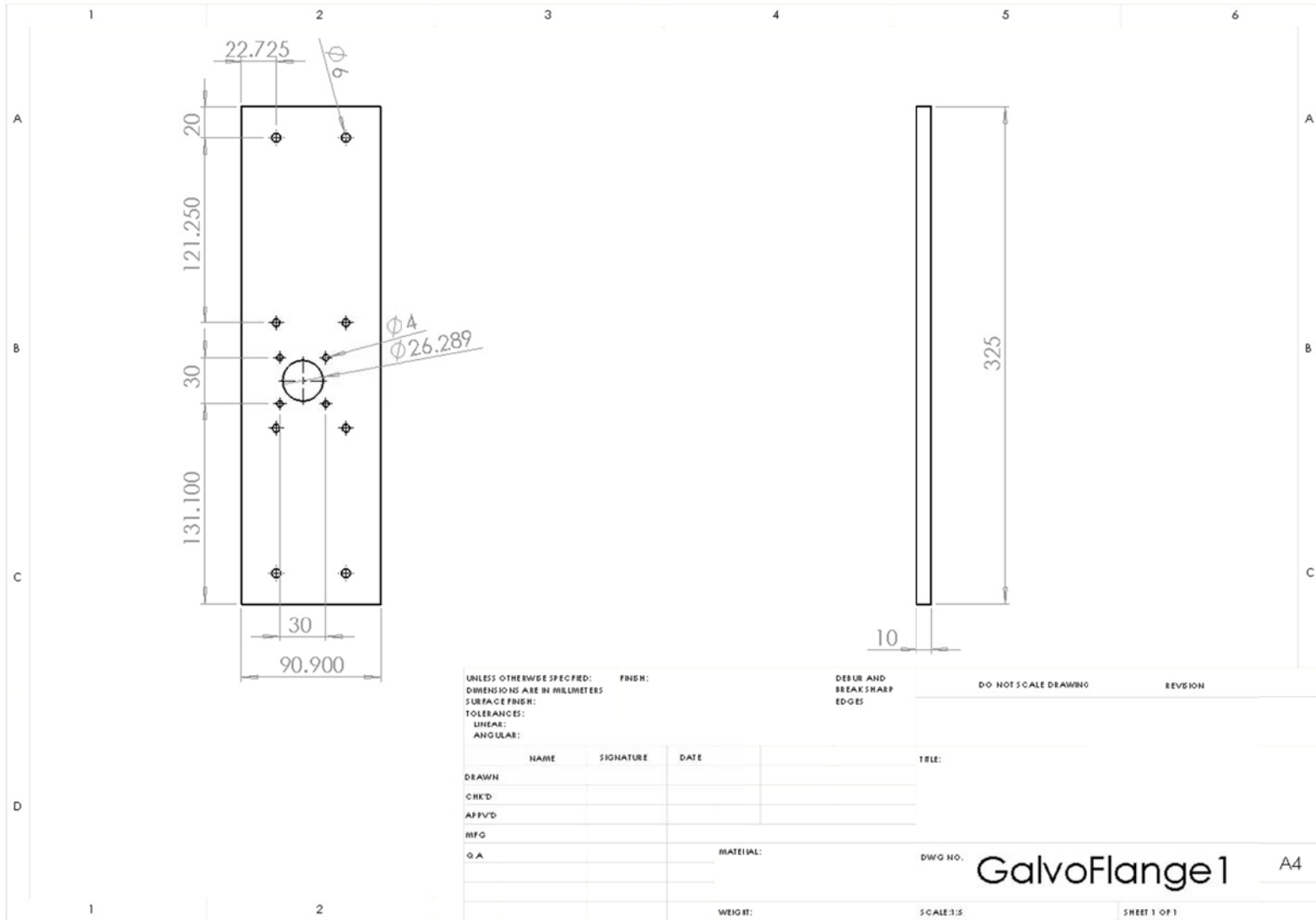


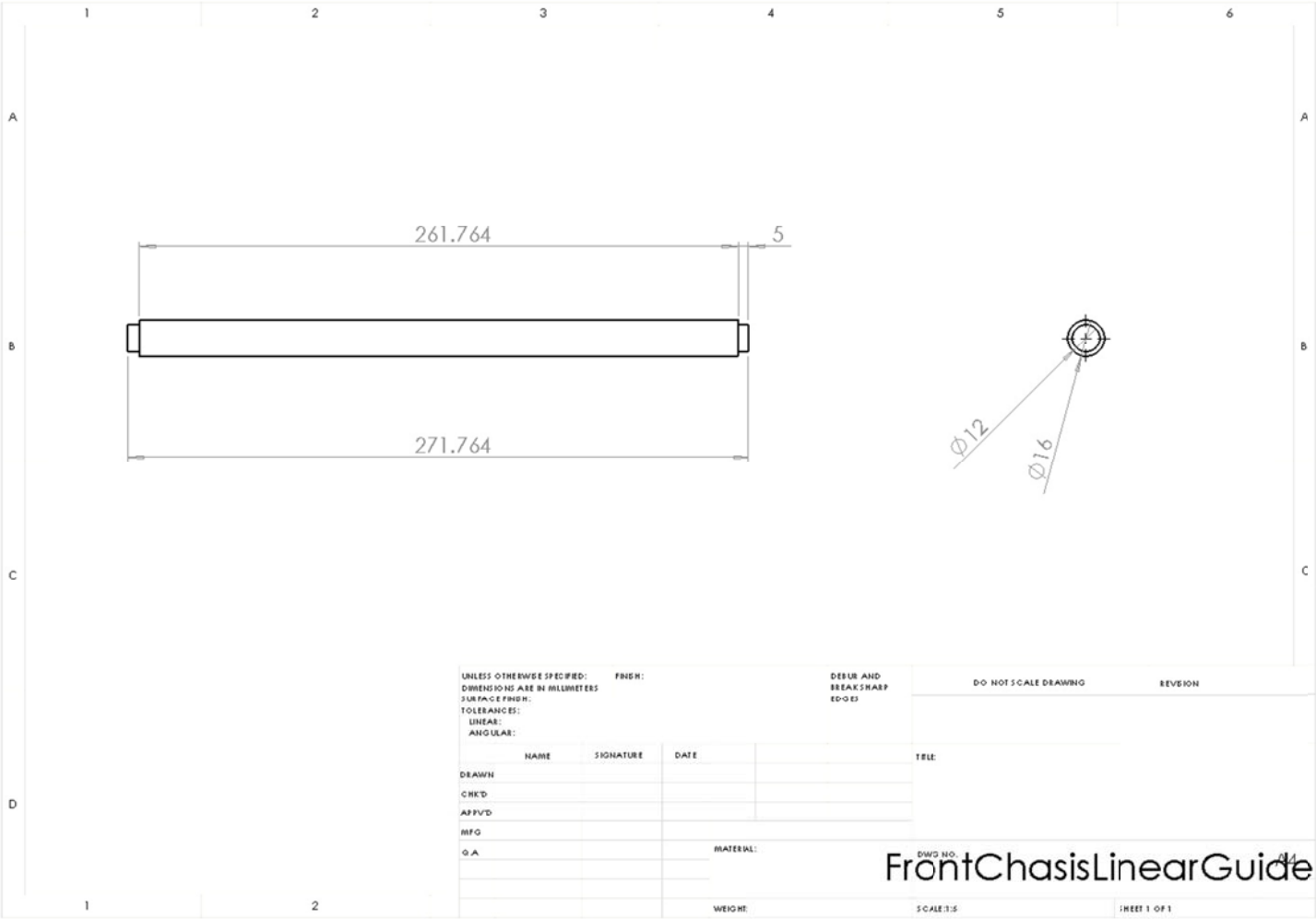


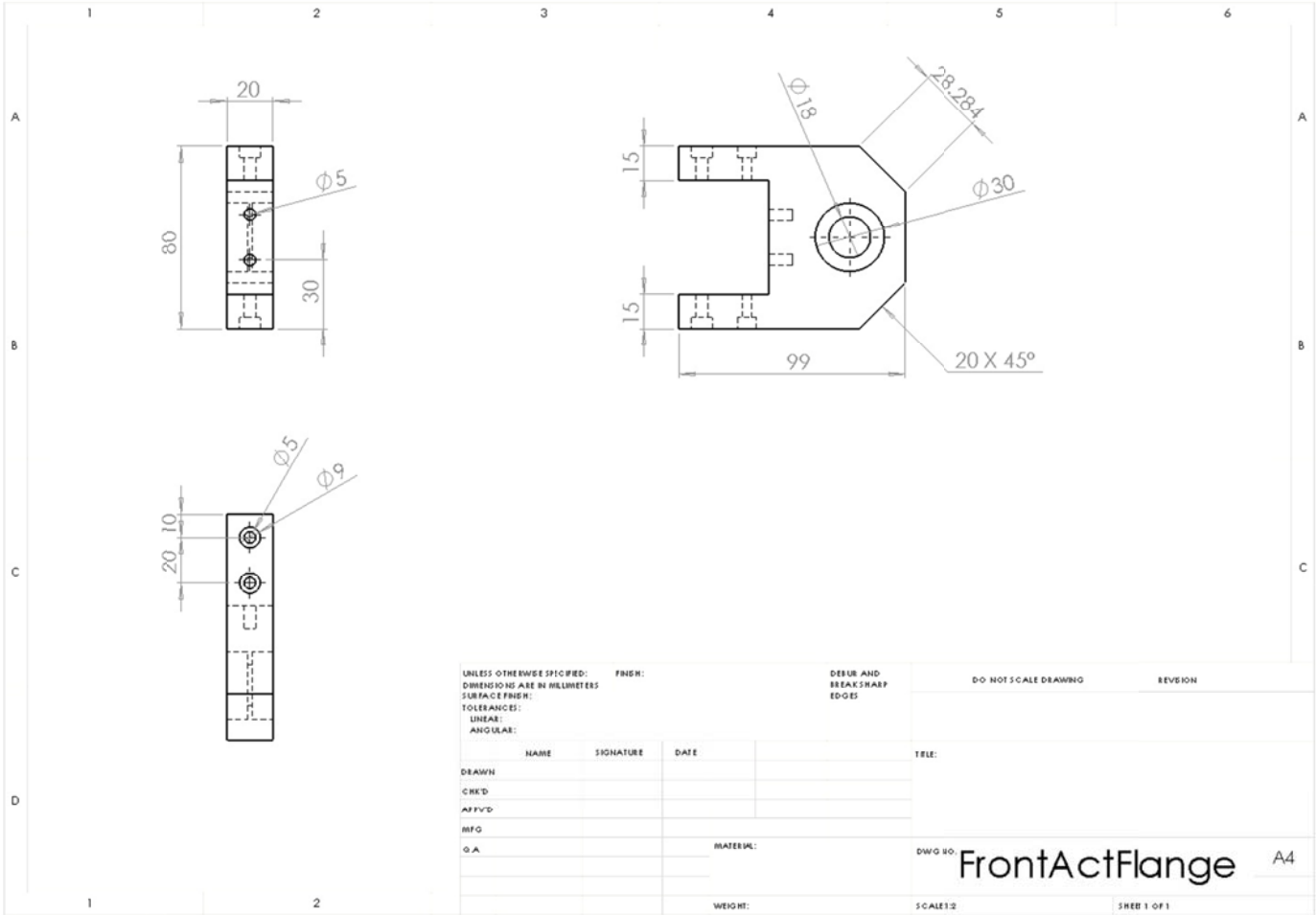


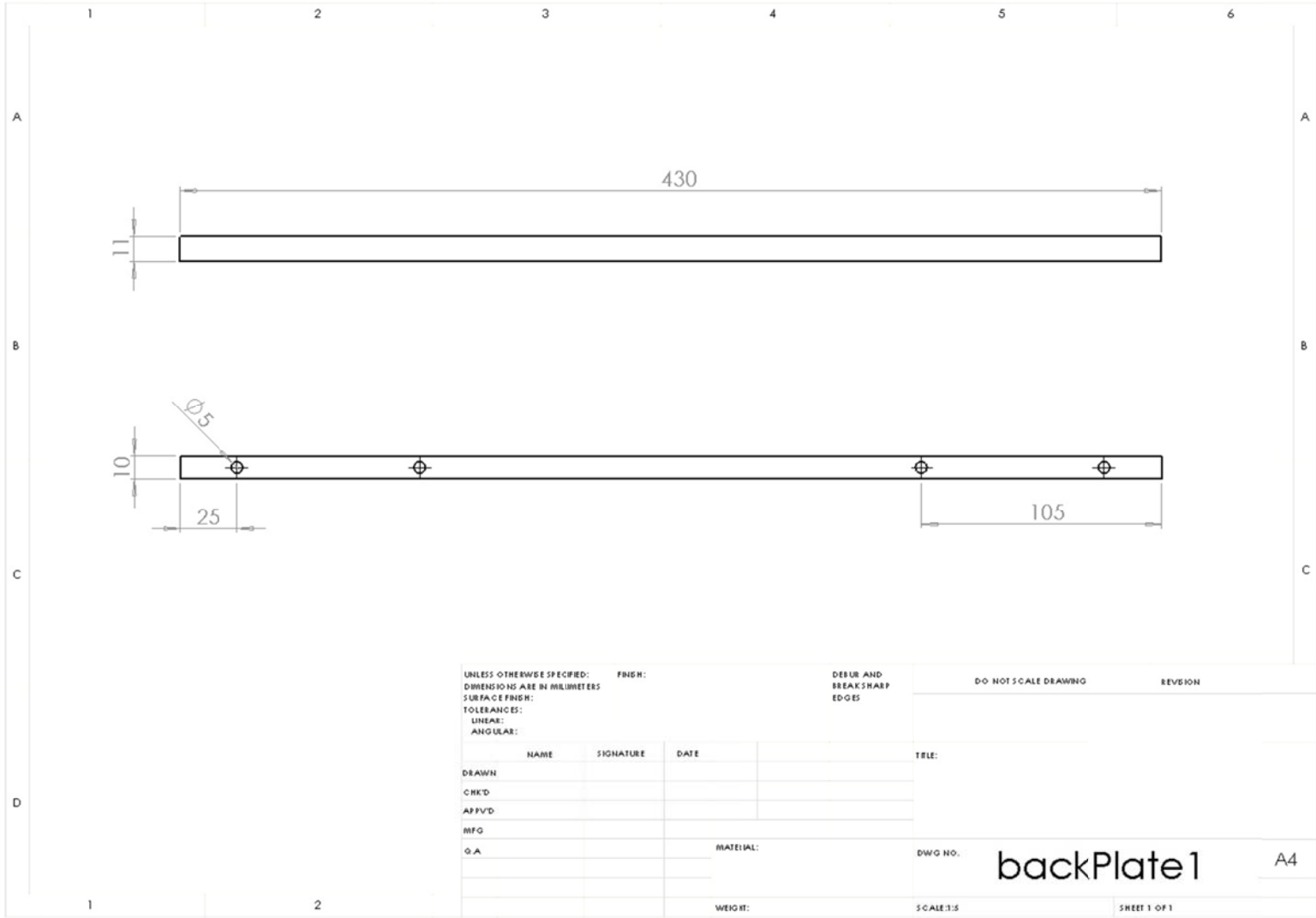


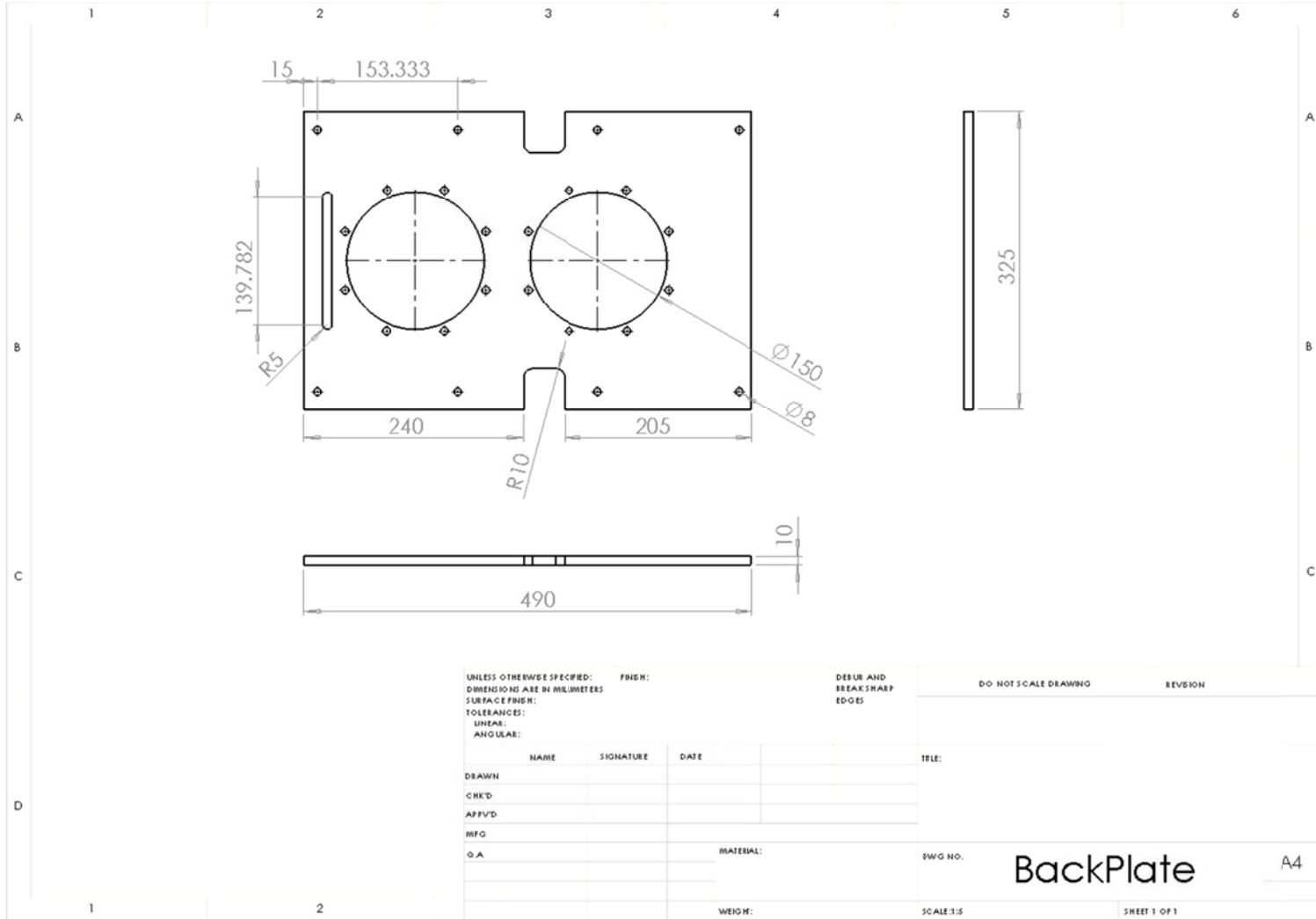




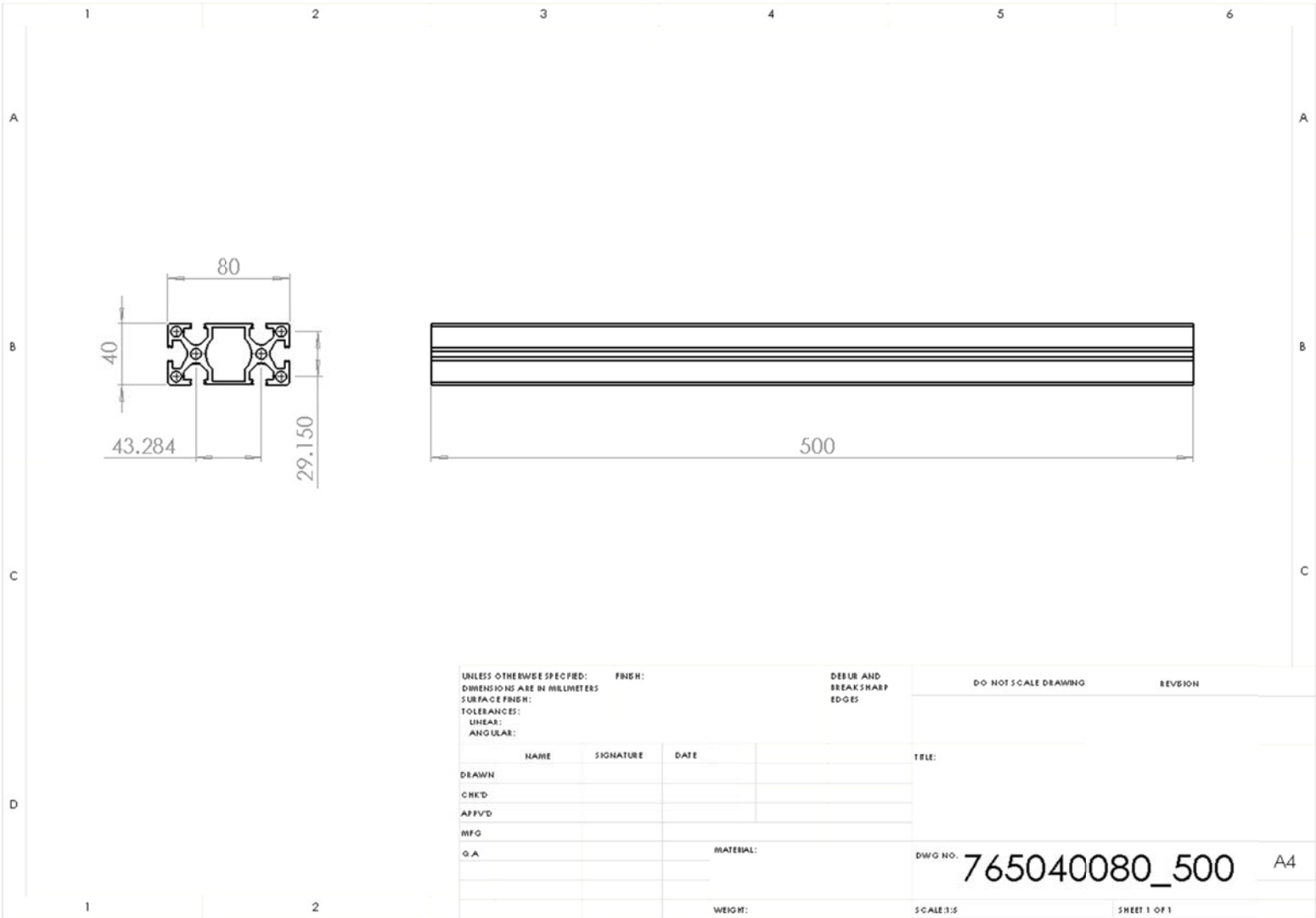




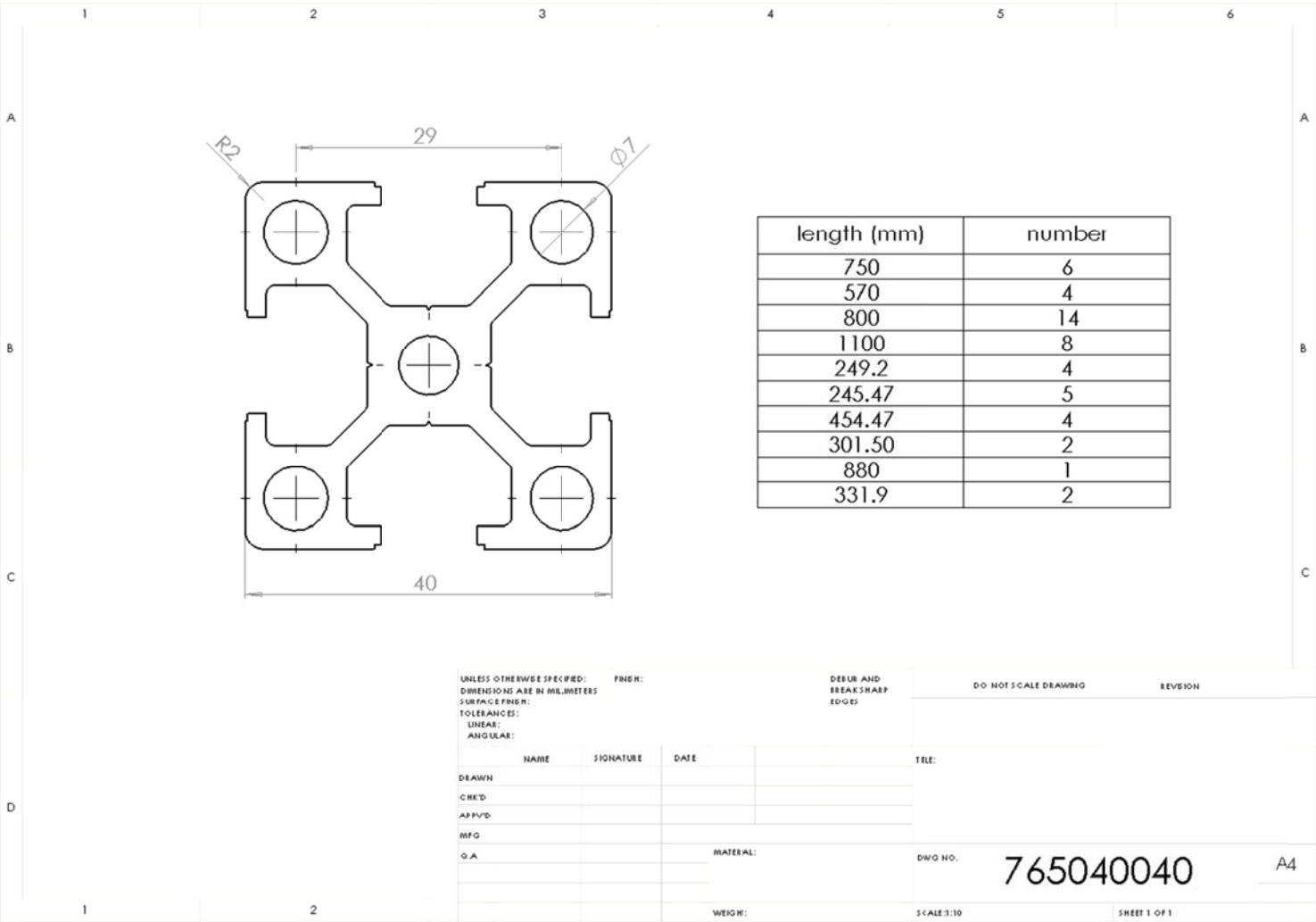








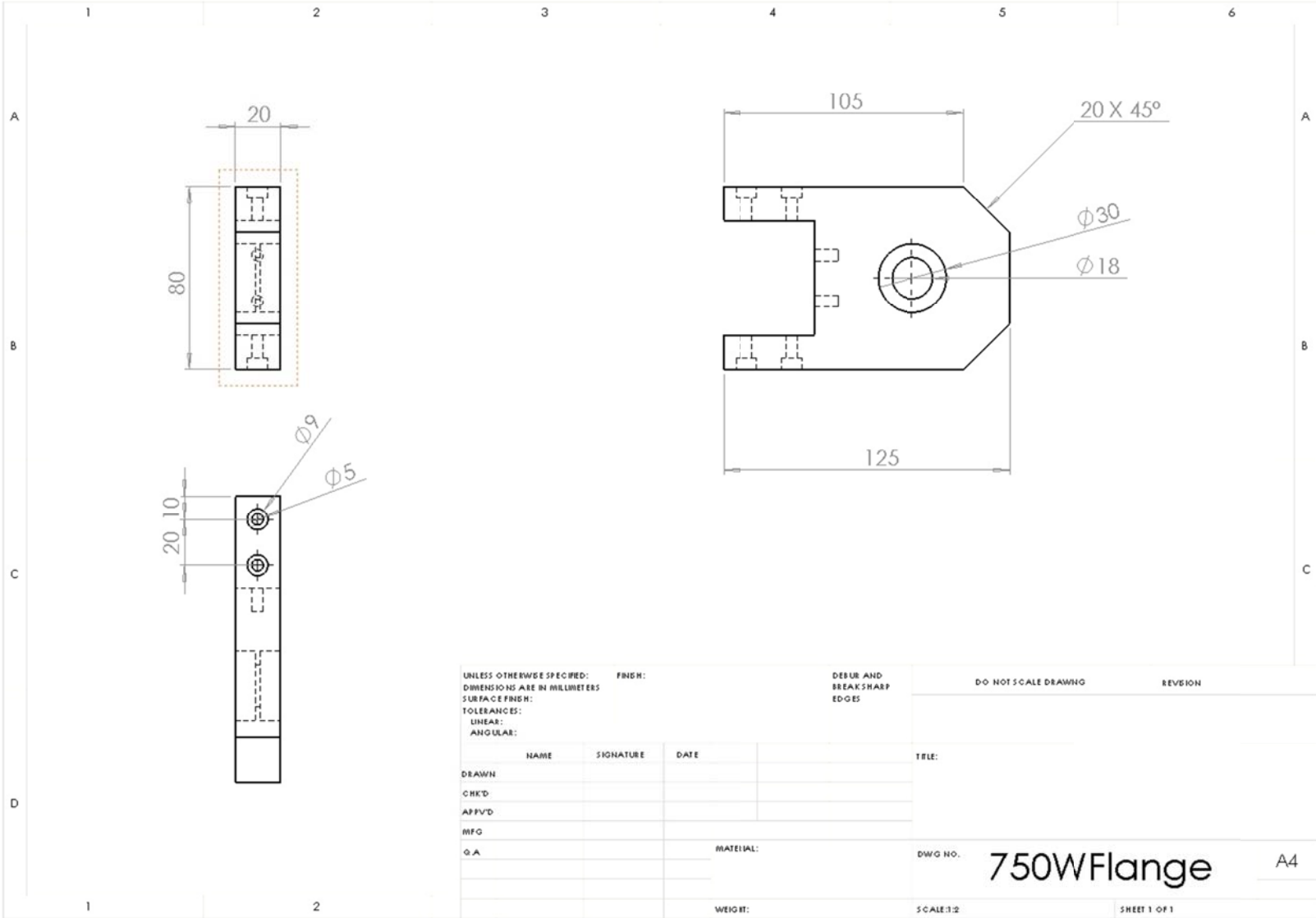
|                               |      |           |                             |           |                              |              |
|-------------------------------|------|-----------|-----------------------------|-----------|------------------------------|--------------|
| UNLESS OTHERWISE SPECIFIED:   |      | FINISH:   | DEBUR AND BREAK SHARP EDGES |           | DO NOT SCALE DRAWING         | REVISION     |
| DIMENSIONS ARE IN MILLIMETERS |      |           |                             |           |                              |              |
| SURFACE FINISH:               |      |           |                             |           |                              |              |
| TOLERANCES:                   |      |           |                             |           |                              |              |
| LINEAR:                       |      |           |                             |           |                              |              |
| ANGULAR:                      |      |           |                             |           |                              |              |
|                               | NAME | SIGNATURE | DATE                        |           | TELE:                        |              |
| DRAWN                         |      |           |                             |           |                              |              |
| CHK'D                         |      |           |                             |           |                              |              |
| APP'VD                        |      |           |                             |           |                              |              |
| MFG                           |      |           |                             |           |                              |              |
| Q.A                           |      |           |                             | MATERIAL: |                              |              |
|                               |      |           |                             |           | DWG NO. <b>765040080_500</b> | A4           |
|                               |      |           |                             | WEIGHT:   | SCALE 1:1                    | SHEET 1 OF 1 |



UNLESS OTHERWISE SPECIFIED: FINISH: DEBUR AND BREAK SHARP EDGES  
 DIMENSIONS ARE IN MILLIMETERS SURFACE FINISH: DO NOT SCALE DRAWING  
 TOLERANCES: LINEAR: REVISION  
 ANGULAR:

| NAME  | SIGNATURE | DATE | TITLE: |
|-------|-----------|------|--------|
| DRAWN |           |      |        |
| CHK'D |           |      |        |
| APP'D |           |      |        |
| MFG   |           |      |        |
| G.A.  |           |      |        |

MATERIAL: DWG NO. **765040040** A4  
 WEIGHT: SCALE: 1:10 SHEET 1 OF 1



## Appendix 3.2 - Optic Component List

Table A.3.1 Opto-Mechanical Components related to the flying optic part of the SAM Workstation

| Component   | Quantity | Description  |
|-------------|----------|--|
| KCB2        | 8        | The 30 mm Right Angle Kinematic Cage Mount mounts an optic in a double-bored adjustment plate for two lines of stable contact and securely holds the optic with a locking nylon-tipped setscrew. The kinematic adjustment plate mounts the optic at a 45° angle with ±4° pitch and yaw adjustment range and is actuated with 100 TPI (Threads Per Inch) adjustment screws for smooth, high sensitivity movement.                                 |
|             |          |  |
| SM1L30      | 2        | These stackable Ø1" lens tubes provide a fast and easy means for building compact optical assemblies. Their stackable design and direct interfacing with any SM1-threaded (1.035"-40) components provide flexibility for complex optomechanical assemblies. One SM1RR retaining ring is included with each lens tube.(V type lens tubes are rotating adjustable)   |
| SM1V10      | 1        |  |
| SM1V05      | 1        |  |
|             |          |  |
| PF10-03-P01 | 1        | Silver coated mirrors offer the highest reflection in the visible-NIR spectrum (450 nm - 2 µm, $R_{avg} > 97.5\%$ ) of any metallic mirror. While excellent in the visible, silver mirrors also offer high reflection in the IR (2 - 20 µm, $R_{avg} > 96\%$ ). Please see the Graphs tab (above) for reflectance curves. In order to protect them from oxidation, these mirrors have a durable SiO overcoat. (Each package includes 10 mirrors) |
|             |          |  |
| PF10-03-M01 | 1        | Protected gold is the most efficient reflective coating over the entire IR range. A protective overcoat is layered over the gold to help protect it from damage and make cleaning easier. The protected gold coating is made by using a proprietary protective overcoat, which allows >96% average reflection from 800 nm to 20 µm. (Each package includes 10 mirrors)   |
|             |          |  |
| LA1131-C    | 2        | N-BK7 Plano-Convex Lens, Ø1", f = 50.0 mm, ARC: 1050-1620 nm   |
| LA1608-C    | 2        | N-BK7 Plano-Convex Lens, Ø1", f = 75.0 mm, ARC: 1050-1620 nm   |
| LA1509-C    | 2        | N-BK7 Plano-Convex Lens, Ø1", f = 100.0 mm, ARC: 1050-1620 nm  |
| LA1229-C    | 2        | N-BK7 Plano-Convex Lens, Ø1", f = 175.0 mm, ARC: 1050-1620 nm  |
| LA7660-F    | 2        | Ø1" ZnSe Plano-Convex Lens, f = 75.0 mm, AR-Coated: 8-12 µm  |
| LA7656-F    | 2        | Ø1" ZnSe Plano-Convex Lens, f = 50.0 mm, AR-Coated: 8-12 µm  |
| LA7261-F    | 2        | Ø1" ZnSe Plano-Convex Lens, f = 100.0 mm, AR-Coated: 8-12 µm   |

Table A.3.1 Opto-Mechanical Components related to the laser feedback part of the SAM Workstation

| Component        | Quantity | Description   |
|------------------|----------|---|
| <b>Mechanics</b> |          |   |
| SM1L10           | 3        | Lens tubes are ideal for several applications, including the creation of optical subassemblies. A single tube can house from one to several optical elements, which are separated and secured by retaining rings. The retaining rings are easy to install using our specialized lens tube spanner wrenches. Five lens tube sizes are available: SM05 ( $\varnothing 1/2"$ ), SM1 ( $\varnothing 1"$ ), SM30 ( $\varnothing 30$ mm), SM2 ( $\varnothing 2"$ ), and SM3 ( $\varnothing 3"$ ) and have adapters to connect lens tubes of different diameters together. |
| SM1M10           | 1        |   |
| SM1S10           | 3        |   |
| SM1S30           | 2        |   |
| SM1CP2           | 1        |   |
| MB3060/M         | 1        | Aluminum Breadboard, 300 mm x 600 mm x 12.7 mm, M6 Threaded   |
| C4W              | 1        | 30 mm Cage System Cube, 4-Way   |
| B3C              | 2        | Rotatable Cage Cube Platform for C4W/C6W  |
| B5C              | 2        | $\varnothing 1"$ Cage Cube Optic Mount For B3C  |
| B1C/M            | 1        | Blank Cover Plate with Rubber O-Ring for C4W/C6W, Metric  |
| MSH075           | 6        | Mini-Post Holder with Swivel Base, 3/4" (19 mm) High  |
| MSH1             | 9        | Mini-Post Holder with Swivel Base, 1" (25 mm) High  |
| MSA4/M           | 6        | Thread Adapter, M4 to M3  |
| MSA25            | 3        | Thread Adapter, 1/4"-20 to 4-40   |
| CP02/M           | 2        | SM1 Threaded 30 mm Cage Plate, 0.35" Thick, Metric  |
| MS1R/M           | 10       | Mini Series Mounting Posts, $\varnothing 6$ mm, 25 mm Long  |
| MS05R/M          | 6        | Mini Series Posts, $\varnothing 6$ mm, 13 mm Long   |
| MS1R             | 2        | Mini Series Mounting Posts, $\varnothing 6$ mm, 1" Long   |
| <b>Optics</b>    |          |   |
| LA1951           | 1        | N-BK7 Plano-Convex Lens, $\varnothing 1"$ , $f = 25.4$ mm, Uncoated (350 nm - 2.0 $\mu$ m range)  |
| ND01A            | 1        | Mounted Reflective $\varnothing 25$ mm ND Filter, Optical Density: 0.1  |
| ND03A            | 1        | Mounted Reflective $\varnothing 25$ mm ND Filter, Optical Density: 0.3  |
| ND10A            | 1        | Mounted Reflective $\varnothing 25$ mm ND Filter, Optical Density: 1.0  |
| ND20A            | 1        | Mounted Reflective $\varnothing 25$ mm ND Filter, Optical Density: 2.0  |
| ND30A            | 1        | Mounted Reflective $\varnothing 25$ mm ND Filter, Optical Density: 3.0  |
| CM1-BS014        | 1        | Cube-Mounted Polarization-Insensitive Beamsplitter, 700 - 1100  |
| FES1000          | 1        | Shortpass Filter, Cut-Off Wavelength: 1000 nm   |
| MVL8L            | 1        | 8 mm EFL, $f/1.4$ , for 2/3" Format Cameras, with Lock  |
| <b>Sensors</b>   |          |   |
| SM1PD2A          | 1        | Mounted UV Enhanced Silicon Photodiode, 200-1100 nm, Cathode Grounded   |
| DCC1545M         | 1        | High Resolution USB2.0 CMOS Camera, 1280 x 1024, Monochrome   |

### Appendix 5.1 - Technological Demonstration Material Properties

SLS Processing material is SLS Innova'PA 1550 (Polyamide 12). The material properties are given below.

| General Properties                              | Method & Condition   |                       |
|---|--|-----------------------|
| Average particle size                           | Diffraction Laser  | 40 – 50 $\mu\text{m}$ |
| Powder packed density                           | Manufacture method   | 0.5 $\pm$ 0.05        |
| Part density                                    | Manufacture method   | 0.98 $\pm$ 0.05       |
| Moisture absorption (%50 RH, 23°C 24 hrs)       | ASTM D570  | 0.5 $\pm$ 0.05        |
| $T_f$ (Melting Point)                           | DSC  | 181<_<185             |
| $T_g$ (Glazing Point)                           | DSC  | 34 $\pm$ 2            |
| Heat deflection temperature at 1.82 MPa         | ASTM D648  | 86 $\pm$ 1            |
| $T_{process}$                                   | Glazing method   | -14 $\pm$ 2           |
| Tensile Strength                                | ISO 527  | 45 $\pm$ 1            |
| Young Modulus                                   | ISO 527  | 1550 $\pm$ 150        |
| Elongation at break                             | ISO 527  | 16 $\pm$ 2            |
| Flexural Modulus                                | ISO 178  | 1350 $\pm$ 25         |
| Charpy – Impact Strength                        | ISO 180  | 34 $\pm$ 2            |
| Charpy – Notched impact strength                | ISO 180  | 6 $\pm$ 0.5           |
| Shore Test (Shore D)                            | ISO R 868  | 68 $\pm$ 3            |
| Chemical Resistance                             | Chemical resistance to alkaline, hydrocarbons, oils, gasolines, gas oil and solvents. May be attacked by acids. No through porosity with sections greater than 1.6 mm thick. |                       |
| Volume Resistivity, 50% HR, 23°C                | CEI 93   | 1.3E <sup>13</sup>    |
|   | CEI 93   | 1.5E <sup>15</sup>    |
| Natural colouration                             | Visual   | white-cream           |
| Upper facing processed & blasting surface $R_a$ | ISO 4287   | 9 $\pm$ 1             |
|   | ISO 4287   | <1 $\pm$ 0.5          |

## References

## Chapter 2 References

1. Chryssolouris, G., *Laser machining - Theory and practice*. 1991. Medium: X; Size: Pages: (292 p).
2. Einstein, A., *On the quantum theory of radiation*. Physik Zeitschrift, 1917.
3. Schawlow, A.L., Townes, C.H., *Infrared and optical masers*. Phys. Rev. , 1958(112): p. 1940.
4. Walter, W.T., Pilch, M., Solimene, N., Gould G., *Pulsed-laser action in atomic copper vapor*. Bulletin of the American Physical Society, 1966. **11**(II): p. 113.
5. Evbatyrov, T., *Pulsed Fiber Laser Specification*. 2008, IPG Laser.
6. Lu, L., Fuh, J.Y.H., *Material Origin shrinkage, distortion and fracture of photopolymerized material*. Material Research Bulletin, 1995. **30**(12): p. 1561-1569.
7. Kruth, J.P., *Material Incess Manufacturing by Rapid Prototyping Techniques*. CIRP Annals, 1991. **40**(2): p. 603-614.
8. Gibson, I., *Advanced Manufacturing Technology for Medical Applications, Reverse Engineering*. 2005, Hoboken, NJ: John Wiley & Sons
9. Exner, H., Regenfuss, P., Hartwig, L., Klötzer, S., Ebert, R., , *Selective Laser Microsintering with a Novel Process*. 2003.
10. Kruth, J.P., Mercelis, P., Ven Varenbergh, J., Froyen, L., Rombouts, M., *Binding mechanisms in selective laser sintering and selective laser melting*. Rapid Prototyping Journal, 2005. **11**(1): p. 26-36.
11. Mukesh Agarwala, D.B., Joseph Beaman, Harris Marcus, Joel Barlow, *Direct selective laser sintering of metals*. Rapid Prototyping Journal, 1995. **1**(1): p. 26-36.
12. Kruth, J.P., Levy, G., Schindel, R., Craeghs, T., Yasa, E., *Consolidation of polymer powder by selective laser sintering*. K.U. Leuven Heverlee, Belgium.
13. Harlan, N.R., *Titanium processing using selective laser sintering*, in *Mechanical Engineering*. 1999, University of Texas, at Austin: Austin.
14. Bunnell, D.E., *Fundamentals of Selective Laser Sintering of Metals*, in *Mechanical Engineering*. 1995, University of Texas, at Austin: Austin.
15. Deckard C.R., B., J.J., *Selective Laser Sintering with Assisted Powder Handling*, U. Patent, Editor. 1990.
16. Sun, M.S., Nelson, J.C., Beaman, J.J., Barlow, J.J., . *A Three Dimensional Model of SLS*. in *Solidfreeform Sym*. 1991.
17. Beaman, J.J., Barlow, J.W., Bourell, D.L., Crawford, R.H., Marcus, H.L., McAlea, K.P., , in *Solid Freeform Fabrication: A new direction in manufacturing*. 1997, Kluwer: Boston. p. 207.
18. Childs, T.H.C., Cardie, S., Brown, J.M. *SLS of Polycarbonate at varying Powers, Scan Speeds and Scan Spacings*. in *Solidfreeform Symposium Proceedings*. 1994.
19. Weissman, E.M., Hsu, M.B., *A finite element model of Multi-Layered Laser Sintering Parts*. in *Solidfreeform Fabrication Symposium Proceeding*. 1991.
20. Williams, J.D., Deckard, C.R., *Variable beam size SLS workstation and enhanced SLS model*. Rapid Prototyping Journal, 1997. **3**(1): p. 4-11.
21. Bugada, G., Cervera, G.B.M., Lombera, G., *Numerical prediction of Temperature and Density Distribution in Selective Laser Sintering Process*. Rapid Prototyping Journal, 1999. **5**(1): p. 21-26.

22. Tontowi, A.E., Childs, T.H.C., , *Density prediction of crystalline polymer sintered parts at various powder bed temperatures*. Rapid Prototyping Journal, 2001. **7**(3): p. 180-184.
23. Migliore, L., ed. *Laser Materials Processing*. 1996, Marcel Dekker Inc.,: Mountain View, California. 311.
24. Haferkamp, K., Marquering, M., Ebsen, H., , *Alloying of copper surface with a pulsed Nd:YAG laser*. SPIE Proc., 1994. **2207**: p. 690.
25. Lü, L., Fuh, J., Wong, Y.S., *Laser-Induced Materials and Processes for Rapid Prototyping*. 2001, Dordrecht: Kluwer Academic Publishers.
26. Lash, J.S., Gilgenbach, R.M., *Copper vapour laser drilling of copper, iron and titanium foils in atmospheric pressure air and argon*. Rev. Sci. Instrum., 1993. **64**: p. 3308-3313.
27. O'Neill W., E., A., Steen, W.M., Volsanger, M., . *Selective Removal of Steel by a Laser Slotting Process*. in *ICALEO '95: Proceedings of the laser materials processing conference*. 1995. San Diego, CA.
28. Chang, J.J., Warner, B.E., , *Laser-plasma interaction during visible ablation methods*. Appl. Phys. Lett., 1996. **69**: p. 473-475.
29. Knowles, M.R.H., *Drilling of shallow angled holes in aerospace alloy using a copper laser*. ICALEO 1995, 1996: p. 321-330.
30. Tunna, L., Khan, A., O'Neill, W., *Micromachining of copper using Nd:YAG laser radiation at 1064, 532 and 355 nm wavelengths*. Optics and Laser Technology, 2001. **33**: p. 135-143.
31. Knowles, M., *Micro-ablation with high power pulsed copper vapor lasers (CVL)*. Opt. Express, 2000. **7**: p. 50-55.
32. Kamalu, J., Byrd, P., Pitman, A., , *Variable angle laser drilling of thermal barrier coated nimonic*. J. Mater. Process. Technol. , 2002. **122**: p. 355-362.
33. Chang, J.J., Warner, B.E., Dragon E.P., Martinez, M.W., , *Precision micromachining with pulsed green lasers*. Journal of laser applications, 1998. **10**(6): p. 285-290.
34. Chang, J.J., Warner, B.E., Dragon E.P., Martinez, M.W., , *Apparatus for Precision Micromachining with Lasers, in United States Patent, T.U.S.o.A.a.r.b.t.U.S.D.o. Energy, Editor*. 1995.
35. Olson, R.W., Swope, W.C., *Laser Drilling with focused gaussian beams*. Journal of Applied Physics, 1992. **72**(8): p. 3686-3696.
36. Pfefferkorn, E.E., Incorpora, F.P., Shin, Y.C., *Surface temperature measurement of semi-transparent ceramics by long-wavelength pyrometry*. Journal of heat transfer, 2003. **125**(1): p. 48-56.
37. Kirby, K.W., Jankiewicz, A.T., , *Laser machining of glass forming ceramics*. Journal of laser applications, 1998. **10**(1): p. 1-10.
38. Barnes, C. *Copper at the cutting edge: the copper vapor laser*. 2001 [24.07.2011]; Available from: [http://www.copper.org/publications/newsletters/innovations/2001/06/cutting\\_edge.html](http://www.copper.org/publications/newsletters/innovations/2001/06/cutting_edge.html).
39. Miyazawa, H., Miyake, S., Watanabe, S., Murakawa, M., Miyazaki, T., *Laser assisted thermochemical processing of diamond*. Applied Physics Letters 1994. **64**(3): p. 387-389.
40. Anonymus, *Laser 'punches' holes in diamond wire-drawing dies*, in *Laser Focus*. 1966. p. 4-7.



41. Schaeffer, R. *Novel high-power Nd:YLF laser for CVD-diamond micromachining*. in *Proceedings of the Conference Micromachining and Microfabrication Process Technology*. 1995. Bellingham.
42. Harryson, R., and Herbertson, H., . *Machining of high performance ceramics and thermal etching of glass by laser*. in *Proceedings of the 4th International Conference Lasers in Manufacturing*. 1987. Birmingham, UK: IFS Publications.
43. Schaeffer, R.D., Kardos, G., Derkach, O., *Laser Processing of Glass* Industrial Laser Solutions, 2002. **17**(9): p. 11-13.
44. Atasanov, P.A., Gendjov, S.I., *Laser cutting of glass tubing- a theoretical model*. Journal of Physics, 1987. **20**(5): p. 597-601.
45. Hallada, M.R., Walter, R.F., Setffert, S.L. *High power laser rock cutting and drilling in mining operations, initial feasibility tests*. in *Proceedings of the Conference High-power Laser Ablation III*. 2000: Bellingham:SPIE.
46. Graves, R.M., O'Brien, D.G., *Targeted literature review: determining the benefits of Star Wars laser technology for drilling and completing natural gas wells, topical report*. 1998, Gas Research Institute: Chicago.
47. Bang, S.Y., Roy, S., Modest, M.F., *CW laser machining of hard ceramics- II. Effects of multiple reflections*. International Journal of Heat and Mass Transfer, 1993. **36**(14): p. 3529-3540.
48. Rozzi, J.C., Pfefferkorn, F.E., Shin, Y.C., Incorpora, F.P., *Experimental evaluation of the laser-assisted machining of silicon nitride ceramics*. Journal of Manufacturing Science and Engineering 2000. **122**: p. 666-670.
49. Kitagawa, A., Matsunawa, A., *Three dimensional shaping of ceramics by using CO2 laser and its optimum processing condition*. in *Proceedings of the Laser Material Processing Conference (ICALEO 90)*. 1990. Orlando: Laser Institute of America, Bellingham:SPIE.
50. Cottam, C.A., *XPS monitoring of the removal of an aged polymer coating from a metal substrate by TEA-CO2 laser ablation*. Journal of Material Science, 1998. **33**: p. 3245-3249.
51. Berrie, P.G., Birkett, E.N., *The drilling and cutting of polymethyl methacrylate (perspex) by CO2 laser* Optics and Lasers in Engineering, 1980. **1**: p. 107-129.
52. Schaeffer, R., O'Connell, J., *Comparing lasers for micromachining plastics*. Industrial Laser Solutions, 2002. **17**(5): p. 16-19.
53. Carslaw, H.S., Jaeger, J.C., *Conduction of Heat in Solids* 1959: Oxford: Clarendon Press.
54. Bass, M., ed. *Laser Heating of Solids*. Physical Processes in Laser Material Interactions, ed. M. Berolotti. 1983, Plenum Press, New York.
55. Ready, J.F., *Effects of High-Power Laser Radiation*. 1971, New York: Academic Press.
56. Rosenthal, D., *Mathematical Theory of Heat Distribution During Welding and Cutting*. Welding Journal, 1941.
57. Rosenthal, D., *The theory of moving sources of heat and its application to metal treatments*. Transactions of the American Society of Mechanical Engineers, 1946. **69**: p. 849-866.
58. Ashby, M.F., Easterling, K.E., *A first report on diagrams for grain growth in welds*. Acta Metallurgica, 1982. **30**(11): p. 1969-1978.
59. Ryakaling, N., Uglov, A., Kokora, A., *Laser Machining and Welding*. 1978, Oxford: Pergamon Press.

60. Ashby, M.F., Easterling, K.E., *The transformation hardening of steel surfaces by laser beams- 1. Hypertoid steels*. Acta Metallurgica, 1984. **32**(11): p. 1935-1948.
61. Grez, J.A.R., *Surface Modification of Ceramic and Metallic Alloy Substrates by Laser Raster Scanning*, in *Material Science and Engineering*. 2003, University of Texas, at Austin: Austin.
62. Ltd., S.O.P., *Nd:YAG Lasers*, S.O.P. Ltd, Editor. 2005: Singapore.
63. Illyefalvi, V., Z., *Laser Processing for microelectronics packaging applications*. Microelectron Reliab, 2001. **41**(4): p. 563.
64. Tolochko, N.K., Laoui, T., Khlopkov, Y.V., Mozzharov, S.E., Titov, V.I., Ignatev, M.B., *Absorptance of powder materials suitable for laser sintering*. Rapid Prototyping Journal, 2000. **6**: p. 155-161.
65. Dowden, J.M., *The Mathematics of Thermal Modelling: An introduction to laser material processing*. 2001, Boca Raton, Florida.
66. G.R.B.E, R., *Matlab Laser Toolbox*. Physics Procedia: p. 412-419.
67. Kreyszig, E., *Advanced Engineering Mathematics*. 2010: John Wiley & Sons.
68. Abramowitz, M., Stegun, I.A., *Handbook of Mathematical Functions: with Formulas, Graphs and Mathematical Tables*. 1965.
69. Birmingham, B.R., *Laser-Based Solidfabrication Techniques for Direct Production of Ceramic and Metal/ Ceramic Shapes*, in *Material Science and Engineering*. 1995, University of Texas, at Austin: Austin.
70. Duley, W.W., *Laser Processing and Analysis of Materials*. 1983, New York: Plenum Press.
71. Weast, R.C., *CRC Handbook of Chemistry and Physics*. 1999, Boca Raton: CRC Press.
72. Boyer, R.G., Collings, E.W., *Materials and Properties Handbook: Titanium Alloys*. 1994, Materials Park: ASM International.
73. Ross, R.B., *Metallic Materials Specification Handbook 4th Ed*. 1992, London: Chapman & Hall.
74. *Metallic Handbook Vol 2: Properties and Selection: Nonferrous Alloys and Special Purpose Materials*. ASM International 10th Edition. Vol. 2. 1990.
75. Nayer, A., *The Metal Databook*. 1997, New York: Mc-Graw Hill.
76. Clegg, D.W., Collyer, A.A., *The structure and properties of polymeric materials*, London: The Institute of Materials.
77. Leaver, K.D., Anderson, J.C., Rawlings, R.D., Alexander, J.M., *Materials Science for Engineers 5th Ed*. 2003, Boca Raton: CRC Press.
78. McCulloch, R.S., *Treatise on the mechanical theory of heat and its applications to the steam-engine*. 1876, New York: D. Van Nostrand.
79. Trouton, F., *On Molecular Latent heat*. Philosophical Magazine, 1884. **18**: p. 54-57.
80. Ashby, M.F., *Materials Selection in Mechanical Design 2nd Ed*. 1999, Oxford: Butterworth-Heinemann.

### Chapter 3 References

1. Chung, H., *Processing and Properties of Functionally Graded Polymer Composites Produced by Selective Laser Sintering*, in *Mechanical Engineering*. 2005, University of Michigan.
2. Lee, J., *Finite Element Models of Laser Welding*, in *Mechanical Engineering*. 1992, University of Michigan.

3. Cheng, M.Y., *High Power Pulsed Fiber Lasers at Near-IR Optical Wavelengths*. 2007, University of Michigan.
4. Hu, Y., *Laser Direct Fabrication of 3D Components*, in *Materials Science and Mechanics*. 2000, Michigan State University.
5. Yuan, D., *Laser Direct-Write Microfabrication and Patterning*, in *Mechanical Engineering*. 2008, University of Michigan.
6. Qi, H., *Synthesis of Designed Materials by Laser-Based Direct Metal Deposition Technique: Experimental and Theoretical Approaches*, in *Mechanical Engineering*. 2005, University of Michigan.
7. Das, S., *Direct Selective Laser Sintering of High Performance Metals- Machine Design, Process Development and Process Control*. 1998, University of Texas, at Austin: Austin.
8. Deckard, C.R., *Selective Laser Sintering*. 1988, University of Texas, at Austin: Austin.
9. Jepson, L.R., *Multiple Material Selective Laser Sintering*. 2002, University of Texas, at Austin: Austin.
10. Ying-Jeng, W., *A minimum time laser tracking control technique for selective laser sintering*. 1992, University of Texas, at Austin: Austin.
11. Mercelis, P., *Control of Selective Laser Sintering and Selective Laser Melting*. 2007, Katholieke Universiteit Leuven: Leuven.
12. Rombouts, M., *Selective laser sintering/ melting of iron based powders*. 2006, Katholieke Universiteit Leuven: Leuven.
13. Shueren, V.D., *Basic contributions to the development of the selective metal powder sintering process*. 1996, Katholieke Universiteit Leuven: Leuven.
14. Regenfuss, P., Petsch, T., Hartwig, L., Klötzer, S., Brabant, Th., Ebert, R., Exner, H., *Microsintering - Ein Verfahren zur herstellung metallischer und keramischer Mirobauteile*. Rapid. Tech, Anwendertagung und Fachausstellung für Rapid Technologien.
15. Slocum, A., *Precision Machine Design*. 1992, Michigan: Society of Manufacturing Engineers.
16. Cerit, E., *Development of a Novel Open-Architecture Rapid Prototyping System*, in *Mechanical Engineering*. 2009, Koc University: Istanbul.
17. Cerit, E., Lazoglu, I., *A CAM-based path generation method for rapid prototyping applications*. Int. J. Adv. Manuf. Technol., 2011.
18. Izbassarov, D., *Open architecture system for biomanufacturing of scaffolds for tissue engineering*, in *Mechanical Engineering*. 2010, Koc University: Istanbul.
19. Sells, E., Smith, Z., Bailard, S., Bowyer, A., Olliver, V., *RepRap: The Replicating Rapid Prototyper: Maximizing Customability by Breeding the Means of Production*. Social Science Research Network, 2009.
20. Malone, E., Lipson, H., *Fab@Home: the personal desktop fabricator kit*. Rapid Prototyping Journal, 2007. 13(4): p. 245-255.
21. Chen, K., *Numerical and Experimental Unvestigation of Interactive Effects in Laser Machining*. 1999, Columbia University: NewYork.
22. Kruth, J.P., Froyen, L., Van Vaerenbergh, J.V., Mercelis, P., Rombouts, M., Lauwers, B., *Selective Laser Melting of Iron Based Powder*. Journal of materials processing technology, 2004. 149: p. 616.
23. Kuar, A.S., *Modelling and analysis of pulsed Nd:YAG laser machining characteristics during micro-drilling of zirconia (ZrO<sub>2</sub>)*. International Journal of Machine Tools and Manufacture, 2005. 46(12-13): p. 1301-1310.

24. Lamikız, A., *Laser Polishing of Parts Built Up by Selective Laser Sintering*. International Journal of Machine Tools and Manufacture, 2007. 47(12-13): p. 2040-2050.
25. Fisher, F., Romoli, L., Kling, R., *Laser-based repair of carbon fiber reinforced plastics*. CIRP Annals Manufacturing Technology, 2010.
26. Li, L., Eghlio, R., Marimuthu, S., *Laser Net Shape Welding*. CIRP Annals Manufacturing Technology, 2011.
27. Das, S., *Direct Selective Laser Sintering of High Performance Metals, Machine Design, Process Development and Process Control "Chapter 6 Technology Demonstration AIM9 Sidewinder Missile Guidance Housing"*, in *Mechanical Engineerign*. 1998, University of Texas Austin: Austin.
28. Lü, L., Fuh, J., Wong, Y.S., *Laser-Induced Materials and Processes for Rapid Prototyping*. 2001, Dordrecht: Kluwer Academic Publishers.
29. Anon., *Panasonic Instruction Manual AC Servo Motor and Driver Minas A4 Series*.
30. Balasubramanian, B., *Study of the Selective Laser Sintering of Metal-Polymer Powders*, in *Material Science and Engineering*. 1995, University of Texas, at Austin: Austin.

#### Chapter 4 References

1. Anon., *Pulsed Fiber Laser Specification Model YLP-1-120-50-50*, I. Laser, Editor. 2008.
2. Steen, W.M., *Laser Material Processing 1991*: Springer-Verlag.
3. *F-theta Ronar Datasheet Specification*. 2011.
4. Foucault, L.M., *Memoire sur la construction des telescopes en verre argente*. Annales de l'Observatoire imperial de Paris, 1859. 5: p. 197-213.
5. Hachfeld, K., D., *Laser-beam quality and brightness in industrial applications*, in *Industrial Laser Handbook*. 1992-1993. p. 48-54.
6. Backes, G., Kreutz, E.W., Stromeyer, R., Wissenbach, K., , *Process monitoring and control during alloying and cladding with CO2 laser radiation*, in *In ECLAT European conference on laser treatment of materials*. 1998. p. 227-236.
7. Bi, G., Gasser, A., Wissenbach, K., Drenker, A., Poprawe, R., , *Identification and qualification of temperature signal for monitoring and control in laser cladding*. Optics and Lasers in Engineering, 2006. 44: p. 1348-1359.
8. Mutabue, T., Colin, C., Malot, T., Aubr, P., . *Influence of process monitoring devices on direct manufacturing by laser cladding for aeronautic components*,. in *In Proc. 23rd International Congress on Applications of Lasers and Electro-Optics*. 2004.
9. Beersiek, J., Devermann, T., Behler, K.,. *Practical applications of in-process monitoring for laser processes- not only for single welds and common materials*. in *In Proc. 23rd International Congress on Applications of Lasers and Electro-Optics 2004*. 2004.
10. Deininger, C., Miler-Borhanian, J., Dausinger, F., Hgel, H. *Development of multi-detector systems for the process monitoring of laser beam welding capable for industrial use*. in *In Proc. of the Laser Assisted Net Shape Engineering (LANE) Conference*. September, 2004. Erlangen, Germany.
11. Negendanck, M., Schwab, J. *Process monitoring in laser beam welding*. in *In Laser Assisted Net Shape Engineering 3, Proceedings of the LANE 2001*. 2001.

12. Schroder, K., Weingartner, Schuker, D., *Optical distance monitoring system for laser materials processing*. in *In Laser Assisted Net Shape Engineering 3, Proceedings of the LANE 2001*. 2001.
13. Poprawe, R., Kanig, W., *Modeling, monitoring and control in high quality laser cutting*. CIRP annals 2001, 2001. **50**(1): p. 129.
14. Alvarez, C., Ramil, A., Nicolas, G., Saavedra, E., Lopez, A.J., Perez, J.A., Yanez, A., Ocana, J.L. *Realtime control and monitoring of laser hardening process: application to cylindrical workpieces*. in *In Laser Assisted Net Shape Engineering 3, Proceedings of the LANE 2001*.
15. Craeghs, T., Florian, B., Berumen, S., Kruth, J.P., *Feedback control of Layerwise Laser Melting using optical sensors*. Physics Procedia, 2010. **5**: p. 505-514.
16. *2-Achsen Laserstrahl-Ablenkeinheiten - Handbuch RLA, SS, TS*, Raylase, Editor. 2011.
17. Das, S., *Direct Selective Laser Sintering of High Performance Metals - Machine Design, Process Development and Process Control*, in *Material Science and Engineering*. 1998, University of Texas, at Austin: Austin.
18. Nelson, J.C., *Selective Laser Sintering: A definition of the process and an empirical sintering model*, in *Material Science and Engineering*. 1993, University of Texas, at Austin: Austin.
19. Benda, J.A., Parasco, A., *Apparatus for temperature controlled sintering*, U.S.P. Office, Editor. 1996.
20. Bollig, A., Abel, D., Kratsch, Ch., Kaieler, S., *Identification and predictive control of laser beam welding using neural networks*.
21. Kuar, A.S., Doloi, B., Bhattacharyya, B., *Modeling and analysis of pulsed Nd:YAG laser machining characteristics during micro-drilling of Zirconia*. Machine Technology and Manufacturing, 2006. **46**: p. 1302-1310.
22. Incropera, F.P., DeWitt, D.P., *Fundamental of Heat and Mass Transfer*. 2002: John Wiley & Sons.
23. Benedict, R.P., *Fundamentals of Temperature, Pressure and Flow Measurements*. 1984: John Wiley & Sons.
24. Bernardini, F., Rushmeier, H., *The 3D Model Acquisition Pipeline*. Computer Graphics Forum, 2002. **21**(2): p. 149-172.
25. Istook, C., Hwang, S., *3D Body Scanning Systems with Application to the Apparel Industry*. Journal of Fashion Marketing and Management, 2001. **5**(2): p. 120-132.
26. Rochini, C., Cignoni, P., Montani, C., Pingi, P., Scopigno, R., *A low cost 3D scanner based on structured light*. Eurographics, 2001. **20**(3).
27. Tognola, G., Parazzini, M., Ravazzani, P., Grandori, F., Svelto, C., *3D acquisition and quantitative measurements of anatomical parts by optical scanning and image reconstruction from unorganized range data*. IEEE Trans. Instrum. Meas., 2003. **52**: p. 1665-1673.
28. Hajeer, M., Millet, D., Ayoub, A., Siebert, J., *Applications of 3D imaging in orthodontics: Part I*. Journal of orthodontics, 2004. **31**: p. 62-70.
29. Hennesy, R., McLearn, S., Kinsella, A., *Facial surface analysis by 3D laser scanning and geometric morphometrics in relation to sexual dimorphism in cerebral-craniofacial morphogenesis and cognitive function*. Journal of Anatomy, 2005. **207**: p. 283-295.
30. Trinh, N., Lester, J., Fleming, B., Tung, G., Kimia, B., *Accurate measurement of cartilage morphology using a 3D scanner*. in *In Proc. of 2nd Int'l ECCV Workshop on*

- Computer Vision Approaches to Medical Image Analysis, CVAMIA '06*. 2006. Graz, Austria.
31. Azouz, Z., Shu, C., Lepage, R., Rioux, M., *Extracting main modes of human body shape variation from 3D anthropometric data*. in *In Proc. 5th Int'l Conf. 3D Digital Imaging and Modeling, 3DIM '05*. 2005. Ottawa, Canada.
  32. Schwenzer-Zimmer K., H., J., Kovacs, L., Boerner, B., Schwenzer, N., Juergens, P., Zeilhofer, H.-F., Holberg, C., *3D surface measurement for medical application-technical comparison of two established industrial surface scanning systems*. *Journal of Medical System*, 2008. **32**: p. 50-64.
  33. Bajcsy, R., Pito, R., *Data acquisition and representation of mechanical parts and interfaces to manufacturing devices*. In *Proc. Int'l Conf. Recent Advances in 3D Digital Imaging and Modeling*, 1997: p. 2-9.
  34. <http://www.3dmd.com>. 2011.
  35. Jalkio, M., Kim, R., Case, S., *Three dimensional inspection using multistripe structured light*. *Optical Engineering*, 1985. **24**: p. 966-974.
  36. Petrov, M., Talapov, A., Robertson, T., Lebedev, A., Zhilyaev, A., Polonsky, L., *Optical 3D digitizers: Bringing life to virtual world*. *IEEE Computer Graphics and Applications*, 1998. **18**: p. 28-37.
  37. Dunn, R., Taylor, D., *A 3D Scanner for you and me*, Cornell University EcE 4760 Final Project.
  38. Bouguet, J.-Y., Perona, P., *3D Photography on your desktop*.
  39. Lichtschnitt, L. [www.sukhamburg.com/onTEAM/pdf/kontur3d\\_e.pdf](http://www.sukhamburg.com/onTEAM/pdf/kontur3d_e.pdf). Laser light section: a key feature in 3D laser measurement technique 2007 10.08.2011].
  40. Bolle, R., Vemuri, B., *On three-dimensional surface reconstruction methods*. *IEEE Trans. Pattern Analysis and Machine Intelligence* 1991. **13**(1): p. 1-13.
  41. Soucy, M., Laurendau, D., *A general surface approach to integration of a set of range views*. *IEEE Trans. Pattern Analysis and Machine Intelligence*, 1995. **17**: p. 344-358.
  42. Kulli, K., Duchamp, T., Hoppet, H., McDonald, J., Shapiro, L., Stuetzle, W., *Robust meshes from multiple meshes*. In *Proc. Int'l Conf. Recent Advances in 3D Digital Imaging and Modeling*: p. 205-211.
  43. Zhang, L.C., Han, M., Huang, S.H., *An effective error tolerance slicing algorithm for STL files*. *International Journal of Advanced Manufacturing Technology*, 2002. **20**: p. 363-367.
  44. Tong, W., Edmund, H.M., Cheung, *Enhanced STL*. *International Journal of Advanced Manufacturing Technology*, 2006. **29**: p. 1143-1150.
  45. Chen, K., *Intelligent Scanning in Selective Laser Sintering*, in *Mechanical Engineering*. 1998, University of Texas, at Austin: Austin.
  46. Kruth, J.P., *Material Ingress Manufacturing by Rapid Prototyping Techniques*. *CIRP Annals* 1991. **40**: p. 603.
  47. Schaub, D.A., Chu, K.R., Montgomery, D.C., *Optimizing the stereolithography throughput*. *Journal of manufacturing systems*, 1997. **16**(4): p. 290.
  48. Jande, Y.A.C., *Manufacturing and Characterization of Uniformly Porous and Graded Porous Polymeric Structures via Selective Laser Sintering*, in *Mechanical Engineering*. December 2009, Middle Eastern Technical University: Ankara.
  49. Tekin, C.M., *Mechanical Characterization and Modeling of Porous Polymeric Materials Manufactured by Selective Laser Sintering*, in *Mechanical Engineering*. December 2009, Middle Eastern Technical University: Ankara.

50. Cheah, C.M., in *Mechanical Engineering*. 2001, National University of Singapore.
51. Donahue, R.J., Turner, R.S., . *CAD model and alternation methods of information transfer for rapid prototyping systems*. in *Proc. of 2nd International Conference on Rapid Prototyping*. 1992. Dayton, Ohio.
52. Sheng, X., Hirsch, B.E., *Triangulation of trimmed surfaces in parametric space*. *Computer-Aided Design*, 1992. **24**(8): p. 437-444.
53. Bjorke, O., *How to Make Stereolithography into a Practical Tool for Tool Production*. *CIRP Annals*, 1991. **40**(1).
54. Lü, L., Fuh, L.H., Wong, Y.S., *Laser-Induced Materials and Processes for Rapid Prototyping*. 2001, Drodrecht: Kluwer Academic Publisher.